Politechnika Wrocławska

FIELD OF SCIENCE: ENGINEERING AND TECHNOLOGY

DISCIPLINE OF SCIENCE: MECHANICAL ENGINEERING

DOCTORAL DISSERTATION

Method of efficient utilization of digital hydraulic concept in multisource hydrostatic drive systems.

MSc. Eng. Ahmed Zubair Jan

Supervisor/Supervisors: dr hab. inż. Krzysztof Kędzia

Keywords: Fluid Power, “Digital” Hydrostatic Transmission, Simulation end Experimental Tests

WROCŁAW 2025

Acknowledgements

I would like to thank ALLAH Almighty, whose benediction bestowed upon me talented professors, provided me sufficient opportunities, and enabled me to undertake and execute this research work. I offer my sincere gratitude to my affectionate, sincere, kind, and most respectful supervisor **dr hab. inż. Krzysztof Kędzia**, whose kinetic supervision, the caution in the correct inclination, and inductance of hard work made my task easy. I completed my dissertation well within time. His ideology and concepts have a remarkable impact on my research contrivances.

I would like to extend my sincere gratitude to **PhD. Eng. Catalin Dumitrescu**, Director of the IHP Institute in Romania, for generously providing me with the opportunity to conduct experimental tests in his state-of-the-art laboratory. His support and access to advanced facilities were instrumental in the successful execution of this research. I am also deeply thankful to **PhD. Eng. Radu Radoi** for his invaluable assistance and technical support during the experimental tests. His expertise and guidance were crucial in overcoming challenges and ensuring the accuracy of the results. Both **PhD. Eng. Dumitrescu and PhD. Eng. Radoi** have made significant contributions to this project, and I am truly grateful for their support.

I would like to thank the authorities Wroclaw University of Science and Technology as they provided me with the opportunity and facilitated me to continue my study. I also feel grateful to my beloved **wife** and **son Muhammad Arham Ahmed** for their unwavering love, patience, and encouragement throughout this journey. Their understanding and support have been my greatest source of motivation. I am also immensely grateful to my **friends Ahsan Khan, Atif Shafi, Ahsan Ali ,Chaman Gul, Mohsan khan,** for their constant encouragement and for being a source of positivity during challenging times. This achievement would not have been possible without their belief in me.

List of content

1 Introduction 8
2 Justification for the Selection of the Topic 10
2.1 Outline of the Current State of Research 12
2.2 PhD Thesis Hypothesis 13
2.3 Contribution of the Expected Results to the Scientific Discipline. 14
2.4 Planned Research Methods 15
2.5 Research Significance 15
3 Components of Digital Hydraulic Technology 17
3.1 Hydraulic Pump. 19
3.2 Hydraulic Actuators 19
3.3 Control Valves 20
3.4 Reservoir 20
3.5 Hoses, Pipes, and Fittings 21
3.6 Hydrostatic Transmission 22
3.7 Open Loop Hydrostatic Drive System 23
3.8 Closed Loop Hydrostatic Drive System 24
3.9 Limitations of Traditional Hydraulic Systems 26
4 Fundamental Concepts of Digital Hydraulics 27
4.1 Digital Hydraulic Valves 29
4.2 Parallel Connection in Digital Hydraulics 33
4.3 Digital Flow Control Unit (DFCU) 34
4.4 Pulse Based Modulation Techniques in Digital Hydraulics 36
4.5 Digital Hydraulic Power Management System (DHPMS) 38
4.6 Comparison of Conventional with Digital Hydraulics 38
5 Simulation Model 40
5.1 Gear Pumps 42
5.2 Directional Valves 43
5.3 Check Valves 44
5.4 Pressure Relief Valve 44
5.5 Hydraulic Fluid 44
5.6 Other Components 44
5.7 Mechanical and Hydraulic Losses 46
5.8 Energy Efficiency Measurement 47
5.9 Model of Hydraulic Losses in Pipes 48
5.10 Ecological Performance Measures 49
5.11 Impact on the Environment 49

5.12 Expanded Economic Analysis 51
5.12.1 Capital Expenditure (CAPEX) 51
5.12.2 Operational Expenditure (OPEX) 51
5.12.3 Total Cost of Ownership (TCO) 52
5.13 Evaluation of the Compatibility of Simulation Models 52
6 Test Scenarios 54
6.1 Test Scenario 1 54
6.2 Test Scenario 2 55
6.3 Test Scenario 3 56
7 Experimental Research Results 58
7.1 Experimental Stand of Digital Hydrostatic Transmission 58
7.2 Experimental Results for Scenario No. 1 (Load 2.8 MPa) 62
7.3 Experimental Results for Scenario No. 1 (Load 5.7 MPa) 66
7.4 Experimental Results for Scenario No. 1 (Load 10 MPa) 70
7.5 Experimental Results for Scenario No. 2 (Load 1.2 MPa) 73
7.6 Experimental Results for Scenario No. 2 (Load 6 MPa) 77
7.7 Experimental Results for Test Scenario 3 (Load 1.2 MPa) 81
7.8 Experimental Results for Test Scenario 3 (Load 1.6 MPa) 84
7.9 Experimental Results for Test Scenario 3 (Load 9 MPa) 88
8 Simulation Research Results 92
8.1 Digital Hydrostatic Transmission 92
8.1.1 Simulation Research Results for Test Scenario No. 1 92
8.1.2 Simulation Research Results for Test Scenario No. 2 98
8.1.3 Simulation Research Results for Test Scenario No. 3 104
8.1.4 Simulation Research Results for Test Scenario No. 3a 110
8.1.5 Simulation Research Results for Test Scenario No. 3b 117
8.1.6 Simulation Research Results for Test Scenario No. 3c 123
8.2 Classic Hydrostatic Transmission 130
8.2.1 Comparison of Experim. and Sim. Results for Scenario No. 2 (Load 1,2 MPa) .. 132
8.2.2 Comparison of Experim. and Sim. Results for Scenario No. 2 (Load 6 MPa) 134
8.3 Comparison of Simulation Results: Classic vs. Digital Transmission 137
8.3.1 Analysis for Scenario No. 3 (20s) 137
8.3.2 Analysis for Scenario No. 3a (10s) 139
8.3.3 Analysis for Scenario No. 3b (5s) 142
8.4 Comparison of simulation of classic and digital simulation drive models 147
8.4.1 Comparison for the 3rd testing signal at 10-20 MPa load pressure 148
8.4.2 Comparison for the 3a testing signal at 10-20 MPa load pressure 150

8.4.3 Comparison for the 3b testing signal at 10-20 MPa load pressure........................ 152
8.4.4 Comparison for the 3c testing signal at 10-20 MPa load pressure........................ 154
9 SUMMARY 157
9.1 Method for Replacing a Classic to Digital Hydrostatic Transmission........................... 161
9.2 Final Conclusions and Verification of the Research Hypothesis 165
9.3 Contribution and Recommendations: 166
10 References:...167
11 Appendix...177
11.1 Appendix A 177
11.2 Appendix B 189
11.3 Appendix C 192

LIST OF NOMENCLATURE

Symbol	Description	Units
g_e	Specific fuel consumption	[g/kWh]
h	Valve orifice opening distance	[m]
k_n	Filling coefficient	[–]
k_{sp}	Loosening coefficient of the processed material	[–]
Δp	Pressure difference across the valve	[Pa]
p_p	Pump load pressure	[Pa]
p_{sh}	Pressure drop in hydrostatic motor	[Pa]
p_{crack}	Cracking pressure	[Pa]
p_{max}	Maximum pressure	[Pa]
Δp_{Reg}	Pressure regulation range	[Pa]
q_0	Geometric capacity of the working vessel	[m^3/rad]
q_k	Deformation of the working chambers	[m^3]
$q_{sh\ max}$	Max unit absorption of the hydrostatic motor	[m^3/rad]
t_c	Working cycle time	[s]
v	Kinematic viscosity coefficient	[m^2/s]
A	Cross-sectional area of the valve opening	[m^2]
A_{prv}	Effective area of the valve opening	[m^2]
$C_{j,i}$	Concentration of individual compounds	[%]
C_l	Dimensionless proportionality factor	[–]
C_t	Dimensionless proportionality coefficient	[–]
C_d	Discharge coefficient of the valve	[–]
CS	Control Signal	[–]
D	pump's volumetric displacement	[m^3/rad]
D_p	Displacement volume per revolution	[m^3/rev]
$G_{sp,i}$	Exhaust gas flow rate	[kg/h]
I	Current	[A]
K_{HP}	Hagen-Poiseuille coefficient for laminar leakage	[m^4s/kg]
K_{TP}	Friction torque vs. pressure gain coefficient	[m^3]
K_e	Back EMF constant	[Vs/rad]
K_t	Torque constant	[Nm/A]

ΔM_p, ΔM_{sh}	Pump and hydrostatic motor torque losses	[N m]
N_{sp}	Power developed by the engine during the cycle	[W]
P_{sys}	System pressure	[Pa]
P_{set}	Set pressure of the valve	[Pa]
Q	Volumetric flow rate, engine absorption	[m^3/s]
Q_p	Flow rate of the hydraulic pump	[m^3/s]
Q_s	Flow rate of the hydraulic motor	[m^3/s]
Q_v	Flow rate through the valve	[m^3/s]
Q_{vl}	Laminar leakage flow rate	[m^3/s]
Q_{vt}	Turbulent flow	[m^3/s]
ΔQ_p, ΔQ_{sh}	Pump and motor volumetric losses	[m^3/s]
T_p	Torque required to drive the pump	[N·m]
V	Voltage	[V]
η	Overall energy efficiency of the system	[–]
η_m	Mechanical efficiency of the pump	[–]
η_v	Volumetric efficiency of the pump	[–]
μ	Coefficient of friction losses	[$kg/(s^2m^3)$]
ρ	Density of the hydraulic fluid	[kg/m^3]
τ	Time constant of the valve	[s]
τ_0	No-load torque	[N·m]
τ_{prv}	Time constant of the pressure relief valve	[s]
ω	Angular velocity	[rad/s]
ω_p	Angular velocity of the pump	[rad/s]
$\omega_{Threshold}$	Threshold of angular velocity	[rad/s]
ε_{sh}	Axial motor absorption control parameter	[–]
ε_p	Axial pump capacity control parameter	[–]

Abstract

This doctoral dissertation analyzes the potential for effective use of the digital hydrostatic transmission concept in classic hydrostatic drive systems. The aim of the research is to determine whether it is possible to replace traditional hydrostatic transmissions, which typically utilize expensive and complex variable-displacement and/or fixed-displacement multi-piston pumps with throttling valves, with digital hydraulics- a concept based on simple sets and low-cost components, such as gear pumps and two-position on/off valves.

The motivation for the research described in this dissertation is primarily the potential for such a solution to significantly reduce system construction costs, increase its reliability, and improve its environmental efficiency both in terms of component manufacturing and energy savings during operation (especially compared to throttling-controlled systems). Simulation and experimental studies of the digital hydrostatic transmission described in this paper have initially confirmed the feasibility of meeting the functional and energy requirements necessary for replacing a classic hydrostatic transmission with an equivalent built according to the digital hydraulics concept in classic hydrostatic drive systems. The advantages of replacing a classic hydrostatic transmission with its digital counterpart are most evident in the areas of capital and operating costs, increased system resilience to critical failures, and reduced environmental impact – particularly in terms of reducing the carbon footprint associated with component production and energy consumption during system operation. In light of these benefits, digital hydraulics represents an interesting alternative for the next generation of intelligent, energy-efficient hydrostatic drive systems, including multi-source systems.

1 Introduction

The origins of fluid power date back to ancient times. Greek thinkers such as Archimedes (3rd century BC) studied the basic properties of fluids, including buoyancy and pressure. In the 17th century, the French scientist Blaise Pascal, in 1653, formulated the fundamental law for these types of systems, which states that pressure exerted on a confined fluid is transmitted equally in all directions [1].

The true flourishing of hydrostatic drives occurred with the Industrial Revolution in Great Britain at the turn of the 17th and 18th centuries. In 1795, the English inventor Joseph Bramah patented the world's first hydraulic press [2]. Using Pascal's law, he created a device capable of generating immense forces, which revolutionized the processes of metal forming and pressing. In the second half of the 19th century, William Armstrong—often called the "father of modern hydraulics"- constructed the first hydraulic crane powered by pressurized water, and later the hydraulic accumulator (weighted type), which allowed for the storage of energy in pressure networks (Fig. 1).

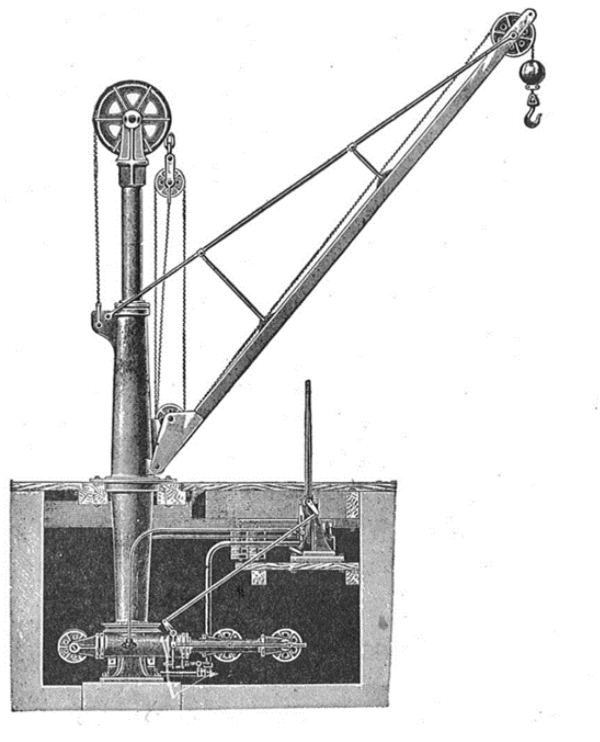

Figure 1. William Armstrong's first hydraulic crane [8].

The 20th century was a time of miniaturization, an increase in operating pressures, and, most importantly, the transfer of fluid power to mobile applications. The key areas where changes occurred are presented below [3]:

- Oil as a Medium: Water was replaced by hydraulic oils, which offered better lubrication, higher operating temperatures, and protection against corrosion.
- Mobile Machinery: The development of compact gear, vane, and finally axial-piston pumps allowed for the widespread use of hydrostatics in construction, agricultural, and forestry machinery.
- Aviation: Hydraulic systems became standard in aviation for controlling landing gear, flaps, and control surfaces due to their reliability and high-power density.
- Electrohydraulic: In the second half of the 20th century, a breakthrough occurred the integration of hydraulics with electronics. The creation of servo-valves and proportional valves allowed for precise, remote control of force and speed.

Currently, development work related to this area concerns energy efficiency and integration with information technology systems (Industry 4.0) [4], [5], [6], [7], such as:

- Intelligent Control: The proliferation of microprocessors and PLC controllers has enabled the implementation of advanced control algorithms that optimize system operation in real-time.
- Digital Hydraulics: It involves replacing continuous regulation realized, for example, by proportional valves or units with adjustable flow rate with discrete, binary switching of many simpler and cheaper components (e.g., a set of gear pumps and their associated on/off valves).
- Diagnostics and Industry 4.0: Modern hydraulic systems are equipped with numerous sensors that monitor their condition. This allows for early fault detection, predictive maintenance, and the integration of machines within an intelligent factory (Internet of Things - IoT).

Recent research indicates substantial energy savings by employing digital pumps together in hydraulic systems. By utilizing several pumps within one system, less energy will be used, particularly during partial load conditions and slow speed movements. It is worth mentioning that there was a 38% decrease in energy use in comparison with the traditional analog pump [9].

2 Justification for the Selection of the Topic

As part of the work, a comparison of various methods of changing the flow rate used in classic hydrostatic drive systems is planned. Currently, the focus is on comparing a classic hydrostatic system (Fig. 2), built of axial piston hydrostatic units, with a digital hydraulic system (Fig. 3) built of gear pumps with different flow rates, e.g., in a binary system $q1 = 3.1831\times10^{-7}m^3/rad$ ($2cm^3/rev$), $q2=6.3662\times10^{-7}m^3/rad$($4cm^3/rev$), $q3=1.2732\times10^{-6}m^3/rad$ ($8cm^3/rev$), $q4=2.5465\times10^{-6}m^3/rad$ ($16cm^3/rev$), with corresponding ON/OFF valves, which provides the ability to change the fluid flow rate in the system [10]. The concept of determining the control of the multi-source drive system after positive verification of the possibility of using a digital drive system instead of the classic one for both cases remains the same- the kinetostatic method [11]. There have been four major areas where developments have been made in digital hydraulic systems with respect to linear actuators:

- Parallel valves
- Single switch valve
- Multiple chamber cylinder
- Multiple pressure cylinders

Such valve configurations enable better energy efficiency as well as provide better precision control. Nevertheless, drawbacks such as high losses during switching and complexity of controls still exist in digital hydraulics systems. The use of model predictive control algorithm has further improved energy performance but poses extra computational burdens [12]. A further innovation in digital hydraulics is the design of multi-poppet valves that can accommodate large flows (of up to 100 l/min) while switching at speeds of 1 ms at 5 bar pressures. This valve is particularly suited for use in cases of high-speed switching where energy efficiency and reliability are paramount, and they do not experience leakage, thus ensuring energy efficiency up to 20 kW [13]. The implementation of fast switching valves and PWM technology in Digital Flow Control Units (DFCU) has helped increase its accuracy in hydraulic control systems [14]. The use of these two technologies enables more accurate control of low flows, which is required in cases where control of cylinders is needed. Research studies show that this integration leads to better velocity control, which can vary between 1 mm/s and 350 mm/s [15]. The use of hydraulic switching control has become one of the most sought-after options to replace traditional proportional and servo valves due to its benefits. These include lower expenses, increased reliability, and higher energy efficiency. Nonetheless, there are certain technical issues associated with this type of control that need to be addressed. These problems include the presence of hydraulic pulses and the design of switching valves, especially when dealing with high-flow applications. Nevertheless, hydraulic switching control will continue to attract more users in various fields, including metals and agriculture [16]. The Digital Hydraulic Pumping System, which utilizes the use of fixed displacement pumps with binary flow modes to provide 15 flow rates, has been experimented on. The system showed high degrees of repeatability, thus proving that the technology of digital hydraulics could make controlling flows very easy without requiring any intricate flow control, and offer a practical alternative for systems without complicated flow regulation [17].

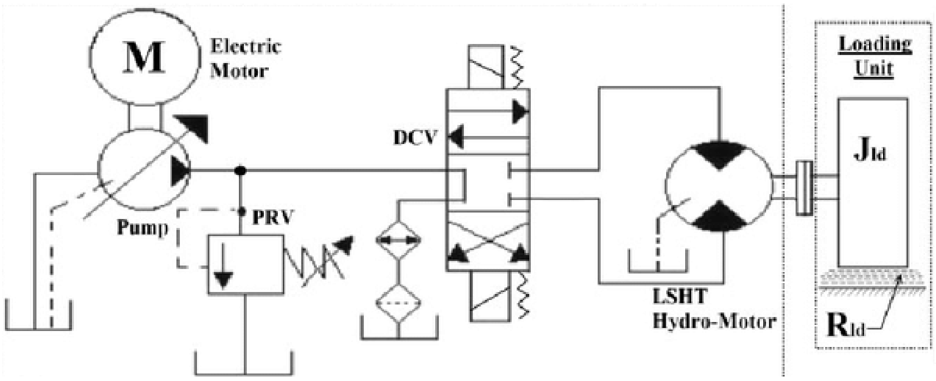

Figure 2. Schematic diagram of the classic hydrostatic drive system [10].

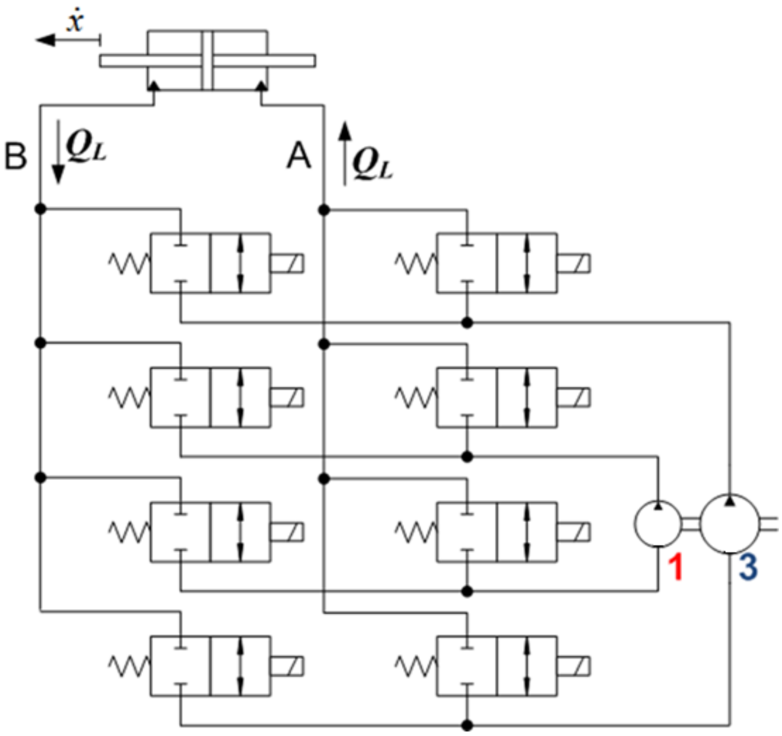

Figure 3. Schematic diagram of digital hydrostatic system (with one of possible set of valves) [10].

The concept of digital hydraulics has been known for many years, but only recently has it found practical application, for example, in the pulp and paper industry [18]. Thanks to the use of digital hydraulics, usually expensive multi-piston units or proportional valves can be replaced by inexpensive gear pumps along with appropriately connected, simple-to-build valves (two-way, two-position). Analyses of experimental studies conducted so far lower energy consumption compared to the throttle control technique as well as lower initial investment and spare parts costs.

Additionally, modern hydrostatic units, especially multi-piston ones despite their impressive parameters: efficiency, nominal working pressure, etc. are many times more expensive than solutions based on gear pumps. The price of the units is closely related to the consumption of resources (materials, energy, time) and technology [18]. The inability to use the latest high-efficiency units- e.g. from financial reasons- can lead to exclusion. Such a situation may affect countries that do not have sufficient financial capabilities as well as a suitably developed technological background. The use of the concept of digital hydrostatic systems can contribute to reducing such exclusion.

2.1 Outline of the Current State of Research

Digital Fluid Power (DFP), as understood in this dissertation, consists of replacing a pump with a variable flow rate (usually expensive and complex in construction, e.g., an axial piston pump) with a set of simple and inexpensive gear pumps mounted on a single shaft of the motor, which is the energy source, and/or using simple hydraulic valves (two-way, two-position) for flow rate control in the system, in place of, for example, a throttle valve. The other components of the hydraulic system remain unchanged.

According to Rudolf Scheidel: "Digital hydraulics is a new branch of fluid technology that offers great potential for innovative solutions. A successful application requires new components, a good understanding of the system and new control principles [19]. In McCloy's book "Control of fluid power Analysis and design," it has been described in detail in terms of its application in both hydraulic and pneumatic systems [20]. The concept of the doctoral dissertation is to investigate the possibility of using DFP in Multi-Source Hydrostatic Drive Systems, aiming to reduce energy consumption and maximize energy recovery in the recuperation process in hydrostatic systems.

2.2 PhD Thesis Hypothesis

"It is possible to replace the proportional technique in hydrostatic drive systems with "digital hydraulics", ensuring a similar output parameter (flow, torque, power) with reducing of the expenditure on the construction of a system by about 30%."

In this dissertation the proportional technique in hydrostatic drive systems is defined as follows: a control method based on the continuous modulation of fluid flow and pressure. It is typically realized through the use of variable-displacement pumps (e.g., axial piston pumps with a tilting swashplate) and/or continuous throttle control using proportional or servo valves, which adjust the flow cross-section smoothly in response to a continuous electrical input signal.

The term "digital hydraulics" means here: a branch of fluid power technology that replaces continuous regulation components with a set of simple components operating in discrete, binary states (on/off). In the context of this dissertation, it specifically refers to replacing a complex variable-displacement pump with a set of fixed-displacement gear pumps mounted on a single shaft, whose flow is controlled by switching simple two-way, two-position (on/off) directional valves, acting as a Digital Flow Control Unit (DFCU).

The efficiency η is calculated using following equation:

$$\eta = \frac{P_{out}}{P_{in}} \tag{1}$$

in which:
η – overall energy efficiency of the system [-],
P_{out} – useful output power (hydraulic power delivered to the load or mechanical power on the motor shaft) [W],
P_{in} – input power (mechanical power supplied to the pump shaft by the prime mover) [W].

Research Problems:

1. Will the replacement of a pump with a variable flow rate (e.g., a multi-piston axial pump with a tilting swashplate) and/or throttle control (e.g., realized by a proportional valve) with a system built according to the "digital hydraulics" concept in which a complicated and expensive pump is replaced by a set of simple and inexpensive gear pumps located on one shaft, and/or the proportional valve controlling the flow rate is replaced by simple to build and relatively inexpensive valves (two-stage, two-way) meet the requirements for power supply and control units used to build hydrostatic drive systems?
2. What will be the energy efficiency of the change described above?

3. Will the dynamic parameters e.g. acceleration, rising time, frequency responses of the hydraulic system subjected to such modifications meet the requirements assumed for the systems?
4. What kinds of savings will result from such a modified system?
5. How will the replacement of a typical hydraulic system with a system built according to the "digital hydraulics" concept affect the areas of efficiency, reliability, safety, and ecology (carbon footprint, emission of harmful substances, e.g., in the case of using an internal combustion engine: carbon dioxide, nitrogen oxides, solid particles)?

The reliability will be understood as the system's ability to maintain its basic functionality even in the event of a partial component failure (fault tolerance/redundancy), which in the digital system is achieved by using multiple parallel gear pumps so that the failure of one only limits the maximum capacity without stopping the entire system. Safety will be understood as the ability of the system to maintain pressures within safe limits (using relief valves) and its structural resilience to the occurrence of dynamic shock loads and high-frequency torque pulsations identified during transient operational phases.

2.3 Contribution of the Expected Results to the Scientific Discipline.

After investigating the above-described concept of replacing a classic hydraulic system with a system built according to the "digital hydraulics" concept, a method of conversion (in a form of algorithm) will be developed. This method will facilitate the potential transformation of the classic system with a digital one. By means of this method, it will be possible to replace an expensive and complicated supply system e.g., one utilizing a multi-piston axial hydrostatic pump with the ability to change the flow rate and/or control realized by means of a throttling technique with a set of gear pumps (simple and inexpensive) and a control system built using a set of simple and reliable valves (two-way, two-position) with an appropriately selected, simple controller.

The benefits of the conducted research and analyses will be:

- The use of less complex, and therefore more reliable and resistant to external and internal factors, components (e.g., sensitivity to contamination or liquid parameters - viscosity, temperature, etc.).
- The possibility of reducing the costs of building the system and its maintenance.

- Improvement of ecological parameters (e.g., reduction of energy consumption as well as carbon footprint, etc.).
- Reducing the possibility of exclusion for financial reasons and/or a suitably developed technological background.

2.4 Planned Research Methods

The first phase will involve simulation studies using appropriate software, such as MATLAB/Simulink. After defining the physical model, a mathematical model will be developed. Based on this, simulation models of both the "classic" system and the one built according to the "digital hydraulics" concept will be constructed. After verifying the simulation results with experimental ones, the models of both simulation systems will be compared with each other in terms of their dynamic and ecological parameters. This comparison will provide an answer to the question of whether it is possible to replace the classic hydrostatic drive system with its digital equivalent. On this basis, an answer will also be provided as to whether it is possible to effective use it in hydrostatic drives (including multisources one).

The second phase of the doctoral dissertation will involve issues related to the construction of an appropriate research stand and the implementation of properly planned experimental research. The results obtained from this research will be used to verify the results obtained during the simulation studies.

The third phase will consist of the possible correction and parameterization of the simulation models.

2.5 Research Significance

Digital hydraulics can be an interesting alternative to classic drive systems due to the many challenges facing the Fluid Power industry today. Hydrostatic drive systems especially those with throttle control are characterized by relatively low efficiency (0.4 to a maximum of 0.8) [11], [21]. As a rule, these losses are generated by the system when it is not performing operational tasks. In systems with throttle control, the pressure in the system during idle operation (without performing useful work) is usually at the level of the relief valve opening pressure (nominal pressure). This means that the entire generated flow rate flows directly to the tank through the relief valve without performing any useful work. In this way, all the energy supplied to the system is converted into heat. Control in digital hydraulics systems should be classified as a type of volumetric regulation. In this way, the efficiency of energy consumption increases. This is achieved by appropriately managing the supply of flow rate to the hydraulic system. This is possible thanks to appropriate sequences of switching valves on and off for the respective pumps. Pumps whose flow rates are not needed to carry out a given cycle generate a flow rate, but by opening the appropriate valve, direct flow from the pump to the tank is enabled (without flowing through the relief valve). Therefore, the only load on such a pump is the resistance resulting from the flow of fluid through the hydraulic installation to the tank. Research results prove that the analysed concept of digital hydrostatic systems reduces energy consumption by up to 40% in specific applications compared to its classic counterparts. This constitutes an interesting solution for companies striving to limit their negative impact on the environment [22], [23], [24].

Digital hydraulic elements come in the form of modules that engineers can combine to create unique systems tailored to specific application conditions. These systems adapt well to various industries, including automotive and renewable energy, thanks to their customizable components. The importance of this research is growing as companies rapidly adopt Industry 4.0 technology, which uses intelligent automation and data exchange systems [25], [26]. Digital hydraulic technology fits current market trends and enables the creation of advanced power system enhancements that are both advanced and energy-efficient, while also meeting the conditions contained in the currently implemented concept of sustainable development [4], [6], [7] (Fig. 4).

Digital hydraulic technology continues to evolve, with several emerging trends shaping its development. Nowadays it is recognizable four areas:

1. Integration with Artificial Intelligence.
   Using AI technology developers are creating algorithms to control of servo drives, anticipate component breakdowns together with dynamic optimization of operational controls to boost system performance.
2. Sustainable Fluid Development.
   The rise of environmentally friendly hydraulic fluids which break down naturally appears in modern industry leading to minimal damage to the environment during hydraulic operations.
3. Additive Manufacturing in Hydraulic Components.
   Through 3D printing operations manufacturers can produce customized hydraulic components featuring complex structures that boost system performance while requiring reduced economic inputs.

4. Hybrid Hydraulic Systems.

Companies are developing hybrid systems which integrate digital and conventional hydraulic technology to achieve peak performance and cut operational costs.

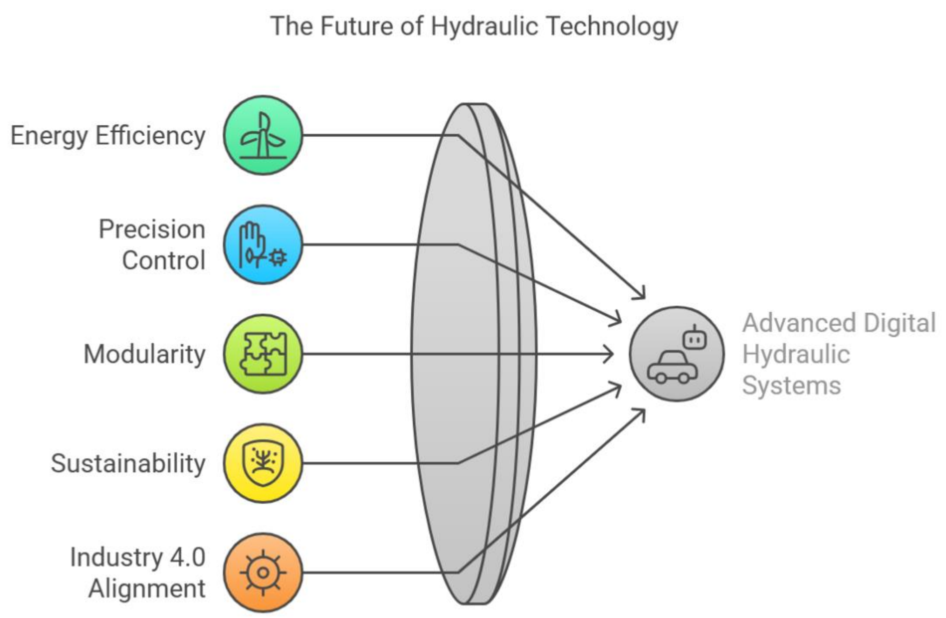

Figure 4. Future of hydraulic technology.

3 Components of Digital Hydraulic Technology

Digital Fluid Power (DFP) is an interesting alternative in the field of fluid power control. Unlike classic systems, which are based on the continuous modulation of flow and pressure using, for example, proportional or servo valves, digital hydraulics uses discrete control based on binary on/off states (ON/OFF). The main idea is to replace single, complex components with smoothly varying characteristics with many simpler elements whose combined operation allows for obtaining the desired, regulated output signal (flow rate Q). This concept is analogous to the operation of digital-to-analog converters (DACs) in electronics, where a high-resolution signal is built from the sum of many simple, weighted binary signals [27].

The implementation of the *DFP* concept in practice involves replacing the key components of a classic hydrostatic transmission with their digital counterparts. The heart of the digital system is the replacement of a single, expensive, and complexly built variable displacement pump (e.g., an axial piston pump) with a set of several simpler and cheaper fixed displacement pumps (e.g., gear pumps). These pumps are usually mounted on a single, common shaft, driven by one motor, which ensures they have the same rotational speed. To achieve a wide range and high control resolution, the displacements of individual pumps are often chosen in a weighted manner, most commonly binary (e.g., 1:2:4:8) or ternary (e.g., 1, 3, 9, 27). The control of the flow rate in the system is not carried out by, for example, throttle valves, which operate on the principle of throttling the flow. Instead, each of the fixed displacement pumps is connected to an individual, fast-switching on/off valve (most often 2/2) [28],[29],[30],[31]. These valves, controlled by digital signals from a central unit (e.g., a *PLC*), only decide whether the stream from a given pump is directed to the working circuit or pressure-free to the tank. The regulation of the entire unit's output is based on the principle of summation. The total flow rate (Q) at the outlet of the pumping unit is the arithmetic sum of the flow rates from those pumps whose control valves are currently in the "*ON*" state (open to the system). By activating the appropriate combinations of valves, the controller can in a discrete (stepped) manner create a resultant stream of the desired value. For a system with four pumps with binary weights, it is possible to obtain $15\ (2^4-1)$ different, non-zero flow levels. Such a "stepped" flow profile approximates the smooth characteristic generated by a classic system. Key advantages and challenges of technology are:

- Energy Efficiency: By eliminating throttling control, the digital system eliminates the main source of energy loss in classic systems. The pumps either operate at their optimal efficiency point, pumping liquid into the system, or they operate without load, and their flow is freely returned to the tank. This leads to a significant reduction in energy consumption, up to 40% compared to systems with throttling regulations.

- Reliability and Costs: The use of standard, mass-produced gear pumps and simple ON/OFF valves, which are much more resistant to contamination than precision proportional valves, leads to a reduction in investment costs (CAPEX) and potentially higher reliability and lower service costs (OPEX). The modular design also provides a degree of fault tolerance and relatively low costs for eventual repairs.

- Dynamic Characteristic: The main engineering challenge and compromise for potentially higher efficiency is a different dynamic characteristic. The discrete, stepped nature of the control inherently generates phenomena in the system such as pressure and torque pulsations and, as shown by experimental studies, shock load spikes at the moments of switching [32],[33],[34],[35],[36] Managing this dynamic to ensure operational stability, low noise levels, and the fatigue life of components is a key aspect of designing digital systems.

3.1 Hydraulic Pump.

The hydraulic pump is the primary energy source in a hydraulic system, responsible for converting mechanical energy into hydraulic energy. Pumps draw fluid from the reservoir and deliver it into the hydraulic circuit, supplying power to different system components.

Hydraulic pumps are classified into two main categories: fixed displacement pumps and variable displacement pumps. Fixed displacement pumps provide a constant flow rate, making them suitable for systems requiring continuous and predictable power output. Common types include gear pumps, vane pumps, and piston pumps, each varying in efficiency, pressure handling, and noise levels. In contrast, variable displacement pumps adjust the flow rate based on system demand, offering greater flexibility and energy efficiency by reducing unnecessary fluid circulation. These pumps are widely used in high-precision applications, such as mobile hydraulic equipment and energy-efficient industrial systems.

The performance of a hydraulic pump is influenced by factors such as fluid viscosity, pump speed, pressure levels, and system load conditions. A well-designed pump ensures efficient energy transfer while minimizing heat generation, fluid cavitation, and mechanical wear.

3.2 Hydraulic Actuators

Actuators are the output elements of a hydraulic system, responsible for converting hydraulic energy back into mechanical motion. These devices generate force and movement, enabling machinery to perform essential tasks such as lifting, pressing, rotating, or pushing loads. There are two primary types of hydraulic actuators: hydraulic cylinders and hydraulic motors. Hydraulic cylinders produce linear motion, utilizing a piston and rod mechanism to extend and retract under fluid pressure. They are commonly found in applications such as hydraulic presses, lifting equipment, and industrial machinery. The force generated by a hydraulic cylinder depends on the fluid pressure and the piston's surface area, with higher pressure producing greater output force.

Hydraulic motors, in contrast, generate rotational motion and function similarly to electric motors, but use pressurized fluid instead of electricity. These motors are widely used in applications requiring continuous or high-torque rotation, such as conveyor systems, winches, and hydraulic drive mechanisms. There are various types of hydraulic motors, including gear, vane, and piston motors, each designed for specific performance requirements in terms of speed, torque, and efficiency. The efficiency of hydraulic actuators is influenced by internal leakage, friction between the seal and the cylinder, and other factors. Proper sealing, lubrication, and load balancing are crucial for ensuring optimal performance and extending the lifespan of actuators.

3.3 Control Valves

Control valves play a critical role in hydraulic systems, regulating fluid flow, controlling pressure, and directing hydraulic power to actuators. These valves ensure that the right amount of fluid is delivered at the proper pressure and in the correct direction, enabling precise system operation.

There are three main types of hydraulic control valves: directional control valves, pressure control valves, and flow control valves. Directional control valves determine the path of the hydraulic fluid, controlling whether actuators move forward, backward, or remain in a neutral position. This group includes spools, poppet, and rotary valves, each suited for different system configurations. Pressure control valves maintain system stability by ensuring that the fluid pressure remains within safe, optimal values. They include relief (overflow) valves, which prevent excessive pressure build-up, and reducing valves, which regulate pressure in specific sections of the system to avoid overloads. Flow control valves regulate the speed of actuators by modulating the volume of fluid entering or exiting a cylinder or motor. Throttle, needle, and orifice valves are commonly used to achieve smooth and controlled motion. In advanced hydraulic systems, servo-valves and proportional valves provide control based on electronic feedback, enabling very precise adjustments also used in automation and robotics.

Proper maintenance, such as filtering the hydraulic oil to prevent contamination, is essential to ensure the smooth operation and reliability of the valves.

3.4 Reservoir

The hydraulic reservoir serves as a storage unit for hydraulic fluid, ensuring a continuous supply to the system, while also playing a crucial role in maintaining fluid parameters and, consequently, system stability. A well-designed reservoir ensures that the hydraulic fluid remains at an optimal temperature and cleanliness level. It allows for the separation of air bubbles and solid particles from the fluid, thus preventing the phenomenon of cavitation. The size and design of the reservoir depend on the system's operational capacity, with larger reservoirs being used in heavy-duty industrial and mobile applications. Efficient filtration and cooling mechanisms are often integrated into hydraulic reservoirs to prevent oil degradation and overheating, ensuring consistent system performance under varying load conditions.

3.5 Hoses, Pipes, and Fittings

Hydraulic hoses, pipes, and fittings form the fluid transmission network within a hydraulic system, allowing fluid to move between components. These elements must be resistant to high pressure, ensuring leak-free and efficient energy transfer.

Hydraulic lines can be rigid or flexible, depending on the application's requirements. Steel and copper pipes are commonly used in high-pressure, stationary hydraulic systems, while flexible hoses are used in mobile applications. The selection of hydraulic lines and fittings depends on factors such as operating pressure, fluid type, temperature, and environmental conditions. Proper routing of lines and periodic maintenance are essential to prevent leaks, pressure drops, and premature wear, which can affect the overall efficiency of the system (Fig. 5).

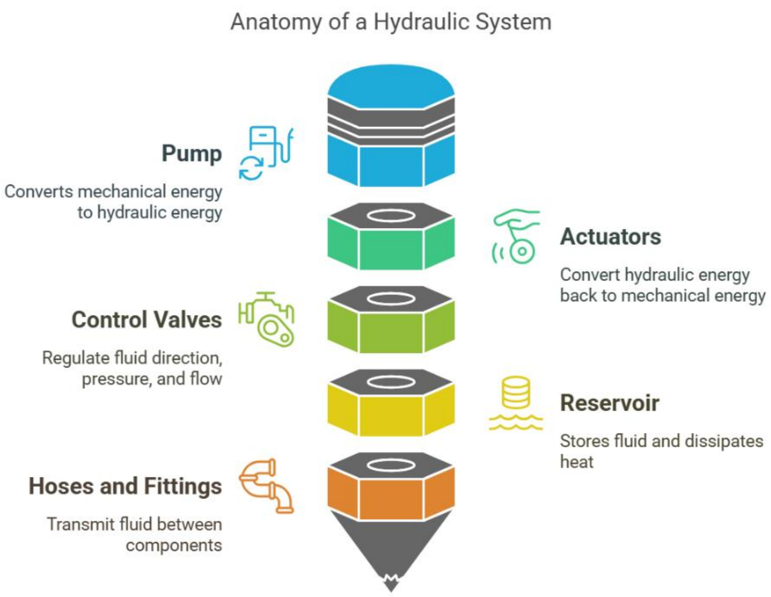

Figure 5. Components of traditional hydraulic systems.

3.6 Hydrostatic Transmission

The Figure 6 illustrates an example of an open loop hydrostatic transmission. It is composed of variable capacity/absorption units, which are controlled by electrohydraulic amplifiers. The power source is usually a combustion in movable machines and vehicles or electric motor in industrial application. Such a system can be also regarded as rotary drive, with volume control.

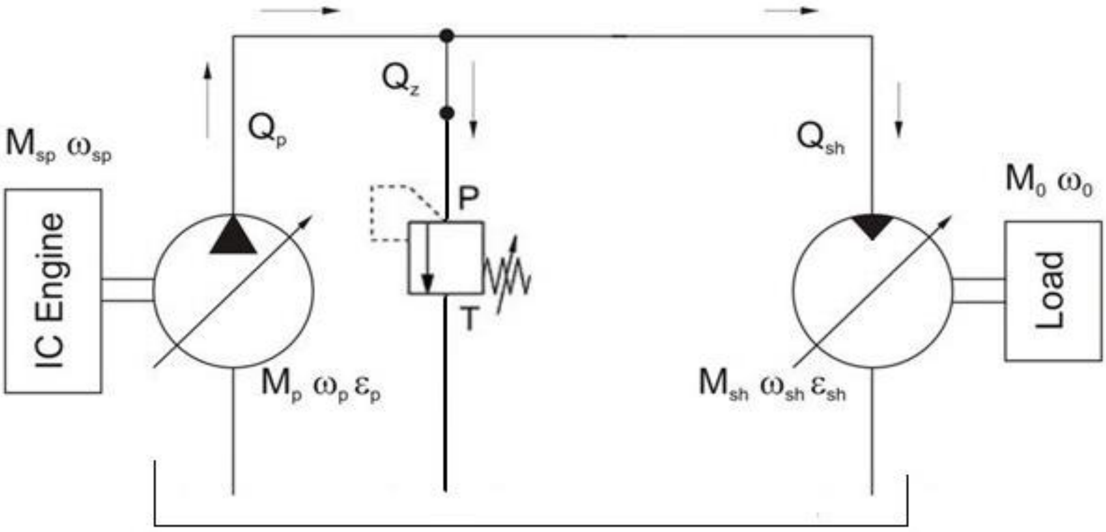

Figure 6. Basic scheme of hydrostatic drive system [42].

In [43], [44] the mathematical models of the hydrostatic pump and motor can generally be represented in the form of equations (2-5):

Hydrostatic pump delivery:

$$Q_p = q_{pmax}\varepsilon_p\omega_p - \Delta Q_p(\varepsilon_p, p_p, \omega_p) \tag{2}$$

Torque on the hydrostatic pump shaft:

$$M_p = q_{pmax}\varepsilon_p p_p + \Delta M_p(\varepsilon_p, p_p, \omega_p) \tag{3}$$

Hydrostatic motor absorption capacity:

$$Q_{sh} = q_{shmax}\varepsilon_{sh}\omega_{sh} + \Delta Q_{sh}(\varepsilon_{sh}, p_{sh}, \omega_{sh}) \tag{4}$$

Hydrostatic motor torque:

$$M_{sh} = q_{shmax}\varepsilon_{sh}p_{sh} - \Delta M_{sh}(\varepsilon_{sh}, p_{sh}, \omega_{sh}) \tag{5}$$

in which:

q_{pmax} – maximum unit capacity of the hydrostatic pump – a design parameter defining the volume of the working chambers [m^3/rad],

$q_{sh\ max}$ – maximum unit absorption of the hydrostatic motor [m^3/rad],

ε_p– axial pump capacity control parameter, dimensionless quantity for pumps operating in an open system 0<, ε_p <1, relationship between the parameter ε_p and the angle of inclination of the retaining disc

$$\varepsilon_p = \frac{tg\alpha_p}{tg\alpha_{pmax}}, \text{usually } \alpha_{pmax} = 18°, \tag{6}$$

ε_{sh} – the axial motor absorption control parameter, a dimensionless quantity in the range of $\varepsilon_{shmin}<\varepsilon_{sh}<1$, the relationship between the hydrostatic motor control parameter and the thrust plate inclination:

$$\varepsilon_{sh} = \frac{tg\alpha_{sh}}{tg\alpha_{shmax}}, \text{"usually" } \alpha_{shmax} = 18°, \tag{7}$$

hydrostatic engine, different values are applied; the following values were used in the work

$$\alpha_{shmin} \approx 5°, \text{"That is" } \varepsilon_{\mathrm{sh}\ min} \approx 0{,}3 \tag{8}$$

p_p – pump load pressure [Pa],

p_{sh} – pressure drop in hydrostatic motor [Pa],

ΔM_p, ΔM_{sh} pump and hydrostatic motor torque losses reduced to the shaft [N m],

ΔQ_p, ΔQ_{sh} – pump and motor volumetric losses (functions of operating parameters) [m^3/s],

ω_p, ω_{sh} – pump and motor angular velocity [rad/s],

Generally, engine volumetric and hydraulic-mechanical losses are represented by the same or similar dependencies as pump losses [45], [46], [47], [48], [49], [50], [51], [52], [53], [54]. Practice demonstrates that engine volumetric losses are lower than pump losses because of the higher filling of the engine working chambers.

Hydrostatic drive systems, depending on the configuration of the hydraulic circuit, are classified into two basic types: open-loop systems and closed-loop systems. The choice between them depends on the application's requirements, such as the nature of the load, the required precision, operating conditions, and costs.

3.7 Open Loop Hydrostatic Drive System

Depending on the hydraulic circuit, construction equipment's hydraulic transmission system can be classified as either an open system or a closed system [55]. When the hydraulic pump is operating in an open circuit, the oil is drawn from the tank, driven by the actuator (such as a hydraulic motor and cylinder) via the hydraulic valve, and then returned to the tank. An air filter that equalizes the fluid's volume change in the pipe network and the actuator connects the tank to the atmosphere. In general, the system is open and connected to the atmosphere. Because the system's oil is recycled back into the oil tank, it has the ability to release heat and precipitate contaminants. In a drive shown in Figure 7, backpressure valve must be installed on the road itself, which will result in further energy loss and raise the oil's temperature because the air can readily enter the system due to the oil's frequent contact with it [56], [57].

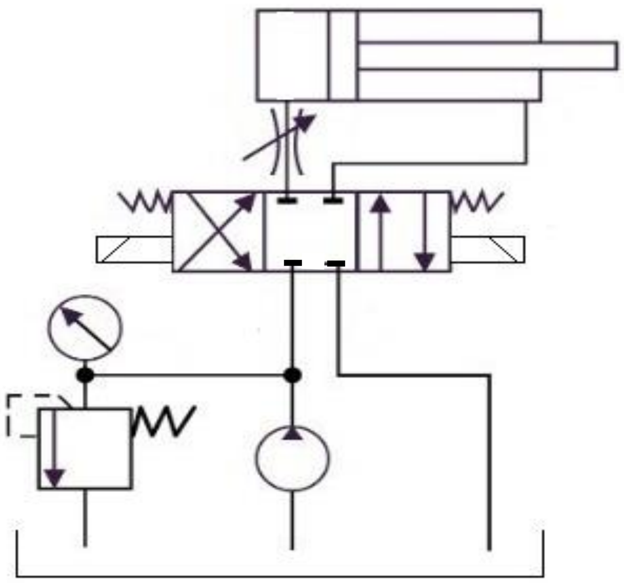

Figure 7. Open loop hydrostatic drive system with throttle control.

There only two advantages of an open loop circuit:

- Less expensive to set up and create.
- Simpler to keep up.

Disadvantages of an open loop circuit are:

- The disturbances are not corrected.
- The accuracy of velocity and positioning is very low.
- The size of the fluid reservoir needs to be sufficient to provide adequate fluid cooling.
- A hydraulic system with an inadequate reservoir may produce excessive heat.
- Troubleshooting issues with complicated open loop systems might be more difficult.

3.8 Closed Loop Hydrostatic Drive System

Because of their capacity to function in four quadrants, based on wheel torque and vehicle velocity, and the less strict requirements for oil reservoir size, hydrostatic transmission's (HT) are more frequently used in heavy-duty applications [58]. Figure 8 displays a closed-circuit HT's fundamental schematic. The prime mover, which is the combustion engine, is usually mechanically coupled to a single variable displacement hydraulic unit (pump), which transfers hydraulic energy through one or more hydraulic units (motor) attached to the wheel axle(s). There are two types of secondary units: variable displacement and fixed displacement. The HT typically has a charge circuit (PC, CV1, CV2, PRC) for oil replenishment, a cross port pressure relief valve (PR1&2) for protection against pressure overload. When it comes to the charging circuit, connecting several motors in series or parallel, and the flushing circuit, there are various variations of the fundamental architecture shown in Figure 8. You can find examples in [58], [59], [60].

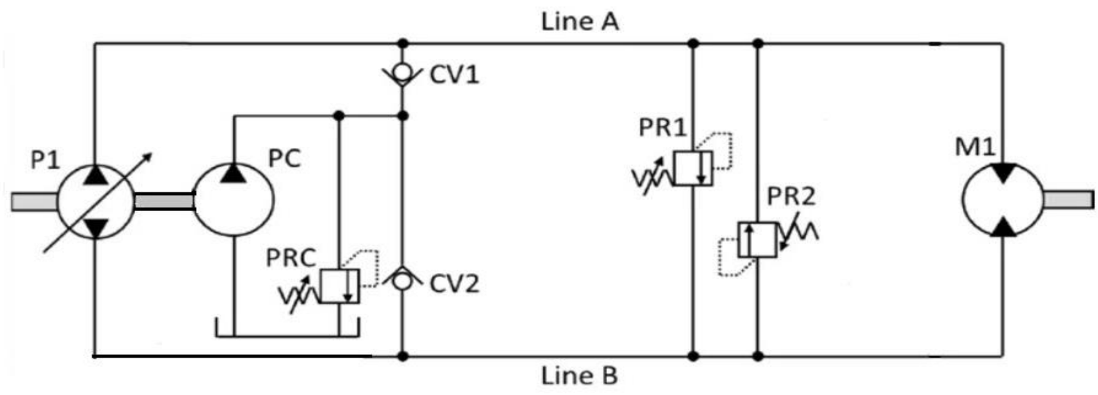

Figure 8. A typical hydrostatic transmission circuit with oil closed loop circuit.

Advantages of a closed loop oil circuit [59]:

- Adapted for hydrostatic transmissions and drives.
- Functions effectively with greater pumps and pressures.
- Systems operate at pressures significantly higher than most.
- Most of the fluid is held inside, so less is needed.
- It has the ability to reverse direction.
- The charge pump replaces lost fluid by supplying fluid to the main pump.
- Increases the versatility with which system designers can create system controls
- Precisely controls a motor in a small, lightweight design.

Disadvantages of a closed loop circuit:

- Increased operational temperature during operation.
- Elevated danger of fluid contamination.
- More expensive to set up and create.
- The need for high-pressure zones hydraulic fluid filtration.

The closed loop control systems linear and rotary is shown in Figure 9. The closed loop consists of: regulator, valve, cylinder, measuring element and a summing node.

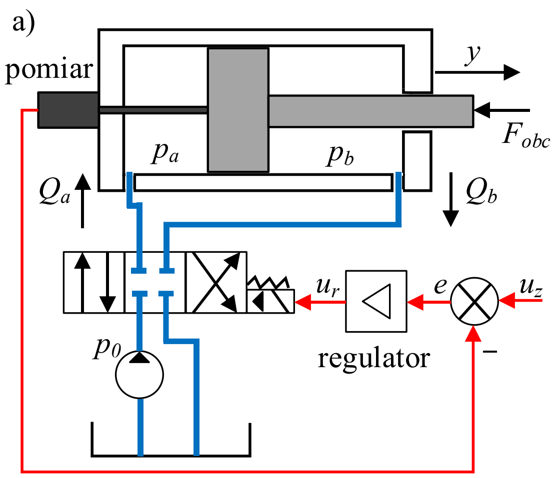

Figure 9. Closed loop control systems [72].

3.9 Limitations of Traditional Hydraulic Systems

Although hydrostatic drive systems have a multitude of positive features and are widely used, several negative features can be mentioned [37], [38] , [39], [40], [41].

- Energy Losses: particularly visible in the case of throttle control, as well as internal leakages, and losses related to flow, fluid viscosity, etc.
- Operational Precision: Mechanical tolerances and excessively slow response times limit the precision of control, especially in high-speed or dynamic applications.
- Maintenance Requirements: It requires much more frequent maintenance than other types of drives (e.g., electric drive).

The demand for systems that can eliminate the above features was the reason for the evolution of hydrostatic systems, introducing advanced control methods with similar efficiency, as well as lower construction costs for hydraulic systems such as digital hydraulics.

4 Fundamental Concepts of Digital Hydraulics

Digital hydraulics is a modern approach to fluid power control that utilizes binary actuation (on/off states) rather than traditional proportional or servo-controlled systems. The core idea is to replace continuously variable hydraulic components with discrete, digital components, leading to improved efficiency, robustness, and energy savings.

A binary control system operates using digital signals (0 and 1) to regulate hydraulic flow. This ensures that the system either fully opens or closes a valve, providing distinct control states rather than gradual changes (Fig. 10).

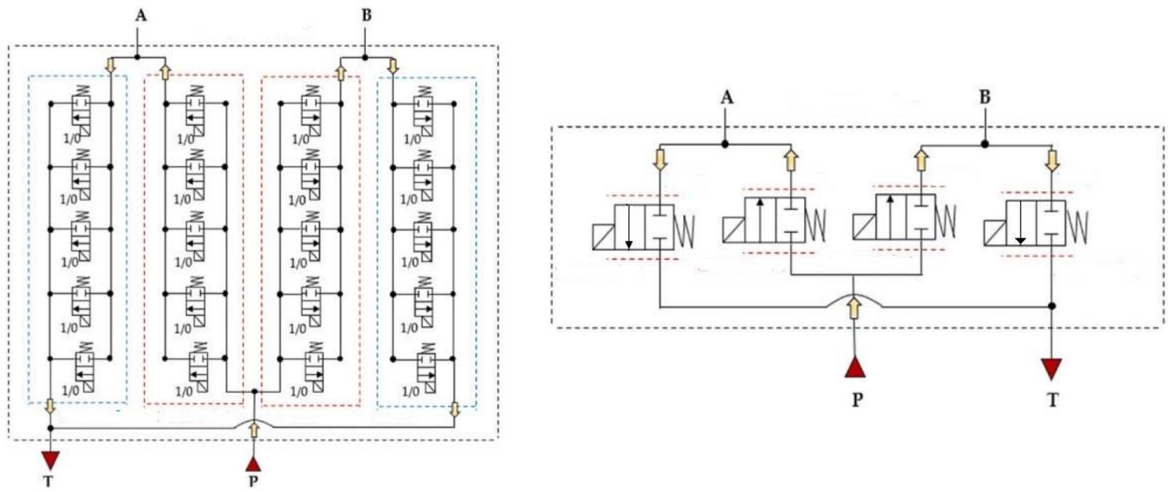

Figure 10. Two schemes of digital hydraulics in binary [61].

Digital hydraulic systems offer several significant advantages over traditional hydraulic systems, making them more efficient, reliable, and adaptable to modern industrial applications. One of the primary benefits is higher energy efficiency, as digital hydraulic systems eliminate throttling losses commonly found in proportional and servo-controlled valves. Traditional hydraulic systems often waste energy due to continuous fluid flow regulation, whereas digital hydraulics use on/off control mechanisms that ensure power is used only when needed, reducing energy consumption and heat generation [62], [63], [64], [65].

Another key advantage is fault tolerance, as digital hydraulic systems are designed with multiple parallel valves. Unlike conventional systems, where the failure of a single valve can compromise performance, digital hydraulic systems can continue to function even if some valves fail by redistributing flow through alternative pathways. This redundancy enhances the overall reliability and durability of the system, making it well-suited for critical applications such as aerospace, heavy machinery, and automated industrial systems.

Digital hydraulic systems also feature simplified control logic, as they do not require complex feedback loops or continuous adjustment mechanisms like servo-controlled systems. Instead, they operate using binary switching, which simplifies system design and reduces the need for advanced electronic controllers. This makes digital hydraulics more cost-effective and easier to integrate into existing industrial infrastructure.

Another significant advantage is improved contamination resistance. Traditional servo and proportional valves rely on precise hydraulic distributor slide positioning, making them highly sensitive to oil contamination and particle accumulation. Digital on/off valves, in contrast, are less prone to clogging and wear since they function in only two states - fully open or fully closed. This increases system longevity and reduces maintenance requirements, making digital hydraulic systems ideal for harsh environments such as construction sites, mining operations, and offshore drilling platforms.

In hydraulics is used two primary types of signals [66], [45].

- Continuous Signals – Traditional hydraulic systems use continuously varying signals, leading to high precision but also increased energy losses (Fig. 11).
- Discrete Signals – Digital hydraulics relies on on/off switching, resulting in energy-efficient and fault-tolerant systems.

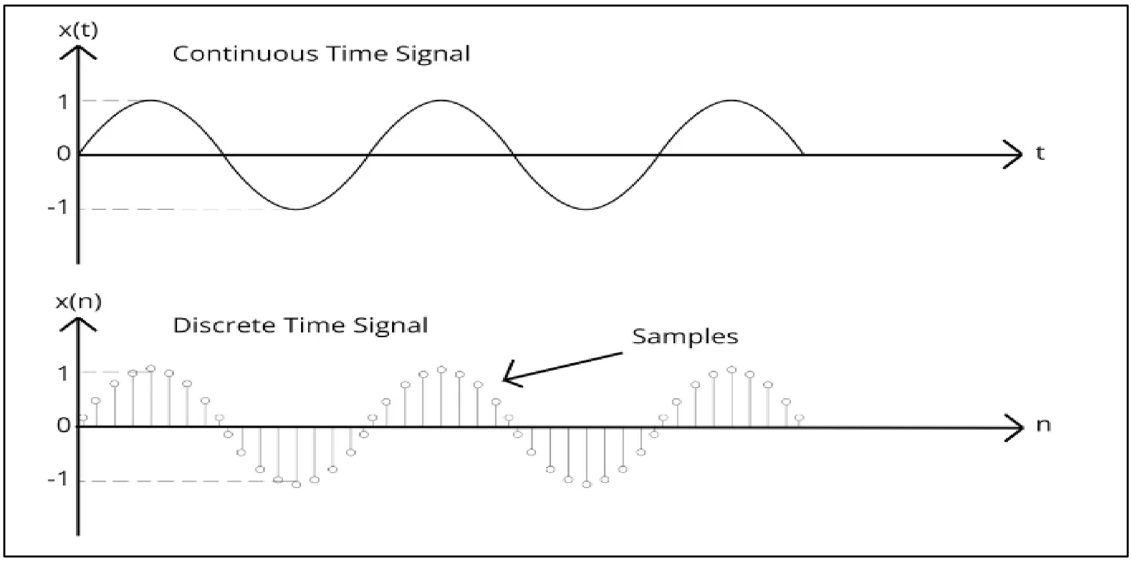

Figure 11. Continuous and discrete signals [67].

Table 1. Comparison: Digital vs. Analog Hydraulics.

Feature	Classic Hydraulics (with proportional valves)	Digital Hydraulics
Signal Type	Continuous (Proportional)	Discrete (On/Off)
Energy Losses	High due to throttling	Minimal
Fault Tolerance	Low – susceptible to minor failures	High – redundant components
Precision	Very High	Depends on valve resolution
Contamination Sensitivity	High	Low

In summary, analog hydraulic systems operate using continuous signals, allowing for high precision and smooth control of hydraulic actuators. However, they suffer from significant energy losses due to fluid throttling and require complex control mechanisms that increase maintenance costs. Additionally, contamination sensitivity is high, as precise valve movements can be easily disrupted by fluid impurities.

In contrast, digital hydraulic systems utilize discrete signals, where components function in a binary (on/off) manner. This approach eliminates unnecessary energy consumption, making these systems more efficient and reliable. While digital hydraulics may not achieve the same level of precision as analog hydraulics, advances in multi-valve configurations and high-speed switching have significantly improved their accuracy and adaptability. Moreover, fault tolerance is higher, as redundant components allow digital hydraulic systems to continue operating even if individual valves fail.

This comparison highlights the superiority of digital hydraulics in terms of efficiency, fault tolerance, and reliability, making it an interesting choice for modern industrial applications that prioritize energy conservation, automation, and system longevity.

4.1 Digital Hydraulic Valves

Digital hydraulic valves are essential components that facilitate fluid control within a hydraulic system through discrete on/off switching. Unlike traditional throttle or servo valves, which regulate flow continuously, digital valves operate in a binary fashion, meaning they are either fully open or fully closed.

Based on their working principles, digital hydraulic valves can be classified into three main types:

- Parallel Digital Hydraulic Valves,

- High-Speed Switching Digital Hydraulic Valves,
- Stepping Digital Hydraulic Valves.

Each of these valve types provides unique advantages, catering to different operational requirements in digital hydraulic systems.

Parallel digital hydraulic valves, also referred to as Digital Flow Control Units (DFCU, function by controlling multiple on/off switching valves arranged in parallel (Fig. 12). The purpose of this configuration is to achieve precise flow regulation by selectively activating specific combinations of valves [68].

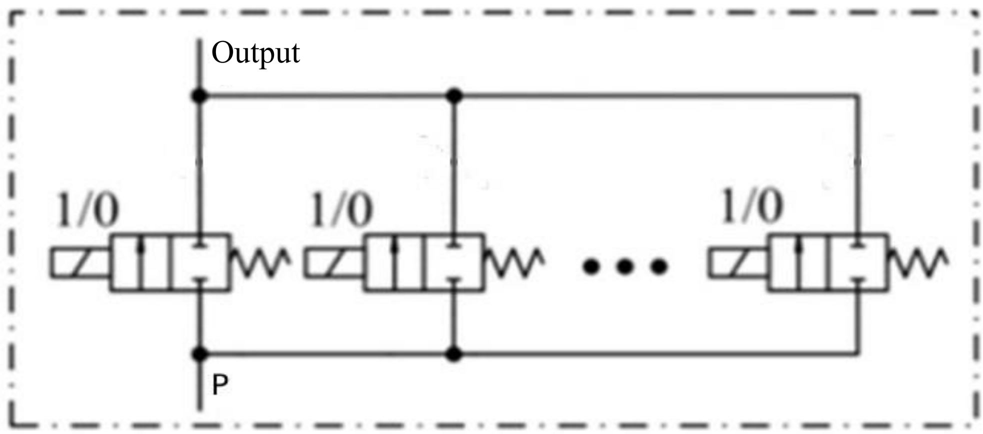

Figure 12. Schema of parallel digital two-way valve [28].

A parallel digital hydraulic valve system consists of multiple independently controlled switching valves. The total flow output is determined by the sum of the flow rates of all valves that are in the "on" state.

The characteristics of a DFCU are influenced by two primary factors:

- The Number of Switching Valves (N): The more valves incorporated in the system, the greater the control resolution.
- The Encoding Method: Various encoding techniques, such as binary encoding, Fibonacci encoding, and Pulse Number Modulation (PNM) encoding, are employed to determine the optimal combination of valve states for a given flow rate.

A parallel digital hydraulic valve system provides 2^N discrete flow output levels, where N is the number of switching valves. This enables highly efficient and precise flow control, eliminating the need for traditional proportional valves.

The key advantage of parallel digital hydraulic valves is their ability to eliminate throttling losses, thereby improving energy efficiency. Unlike proportional valves, which waste energy by continuously regulating flow through partial openings, digital flow control units operate with discrete states, minimizing unnecessary energy dissipation.

Parallel digital valves are commonly used in mobile hydraulics, industrial automation, and high-efficiency fluid power systems, where precise flow control is required with minimal energy loss.

High-speed switching digital hydraulic valves, also known as Pulse Modulation Switching Digital Valves, utilize high frequency switching techniques to regulate flow dynamically (Fig. 13). These valves do not require multiple parallel connections like DFCU's [69]; instead, they achieve flow control by rapidly alternating between "on" and "off" states (Fig. 14).

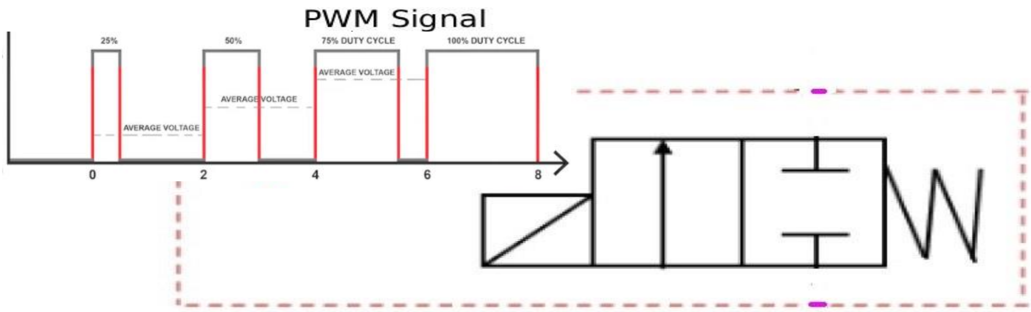

Figure 13. High-speed switching two-way valve controlled by pulse width modulation (PWM) [28].

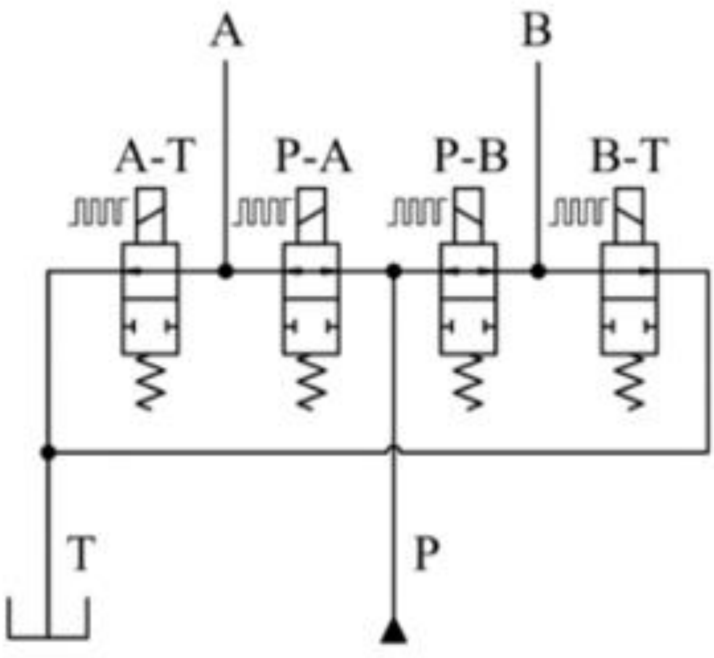

Figure 14. High-speed switching four-way valve [28].

The core mechanism of high-speed switching digital valves relies on pulse width modulation (PWM) (Fig. 15). In this method, the duty cycle of an electrical pulse signal determines the proportion of time the valve remains open within each cycle. By modulating the frequency and duration of these pulses, the system effectively controls the average flow rate.

While theoretically, the flow rate of a high-speed switching valve can be adjusted to any value, in practice, the ratio of maximum to minimum flow rate is constrained by the valve's dynamic characteristics. A lower switching frequency results in better control performance but introduces pressure pulsations, whereas a higher frequency smoothens the flow output but may be limited by the valve's response time.

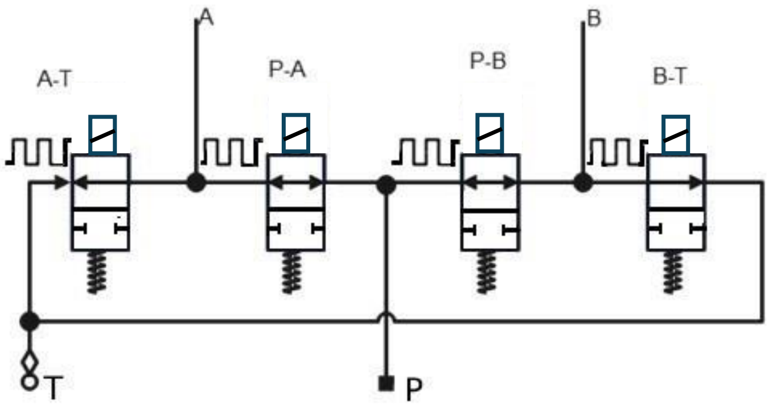

Figure 15. Idea of new high-speed switching valve [70].

High-speed switching digital valves offer several benefits:

- Proportional-Like Control: By leveraging PWM, these valves can effectively simulate continuous variable flow, despite operating in a binary manner.
- Energy Efficiency: The elimination of throttling losses enhances overall energy savings.
- Fast Response Time: The ability to switch states within milliseconds enables rapid adjustments in flow and pressure.

One of the primary applications of high-speed switching digital hydraulic valves is in digital displacement pumps (DDP), where high-speed solenoid valves control individual pumping chambers. This method significantly reduces fuel consumption in mobile hydraulic applications while enhancing overall system efficiency. Additionally, these valves are commonly integrated into high-performance hydraulic actuators, where fast response times are critical. They are particularly valuable in automotive hybrid systems, industrial automation, and high-speed fluid power applications. Stepping digital hydraulic valves utilize a stepper motor to precisely control the movement of a hydraulic valve spool. Unlike parallel and high-speed switching valves, which rely on binary on/off states, stepping valves operate through incremental position adjustments (Fig. 16) [71], [72].

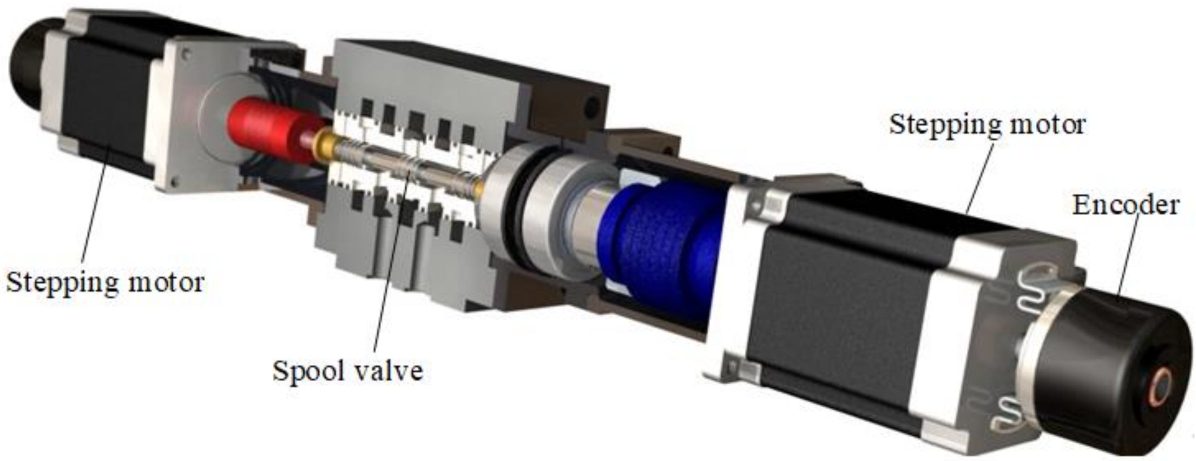

Figure 16. Electrohydraulic linear actuator with two stepping motors controlled by overshoot-free algorithm [72].

The proportional valve with two stepping motor is presented in Figure 17.

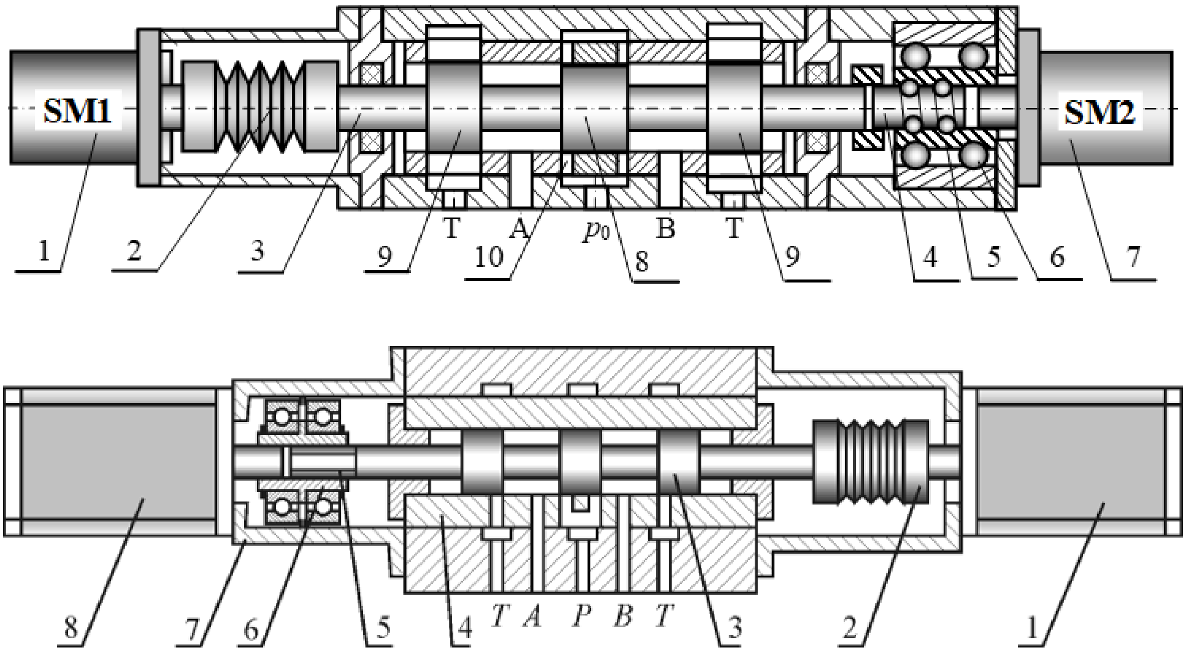

Figure 17. Drawing of the proportional valve with two stepping motors [72.]

4.2 Parallel Connection in Digital Hydraulics

Digital hydraulic technology introduces various control methods that enhance efficiency, precision, and energy savings compared to traditional hydraulic systems. One of the most widely used methods in digital hydraulic control is the parallel connection of hydraulic components, which plays a critical role in improving flow regulation and system response.

Parallel connection technology primarily consists of Digital Flow Control Units (DFCU), which enable precise flow control through binary and pulse-based modulation methods. This section explores the characteristics, working principles, and various modulation techniques employed in parallel digital hydraulics, such as Pulse Number Modulation (PNM), Pulse-Width Modulation (PWM), Pulse-Width-Pulse-Frequency Modulation (PWPFM), and Pulse Frequency Modulation (PFM).

4.3 Digital Flow Control Unit (DFCU)

A Digital Flow Control Unit (QA) consists of multiple on/off valves connected in parallel to regulate hydraulic flow in discrete steps (Fig. 18). Unlike traditional proportional valves, which rely on continuous flow modulation, DFCUs utilize binary control methods, wherein different valves determine the net flow output.

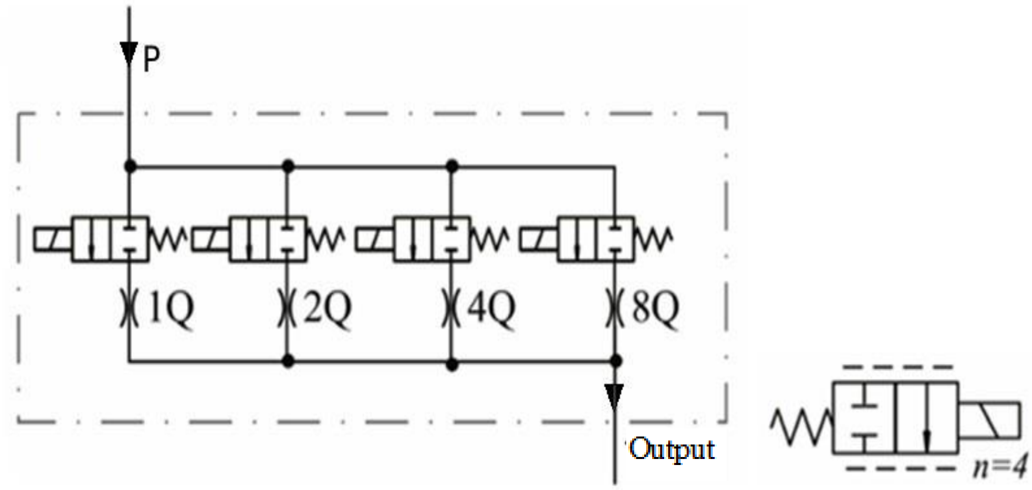

Figure 18. Digital flow control unit (left) and its simplified drawing symbol (right) [73].

In a DFCU system, the total flow rate is the sum of the flow rates of all switching valves in the “on” state. The number of distinct flow levels achievable depends on:

- the number of switching valves (N),
- the encoding method used for switching (Binary, Fibonacci, or PNM encoding).

With N switching valves, the system can achieve 2^N discrete flow levels, allowing for fine control of fluid power (Fig. 19). This stepwise regulation enables accurate, energy-efficient control. while reducing pressure losses associated with traditional hydraulic throttling methods.

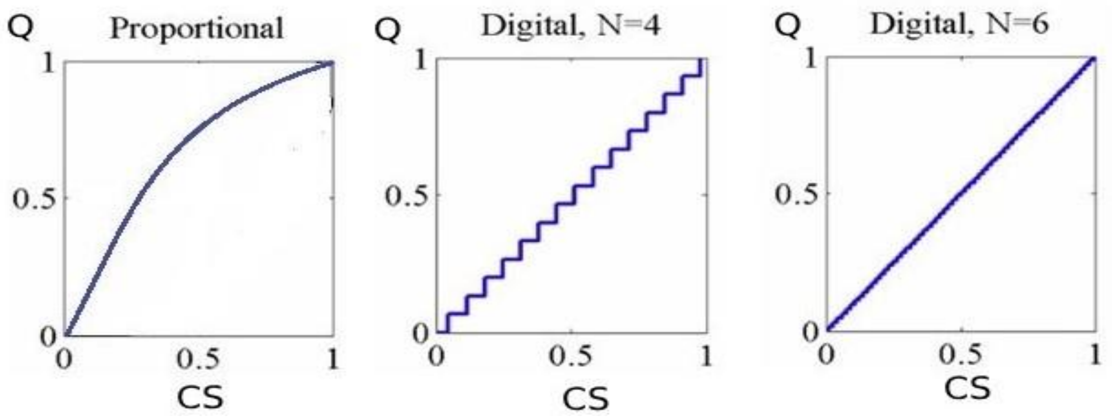

Figure 19. Comparation between proportional valve and DFCU of control signal (CS) [32].

The key characteristics of a DFCU-based system include:

- DFCUs eliminates the need for continuous throttling, reducing hydraulic losses.
- The system enables stepwise regulation of hydraulic output using binary encoding methods.
- Increasing the number of valves enhances resolution, allowing for greater control precision.
- Unlike traditional proportional valves, which are sensitive to contamination, DFCUs are more resistant to fluid impurities due to their simple on/off operation.

A 5-bit DFCU was tested in a single-acting cylinder system to regulate actuator velocity using an I-type velocity controller (Fig. 20). The experiment demonstrated that while exact target velocity could not always be achieved due to discrete state switching, the system effectively modulated flow rate and actuator speed with minimal energy loss [32], [73].

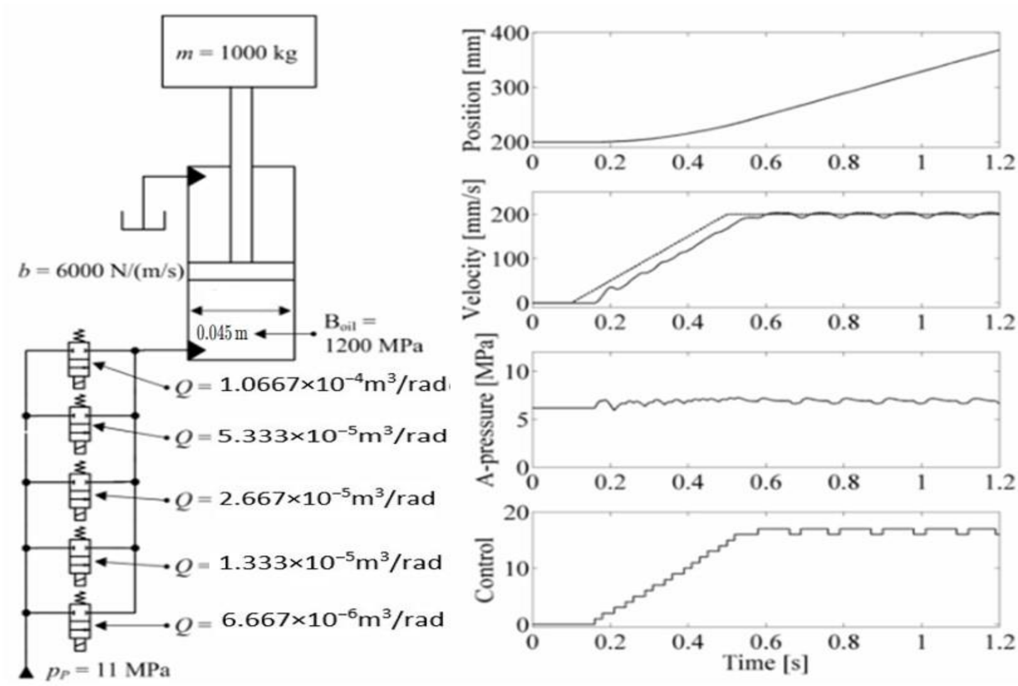

Figure 20. The example of 5-bit DFCU [73].

4.4 Pulse Based Modulation Techniques in Digital Hydraulics

Pulse Number Modulation (PNM) is a digital control technique where multiple identical valves are connected in parallel to regulate flow through pulse sequences. The fundamental idea behind PNM is to control flow by adjusting the number of active valves over a specified period [84]. Uses equal-sized parallel valves to control discrete flow steps [33], [14]. Uses equal-sized parallel valves to control discrete flow steps (Fig. 21).

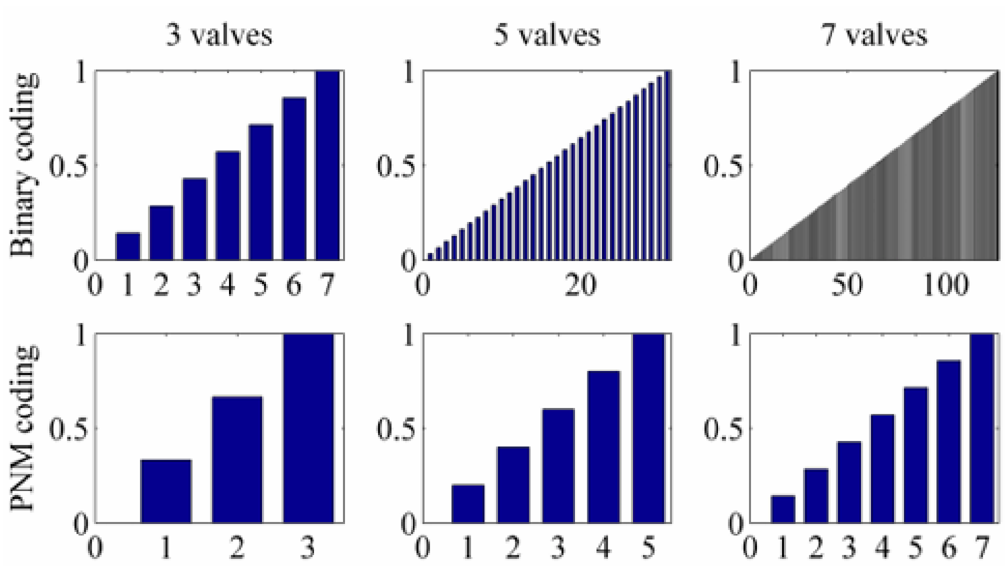

Figure 21. PNM coding for 3, 5 and 7 valves [33].

- The number of active valves determines the flow output, rather than the duration of each pulse.
- More precise than on/off binary switching but requires a large number of valves for high resolution.[74].

Compared to binary encoding, PNM requires more valves to achieve the same resolution. For instance, a binary-encoded system may require only four valves to achieve 16 discrete states, while a PNM-based system would require 15 valves for similar control resolution.

Pulse-Width Modulation (PWM) is one of the most widely used modulation techniques in digital hydraulics (Fig. 22). Unlike PNM, where the number of valves determines flow, PWM regulates flow by varying the "on" time of a single high-speed switching valve.[75]

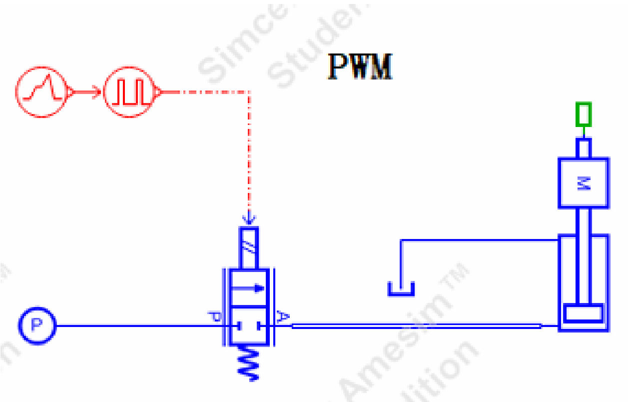

Figure 22. Simple structure of PWM open loop control of hydraulic cylinder [73].

Experiments have shown that PWM-based hydraulic systems can experience pressure oscillations at high switching frequencies [76]. Research into oscillation amplitude has helped optimize control strategies, ensuring smoother system responses. Other studies indicate that at pulse frequencies above 200 Hz, oscillations become negligible, improving system stability as well as in a closed-loop digital hydraulic control system, PWM improves positional accuracy and minimizes transient pressure fluctuations.

Pulse-Width-Pulse-Frequency Modulation (PWPFM) combines PWM and PFM (Pulse Frequency Modulation) to improve digital hydraulic control. It is particularly useful in high-speed digital valves where flow precision must be maintained across varying load conditions.[77].

In PWPFM control, switching frequency is dynamically adjusted based on system requirements [78]:

- during acceleration/deceleration, lower frequencies are used to enhance system response,
- during steady-state operation, higher frequencies reduce flow fluctuations and improve efficiency.

This technique is commonly applied in Remotely Operated Vehicles (ROVs) and other high-speed hydraulic systems. where both response time and flow stability are critical.

4.5 Digital Hydraulic Power Management System (DHPMS)

A Digital Hydraulic Power Management System (DHPMS) is an advanced system designed to optimize hydraulic power distribution using digital switching valves. By dynamically controlling hydraulic flow using on/off valves, DHPMS enhances energy efficiency, reduces system losses, and improves operational flexibility [79]. The most important features of DHPMS are:

- Power balancing at multiple hydraulic outlets.
- Torque control for prime movers to ensure efficient energy use.
- Accumulator-based energy storage to minimize pressure fluctuations.
- Adaptive valve configurations to optimize power transfer across actuators, pumps, and transformers.

DHPMS is widely implemented in mobile machinery, industrial automation, and aerospace systems, where energy-efficient hydraulic control is crucial.

4.6 Comparison of Conventional with Digital Hydraulics

The transition from conventional analog hydraulic systems to digital hydraulic technology marks a transformative shift in the way fluid power is managed and controlled. Digital hydraulics leverages modern electronics and computational power to introduce discrete control, replacing continuous flow regulation with on/off switching mechanisms. This fundamental change not only enhances performance but also aligns with modern industrial trends, such as Industry 4.0, emphasizing automation, efficiency, and connectivity [80].

Table 2. Key Differences Between Conventional and Digital Hydraulics.

Aspect	*Conventional Hydraulics*	*Digital Hydraulics*
Control Method	Continuous, analog	Discrete, digital
Energy Efficiency	Energy losses due to throttling	Minimal losses due to precise switching
Precision	Limited by mechanical tolerances	High precision through digital control
Complexity	Requires proportional/servo mechanisms	Simplified with high-speed switching valves
Integration	Minimal integration with digital systems	Compatible with IoT and automation systems

5 Simulation Model

The attached schematic (Fig. 23) shows a simulation model of a digital hydrostatic transmission, built in the MATLAB/Simulink environment using the Simscape Fluids library. This model reflects the architecture of the physical test stand and allows for the analysis of the system's behavior under various operating conditions. The system can be divided into the following functional sections. The drive source is represented by the "Velocity Source" block, which sets a constant rotational speed (marked as C = 154 rad/sec), simulating the operation of an electric motor. It drives four pumps with fixed geometric displacement (FDP 2cm^3/rev – FDP 16 cm^3/rev), whose capacities are selected in a binary system: $q1$=3.1831×10^{-7}m^3/rad (2 cm^3/rev), $q2$=6.3662×10^{-7}m^3/rad (4 cm^3/rev), $q3$=1.2732×10^{-6}m^3/rad (8 cm^3/rev), $q4$=2.5465×10^{-6} m^3/rad (16 cm^3/rev). They constitute the digital supply unit. The "Scenario Signal" block is responsible for generating the master control signal that defines the commanded work profile. It consists of four Scenario Signal 1 blocks. This signal is then directed to four 2/2 directional valves. These valves, controlled by binary signals (ON/OFF), perform a key function in the system: they decide whether the flow from a given pump is directed to the common pressure line or back to the tank. The flows from the currently active pumps are summed in the main pressure line. A check valve is located after each pump to prevent high-pressure oil from flowing back into an inactive pump circuit. The model also includes standard Simscape blocks, such as a hydraulic reference (representing the tank) and a solver (marked as f(x)=0). The summed fluid stream from the main line drives a fixed-displacement hydraulic motor (FDM), which is the power receiver in the system. The load for the FDM motor is simulated by a pressure relief valve (Pressure Relief Load) that sets the pressure in the loading circuit. It maintains constant pressure in the system, thereby generating a constant resistive torque on the hydraulic motor's shaft.b.

Tables C1 to C19 in Appendix C present the parameters of the components of the modelled digital hydrostatic drive system (Fig. 23).

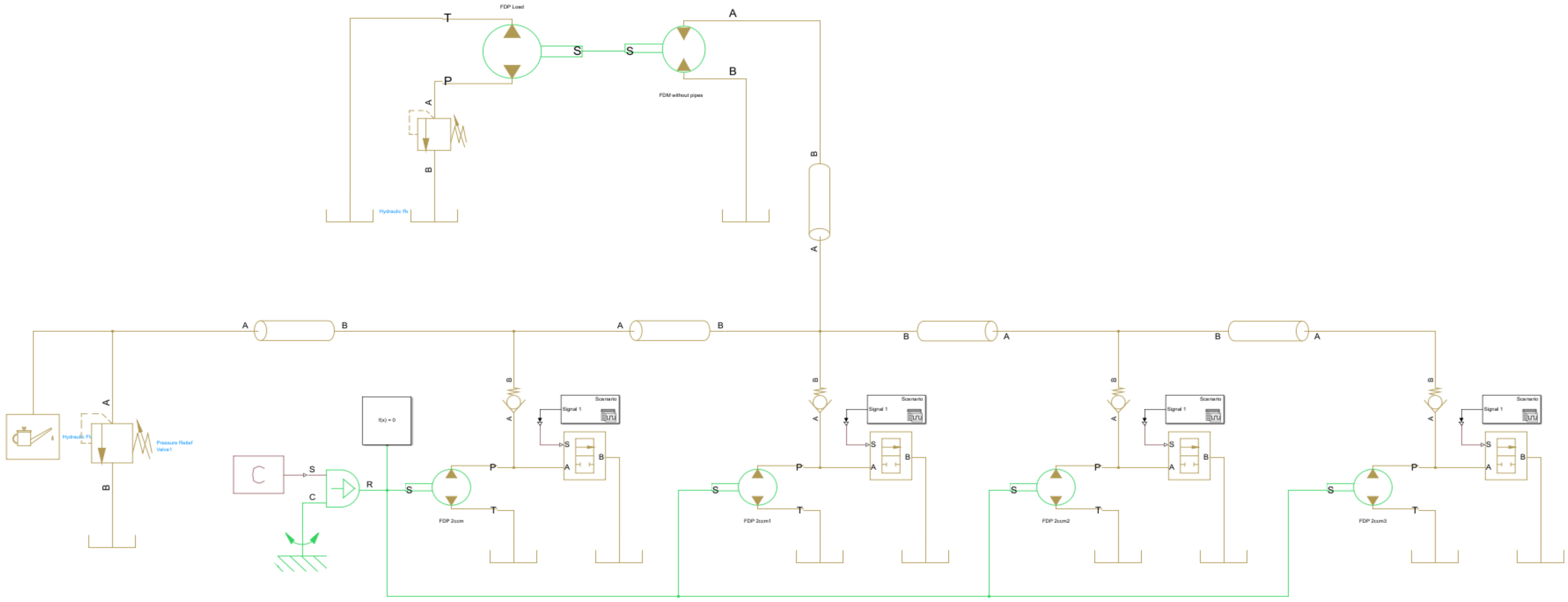

Figure 23. Schematic diagram of digital hydraulic simulation model.

5.1 Gear Pumps

The four gear pumps (P1-P4) are the core of the digital pumping unit. Each is modelled using the Fixed-Displacement Pump block from the Simscape library. This block represents a pump that converts mechanical power at its shaft into hydraulic power. The main parameter of the is geometric volume per revolution V_g or per radian V_r.

The fundamental relationships governing the pump's behavior are:

- Net Volumetric Flow Rate (q): The actual flow rate delivered by the pump is the ideal flow rate minus internal leakage

$$q = q_{\mathrm{Ideal}} - q_{\mathrm{Leak}} \tag{9}$$

- Net Driving Torque (τ): The torque required to drive thevery pump is the ideal torque plus the torque needed to overcome frictional losses

$$\tau = \tau_{\mathrm{Ideal}} + \tau_{\mathrm{Friction}} \tag{10}$$

The ideal flow rate and torque are defined as follows (10) and (11):

$$q_{\mathrm{Ideal}} = D \cdot \omega \tag{11}$$

and

$$\tau_{\mathrm{Ideal}} = D \cdot \Delta p \tag{12}$$

where:

- D is the pump's volumetric displacement [m³/rad],
- ω is the instantaneous angular velocity of the pump shaft [rad/s],
- Δp is the pressure differential across the pump (outlet minus inlet) [Pa].

The internal leakage q_{Leak} and friction torque $\tau_{Friction}$ are modelled based on one of several parameterization options. In this study, the Analytical parameterization was used, where losses are calculated based on specified nominal conditions.

Under this setting, the leakage flow rate is modelled based on laminar flow characteristics:

$$q_{\mathrm{Leak}} = K_{HP} \cdot \Delta p \tag{13}$$

And the friction torque is given by:

$$\tau_{\mathrm{Friction}} = \tau_0 + K_{TP}|\Delta p|\, tanh\left(\frac{4\omega}{\omega_{\mathrm{Threshold}}}\right) \tag{14}$$

where:

- K_{HP} is the Hagen-Poiseuille coefficient for laminar leakage, computed from nominal parameters,
- τ_0 is the no-load torque [N·m],
- K_{TP} is the friction torque vs. pressure gain coefficient,
- $\omega_{Threshold}$ is the threshold angular velocity for the pump-motor transition.

The Hagen-Poiseuille coefficient is determined from nominal fluid and component parameters:

$$K_{HP} = \frac{bh_s^3}{12l\mu} \tag{15}$$

Where: b – wheel width, h_s – tooth height, l – gap length, μ — dynamic viscosity, the subscript '*Nom*' refers to the nominal values (kinematic viscosity, fluid density, angular velocity, pressure gain, and volumetric efficiency) at which the component is characterized.

The pump volumetric efficiency is:

$$\eta_{HP} = \frac{q_{\text{Ideal}} - q_{\text{Leak}}}{q_{\text{Ideal}}} \tag{16}$$

The pump mechanical efficiency is:

$$\eta_{MHP} = \frac{\tau_{\text{Ideal}}}{\tau_{\text{Ideal}} + \tau_{\text{Friction}}} \tag{17}$$

5.2 Directional Valves

The on/off valves (DV1-DV4) that direct flow from each pump are modelled using the 2-Way Directional Valve block. This block models a spool-type valve that controls the connection between two hydraulic ports *A* and *B*. The spool position is controlled by a physical signal at port S.

The instantaneous opening distance *h* of the valve orifice is computed as:

$$h = x_0 + x \tag{18}$$

in which: x_0 is the initial opening and x is the control member displacement from the initial position. A positive signal at port S opens the orifice.

The flow rate Q_v through the valve is calculated using the standard orifice equation:

$$Q_v = C_d \cdot A \cdot \sqrt{\frac{2\Delta p}{\rho}} \tag{19}$$

In which: C_d is the discharge coefficient, A is the cross-sectional area of the valve opening, ΔP is the pressure difference across the valve, and ρ is the fluid density. The valve's opening and closing dynamics can be modelled as a first-order system with a specified time constant τ.

5.3 Check Valves

The Check Valve block models (CV1-CV4) a valve that permits flow in one direction and blocks it in the reverse direction. Its behaviour is defined by the relationship between the valve passage area A and the pressure differential $\Delta p = p_A - p_B$. The valve remains closed (with a small leakage area A_{leak} until the pressure differential reaches the cracking pressure p_{crack}. As the pressure increases further, the passage area opens linearly until it reaches its maximum value A_{max} at the maximum pressure p_{max}.

5.4 Pressure Relief Valve

The Pressure Relief Valve block models a valve that opens to limit the system pressure. The valve is normally closed and begins to open when the pressure at its inlet exceeds the valve pressure setting Δp_{Set}. The opening area increases linearly over the pressure regulation range Δp_{Reg} until it reaches its maximum passage area S_{Max}, preventing the system pressure from rising further.

5.5 Hydraulic Fluid

The properties of the working fluid are defined globally for each hydraulic loop using the Hydraulic Fluid block. This block specifies crucial parameters such as kinematic viscosity, density, and bulk modulus. The model accounts for a small amount of entrained air, which allows for an approximate model of cavitation by reducing the fluid's effective bulk modulus at pressures near atmospheric pressure. This prevents simulation failure at negative pressures and provides a more realistic system response.

5.6 Other Components

- Signal Editor: Used as a source block to create and manage input control signals (scenarios) for the directional valves.
- Hydraulic Flow Rate Sensor: Modelled as an ideal flow meter that measures volumetric and mass flow rate without introducing pressure loss or dynamic delays.

- Hydraulic Reference: Represents the connection to atmospheric pressure (e.g., the hydraulic tank).
- Hydraulic Pipeline: Models the pipelines connecting components, accounting for frictional losses and fluid compressibility, but neglecting fluid inertia (water hammer effects).

Decreasing the theoretical efficiency of the units, are connected with the leaks of the work medium from the displacement chambers due to the clearance between the displacement elements and work chamber or casing walls [81]. Wilson and Thomas [82] draw attention only to the laminar nature leakage flow rate Q_{vl} and define such losses as (17):

$$Q_s = Q_{vl} = \frac{C_1}{\mu}\frac{V_t}{2\pi}\Delta p \tag{20}$$

where: C_l – dimensionless proportionality factor found experimentally for a given hydraulic machine [–], μ – coefficient of friction losses [kg/(s^2 m^3)], which characterizes the resistance of the fluid flowing in the pipe, V_t – critical velocity [m/s], Δp – pressure difference [P$_a$] (Fig. 24).

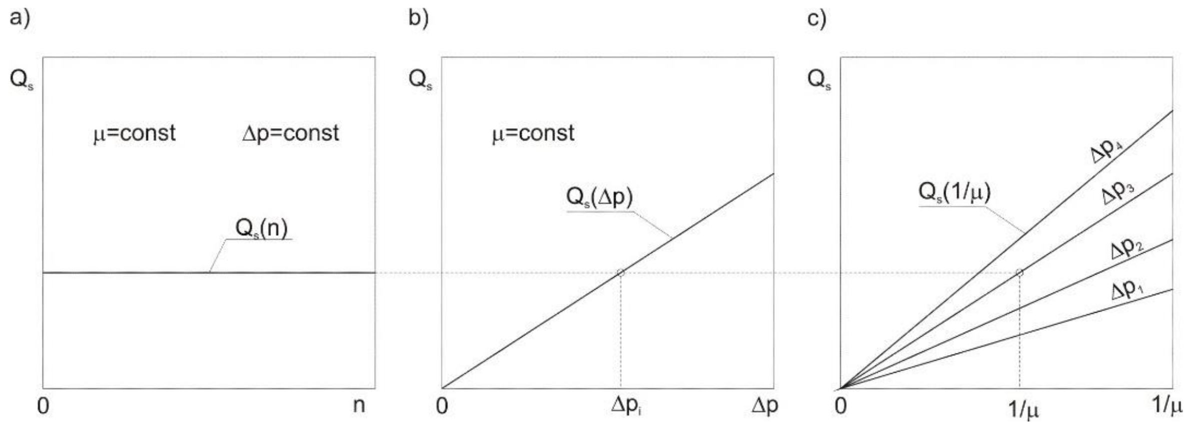

Figure 24. Volumetric loss model according to Wilson [53], [82].

This is the most straightforward model of the volumetric losses' phenomena in these pumps. It is linear and simple to interpret physically. Schlosser and Hilibrands [83], [53], based on laboratory tests of pumps of different types, approximated the volumetric losses Q_s (as leaks only) by a sum of two components: O_{vl} – laminar flow type (as in Wilson) and Q_{vt} – turbulent flow type:

$$Q_s = Q_{vl} + Q_{vt} \tag{21}$$

The volumetric losses Q_{vt} were defined by the equation of turbulent flow:

$$Q_{vt} = C_t \sqrt{\frac{2\Delta p}{\rho}} \sqrt[3]{\left(\frac{\nu_t}{\pi}\right)^2} \tag{22}$$

where C_t – dimensionless proportionality coefficient [–], ρ – density of the liquid [kg/m^3].

The total cross-sectional area and all parallel gaps where there is turbulent flow is called the area of the equivalent gap expressed by the square of the characteristic dimension D_t. (Fig. 25).

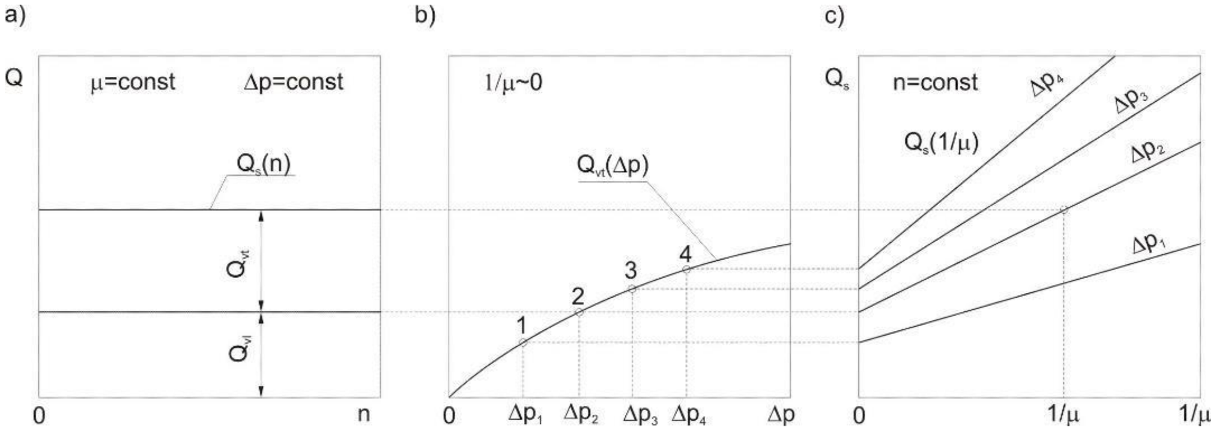

Figure 25. Schlosser's volumetric loss model [83], [53].

This model, though, doesn't consider the flow due to compressibility of the working fluid (q_c) and the flow due to the cyclic deformation of the working chambers (q_k). The leakage phenomenon is described by equations or approximations in the Balawender model [45]. On the one hand, it provides a more precise description of the unit characteristics, but on the other hand, it complicates the analysis of the influence of separate parameters on their characteristics directly. Nevertheless, most commonly, practitioners who apply the findings of scientists' research in practice employ a linear model of volumetric losses in calculations.

5.7 Mechanical and Hydraulic Losses

It results in the actual torque to be transmitted to the shaft to be higher (pump) or the developed torque to be lower (engine) than the theoretical torque [50], [84], [51]. Hydraulic losses relate to the flow resistance of the medium in all internal channels of the pump, and mechanical losses relate to friction on the surface of all elements remaining in relative motion when the units are running. Because of the impossibility of their separation in bench tests, these losses are combined under the term hydraulic-mechanical losses. Using relationships, the efficiency of hydrostatic units can be determined for:

Pumps:

$$\eta_p = \eta_{HP}\eta_{MHPvp} = \frac{q_{\text{Ideal}} - q_{\text{Leak}}}{q_{\text{Ideal}}} \frac{\tau_{\text{Ideal}}}{\tau_{\text{Ideal}} + \tau_{\text{Friction}}} \tag{23}$$

Hydraulic motor:

Theoretical (ideal) flow of the hydraulic motor:

$$Q_{HM} = V_M \omega_M \tag{24}$$

where: V_M is theoretical volume [m^3/rad], ω_M - is angular velocity of the motor shaft [rad/s]

Real flow:

$$Q_{HMrf} = Q_{HM} + Q_{HMleak} \tag{25}$$

where: Q_{HM} – flow thru hydraulic motor [m^3/s], Q_{HMleak} – leakage [m^3/s].

The motor volumetric efficiency is:

$$\eta_{HMv} = \frac{Q_{HM}}{Q_{HMrf}} = \frac{Q_{HM}}{Q_{HM} + Q_{HMleak}} \tag{26}$$

The motor mechanical efficiency is:

$$\eta_{MHP} = \frac{\tau_{\text{MIdeal}}}{\tau_{\text{MIdeal}} + \tau_{\text{MFriction}}} \tag{27}$$

The hydraulic motor efficiency is:

$$\eta_{HMv}\eta_{MHP} = \frac{\tau_{\text{MIdeal}}}{\tau_{\text{MIdeal}} + \tau_{\text{MFriction}}} \frac{Q_{HM}}{Q_{HM} + Q_{HMleak}} \tag{28}$$

$$\eta_{sh} = \eta_{hmsh}\eta_{vsh} = \frac{M_{sht} - \Delta M_{sh}}{M_{sht}} \frac{Q_{sh}}{Q_{sht} + \Delta Q_{sh}} \tag{29}$$

5.8 Energy Efficiency Measurement

One of the most common measures of efficiency is efficiency as a ratio of useful work (energy, power) to delivered work (energy, power). Efficiency can be calculated for every drive system element individually, for the whole drive system or for the working machine. Drive system element efficiency is not constant and is a function of the drive system operating parameters. The performance analysis of sophisticated drive systems is demanding because of the interaction and reciprocity between drive system parameters and components [85], [86], [87], [88], [89], [90].

The hydraulic drive is powered by electricity, supplied to the electric motor. This motor drives the pump, and the pump drives the hydraulic motor. So, the efficiency of this drive η_{HD} should be calculated as:

$$\eta_{HD} = \frac{P_{\text{out}}}{P_{\text{inp}}} = \frac{\tau_{\text{out}}\omega_{\text{out}}}{U_{\text{inp}}I_{\text{inp}}} = \frac{\tau_{\text{out}}Q_{HM}}{U_{\text{inp}}I_{\text{inp}}\,V_M} \tag{30}$$

In the simulation and laboratory investigations, also time should be considered, thus the equation should be converted as follows

$$\eta_{HDW} = \frac{W_{\text{out}}}{W_{\text{inp}}} = \frac{\tau_{\text{out}}\omega_{\text{out}}}{U_{\text{inp}}I_{\text{inp}}} = \frac{\tau_{\text{out}}Q_{HM}}{U_{\text{inp}}I_{\text{inp}}\,V_M} = \frac{\int_0^T \tau_{\text{out}}(t)Q_{HM}(t)dt}{V_M\int_0^T U_{\text{inp}}(t)I_{\text{inp}}(t)dt} \tag{31}$$

5.9 Model of Hydraulic Losses in Pipes

The primary challenge in pressure loss calculation is that in one circuit numerous flow types may exist with pressure drops of different magnitudes, and there is no way of predicting in advance what type of flow will actually take place [45], [91]. One can check whether the flow through a particular element will be laminar or turbulent by comparing the dimensionless quantity known as the Reynolds number given by:

$$Re = \frac{vD}{\mu} \tag{32}$$

in which:
D – internal diameter of the pipe [m],
v– flow velocity at a specific point of the element [m/s],
μ– kinematic viscosity coefficient of the liquid [m^2/s], with a constant so-called critical

If $R_e < Re_{kr}$, the flow will be laminar, if $Re > Re_{kr}$, the flow will be turbulent. For pipes, if we take the pipe diameter d as the dimension and the uniform flow velocity v within the pipe (mean velocity), then the critical Reynolds number will be approximately 2500. For elements with a more complicated shape, there is no abrupt transition between the stratified and turbulent region, for both varieties may exist simultaneously at various locations of the element. Here, in this study, hydraulic losses were assumed to be linear losses just in pipes [92], [93], [53]. Hence, hydraulic losses will be calculated based on the following relation:

$$\Delta p = \begin{cases} \frac{64}{Re}\frac{\rho L v^2}{2d} & \text{dla} \quad Re \le 2300 \\ 0{,}3164 Re^{-0{,}25}\frac{\rho v^2 L}{2d} & \text{dla} \quad Re > 2300 \end{cases} \tag{33}$$

5.10 Ecological Performance Measures

Those parameters are established, for instance, for combustion engines in construction machinery, by the European standards and legal acts [94], [95], [96], [97]. Based on them, the average exhaust of individual components of exhaust per unit of power of the examined engine is calculated (25).

The hourly emission of individual toxic components for each i^{th} of the thirteen test phases [88], which is calculated based on the relationship:

$$E_{j,i} = a_j C_{j,i} G_{sp,i} [\, kg/h] \tag{34}$$

in which:
j – CO, HC or NO_x, SMOKE criterion,
a_j – characteristic coefficient for a given compound j,
$C_{j,i}$ – concentration of individual compounds [%], [ppm],
$G_{sp,i}$ – exhaust gas flow rate [kg/h].

The average unit emission e_j is calculated from the relationship:

$$e_j = \frac{\sum_{i=1}^{13} E_{j,i}}{\sum_{i=1}^{13} N_{ei}} \left[\frac{g}{kWh}\right] \tag{35}$$

where N_{ei} – useful power reduced in the i^{th} stage in [kW].

Another form of energy or environmental assessment indicator may be the concept of global efficiency, allowing assessment of the drive system during the operation time of the machine or device [45], [98], [99], [100]. For combustion engines of construction machines ecological parameters are determined by requirements laid down in the ECE R49 standard and in the company standard BN-84/1374-12 with later amendments [97], [105]. This indicators will be used in the future to assess the quality of control of a multi-source drive system.

5.11 Impact on the Environment

Nowadays, the need for ruling in every type of examinations are increasingly directly related to ecology [99]. An example can be the ubiquitous provisions in European standards and regulations, inter alia, concerning noise and vibrations (Journal of Laws 2005 No. 157, item 1318, PN-EN 458:2006).

Noise and vibration are environmental pollutants with a wide range of sources and ubiquitous presence [101], [102]. The effect of noise on humans is underrated since the influence of noise is not directly perceived. Noise, as defined, is any unwanted, unpleasant, bothersome or damaging mechanical vibrations of an elastic medium, acting through the air on the hearing organ and other senses of the human body. Depending on the frequency of vibration, noise is classified:

- infrasonic, not audible but can be felt, with a vibration frequency below 20 Hz,
- perceived at a pitch within the range of 20–20,000 Hz.
- ultrasonic, inaudible, above 20,000 Hz. "Vibration" is reserved for vibrations functioning not via air but via solid bodies [103], [101], [102].

Harmful noise on the human body influences the condition of its health, the activity of independent organs and systems, and most importantly the hearing organ. Noise influences not only the hearing organ, but also via the central nervous system on other organs.

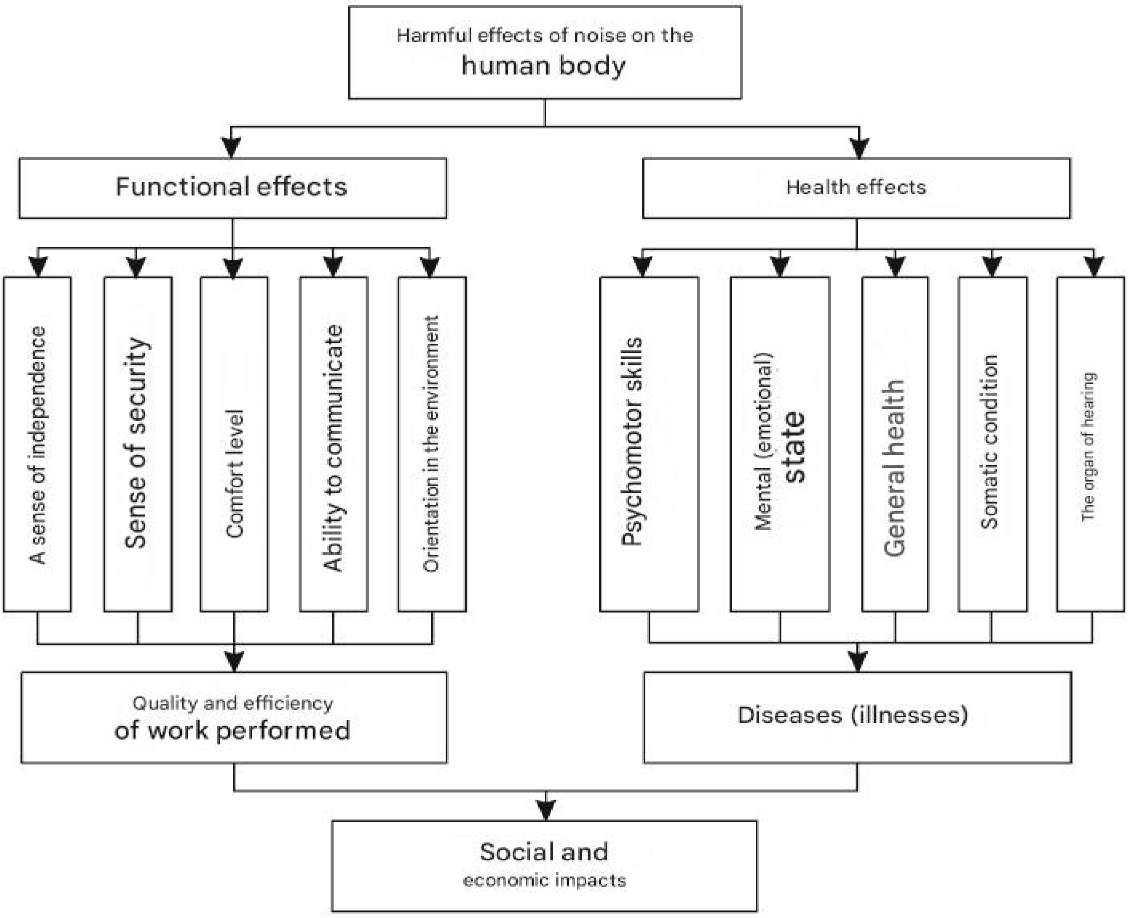

Figure 26. Diagram of the impact of noise on the human body [104].

The effect of noise on psychological condition, mental performance, productivity and quality of work is of very high significance. Figure 26 illustrates a chart of the effect of noise on the human body.

5.12 Expanded Economic Analysis

A full assessment of the viability of implementing a new technology, such as digital hydrostatic transmission, requires going beyond the analysis of purely technical and efficiency parameters. It becomes crucial to conduct a thorough economic analysis that allows for an objective comparison with existing solutions. The contemporary approach to evaluating investments in machinery and industrial systems is based on the Total Cost of Ownership (TCO) methodology, which considers all costs incurred throughout the product's entire life cycle, from purchase to disposal [106]. The TCO methodology is particularly useful when comparing systems that differ in their cost structure, e.g., low investment costs but high operating costs, and vice versa [107].

5.12.1 Capital Expenditure (CAPEX)

Capital Expenditure (CAPEX) is defined as the one-time costs incurred during the design, purchase, and implementation phase of a system. These are all the expenses necessary for the system to achieve operational readiness. In the context of hydrostatic systems, CAPEX includes:

- The purchase cost of key components: the pump (or pump assembly), hydraulic motor, control valves, drive unit (electric motor), and PLC controller.
- The costs of other hydraulic fittings: hoses, connectors, reservoir, and filters.
- The costs of assembly, commissioning, and integration of the system with the working machine.

Traditionally, CAPEX has been the main decision-making criterion when choosing a technology. However, an analysis based solely on the initial cost is incomplete because it ignores the expenses that will arise during many years of operation [108]]. The research hypothesis of this work assumes that the use of standard, mass-produced gear pumps and on/off valves in a digital system allows for a significant reduction in CAPEX compared to expensive, precision-made axial piston pumps and proportional valves in a classic system.

5.12.2 Operational Expenditure (OPEX)

Operational Expenditure (OPEX) comprises all cyclical and ongoing expenses that are necessary to keep the system running and to ensure its proper functioning. Over the entire life cycle of a machine, the sum of OPEX costs often exceeds the initial CAPEX by many times [109]. The main components of OPEX for a hydrostatic drive system are:

- Energy Costs: This is typically the largest and most important component of OPEX. It includes the cost of consumed fuel (in mobile machinery) or electrical energy (in stationary applications). The amount of these costs is directly proportional to the energy efficiency of the system. Systems with higher efficiency that minimize energy losses (e.g., by eliminating throttling) generate direct and constant financial savings throughout their operational life [107].
- Maintenance and Repair Costs: These include the costs of scheduled inspections (preventive maintenance), emergency repairs (corrective maintenance), the purchase of spare parts, and service labor. Systems based on simpler and more reliable components are characterized by lower costs in this category.
- Downtime-Related Costs: Every failure and the associated machine downtime generate measurable economic losses resulting from a break in production or work. Higher system reliability directly translates into a reduction of these costs.

5.12.3 Total Cost of Ownership (TCO)

The TCO methodology allows for a synthetic summary of all the above costs, providing a complete economic picture of a given solution. TCO can be simply presented as:

$$\mathrm{TCO} = \mathrm{CAPEX} + \sum \mathrm{OPEX}\ (\text{over the entire life cycle}) \tag{36}$$

in which:
TCO - Total Cost of Ownership,
CAPEX - Capital Expenditure,
OPEX - Operating Expenditure.

This holistic approach is essential for making informed investment decisions. A system with a higher initial cost (CAPEX) but with significantly lower operating costs (OPEX) may ultimately prove to be much cheaper. In the context of this work, the TCO analysis allows for the verification of the hypothesis that digital transmission, offering both potentially lower CAPEX and, as proven in simulations, lower energy costs, is an economically superior solution to the classic transmission over the entire life cycle [110].

5.13 Evaluation of the Compatibility of Simulation Models

RMSE is a standard and widely accepted indicator for assessing the fidelity of simulation models. To determine the differences between the simulation research results obtained when comparing simulation studies of a classic hydrostatic transmission and its corresponding transmission built according to the concept of digital hydraulics, the Root Mean Square Error

(RMSE) was used. It is a statistical measure that determines how much the values predicted by a model (e.g., from a simulation) differ from the actual values (measured in an experiment). To calculate the "Root Mean Square Error" the following computational steps should be performed:

For each measurement point in time (*i*), the difference, or error (e_i), between the experimental value and the simulated value is calculated:

$$e_i = \left(y_{exp,i} - y_{sim,i}\right) \tag{37}$$

Each calculated error is squared. This is done for two key reasons:

- Sign Elimination: This ensures that positive errors (when the simulation is lower than reality) and negative errors (when the simulation is higher) do not cancel each other out.
- Reinforcement of Large Errors: Squaring makes large deviations have a much greater impact on the final result than small ones, which is desirable when evaluating a model.

$$e_i^2 = \left(y_{exp,i} - y_{sim,i}\right)^2 \tag{38}$$

All the squared errors are summed, and then this sum is divided by the number of measurement points (*N*) to obtain the average. This is the Mean Squared Error (*MSE*):

$$MSE = \frac{1}{N}\sum_{i=1}^{N} e_i^2 = \frac{1}{N}\sum_{i=1}^{N}\left(y_{exp,i} - y_{sim,i}\right)^2 \tag{39}$$

Finally, the square root of the *MSE* is taken. This step "reverses" the squaring operation, so the result (*RMSE*) returns to the original units of the measured quantity (e.g., Nm, m^3/s, rad/s):

$$RMSE = \sqrt{\frac{1}{N}\sum_{i=1}^{N}\left(y_{exp,i} - y_{sim,i}\right)^2} \tag{40}$$

where:

N- Total number of measurement points used for comparison,
$y_{exp,i}$ - i^{th} experimental value,
$y_{sim,i}$ - i^{th} simulated value,

Interpretation of the result: The *RMSE* value is the standard deviation of the model's errors. The lower the result, the better the model fits the data. *RMSE* = 0 would mean a perfect match.

6 Test Scenarios

To evaluate the performance of the classic and digital hydrostatic systems, a series of tests were designed and conducted (both for simulation and experimental). The tests were based on three distinct control signal profiles, or scenarios, which dictated the activation sequence of the four digitally controlled pumps. This chapter defines these test scenarios.

6.1 Test Scenario 1

The first test scenario was designed to generate a symmetrical flow rate profile, with a stepped ramp-up phase, a brief hold at maximum flow, and a symmetrical, stepped ramp-down phase. The activation sequence for the four pumps $P1$=3.1831×10^{-7}m³/rad (2cm³/rev), $P2$=6.3662×10^{-7}m³/rad (4cm³/rev), $P3$=1.2732×10^{-6}m³/rad (8 cm³/rev), $P4$=2.5465×10^{-6} m³/rad (16cm³/rev) followed a binary pattern to achieve precise, discrete flow combinations. Each pump is controlled by a dedicated 2-way directional valve that directs flow either to the main circuit or back to the tank based on a digital (ON/OFF) signal. The sequence is detailed in Table 3 (below).

Table 3: Pump Activation Sequence for Test Scenario 1.

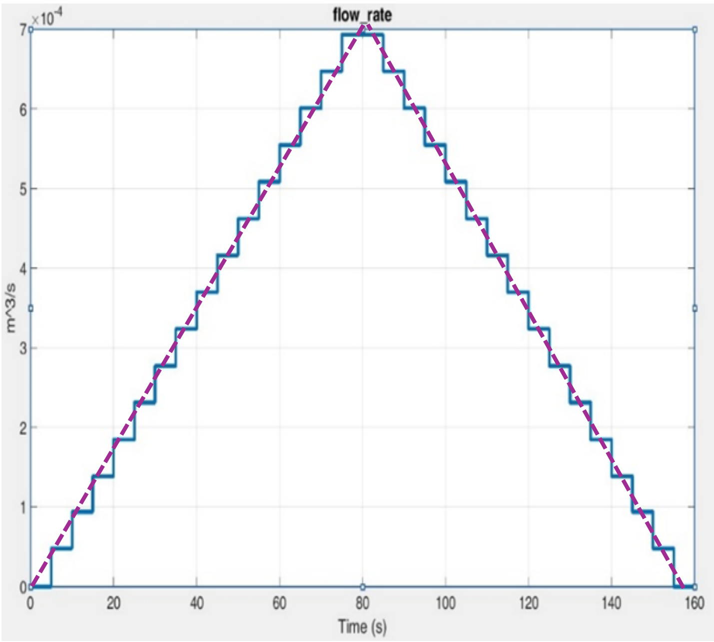

Figure 27. Flow rate of 1st testing signals. Input signal.

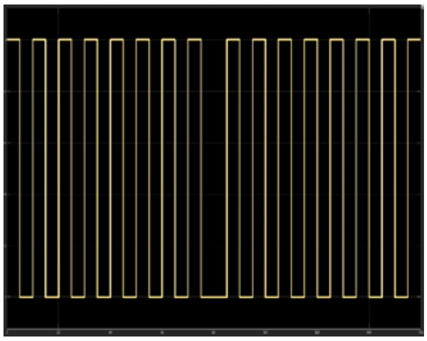

Control signal for pump 1 (2 cm^3)

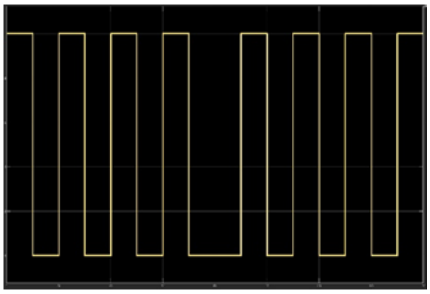

Control signal for pump 2 (4 cm^3)

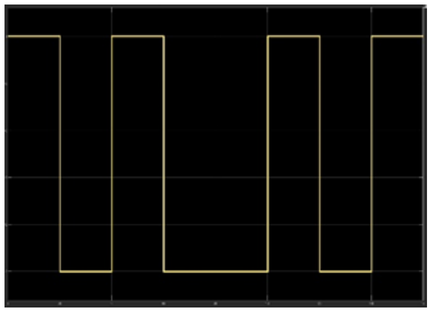

Control signal for pump 3 (8 cm^3)

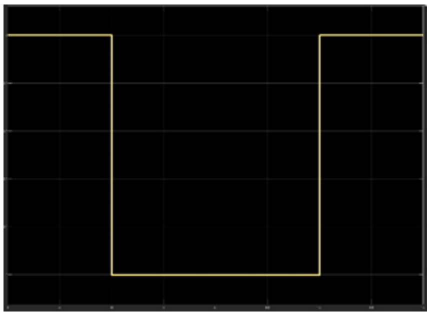

Control signal for pump 4 (16 cm^3)

6.2 Test Scenario 2

The second test scenario was designed to evaluate the system's response to a series of intermittent, step-increasing flow commands. This configuration tests the system's performance during frequent start-stop cycles at progressively higher load levels. The control system combines the pump outputs to generate a series of flow pulses, where each subsequent pulse corresponds to a higher discrete flow rate, as defined in Table 4 (below).

Table 4: Pump Activation Sequence for Test Scenario 2.

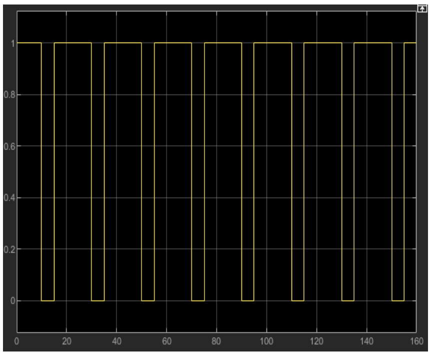

Control signal for pump 1 (2 cm^3)

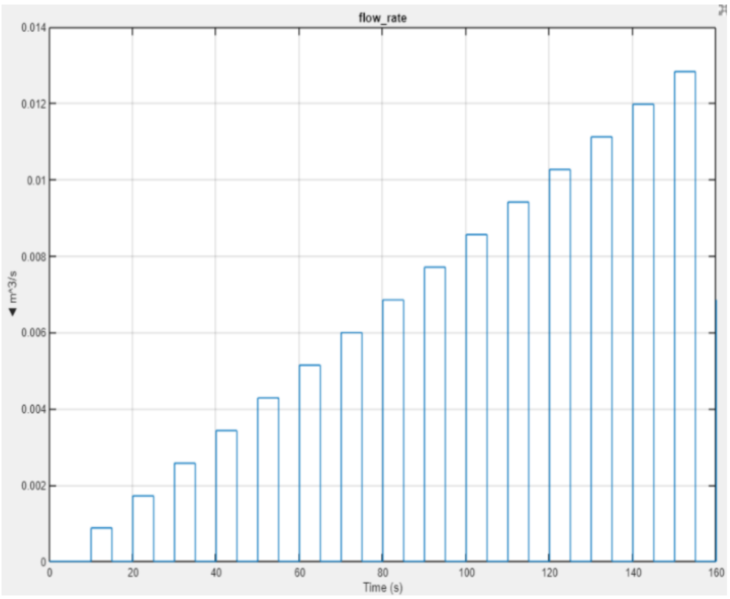

Figure 28. Flow rate of 2nd testing signals. Input signal.

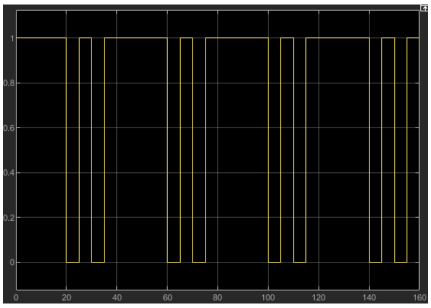

Control signal for pump 2 (4 cm^3)

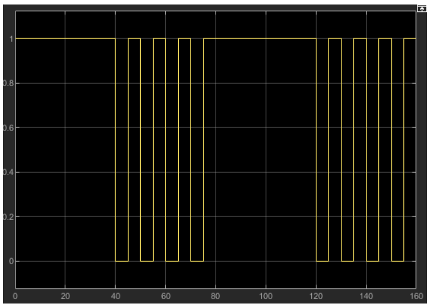

Control signal for pump 3 (8 cm^3)

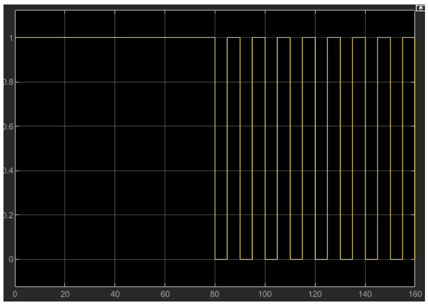

Control signal for pump 4 (16 cm^3)

6.3 Test Scenario 3

The third experimental scenario utilized the same four-pump configuration, with each unit controlled by a 2-way directional valve via digital ON/OFF signals. This profile was designed to demonstrate a different, well-coordinated flow control process, again using binary signal combinations to achieve a specific operational cycle. It is detailed in the sequence Table 5.

Table 5: Pump Activation Sequence for Test Scenario 3.

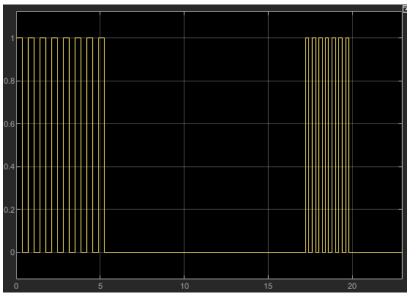

Control signal for pump 1 (2 cm^3)

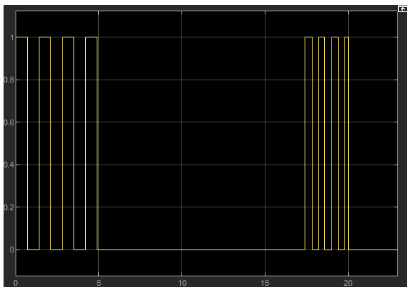

Control signal for pump 2 (4 cm^3)

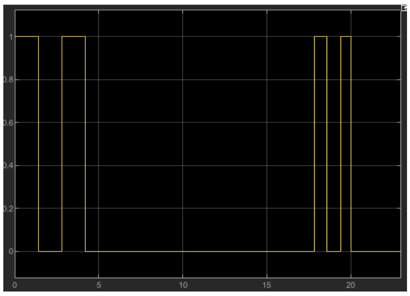

Control signal for pump 3 (8 cm^3)

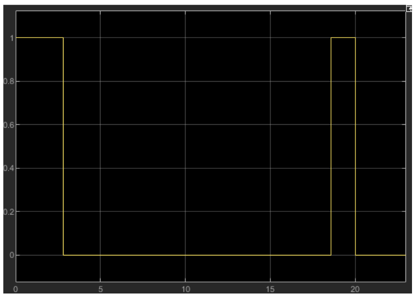

Control signal for pump 4(16cm^3)

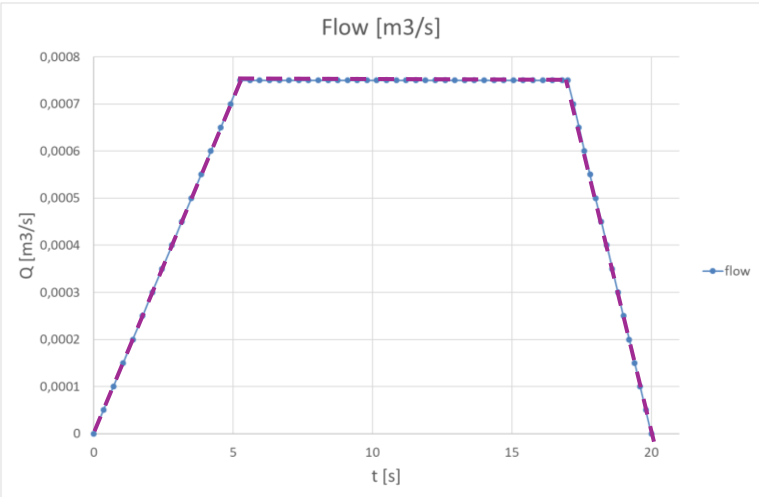

Figure 29. Flow rate of 3rd testing signals. Input signal.

This profile is typical of vehicle traffic. It consists of an acceleration phase (from zero speed), a constant speed phase, and a braking phase (to zero speed).

7 Experimental Research Results

The experimental studies were carried out in cooperation with the Hydraulic and Pneumatic Research Institute INOE 2000 - IHP from Bucharest within the framework of a research mini-grant obtained by the PhD student entitled: Method of effective use of digital hydraulics concept in multisource hydrostatic drive systems, Budget: PLN 19,995. Data on the conducted experimental studies are presented below.

7.1 Experimental Stand of Digital Hydrostatic Transmission

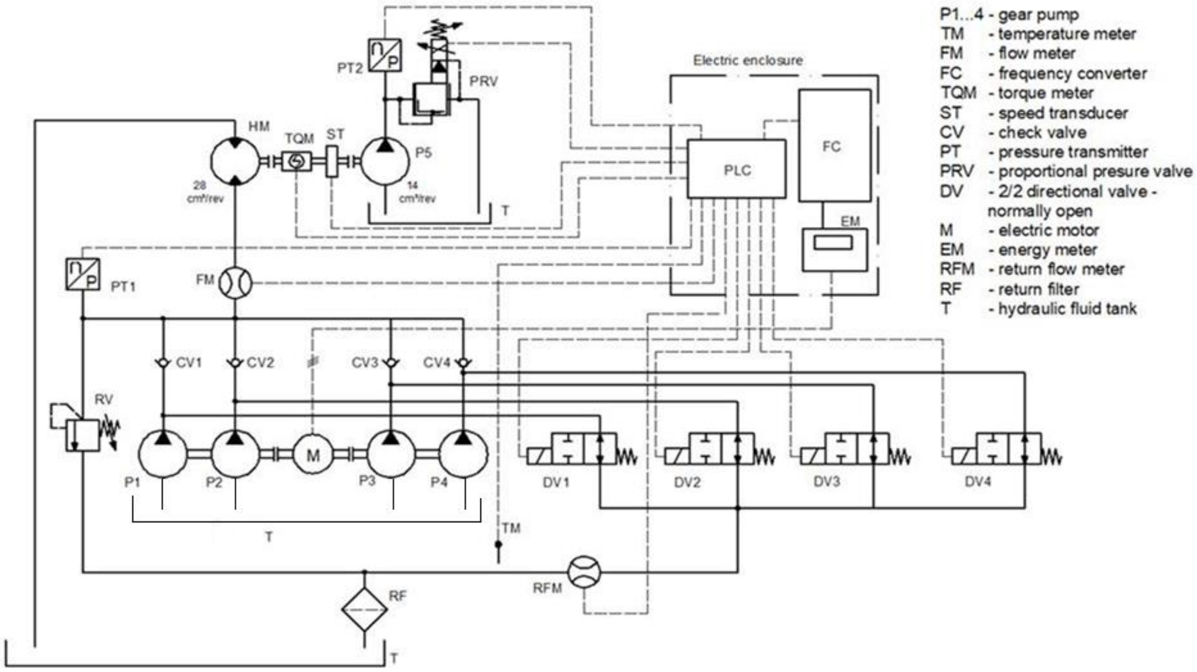

Figure 30. Experimental stand of digital fluid power transmission scheme.

The figure 30 provided schematic illustrates a complete research stand designed for testing and analyzing digital hydrostatic transmission. This system can be divided into three main parts: the digital supply unit, the motor and load unit, and the measurement system.

Digital Supply Unit is the heart of the entire system, responsible for generating a hydraulic fluid stream with a regulated, discrete flow rate. It consists of the following components:

- Main Drive: An electric motor (M) whose rotational speed is regulated by a frequency converter (FC). This allows for precise setting of the rotational speed for the entire pump assembly.
- Pump Assembly (P1-P4): Four gear pumps with fixed but different geometric displacements are mounted on a single shaft driven by the motor (M). These pumps constitute the "digital" element of the supply system.

- Flow Control System: Each of the pumps (P1-P4) is connected to a 2-way, 2-position directional valve (DV1-DV4), which is electrically controlled by a PLC. In their rest state (normally open), these valves direct the flow from the pumps back to the tank (T). Upon receiving a signal from the PLC, the valve switches, directing the flow to the common pressure line.
- Check Valves (CV1-CV4): A check valve is located after each pump-valve pair to prevent the backflow of high-pressure oil from the main line into a momentarily inactive pump circuit.
- Main Relief Valve (RV): A relief valve is installed on the main pressure line to protect the entire system from excessive pressure increases.

Hydraulic Motor and Load Unit is responsible for receiving the hydraulic energy and simulating a controlled load.

- Hydraulic Motor (HM): This is a fixed-displacement hydrostatic motor 4.4563×10^{-6} m^3/rad (28 cm^3/rev) that converts hydraulic energy from the pressure line back into mechanical energy in the form of rotational motion of the shaft.
- Braking (Loading) Unit: The shaft of the hydraulic motor (HM) is mechanically connected to a second pump (P5) with a fixed displacement 2.2282×10^{-6} m^3/rad (14 cm^3/rev). This pump acts as a hydraulic brake its function is to generate a load torque for the HM motor.
- Load Regulation: The load is precisely regulated by a proportional pressure valve (PRV) located at the outlet of the braking pump (P5). By changing the pressure setting on the PRV, the resistive torque, and thus the load on the entire transmission, can be smoothly adjusted.

The stand is extensively equipped with measurement instrumentation, allowing for a comprehensive analysis of operating parameters:

- Pressure Measurement: Two pressure transducers (PT1, PT2) measure the pressure in the main supply line and the loading circuit, respectively.
- Flow Measurement: A flow meter (FM) measures the flow rate of the fluid supplied to the HM hydraulic motor. Additionally, a flow meter on the return line (RFM) allows for the analysis of, for example, leakages.
- Mechanical Parameter Measurement: A torque meter (TQM) and a speed transducer (ST) are installed on the shaft connecting the HM motor with the

braking pump P5. They enable the direct measurement of the output torque and speed, and consequently, the mechanical power.

- Additional Parameter Measurement: The system also features a temperature meter (TM) and an electric energy meter (EM) for the power consumed by the main drive motor.

Based on a set program or signal, the PLC sends binary (on/off) signals to the coils of the DV1-DV4 valves. The activation of a selected combination of valves causes the oil streams from the corresponding P1-P4 pumps to be directed into the common pressure line. The combined stream powers the hydraulic motor HM, which performs work by overcoming the resistive torque generated by the pump P5 and the valve PRV. Simultaneously, the sensor system continuously measures all key parameters, which are recorded for further analysis.

Pumping system technical data of the Experimental part:

- Three – phase induction motor power ………. 11 kW;
- 3-phase supply voltage ………………………. 380 V 50 Hz;
- Motor speed ………………………………….. 1475 rev/min;
- Variable speed drive …………………………. Altivar 71; 15 kW;
- Motor speed adjustment range ……………….. 10÷50 Hz ;
- Max. flow ……………………..…………... $Q = 0.00075$ m³/s, (45 l/min)
- Max. pressure ………………………………… f(Q): 10÷20 MPa;(0.05 MPa)
- Pumps displacement ………………….……… $q1=3.1831\times10^{-7}$m³/rad (2 cm³/rev), $q2=6.3662\times10^{-7}$m³/rad (4 cm³/rev), $q3=1.2732\times10^{-6}$m³/rad (8 cm³/rev), $q4=2.5465\times10^{-6}$ m³/rad (16 cm³/rev),
- Working fluid: …………….……………….…… HP 46 hydraulic oil;
- Filter fineness: …………….…………….……. 10 mm;
- Maximum temperature of the working fluid: …(313 K)

Equipment used:

- Flow transducer: accuracy class 2.0;
- Speed transducer: accuracy class 1.0;
- Torque meter: accuracy class 1.0;
- Thermometer (373 K) accuracy class 2.0;
- Pressure transducer: (16 MPa)
- Power supply: 24 V / 10A.

Test auxiliary necessaries:

- Fittings, nipples, etc;
- Electrical cables.

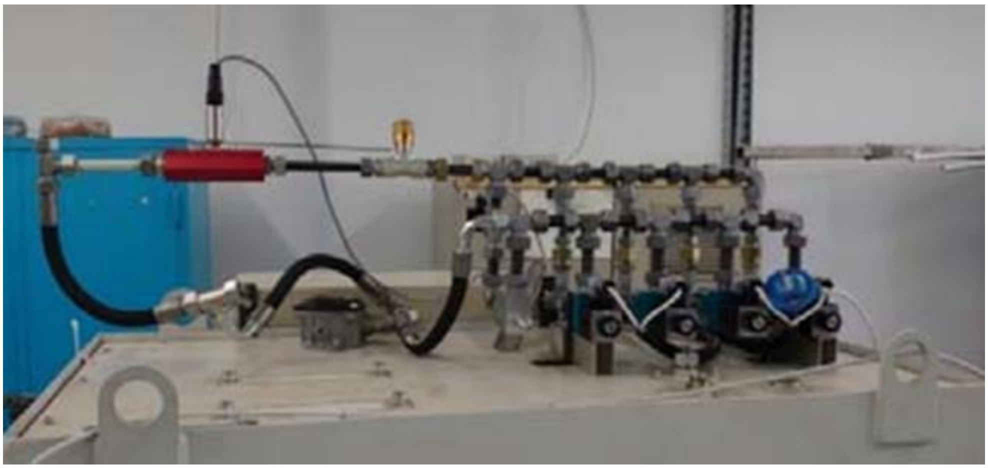

Figure 31. Valves and connection block.

Figure 32. Pumping group.

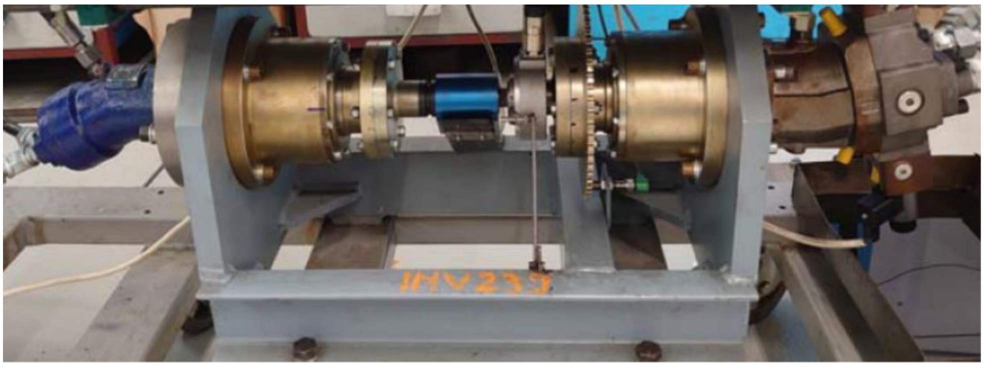

Figure 33. Hydrostatic motor with load.

The presented below set of four graphs (Fig 32 to Fig. 35) presents key parameters of the digital pump system recorded as a function of time during the first experimental test. The analysed quantities are flow rate (*Q*), load pressure (*p*), torque (*M*) and active power (*P*). The active power is calculated as: $P_{ac} = I\,U$ [AV].

The aim of the study was to characterize the dynamic performance of the system during a work cycle with symmetrically increasing and decreasing flow rate. The study was conducted on a laboratory stand equipped with an 11-kW induction motor, powered by 3x380 V / 50 Hz and controlled by an Altivar 71 frequency converter. The hydraulic system consisted of four pumps with geometric volumes of: $q1=3.1831\times10^{-7} m^3/rad$ ($2 cm^3/rev$), $q2=6.3662\times10^{-7} m^3/rad$ ($4 cm^3/rev$), $q3=1.2732\times10^{-6} m^3/rad$ ($8 cm^3/rev$), $q4=2.5465\times10^{-6} m^3/rad$ ($16 cm^3/rev$). The working fluid was hydraulic oil HP 46, maintaining its maximum temperature at (313 K). The test load pressure for this test was 2.8 MPa.

7.2 Experimental Results for Scenario No. 1 (Load 2.8 MPa)

The presented set of four graphs (Fig.34 to Fig.37) documents the basic operating parameters of the digital hydrostatic transmission recorded as a function of time. The study was conducted for the first test scenario (symmetrical profile) at a constant load pressure of 2.8 MPa. A key element of this analysis is the comparison of results from three independent test repetitions (designated as Test 1, Test 2, and Test 3), which allows for the assessment of the system's repeatability and operational stability.

All four analyzed parameters flow rate (Q), pressure (p), torque (M), and active power (P) exhibit very high repeatability on a macroscopic scale. The profiles from the three successive tests largely overlap, following the same symmetrical profile of ramp-up, steady-state operation, and ramp-down. This confirms that the control system (PLC and valves) precisely executes the commanded pump switching sequence in each cycle.

- The flow rate (Q) graph shows an almost ideal overlap of the curves from the three tests. This confirms that the main output parameter of the system is controlled in a highly repeatable manner, reaching a maximum output of approx. $0.00075 m^3/s$ (45 l/min) in each cycle.
- The pressure (p) graph also shows great consistency. The pressure stabilizes at the set level of approx. 2.8 MPa, with minor fluctuations.
- The active power (P) graph, similarly to the flow rate, is characterized by very good repeatability. The profile is smooth, and the curves from the three tests are nearly identical, reaching a peak value of approx. 6.5 kW.

The most interesting and important conclusions come from the analysis of the differences between the individual repetitions, which are most visible on the torque (M) graph.

- Nature of the Torque Profile: In contrast to the smooth profiles of power and flow, the torque graph is very "noisy" and is characterized by sharp, high-frequency oscillations around the mean value. This is not a measurement error, but a physical signature of the digital transmission's operation. These oscillations are the result of two main phenomena:
  - Pressure and flow pulsations generated by the gear meshing of the gear pumps.
  - Hydraulic and mechanical shocks arising from the stepwise connection or disconnection of successive pumps to the common pressure line.
- Differences in Oscillations Between Tests: A key observation is that while the averaged profile of the torque is repeatable, the profile of the instantaneous oscillations is unique for each of the three tests. The peaks and valleys on the graphs do not align perfectly. This phenomenon on a micro-scale may result from several factors:
  - Non-deterministic initial conditions: The meshing phase of the individual pumps at the moment of switching is random (i.e., whether the teeth are in a "pumping" or "transition" phase at the moment a new pump is connected).
  - Minimal differences in valve dynamics: Microsecond-level differences in the response time of the solenoid coils in successive cycles can lead to a slightly different shape of the pressure wave.
  - Influence of temperature and oil viscosity: Changes in oil temperature between successive tests affect its viscosity, which in turn changes the characteristics of vibration damping and pressure wave propagation in the system.

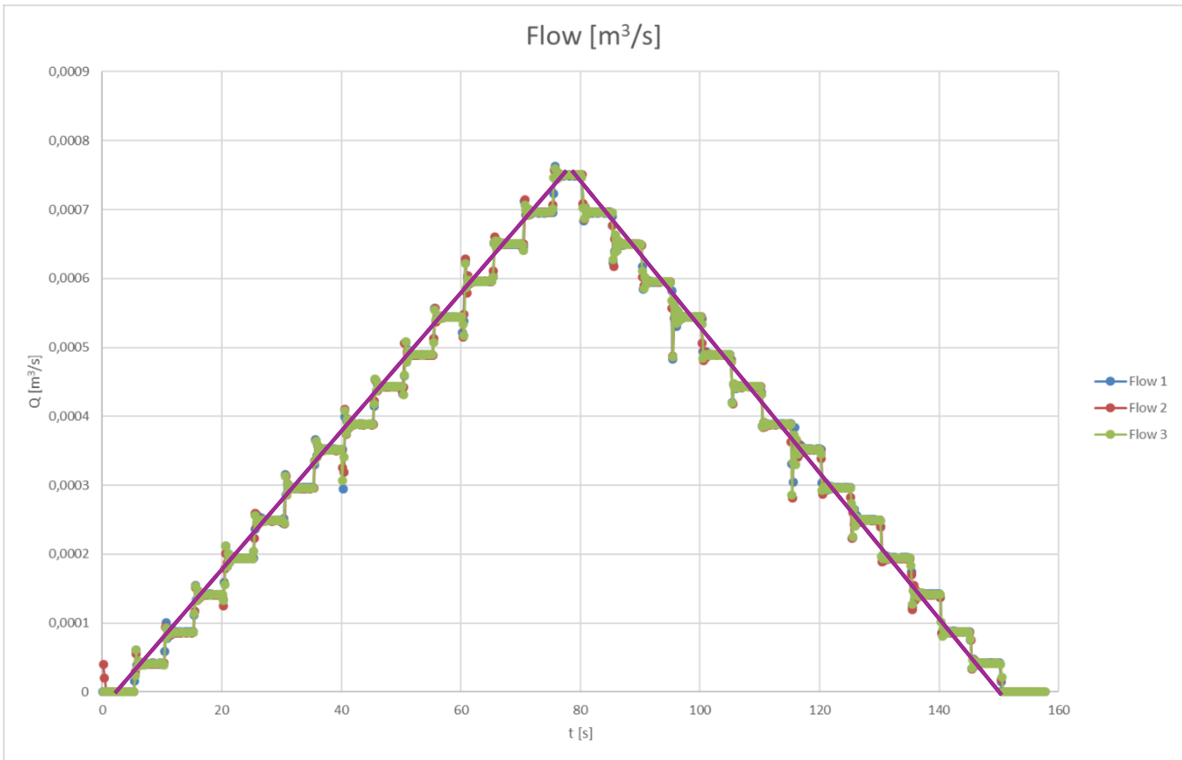

Figure 34. Flow rate of 1st experimental test CS (control signal defined in Table 3).

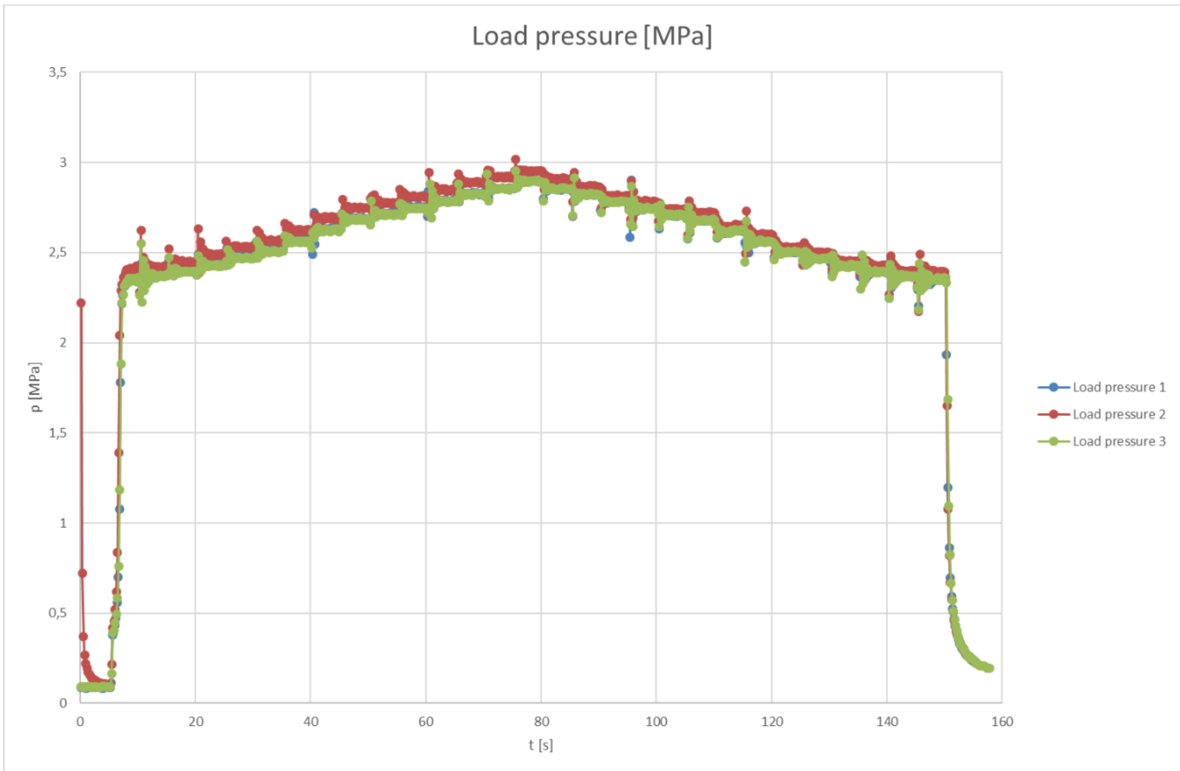

Figure 35. Load pressure of 1st experimental test (defined in Table 3).

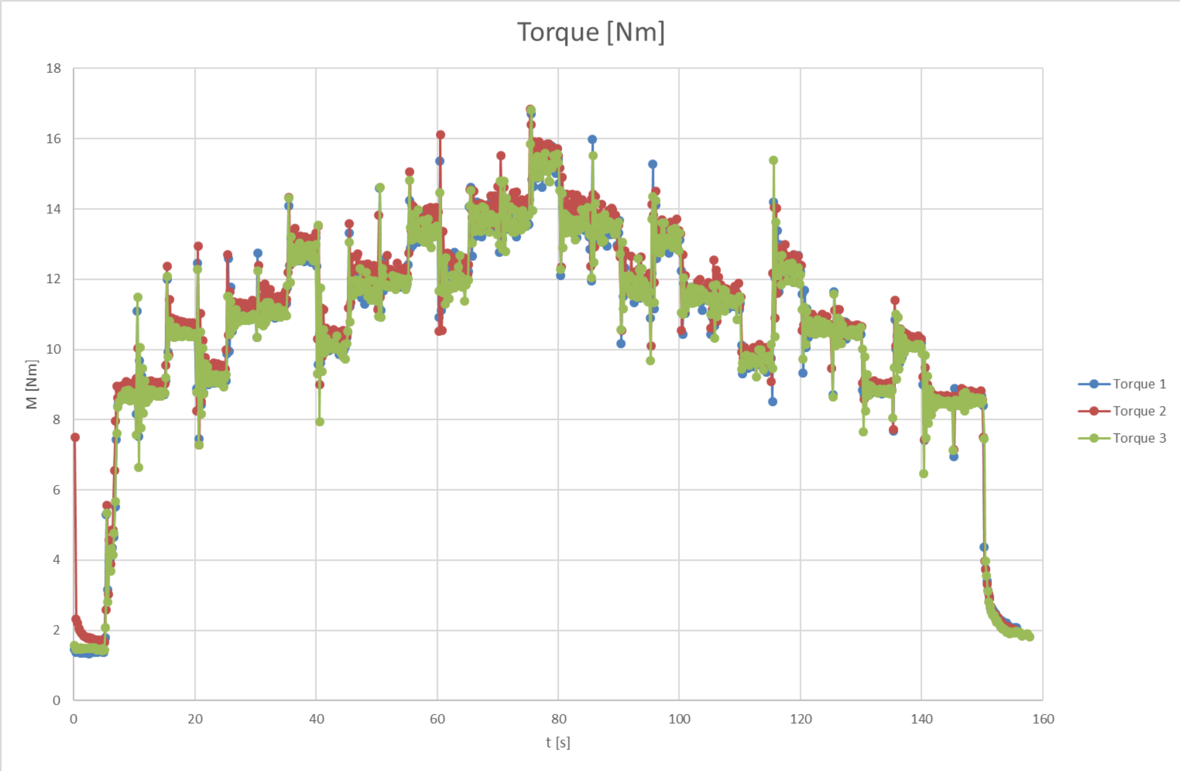

Figure 36. Torque of 1st experimental test (defined in Table 3).

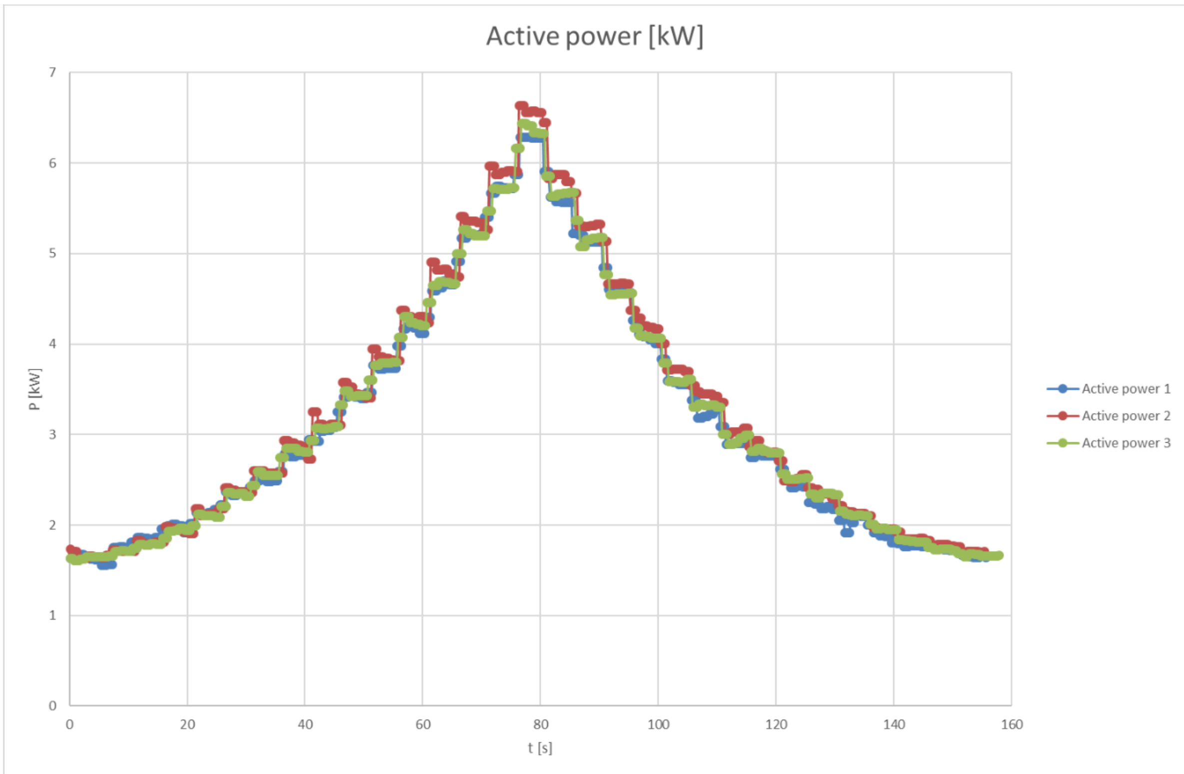

Figure 37. Active power of 1st experimental test (defined in Table 3).

Summary of a conducted experiment with three repetitions:

- High Macroscopic Repeatability: The system exhibits very good repeatability in the control of key output parameters (flow rate and active power consumption), which can attest to its reliability in executing set work cycles.
- Characteristic Torque Dynamics: The results confirm that an inherent feature of the digital transmission's operation is the generation of significant, high-frequency torque pulsations. This is a fundamental difference compared to the "smooth" operation of ideal systems with axial-piston pumps.
- Filtering of Oscillations by the Drive System: The comparison of the noisy torque graph with the very smooth active power graph shows that the inertia of the rotating masses (shaft, coupling, electric motor rotor) act as a low-pass filter, which effectively "smooths out" the rapid mechanical pulsations.

7.3 Experimental Results for Scenario No. 1 (Load 5.7 MPa)

The presented set of four graphs (Fig.38 to Fig.41) documents the key operating parameters of the digital hydrostatic transmission in response to the first test scenario (symmetrical profile), this time at a constant load pressure of 5.7 MPa. The analysis of these results, including a comparison of the three test repetitions, allows for an assessment of the system's behavior under increased load.

Similar to the test at a lower pressure, the system exhibits very high repeatability on a macroscopic scale. The profiles from the three successive tests for flow rate (Fig. 38) and active power (Fig. 41) almost perfectly overlap, which once again demonstrates the precision and reliability of the digital control of the pump operating sequence. The load pressure (Fig. 39) also stabilizes, although in this case, the fluctuations around the mean value are slightly more visible than at the 2.8 MPa load

A comparison of the current results with the test at 2.8 MPa allows for key conclusions regarding the influence of load on the transmission's operation.

- Increase in Power and Torque: As expected, the average steady-state torque has increased up to approx. 20-22 Nm (from approx. 16 Nm), and the peak active power has increased up to approx. 7.8 kW (from previous 6.5 kW). This is a direct verification of the energy relations in hydrostatic systems.

- Decrease in Flow Rate: A very important observation is the slight but noticeable decrease in the maximum flow rate (Fig. 38) compared to the test at a lower pressure. This is the combined effect of two phenomena:
    - Decrease in rotational speed: The higher required torque causes a slight "lugging" of the drive motor, which operates at a minimally lower rotational speed.
    - Increase in volumetric losses: The higher operating pressure causes greater internal leakages in the pumps, which further reduces the effective delivery rate.

The most important conclusions again come from the analysis of the torque profile (Fig. 40):

• Increase in Oscillation Amplitude: Although the overall profile is repeatable, the instantaneous torque oscillations are unique for each test. Crucially, a visual analysis suggests that the amplitude of these oscillations is greater at a pressure of 5.7 MPa than at 2.8 MPa. This means that higher operating pressure not only raises the average required torque but also intensifies the pulsations and mechanical shocks in the system.

• Filtering by the Drive System: Despite the intensified mechanical torque oscillations, the profile of the active power (Fig. 41) consumed by the motor remains extremely smooth and repeatable. This confirms once again that the inertia of the drive system and the control algorithms of the frequency converter effectively filter these rapid load changes, stabilizing the energy consumption from the grid.

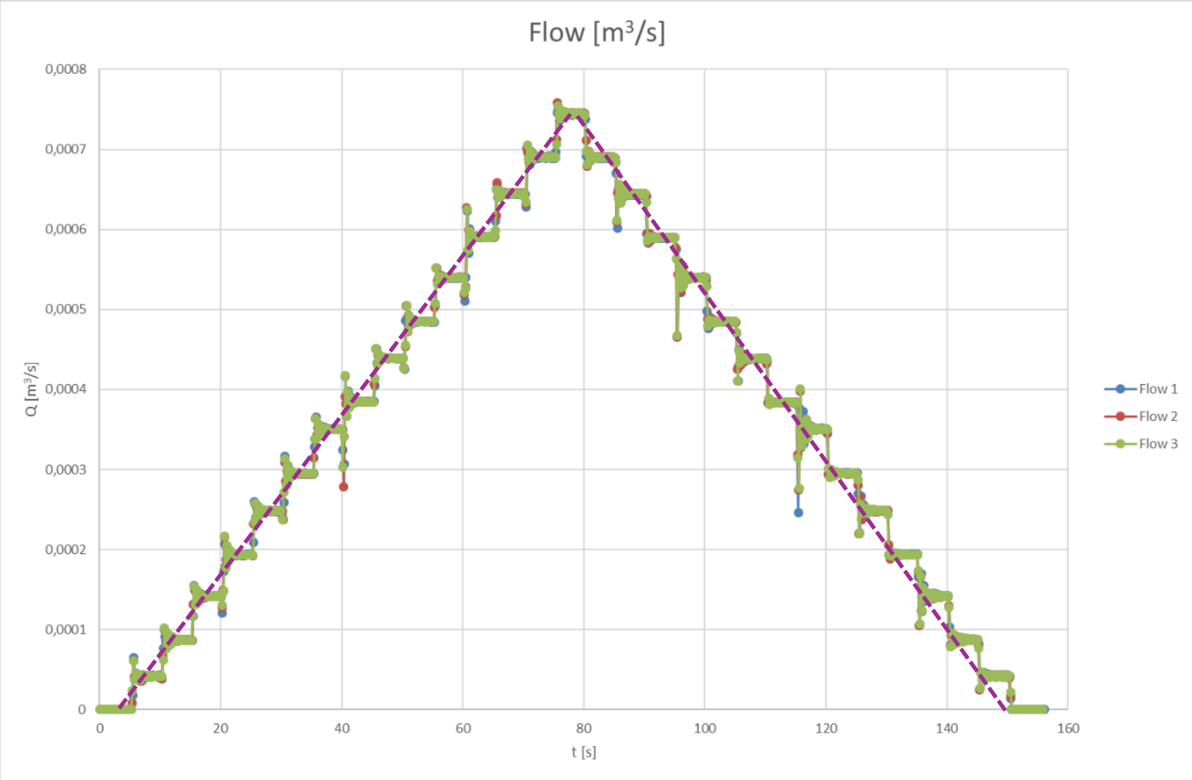

Figure 38. Flow rate of 1st experimental test 5,7 MPa (defined in Table 3).

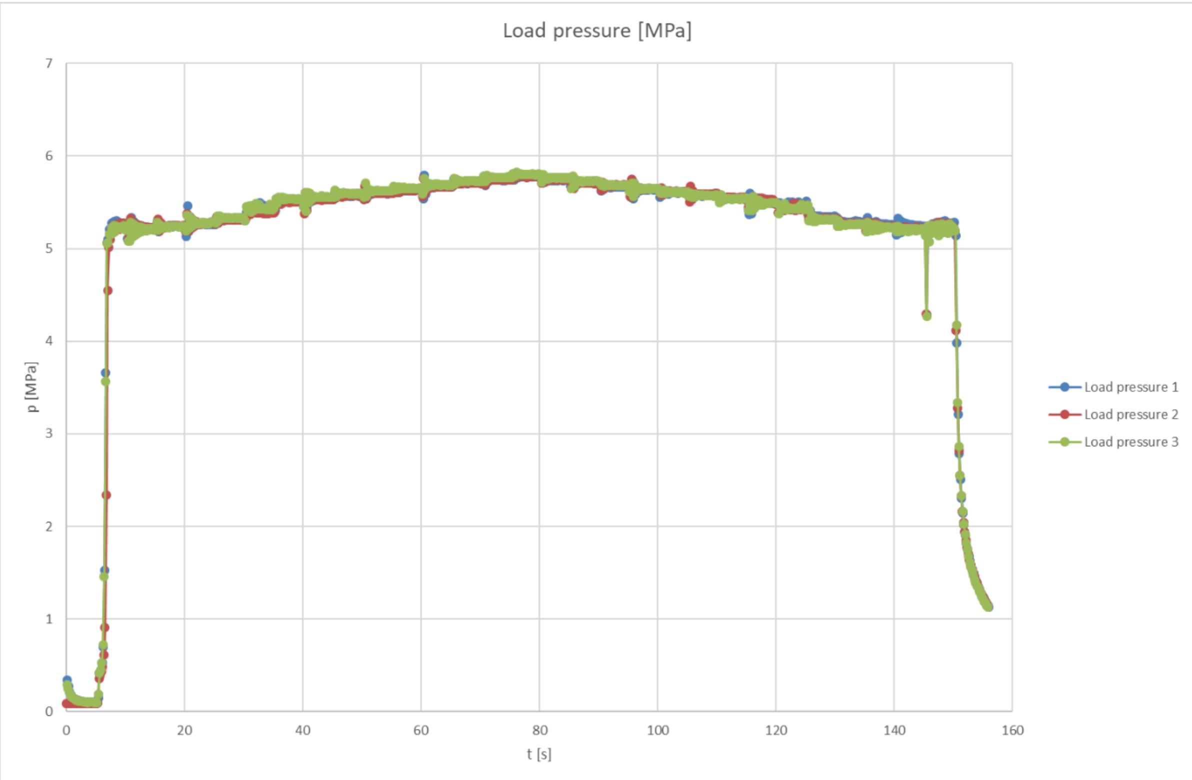

Figure 39. Load pressure of 1st experimental test 5,7 MPa (CS defined in Table 3).

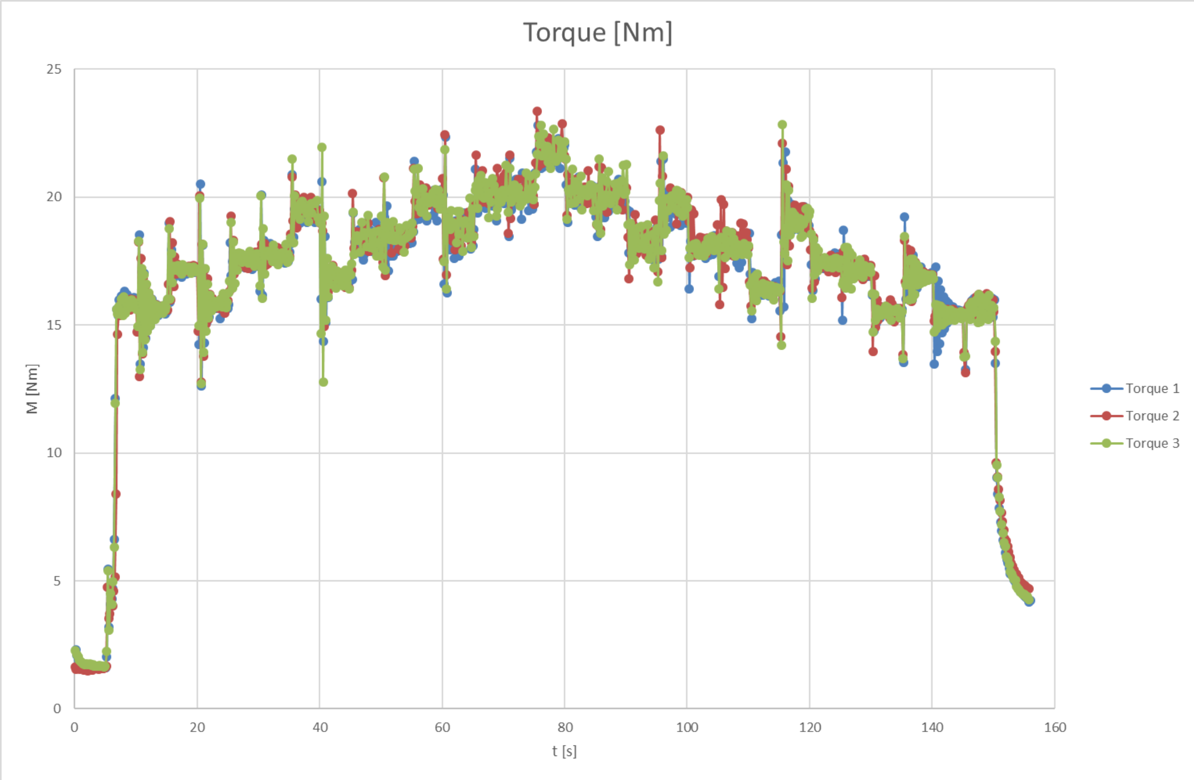

Figure 40. Torque of 1st experimental test 5,7 MPa (defined in Table 3).

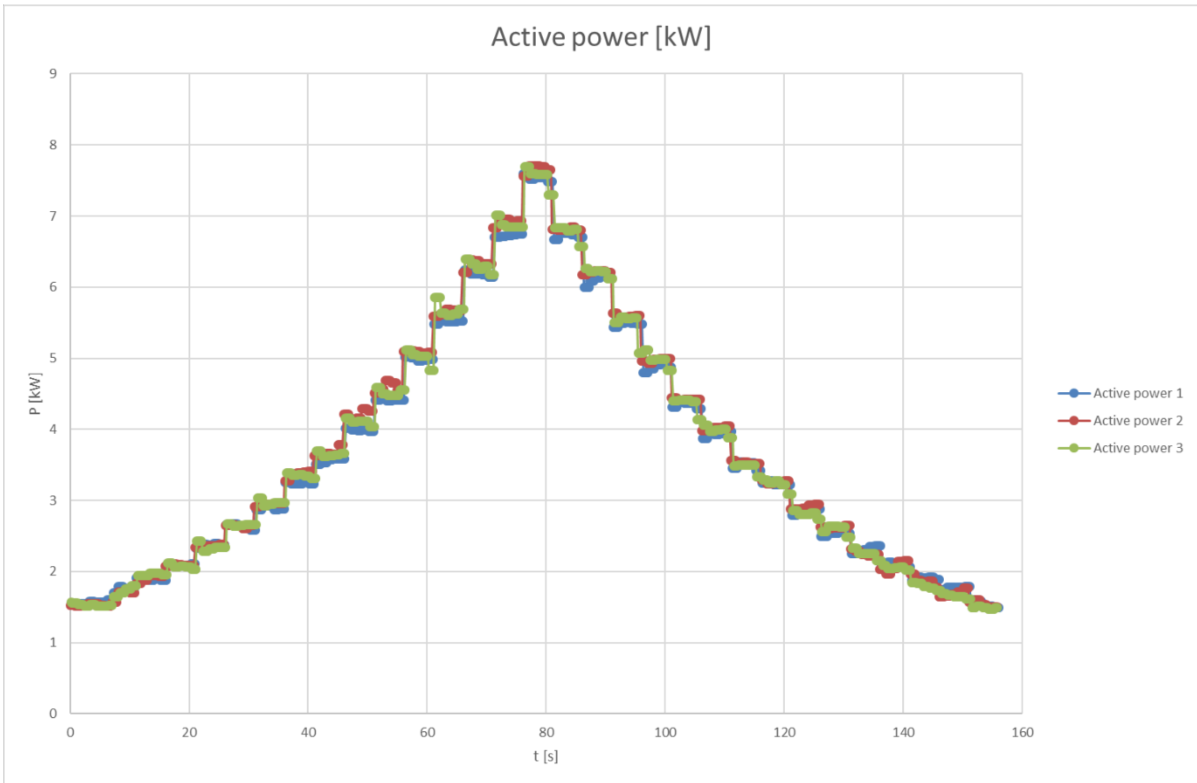

Figure 41. Active power of 1st experimental test 5,7 MPa (defined in Table 3).

The experiment conducted at a load pressure of 5.7 MPa confirms the relationships observed at lower loads and provides new, key information.

• Confirmation of Dependencies: The system behaves in a predictable manner an increase in load leads to a proportional increase in the required torque and power.

• Identification of Performance Decrease: Higher pressure causes a slight decrease in the maximum flow rate, which is an effect of both the drive motor's characteristics and increasing volumetric losses.

• Intensification of Dynamic Phenomena: The key conclusion is that higher operating pressure intensifies the dynamic torque pulsations, which increases the fatigue loads on the mechanical components and may have an impact on the generated noise and vibration. This is a fundamental characteristic of the studied digital transmission.

7.4 Experimental Results for Scenario No. 1 (Load 10 MPa)

The presented set of four graphs (Fig.42 to Fig. 45) documents the operating parameters of the digital hydrostatic transmission for the first test scenario (symmetrical profile) at a load pressure of 10 MPa.

The system continues to exhibit very good repeatability on a macroscopic scale, which is visible on the graphs of flow rate (Fig. 42) and active power (Fig. 45). The profiles from the three successive repetitions largely overlap, which attests to the stability and reliability of the digital control. Concurrently, on the pressure (Fig. 43) and torque (Fig. 44) graphs, it is evident that as the load increases to 10 MPa, the differences between the individual trials become more noticeable, especially in the range of fluctuations.

Operation at a pressure of 10 MPa highlights the trends observed in previous tests and allows for further conclusions to be drawn:

- Increase in Power and Torque: As predicted by theory, operation at a significantly higher pressure requires a proportionally greater torque (Fig. 44) and power (Fig. 45). The average steady-state torque increased to approx. 28-32 Nm, and the peak active power reached 10 kW.
- Decrease in Performance (Flow Rate): The flow rate (Fig. 42) graph shows a further, distinct decrease in maximum output compared to the tests at lower pressures, reaching a peak of approx. 0.00073 m^3/s. This phenomenon is now more pronounced and is the combined effect of a greater drop in the drive motor's rotational speed under the high load torque and significantly larger volumetric losses (leakages), which are directly proportional to the pressure.

The analysis of the profiles on a micro-scale, especially for torque and pressure, provides key information about the system's operation under high load.

- Intensification of Torque Oscillations: The torque (Fig. 44) graph shows that the high-frequency oscillations are the most intense among all tests conducted so far. Their amplitude is clearly larger, and the peaks reach values of over 35 Nm. This confirms the conclusion that an increase in operating pressure not only raises the average mechanical load but also significantly intensifies the dynamic shock loads, which has a direct impact on material fatigue and component durability.
- Pressure Fluctuations and Drop: On the pressure (Fig. 43) graph, a slight but systematic drop in pressure can be observed in the second part of the steady-state phase (from approx. 110s). This may suggest the influence of thermal phenomena- the oil loses viscosity, which in turn increases internal leakages and leads to a slight drop in pressure at a constant output.
- Stability of the Drive System: Despite the extremely "noisy" and dynamic profile of the mechanical torque, the active power (Fig. 45) graph remains smooth and highly repeatable. This is definitive proof of the effectiveness of the drive system in "filtering" the mechanical pulsations.

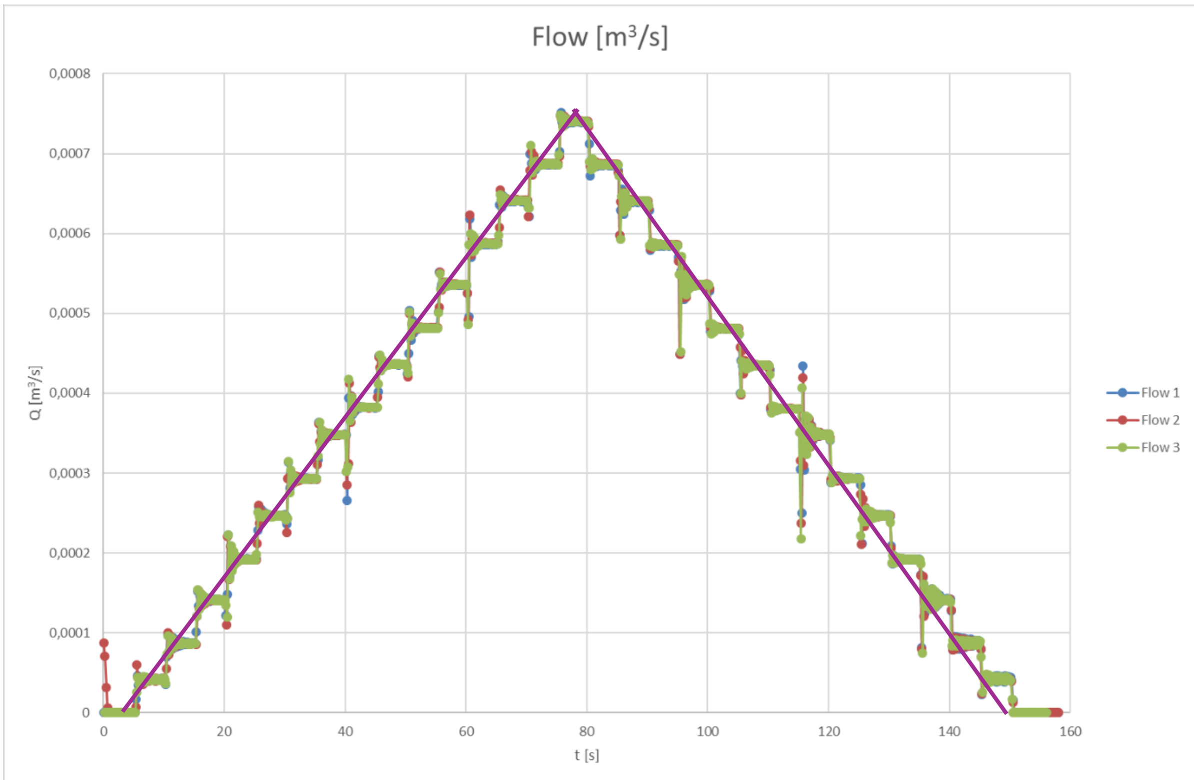

Figure 42. Flow rate of 1st experimental test 10 MPa (defined in Table 3).

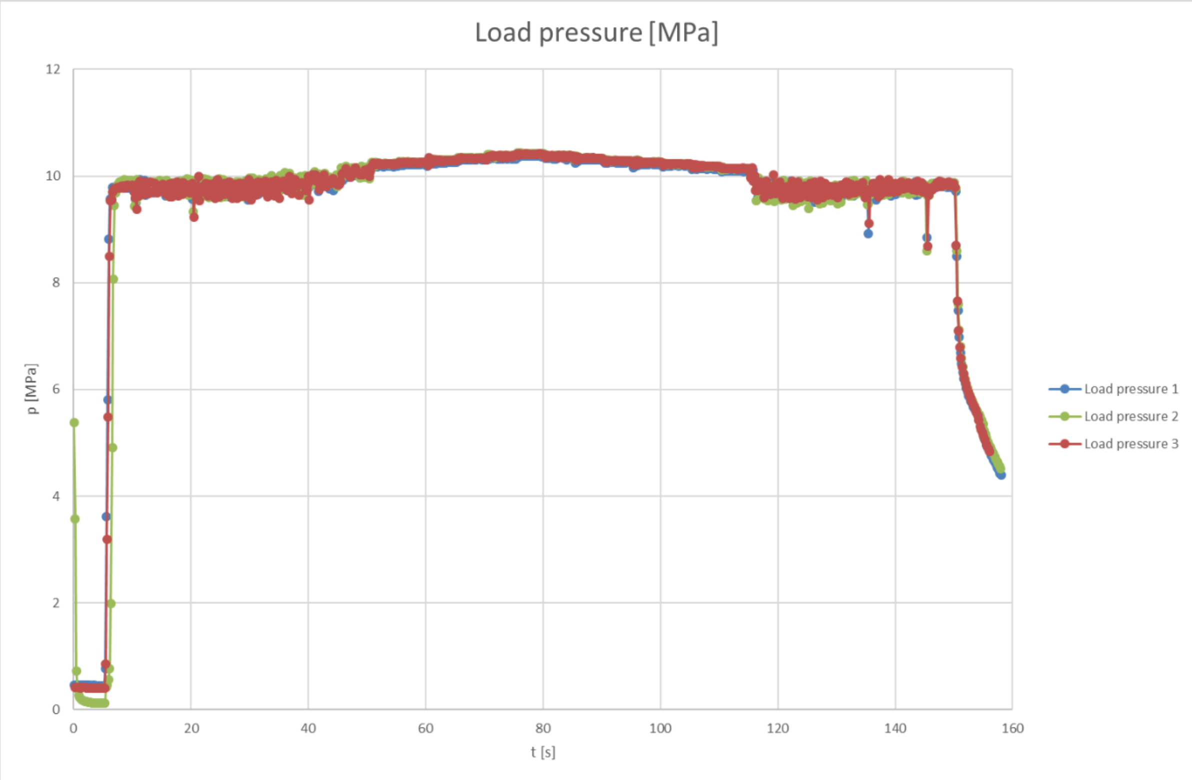

Figure 43. Load pressure of 1st experimental test 10 MPa (defined in Table 3).

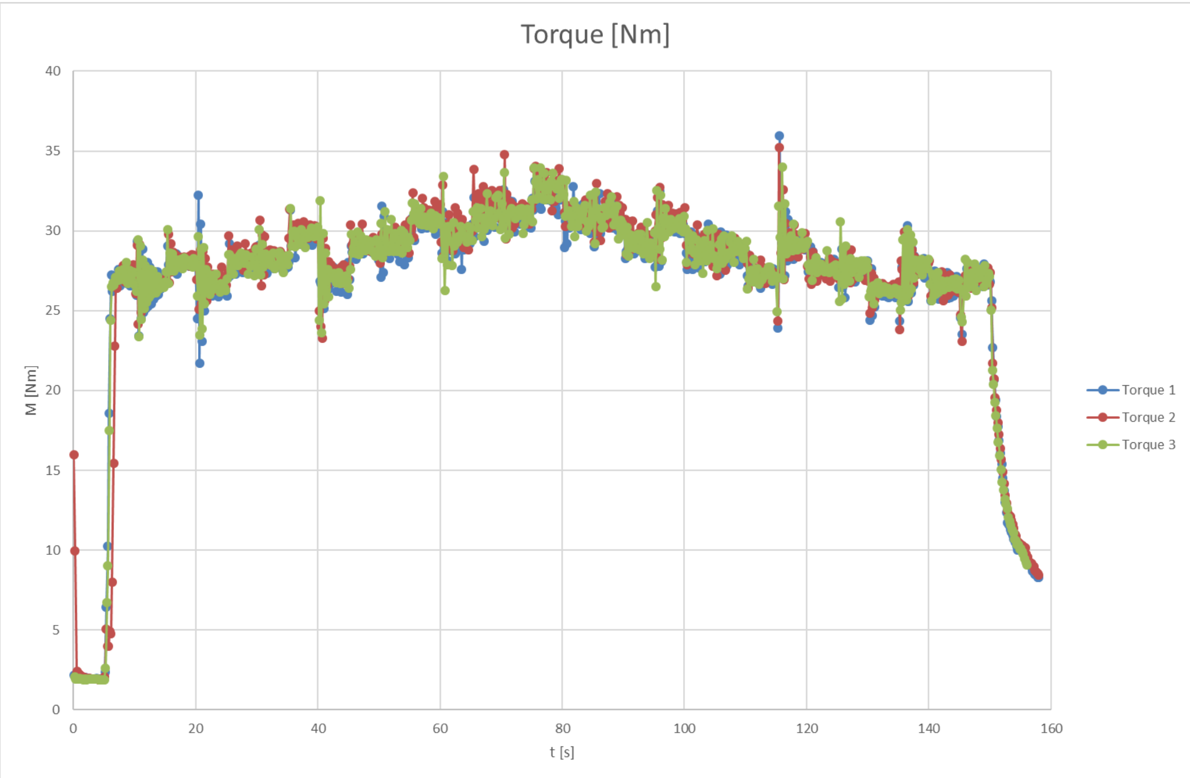

Figure 44. Torque of 1st experimental test 10 MPa (defined in Table 3).

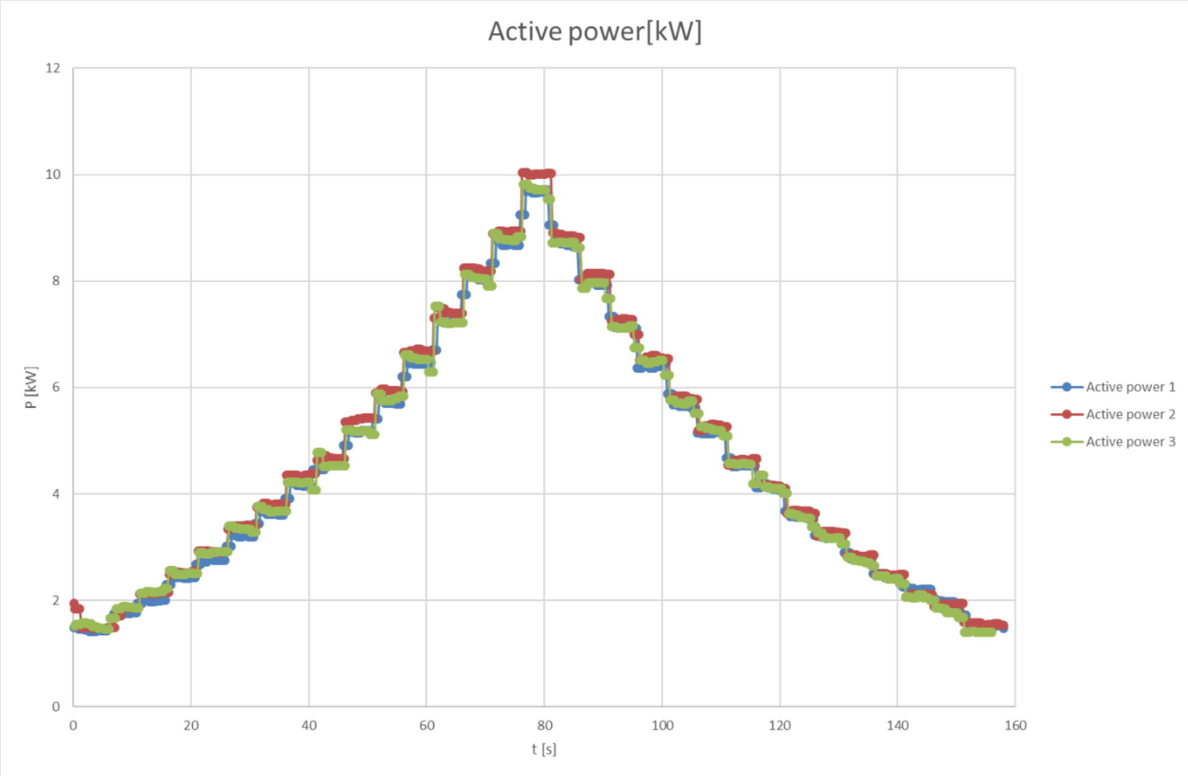

Figure 45. Active power of 1st experimental test 10 MPa (defined in Table 3).

Conclusions from the experiment conducted at a load pressure of 10 MPa for 1st testing load:

- Confirmation and Intensification of Trends: This test confirms and strengthens all trends observed at lower pressures: a proportional increase in power and torque demand, a decrease in flow rate, and an intensification of dynamic pulsations.
- Identification of Performance Limits: The distinct drop in flow rate and the intensified oscillations indicate that the system is approaching its practical limits of performance and stability (due to the maximum power of the electric motor).
- Key Importance of Dynamics: The analysis unequivocally proves that the greatest challenge in digital technology is dynamic phenomena. While the system is capable of operating under high static pressure, the pulsations generated in the process are a key factor that must be considered in the mechanical design and durability assessment of the hydrostatic transmission.

7.5 Experimental Results for Scenario No. 2 (Load 1.2 MPa)

The presented set of four graphs (Fig. 46 to Fig. 49) documents the operating parameters of the digital hydrostatic transmission in response to the second test scenario. This profile is characterized by the generation of a series of separate flow pulses with a step-increasing amplitude. The analysis of results from two independent test repetitions allows for the assessment of the system's behavior under dynamic, intermittent loads and for the verification of its repeatability.

All four analyzed parameters flow rate (Fig. 46), load pressure (Fig. 47), torque (Fig. 48) and active power (Fig. 49) faithfully replicate the pulsating nature of the control. The system correctly executes a series of pulses with increasing amplitude, which demonstrates the proper functioning of the digital control. The macroscopic repeatability is good—both test profiles have the same shape and similar values. However, a slight but systematic difference between the two repetitions can be observed. The "Load pressure 1" profile maintains a constant, slightly higher level than "Load pressure 2". This difference in pressure directly translates to higher values for "Active power 1" compared to "Active power 2". This may result from minimal differences in conditions between the tests, e.g., a slightly different oil temperature affecting its viscosity and pressure losses.

The most important and striking conclusion from this analysis is the characteristic of the torque profile (Fig. 48).

- Comparison with Simulation: In contrast to the "flat" torque pulses obtained in the simulation model for the same scenario, the experimental results show a completely different phenomenon. Each torque pulse begins with a sharp, very high peak, which exceeds the torque value in the steady-state phase of the pulse.
- Physical Interpretation: These torque peaks are not a measurement error. They are a real, dynamic mechanical load, resulting from the necessity to immediately overcome the fluid's inertia and rapidly build up pressure from zero at the beginning of each pulse. This is a classic example of a hydraulic shock, which manifests as a short-term but very large load on the drive shaft.
- Micro-Scale Repeatability: As in the previous experiment, the exact shape and amplitude of these peaks and subsequent oscillations are unique for each repetition. This confirms that dynamic phenomena of high frequency have a non-deterministic element, dependent on the instantaneous conditions in the system.

The comparison of the torque graph (Fig. 48) with the active power graph (Fig. 49) is extremely important. Despite the occurrence of short-term torque peaks reaching over 20 Nm, the active power profile is much smoother. Only slight overshoots are visible on it at the beginning of each pulse. This phenomenon proves once again that the drive system (the electric motor with its inertia and the VFD controller) acts as an effective mechanical filter. It absorbs and smooths out the sharp, short-term mechanical jolts, so they do not translate into equally sharp spikes in power consumption from the electrical grid.

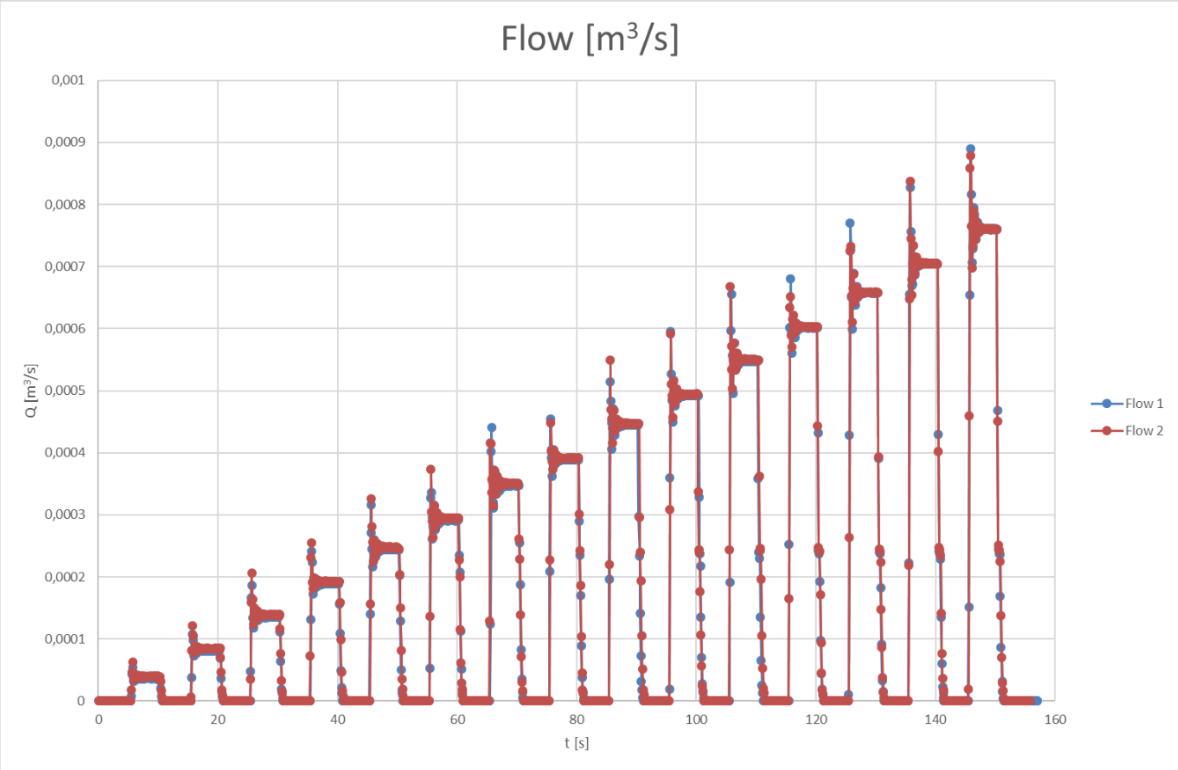

Figure 46. Flow rate of 2nd experimental tests 1,2 MPa CS (control signal defined in Table 4).

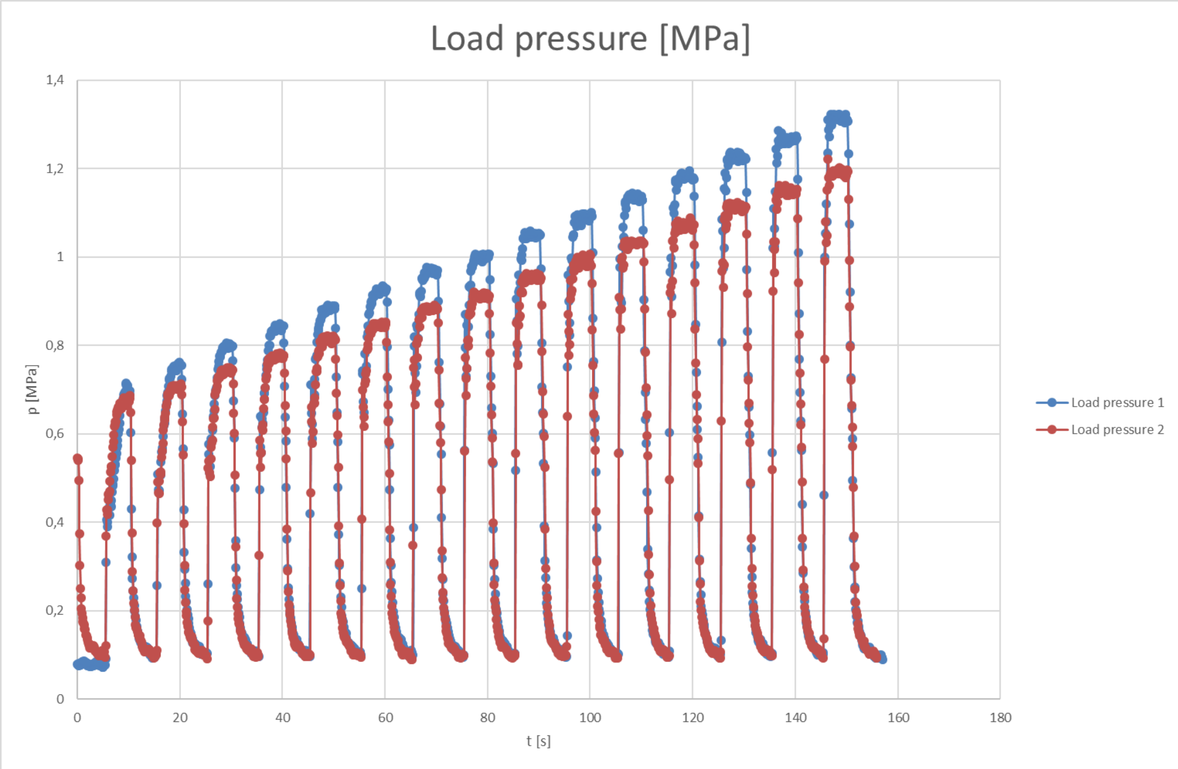

Figure 47. Load pressure of 2nd experimental tests 1,2 MPa (defined in Table 4).

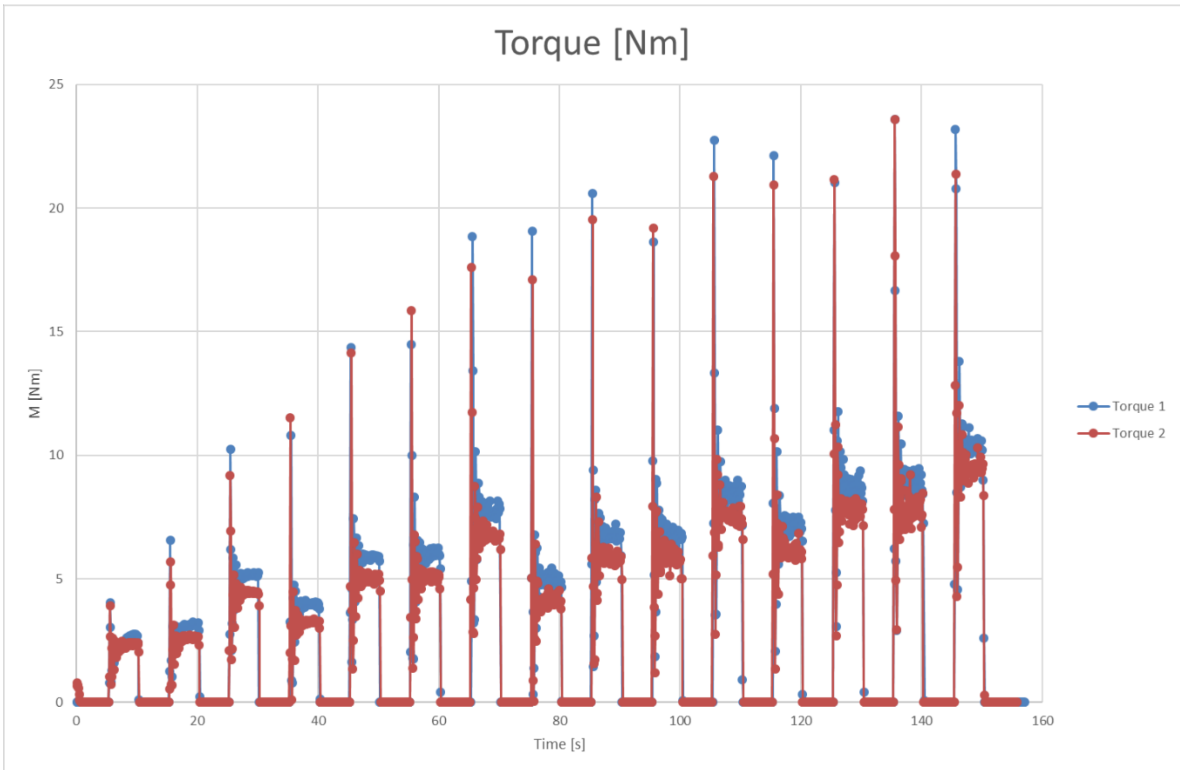

Figure 48. Torque of 2nd experimental tests 1,2 MPa (defined in Table 4).

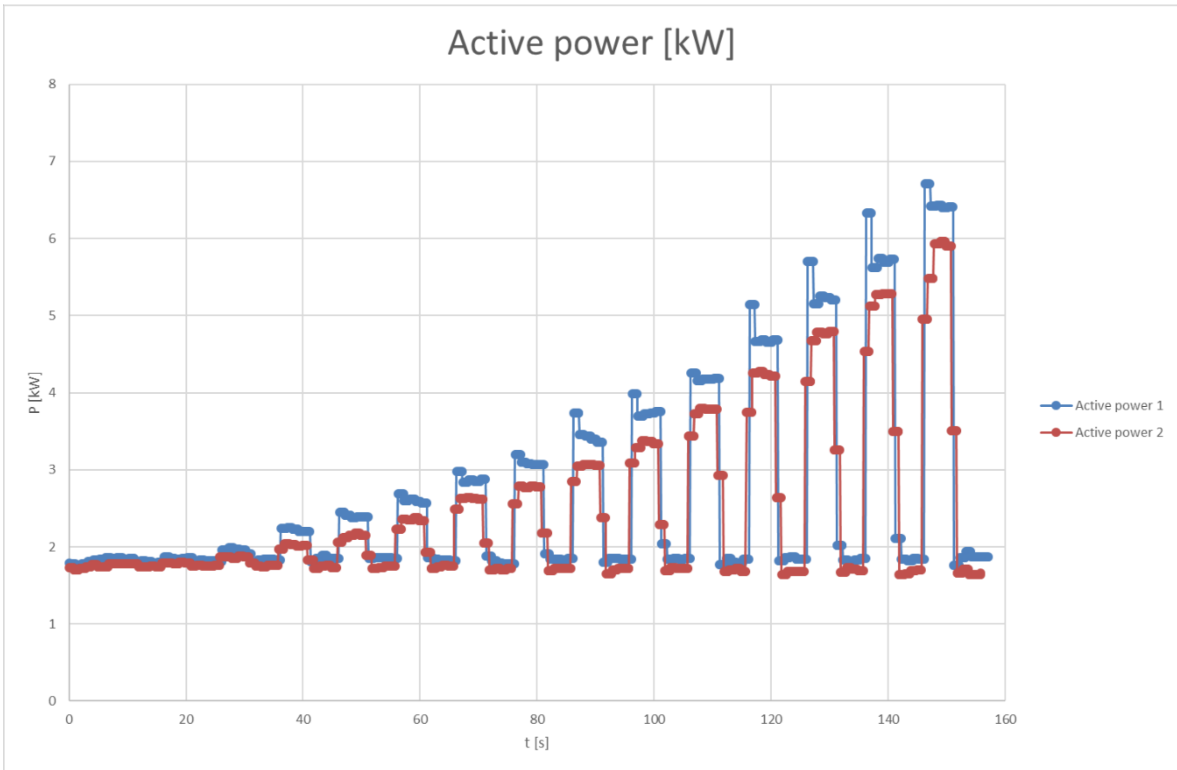

Figure 49. Active power of 2nd experimental tests 1,2 MPa (defined in Table 4).

Conclusions from the experiment conducted under pulsating operating conditions:

- Identification of Shock Loads: The most important discovery is the existence of very high, transient torque peaks at the beginning of each flow activation cycle. This is critical information for assessing the fatigue life of the shaft, coupling, and other mechanical components.
- Role of the Drive System: The experiment confirms the key role of the electric motor as an element that dampens and filters sharp mechanical load pulsations, which is fundamental for the stability of the entire system.

7.6 Experimental Results for Scenario No. 2 (Load 6 MPa)

The presented set of four graphs (Fig. 50 to Fig. 53) documents the operating parameters of the digital hydrostatic transmission in response to the second test scenario (pulsating operation with increasing amplitude) at a load pressure of 6 MPa. This analysis, especially in the context of previous tests at lower pressures, allows for an assessment of the system's behavior under higher, dynamic load.

The system continues to exhibit very good macroscopic repeatability, as seen on the graphs of flow rate (Fig. 50) and active power (Fig. 53). The two successive test repetitions follow the same pulsating control profile, which indicates the reliability of the control logic. Similar to previous tests, a slight but systematic difference can be observed between the "1" and "2" profiles on the pressure and power graphs, which likely results from minimal changes in operating conditions between the tests.

Operation at a pressure of 6 MPa highlights and reinforces the trends observed at lower loads.

- Increase in Power and Torque: As expected from theory, operation under increased pressure demands an increased torque (Fig. 52) and power (Fig. 53) proportionally. The average steady-state torque in the final pulses is approx. 20-22 Nm, and the peak active power reaches approx. 8.5 kW.
- Decrease in Performance (Flow Rate): The flow rate (Fig. 50) graph shows that the maximum output is slightly lower than in the test at 1.2 MPa. This is the combined effect of the drive motor's speed drop under the high load torque and the increase in volumetric losses (leakages), which are significantly greater at a pressure of 6 MPa.

The most important conclusions come from the analysis of the torque profile (Fig. 52) under high pressure.

- Comparison with Simulation and Previous Tests: This profile differs from the "flat" simulation results and represents an intensification of the phenomenon observed in the test at 1.2 MPa. Each torque pulse begins with a sharp peak, whose amplitude is now even greater and reaches over 30 Nm.
- Physical Interpretation: Such high torque peaks are a real, dynamic shock load, which is greater the higher the pressure the system must overcome at the moment of flow activation. This is proof that the mechanical loads in the system do not scale in a simple linear fashion dynamic phenomenon (hydraulic shocks) intensify at higher pressures.
- Micro-Scale Repeatability: It is again visible that the exact shape and amplitude of the torque peaks and subsequent oscillations are unique for each repetition, which confirms the non-deterministic nature of these phenomena.

The comparison of the torque graph (Fig. 52) with the active power graph (Fig. 53) at a pressure of 6 MPa is extremely telling. Despite the occurrence of huge, short-term torque peaks (over 30 Nm), the active power profile remains relatively smooth, with only minor overshoots. This confirms once again the key role of the drive system's inertia as an effective mechanical filter.

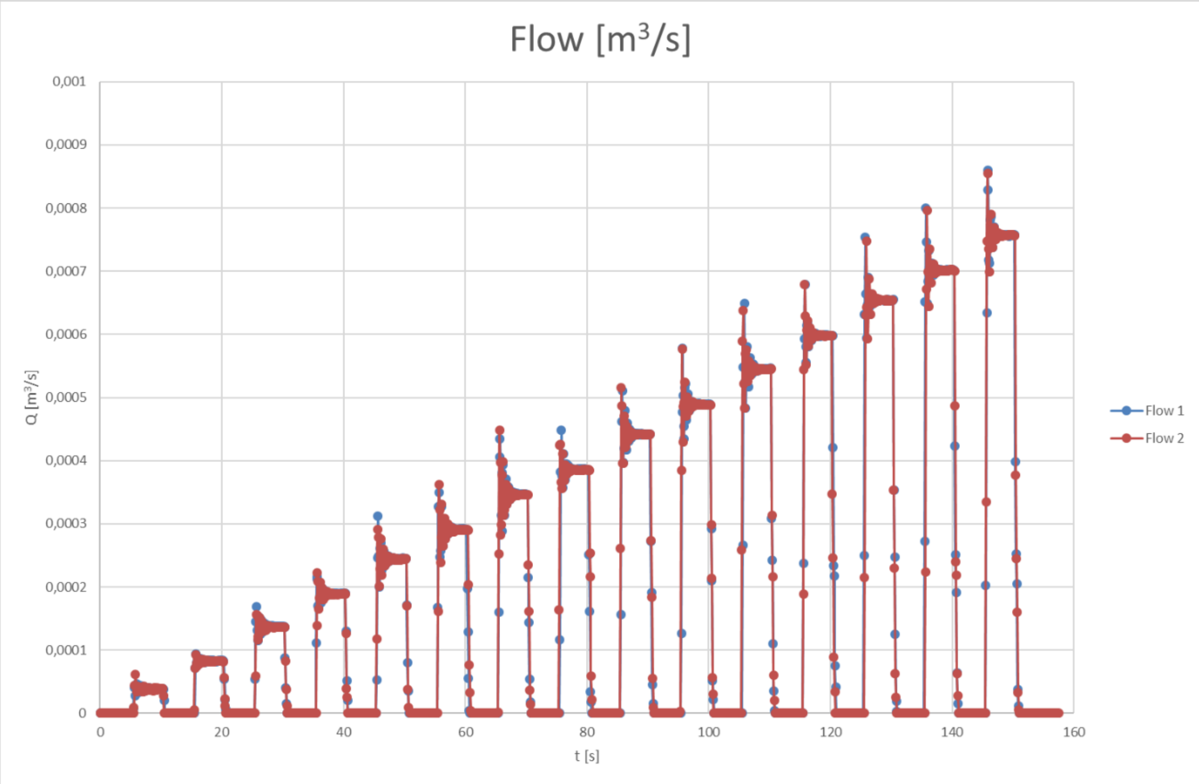

Figure 50. Flow rate of 2nd experimental tests 6 MPa (defined in Table 4).

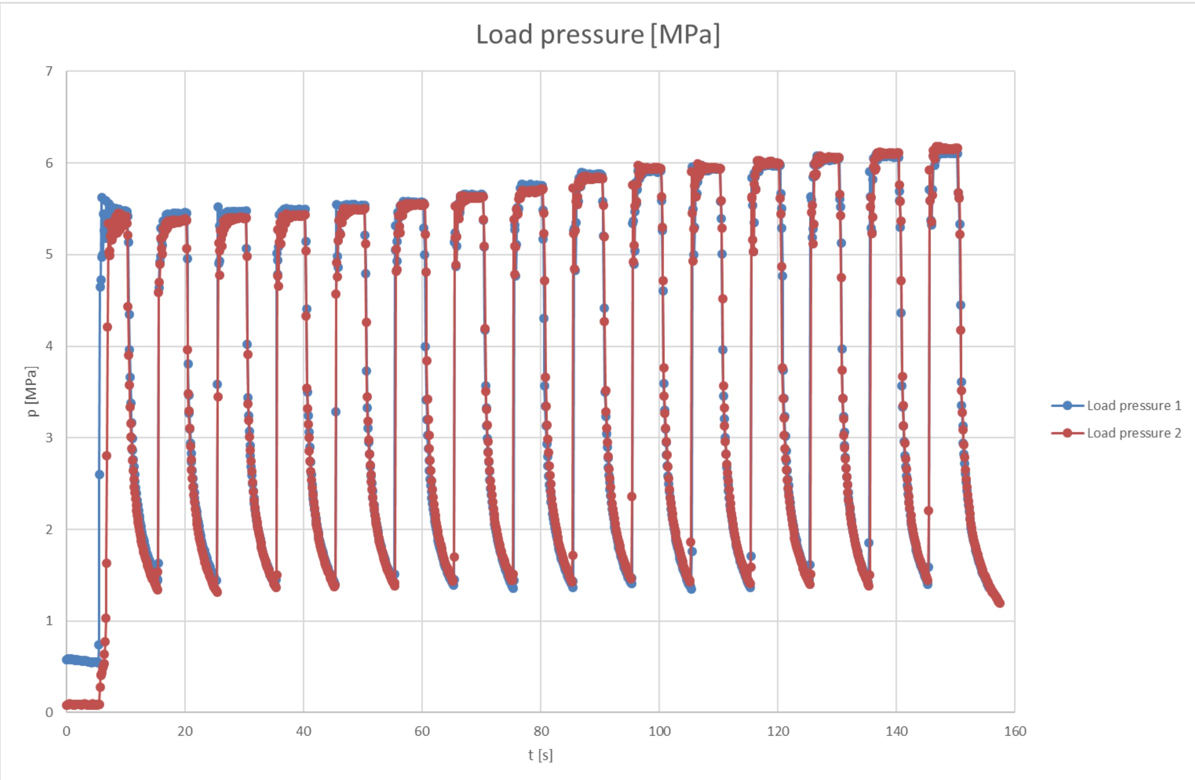

Figure 51. Load pressure of 2nd experimental tests 6 MPa (defined in Table 4).

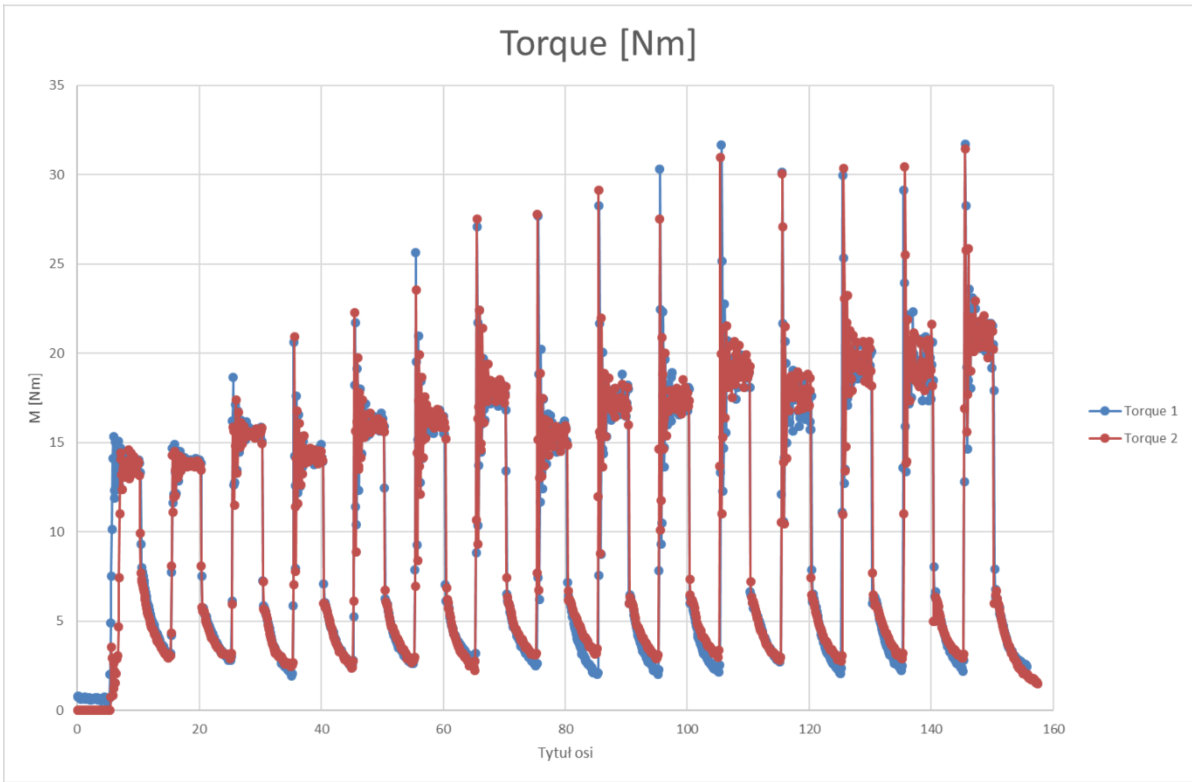

Figure 52. Torque of 2nd experimental tests 6 MPa (defined in Table 4).

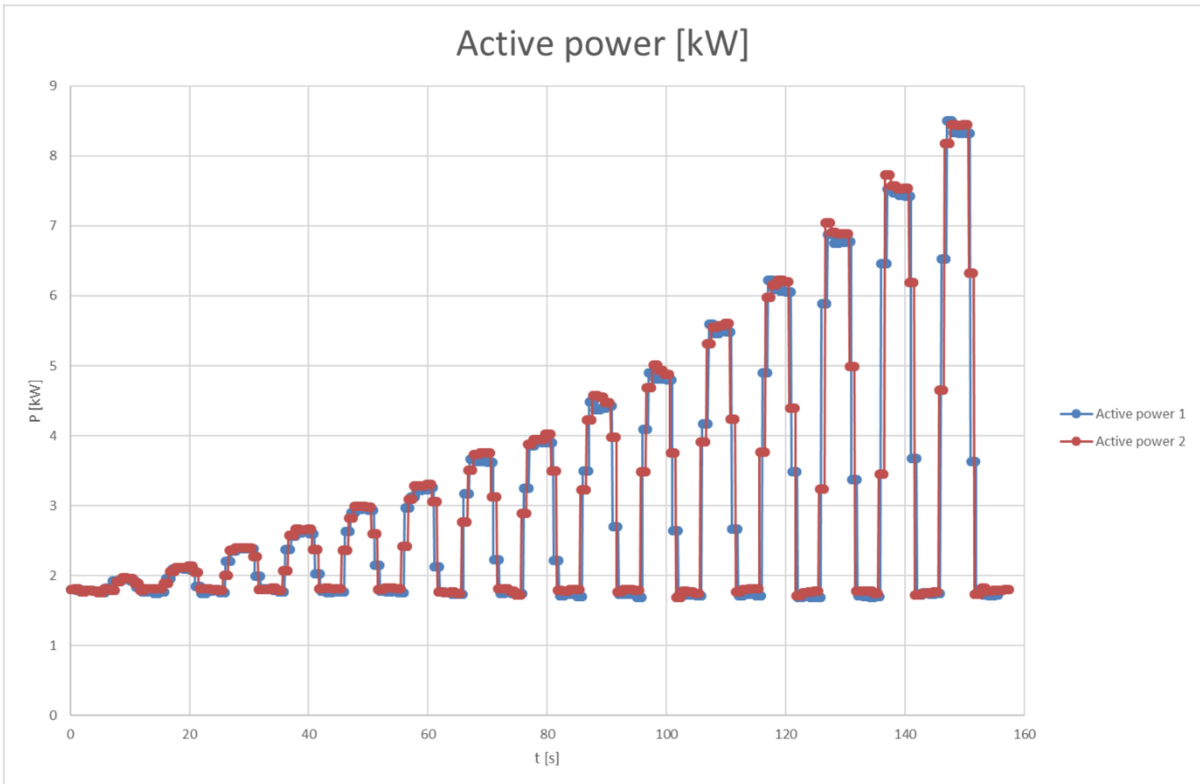

Figure 53. Active power of 2nd experimental tests 6 MPa (defined in Table 4).

Conclusions from the experiment conducted at a pressure of 6 MPa:

- Confirmation of Dependencies: The system behaves in a predictable manner an increase in load leads to a proportional increase in the required torque and power and to a slight decrease in flow rate.
- Identification of Critical Loads: The key discovery is the fact that the transient torque peaks, generated at the beginning of each cycle, are much more severe at higher operating pressures. It is these shock loads, and not the steady-state load, that pose the greatest challenge to the fatigue life of the mechanical components of the system.

7.7 Experimental Results for Test Scenario 3 (Load 1.2 MPa)

The presented set of four graphs (Fig. 54 to Fig. 57) documents the key operating parameters of the digital hydrostatic transmission in response to the Test Scenario 3. This profile is characterized by a trapezoidal shape, simulating a work cycle with a ramp-up phase, a steady-state phase, and a ramp-down phase, at a constant load pressure of approx. 1.2 MPa. The analysis of results from three independent test repetitions allows for an assessment of the system's behavior under continuous load and for the verification of its repeatability.

All four analyzed parameters faithfully replicate the trapezoidal character of the commanded cycle. We observe a ramp-up phase (approx. 0 - 6s), a steady-state phase (approx. 6 - 17s), and a ramp-down phase (after 17s). On a macroscopic scale, the system exhibits very good repeatability, which is particularly visible on the graphs of flow rate (Fig. 54) and active power (Fig. 55). The profiles from the three successive tests largely overlap, which attests to the precision of the digital control. The pressure (Fig. 55) and torque (Fig. 56) graphs also follow the same trend, although they show greater variability on a micro-scale.

The most characteristic element, which is the "fingerprint" of the digital technology, is the stepped nature of the profiles. It is perfectly visible on the active power (Fig. 57) and flow rate (Fig. 54) graphs during the ramp-up and ramp-down phases. These distinct "steps" are not an error but a reflection of the control strategy, which consists of sequentially engaging successive pumps with fixed displacement to achieve a quasi-smooth change in the total flow.

Similar to previous analyses, key conclusions regarding the system's dynamics come from the analysis of the torque profile (Fig. 56).

- Nature of the Torque Profile: Even in the steady-state phase, where flow and pressure are relatively constant, the torque profile is very "dynamic" and full of sharp, high-frequency oscillations. This is the physical result of the summation of pressure and flow pulsations generated by the meshing process in each of the simultaneously operating gear pumps.

- Micro-Scale Repeatability: Although the average steady-state torque value (approx. 8-10 Nm) is repeatable, the instantaneous oscillations are unique for each of the three tests. This confirms once again that the system's micro-dynamics have a non-deterministic element, dependent on instantaneous conditions, such as the mutual phase of the gearings of the individual pumps.

The comparison of the torque graph (Fig. 56) with the active power graph (Fig. 57) is extremely important. Even though sharp, mechanical torque oscillations occur on the drive shaft, the profile of the active power drawn from the grid by the motor is extremely smooth and stable (with distinct, but stable, steps).

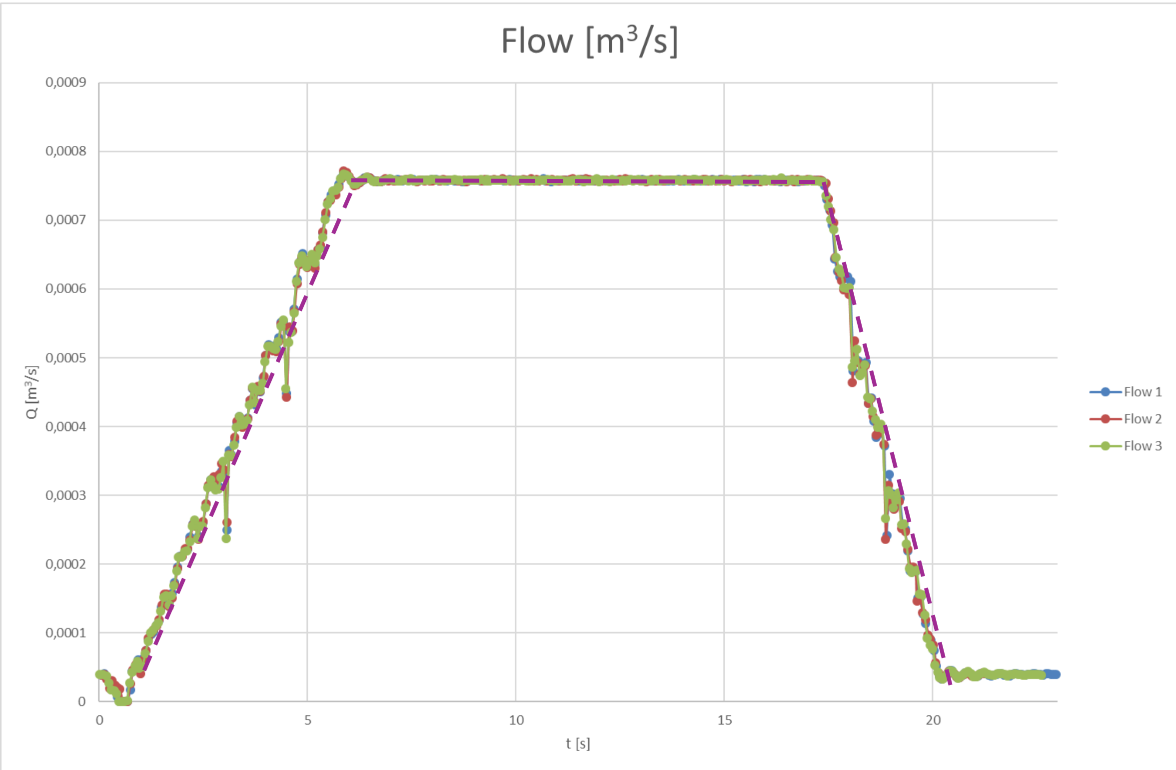

Figure 54. Flow of 3rd experimental tests 1,2 MPa CS (control signal defined in Table 5).

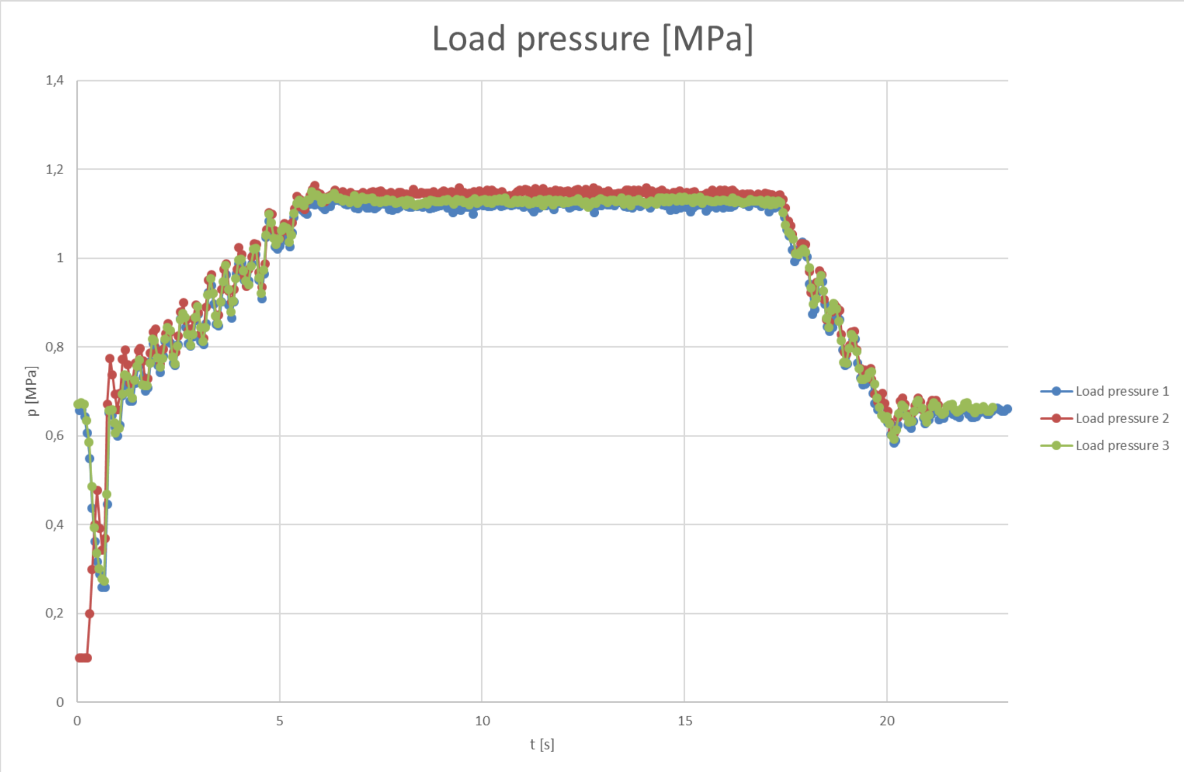

Figure 55. Load pressure of 3rd experimental tests 1,2 MPa (control signal defined in Table 5).

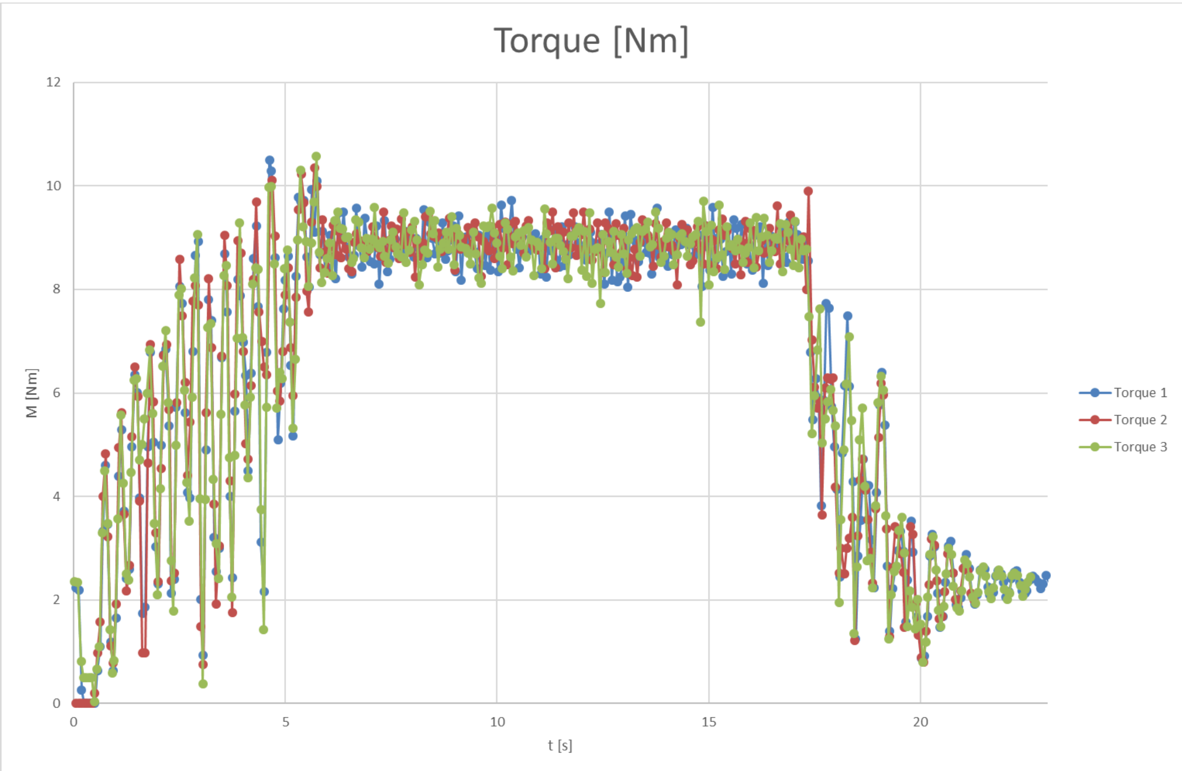

Figure 56. Torque of 3rd experimental tests 1,2 MPa (control signal defined in Table 5).

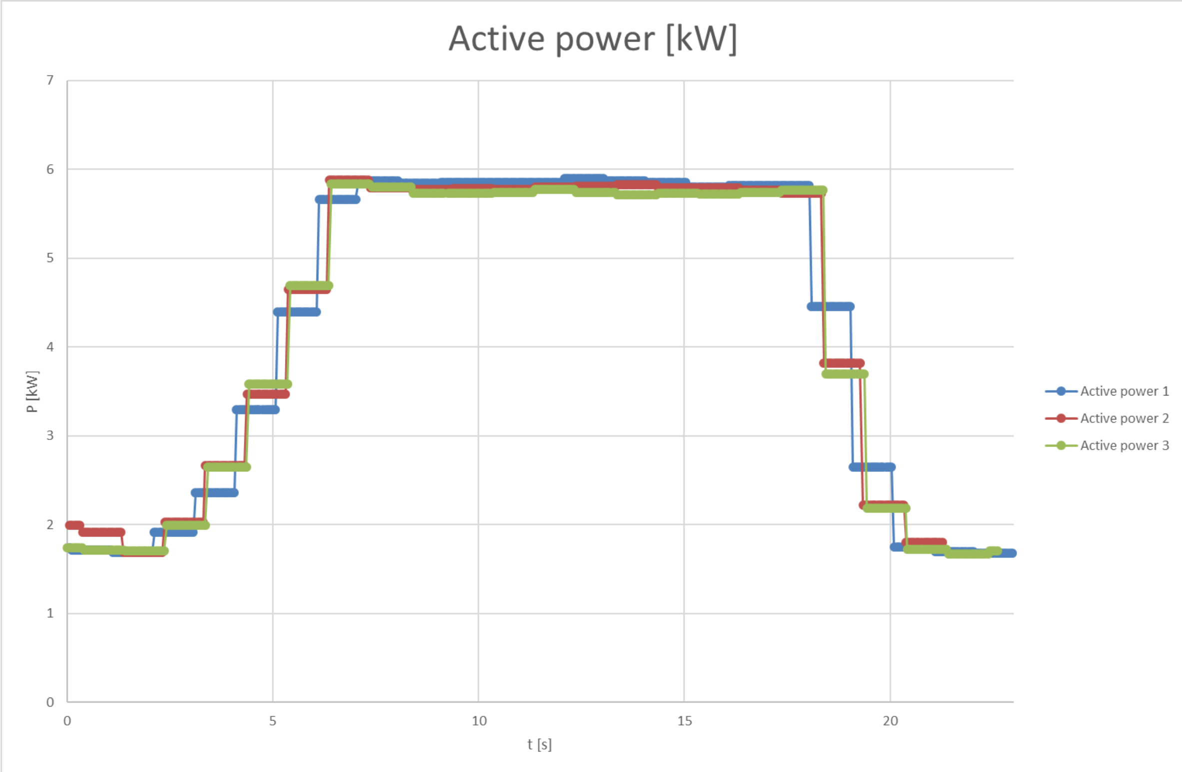

Figure 57. Active power of 3rd experimental tests 1,2 MPa (control signal defined in Table 5).

Conclusions from the experiment for the Test Scenario 3 at a pressure of 1.2 MPa:

- The digital system is able to precisely and repeatably execute complex, multi-phase work cycles, such as the trapezoidal profile.
- A key discovery is the fact that even during steady-state operation, the system generates significant, high-frequency torque pulsations. This is an inherent feature of the multi-pump digital system's operation.

7.8 Experimental Results for Test Scenario 3 (Load 1.6 MPa)

The presented set of four graphs (Fig. 58 to Fig. 61) documents the key operating parameters of the digital hydrostatic transmission in response to the Test Scenario 3 (trapezoidal profile) at a load pressure of 1.6 MPa. The analysis of results from three independent test repetitions allows for an assessment of the system's behavior under a slightly increased load compared to the previous test (1.2 MPa).

The system continues to execute the commanded trapezoidal work cycle, which is visible on all graphs. In the steady-state phase (approx. 7-17s), parameters such as flow rate (Fig. 58) and active power (Fig. 61) exhibit very good repeatability, with the profiles from the three tests almost perfectly overlapping. However, the most important observation in this dataset is the problem with repeatability during the ramp-up phase. The pressure graph (Fig. 59) clearly shows that one of the tests (the red line, "Load pressure 2") is characterized by a much slower pressure build-up in the initial phase of the cycle (0-5s) compared to the other two trials.

The increase in load pressure from 1.2 MPa to 1.6 MPa results in predictable changes in the operating parameters:

- Increase in Power and Torque: As expected from theory, running at higher pressure requires more torque (Fig. 60) and power (Fig. 61). The average steady-state torque increased to approx. 10 Nm (from approx. 8-10 Nm), and the peak active power reached approx. 7 kW (previously approx. 6 kW).

This dataset is particularly interesting due to the observed anomaly in repeatability.

- Problem with Pressure Ramp-up: The significantly slower pressure build-up in the second test (red line) may result from:
  - A momentary fault or delay of one of the control valves (DV) in the early stage of the sequence, which caused one of the initial pumps not to be connected to the system on time.
  - Differences in the initial conditions of the test, e.g., a lower oil temperature, which increased its viscosity and flow resistance at the beginning of the cycle.
- Correlation with Other Parameters: This problem is not a measurement artifact of the pressure transducer. The torque (Fig. 60) and power (Fig. 61) graphs show that the red lines ("Torque 2" and "Active power 2") also exhibit a slower ramp-up in the same initial phase of the test, which is a direct consequence of the slower build-up of the hydraulic load.
- Torque Oscillations in Steady State: Despite the problems in the ramp-up phase, in the steady-state phase, the torque profile (Fig. 60) is again characterized by strong, high-frequency, and non-deterministic oscillations, which is a constant feature of this system.

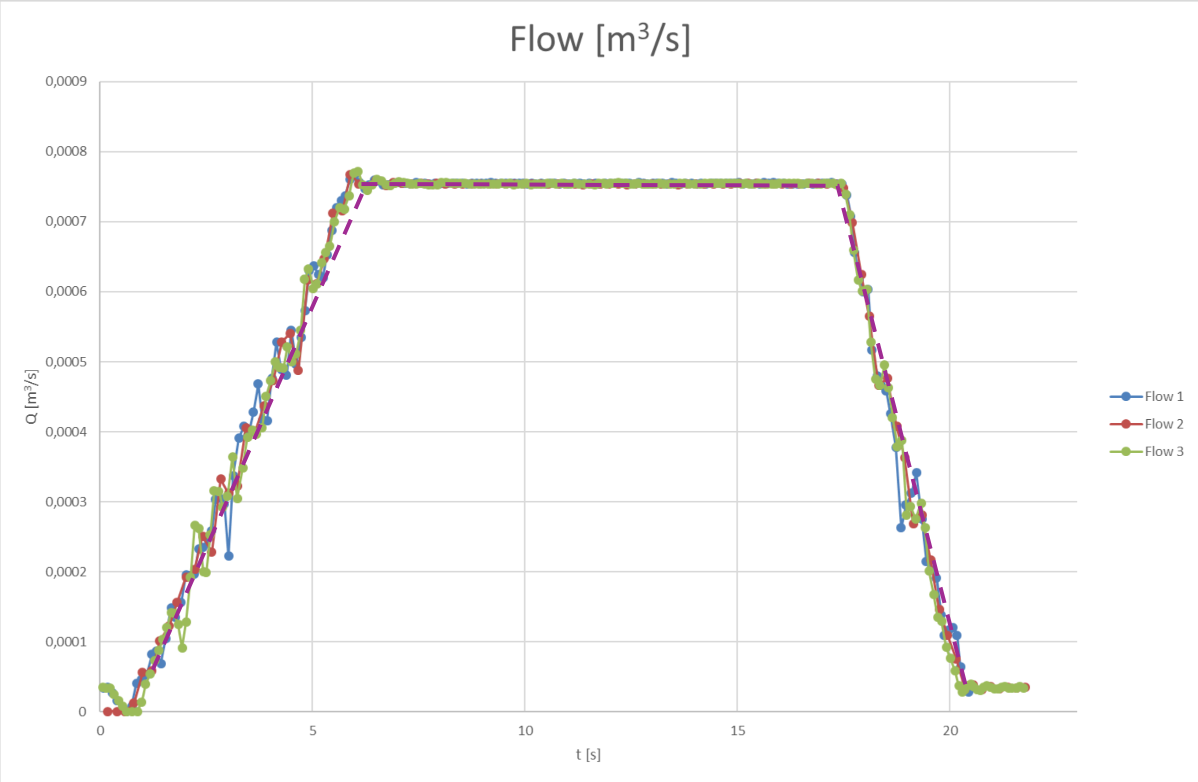

Figure 58. Flow of 3rd experimental tests 1,6 MPa (control signal defined in Table 5).

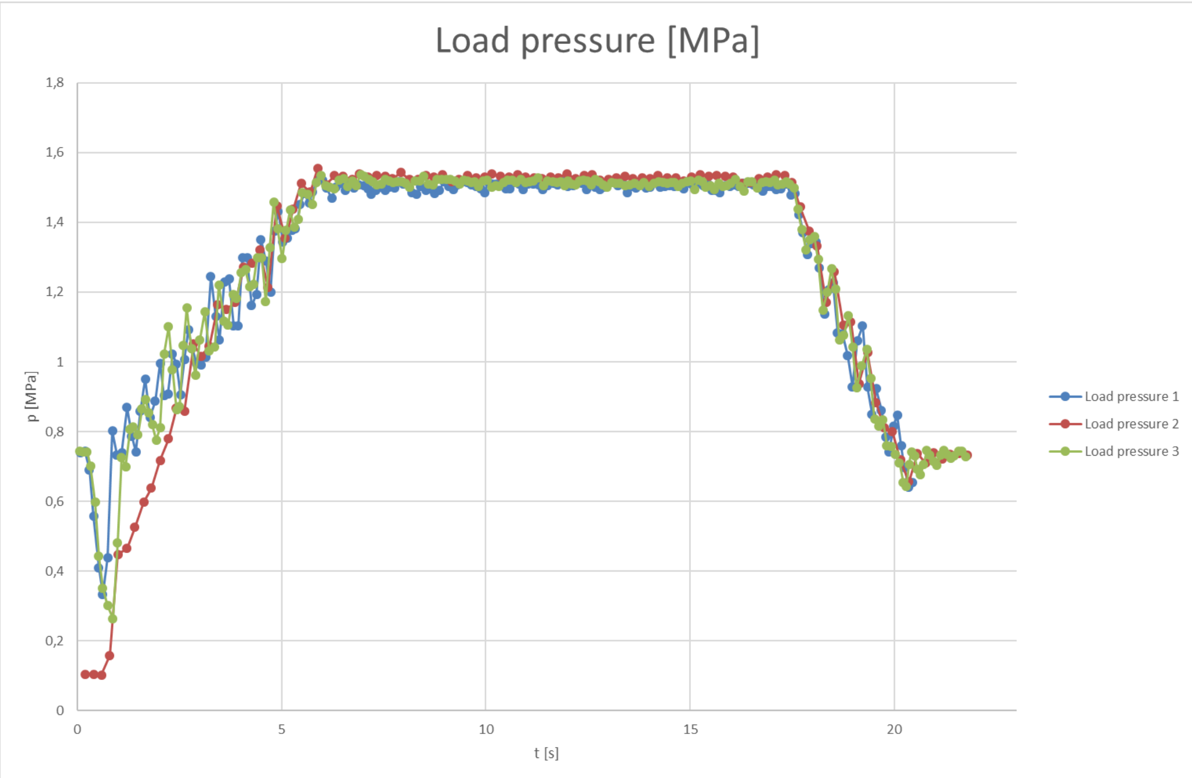

Figure 59. Load pressure of 3rd experimental tests 1,6 MPa (control signal defined in Table 5).

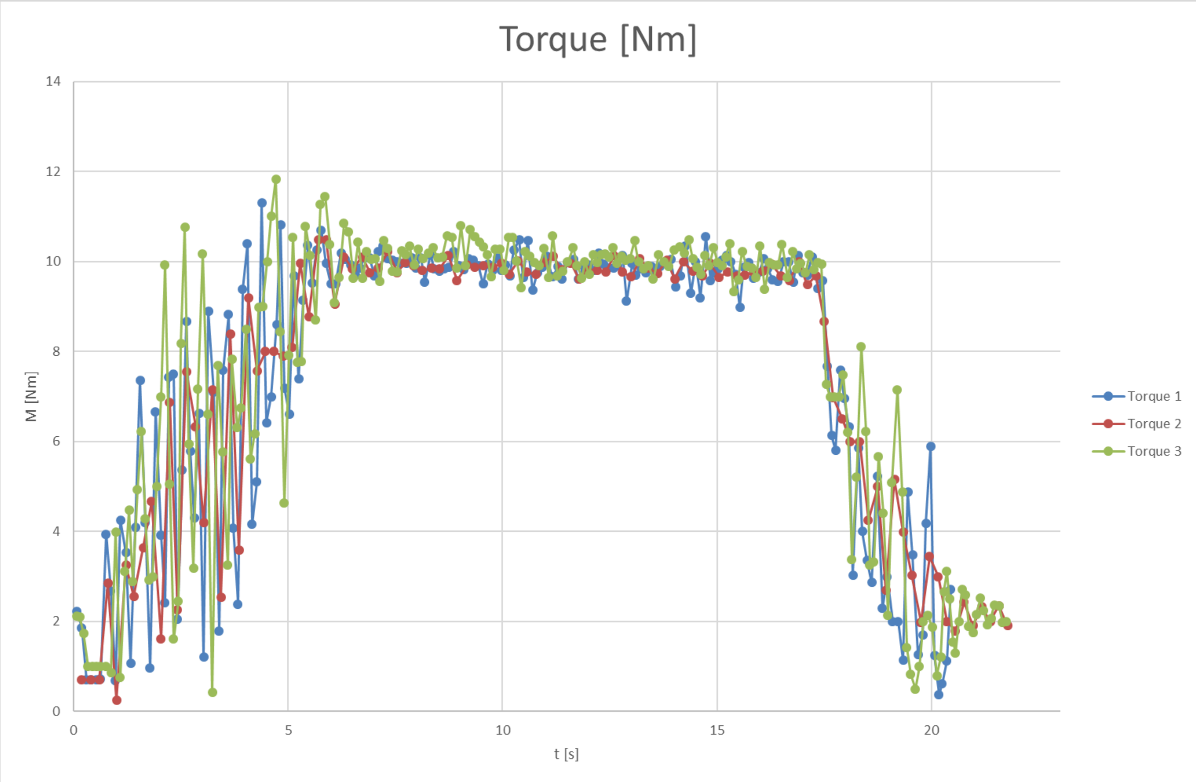

Figure 60. Torque of 3rd experimental tests 1,6 MPa (control signal defined in Table 5).

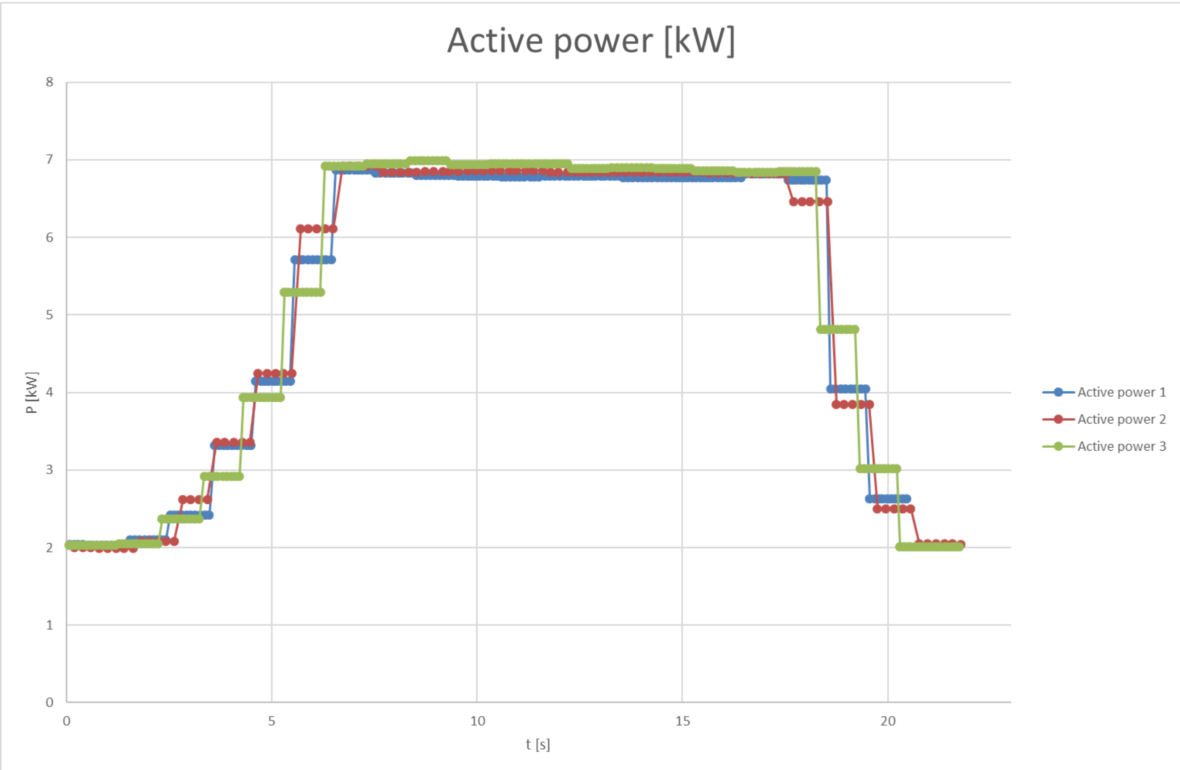

Figure 61. Active of 3rd experimental tests 1,6 MPa (control signal defined in Table 5).

Conclusions from the experiment for the Test Scenario 3 at a pressure of 1.6 MPa:

- The system exhibits good repeatability of operation under steady-state conditions, maintaining the set parameters with minor deviations.
- A key discovery is the fact that the load ramp-up phase is sensitive to potential disturbances, which manifested in one of the tests as a much slower pressure increase. This highlights the importance of the reliability and precision of the control valves' operation in digital systems.
- The test confirms that even a slight increase in operating pressure leads to a proportional increase in the required torque and power, in accordance with basic physical laws.
- The system generates significant torque pulsations, which remains its fundamental characteristic distinguishing it from classic systems.

7.9 Experimental Results for Test Scenario 3 (Load 9 MPa)

The presented set of four graphs (Fig. 62 to Fig. 65) documents the operating parameters of the digital hydrostatic transmission in response to the Test Scenario 3 (trapezoidal profile), this time at a high load pressure of 9 MPa. The analysis of results from four independent test repetitions allows for an assessment of the system's behavior under conditions close to its maximum loads.

The system continues to execute the commanded trapezoidal work cycle, and the repeatability on a macroscopic scale remains very high, as seen on the graphs of flow rate (Fig. 62) and active power (Fig. 65). The profiles from the four successive tests almost perfectly overlap, which once again demonstrates the reliability of the digital control. At the same time, the pressure (Fig. 63) and torque (Fig. 64) graphs show that at such a high load, the variability and dynamics on a micro-scale become even more intense.

Operation at a pressure of 9 MPa confirms and reinforces the trends observed in previous tests at lower pressures.

- As predicted by theory, operation at a high pressure requires a proportionally greater torque (Fig. 64) and power (Fig. 65) The average steady-state torque increased to approx. 27-29 Nm, and the peak active power reached nearly 10 kW, which is consistent with the maximum power of the drive motor.
- The flow rate graph (Fig. 62) shows the most distinct decrease in maximum output so far, reaching a peak of approx. 0.00076 m^3/s. This phenomenon is now more pronounced and is the combined effect of a significant drop in the drive motor's

rotational speed under the very high load torque and large volumetric losses (leakages), which become a significant factor in reducing volumetric efficiency at a pressure of 9 MPa.

- A new observation is the distinct, dynamic pressure "dips" (drops) visible on the graph (Fig. 63) at the beginning (approx. t = 6s) and end (approx. t = 17s) of the steady-state phase. This phenomenon, not visible at low pressures, suggests that at high load, rapid changes in the configuration of the operating pumps (engaging the last pump or disengaging the first) cause a momentary instability of the pressure in the main line. This may be related to complex wave phenomena or the dynamics of the control system's response.
- The torque graph (Fig. 64) is chaotic. The amplitude of the oscillations in the steady-state phase is the largest of all tests conducted, which confirms that the mechanical pulsations are stronger the higher the operating pressure.

- Immutability of the Filtering Effect: Despite the extremely unstable profile of the mechanical torque, the active power graph (Fig. 65) consumed by the motor still remains incredibly smooth and repeatable.

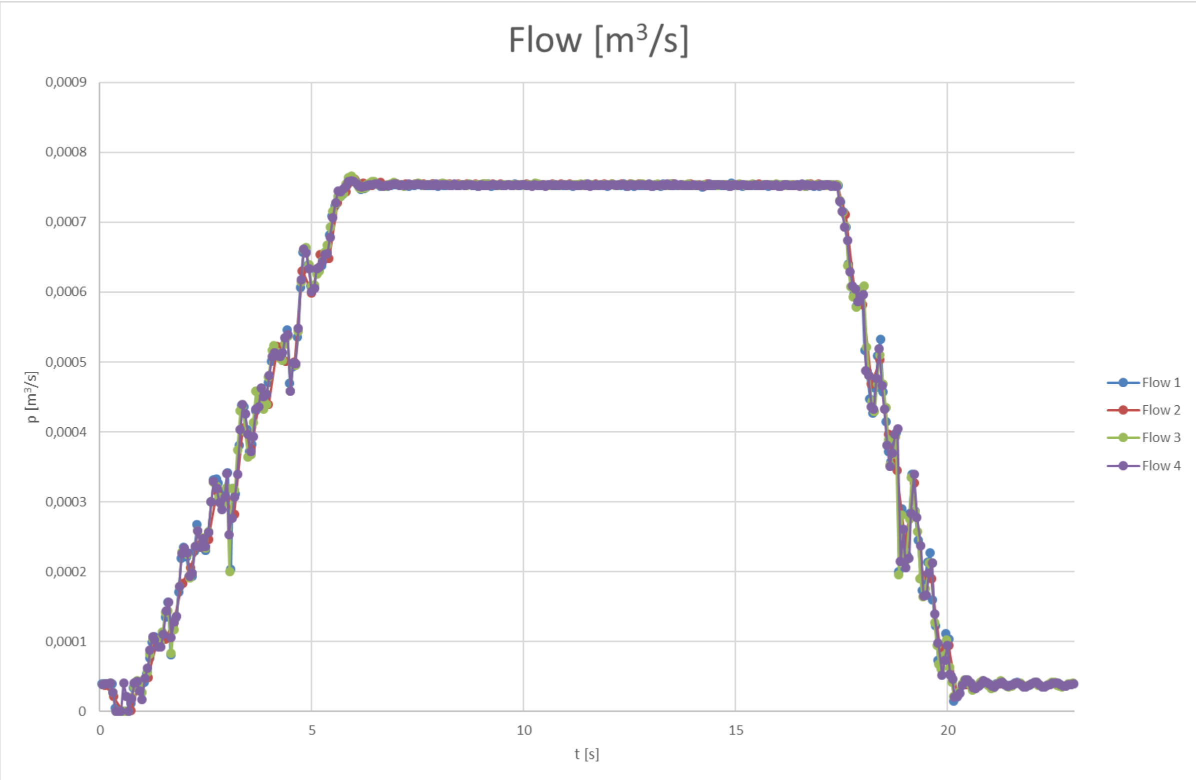

Figure 62. Flow of 3rd experimental tests 9 MPa (control signal defined in Table 5).

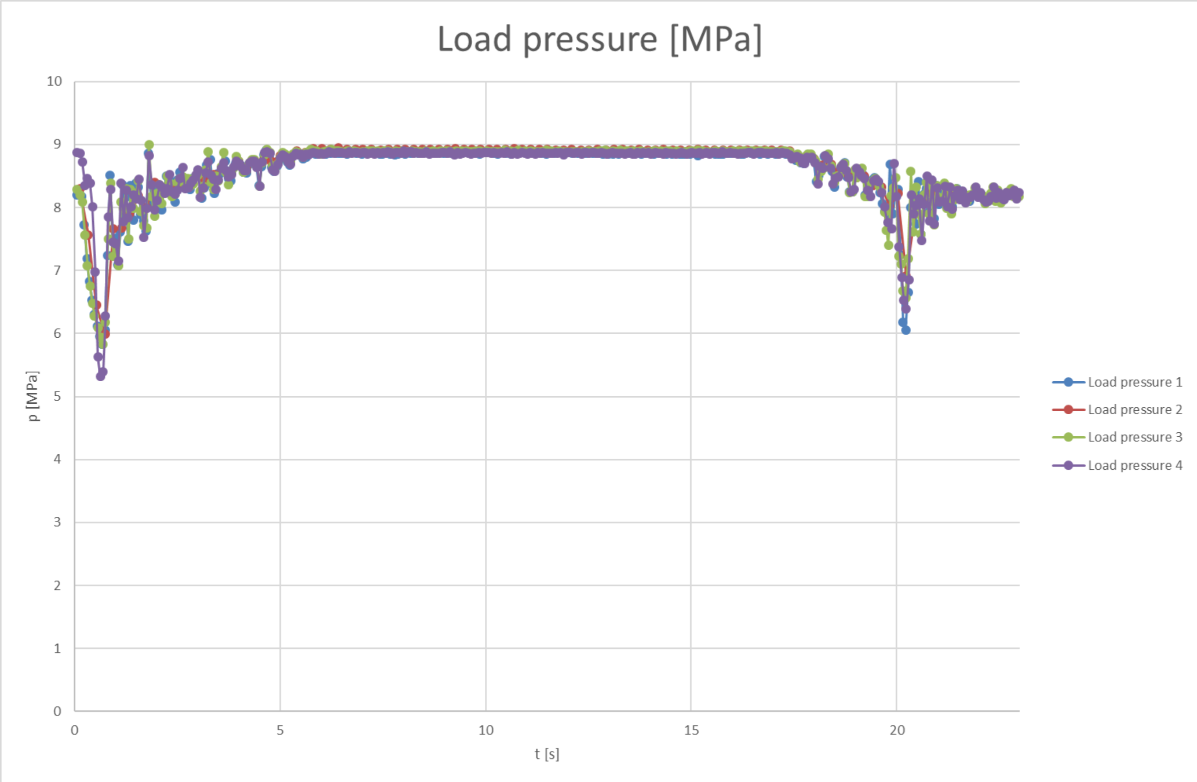

Figure 63. Load pressure of 3rd experimental tests 9 MPa (control signal defined in Table 5).

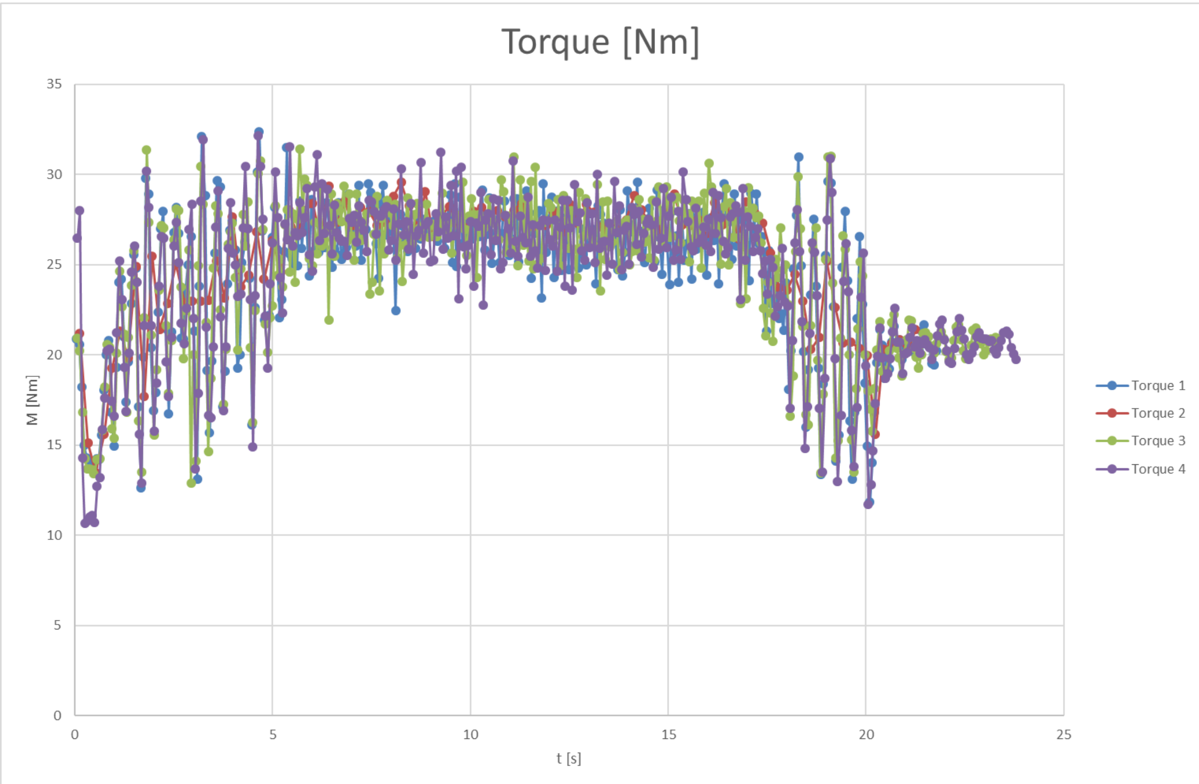

Figure 64. Torque of 3rd experimental tests 9 MPa (control signal defined in Table 5).

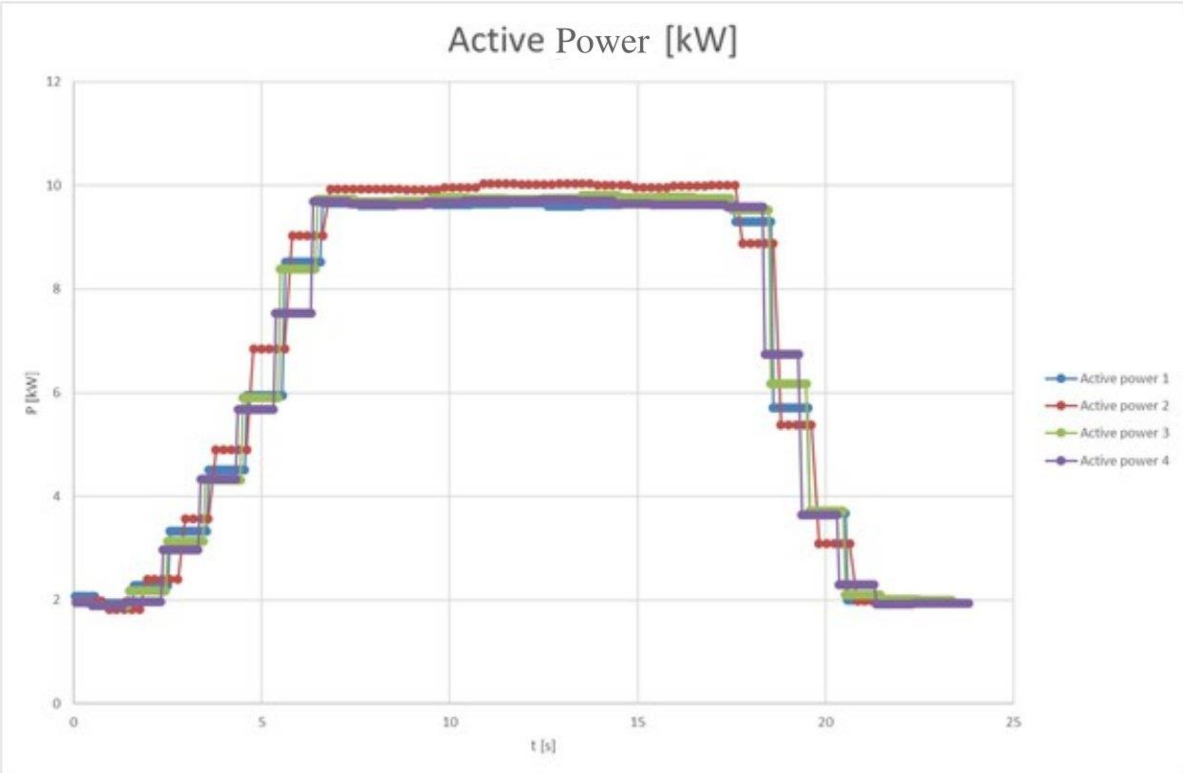

Figure 65. Active power of 3rd experimental tests for 9 MPa load (control signal defined in Table 5).

Conclusions from the experiment conducted at a pressure of 9 MPa:

- The appearance of significant pressure drops in the transient phases indicates potential problems with pressure stability during rapid control changes under high load.
- The distinct drop in flow rate and the maximum intensification of torque pulsations indicate that the system is operating at the limit of its practical capabilities, where losses and dynamic loads become dominant factors.
- The greatest challenge in digital technology is dynamic phenomena. While the system is capable of operating under high static pressure, the pulsations and instabilities generated in the transient phases are a key factor that must be considered in the mechanical design and durability assessment of the transmission.
- The system generates significant torque pulsations, which remains its fundamental characteristic distinguishing it from classic systems.

8 Simulation Research Results

8.1 Digital Hydrostatic Transmission

The results of simulation tests for six load variants are presented below.

8.1.1 Simulation Research Results for Test Scenario No. 1

The presented set of simulation results illustrates the behaviour of the digital hydraulic system during operation under the first test scenario, which is characterized by a symmetrical, stepped profile of the commanded flow rate. The research was conducted for five different levels of constant load pressure, ranging from 10 MPa to 20 MPa, in order to investigate the influence of load on the key operating parameters of the system.

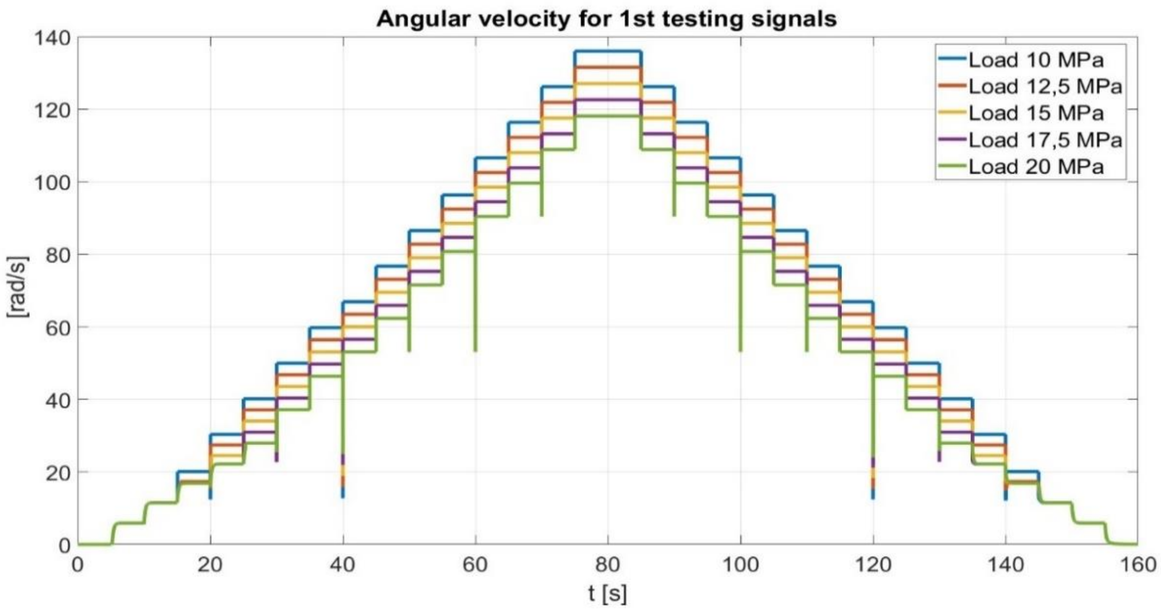

Figure 66. Angular velocity Scenario No. 1.

The graph (Fig. 66) presents the simulated angular velocity of the drive shaft for five different levels of load pressure. It can be observed that as the load increases (from 10 to 20 MPa), the rotational speed slightly decreases at each of the pressure increasing. This phenomenon reflects the characteristics of the motor, which slightly reduces its speed under the influence of a higher load torque.

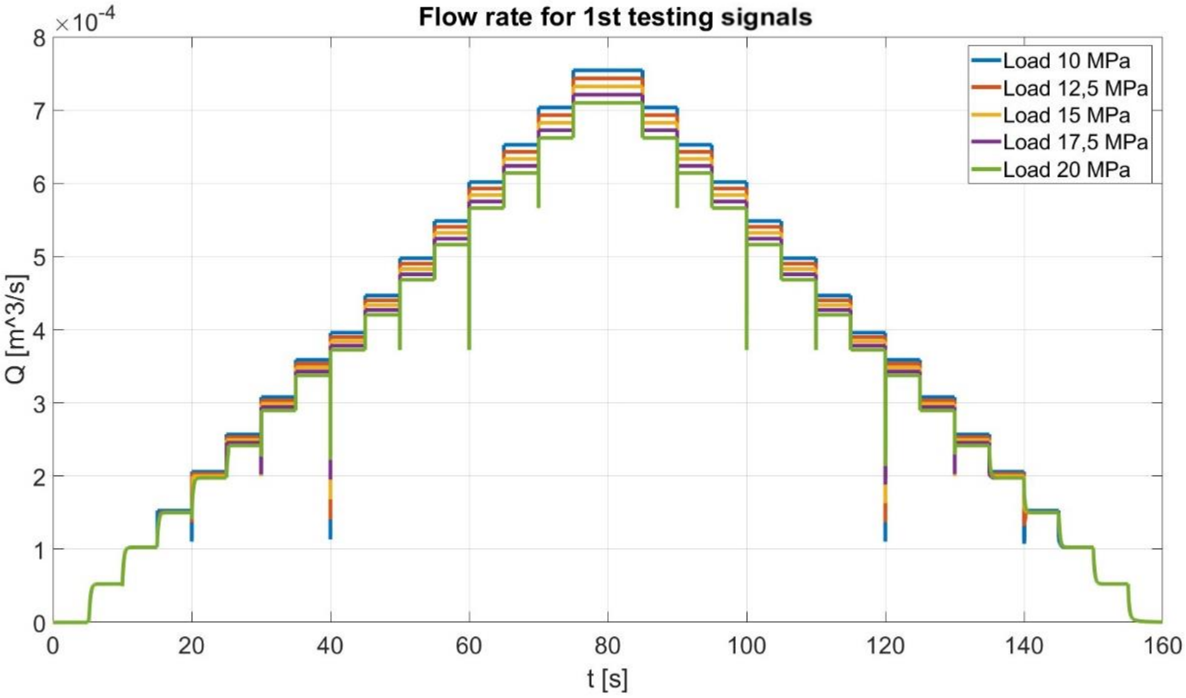

Figure 67. Flow rate Scenario No. 1.

The flow rate profile (Fig. 67) is directly linked to the angular velocity shown in the previous graph. A slight decrease in pumping performance is visible at higher load pressures, which is a result of the increase in volumetric losses (internal leakages) in the pumps.

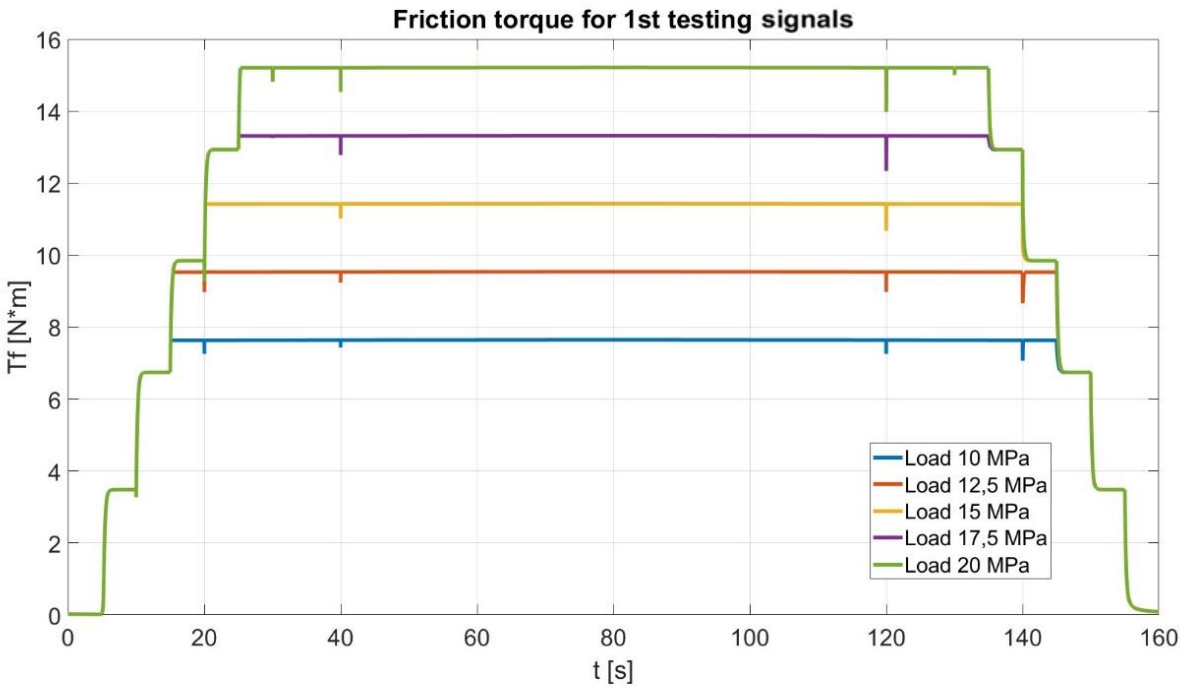

Figure 68. Friction torque Scenario No. 1.

The graph (Fig. 68) illustrates the total friction torque in the pump assembly, which is one of the components of mechanical-hydraulic losses. According to the assumed model, the value of the friction torque increases with the increase of the load pressure in the system, which reflects, among other things, the greater contact forces and motion resistance of the moving parts of the pumps.

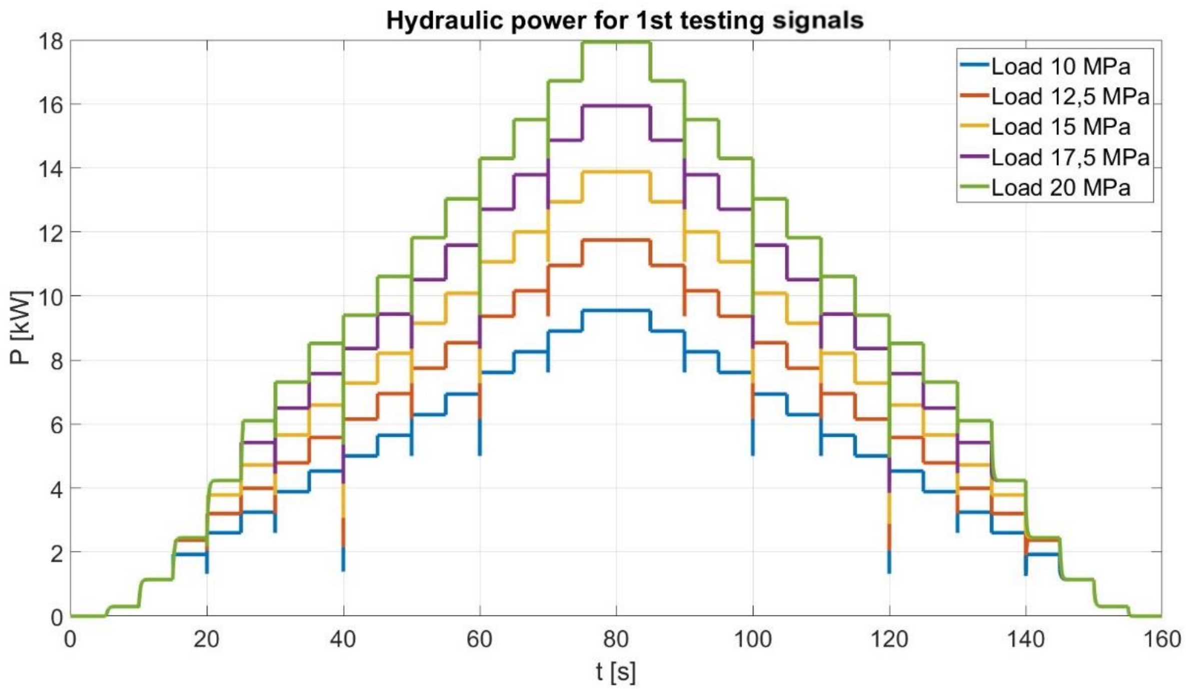

Figure 69. Hydraulic power Scenario No. 1.

This graph (Fig. 69) clearly illustrates the influence of load pressure on the hydraulic power generated by the system. Hydraulic power, being the product of pressure and flow increases almost proportionally to the set load pressure. The stepped shape of the curves corresponds to the discrete performance levels achieved by switching on successive pumps.

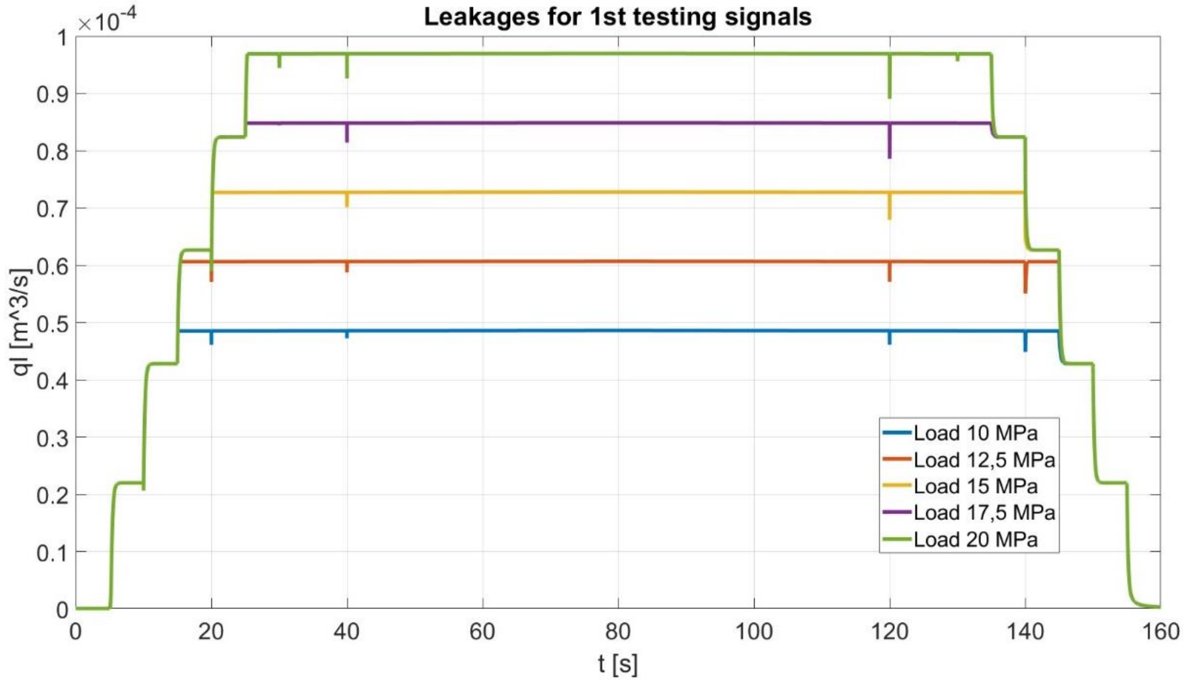

Figure 70. Leakages Scenario No. 1.

The Figure 70 shows the total volumetric losses (internal leakages) in the pump assembly. In accordance with models of losses in positive-displacement machines, the magnitude of the leakages is approximately proportional to the pressure difference. The simulation confirms this relationship, showing increasing volumetric losses for progressively higher operating pressures.

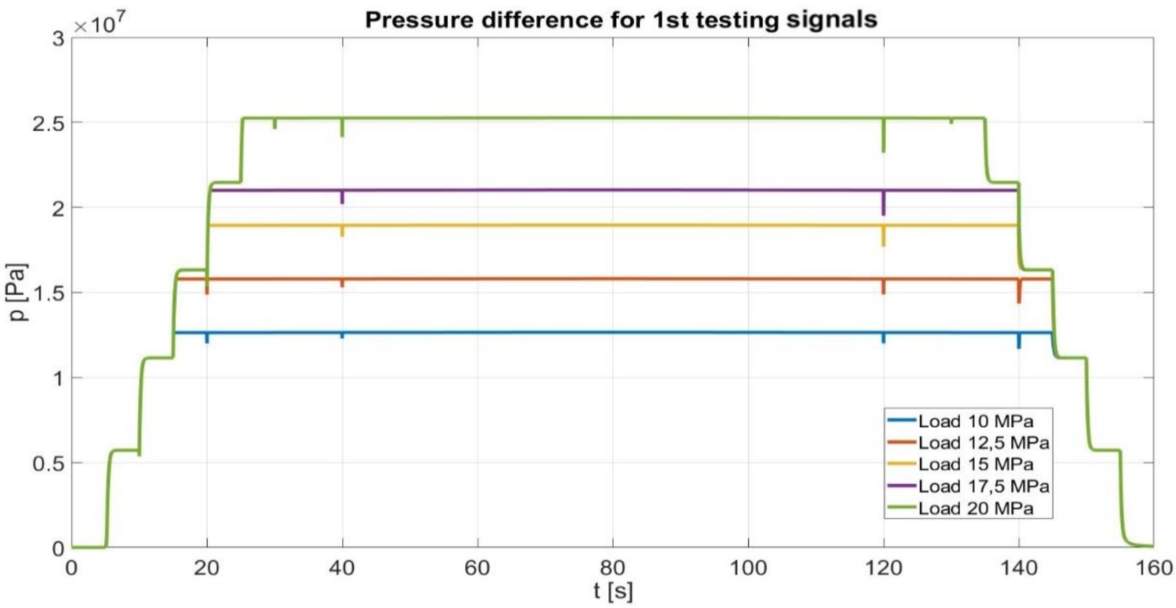

Figure 71. Pressure difference Scenario No. 1.

Figure 71 shows the pressures in hydraulic system. It confirms that for each of the five-test load (10, 12.5, 15, 17.5, and 20 MPa), the digital system pressure stabilized at a constant, increasing level.

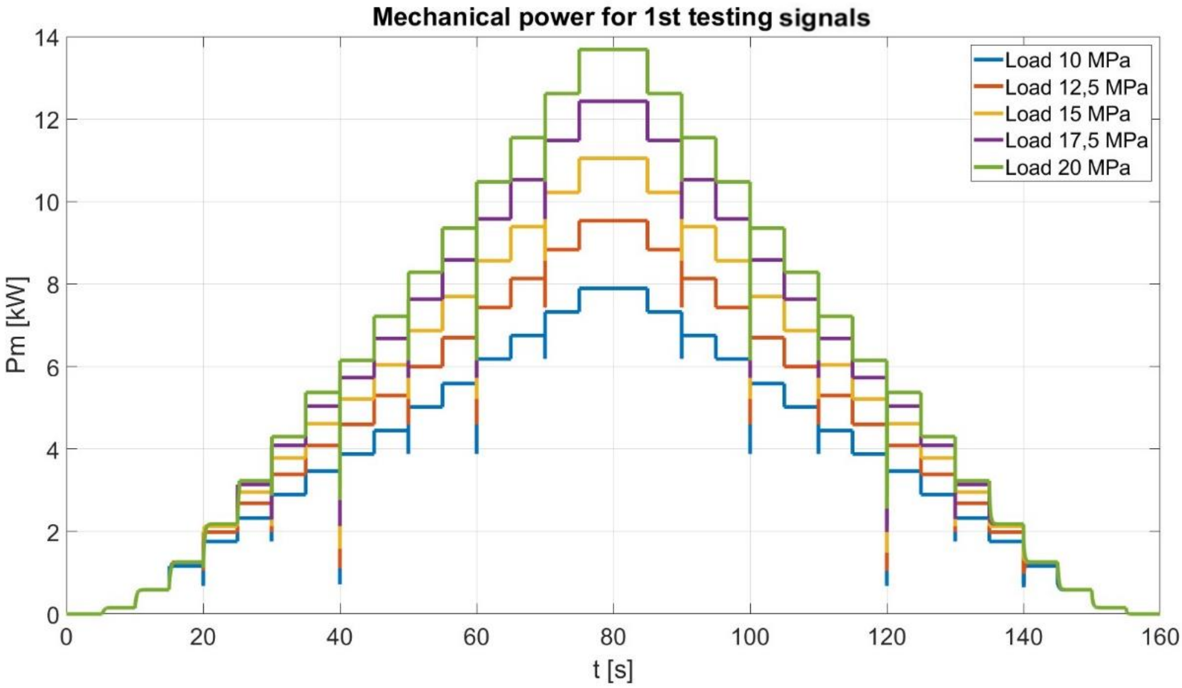

Figure 72. Mechanical power Scenario No. 1.

Figure 72 shows the total mechanical power required on the motor shaft to drive the pumps assembly. This power is the sum of the useful hydraulic power and the power needed to cover volumetric and mechanical-hydraulic losses. Therefore, its values are higher than the hydraulic power, and this difference increases with the load, which is a natural consequence of increasing losses

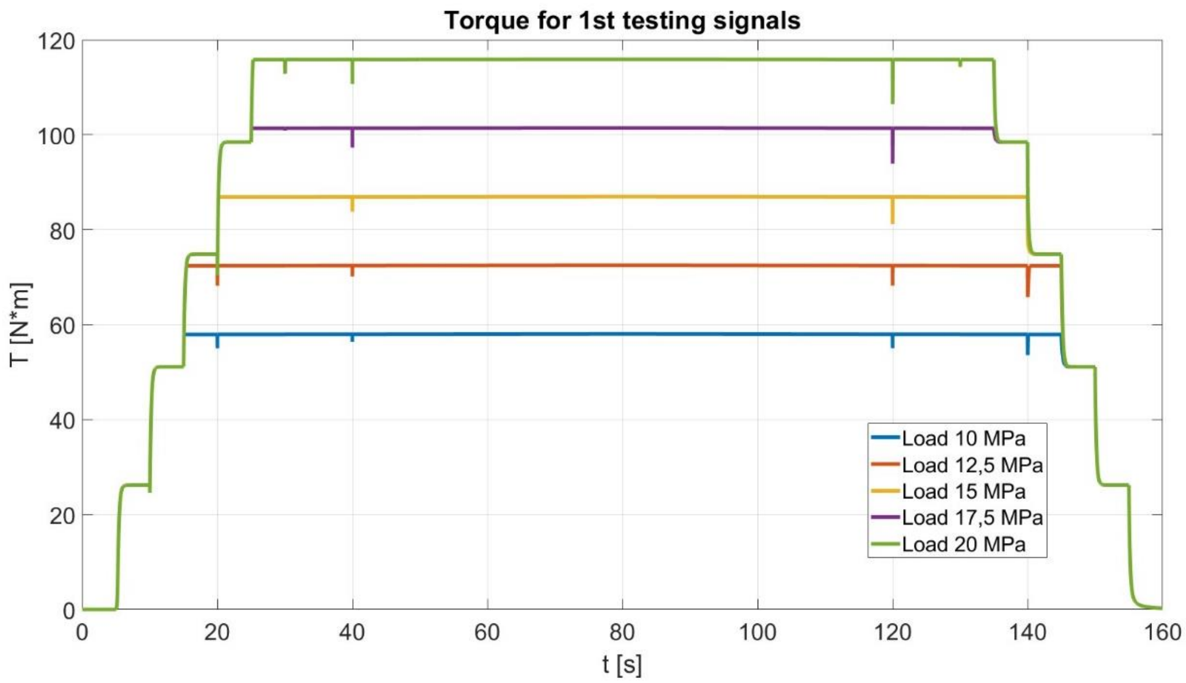

Figure 73. Torque Scenario No. 1.

Figure 73 shows the total torque required to drive the pump assembly at different loads. According to theory, the required torque is proportional to the operating pressure in the system.

A key observation from above analysis is the behaviour of the angular velocity. The graph shows that as the load pressure increases, the rotational speed slightly decreases at each discrete flow rate level (the influence of higher volumetric losses). Additionally, the graph shows sharp, momentary drops in velocity, which correlate with the moments of pump switching and the step change in mechanical load. The angular velocity profile is directly linked to the flow rate. Analysis of Internal Losses in the Model

The graphs of leakages and friction torque provide insight into the modelled internal losses within the pump assembly. In accordance with theoretical assumptions, the simulation shows that the magnitude of volumetric losses (leakages) increases almost linearly with the increase in load pressure. This is consistent with models of laminar flow in clearances, where the flow rate is directly proportional to the pressure difference. Similarly, the friction torque, which represents the sum of mechanical and hydraulic losses, also shows a strong dependence on the operating pressure. The increase in forces acting on the moving parts (bearings, seals) at higher pressures leads to an increase in frictional resistance, which has been represented in the model as a stepped increase in the loss torque for subsequent load levels.

A comparison of the power and torque graphs allows for a full energy assessment of the simulated system. The total torque required on the drive shaft increases in steps with the increase in pressure, which is a fundamental principle of positive-displacement machines. It is the sum of the ideal torque, needed to compress the fluid, and the loss torque (friction), which explains its strong correlation with the friction torque graph.

The comparison of hydraulic power (useful) with mechanical power (supplied to the shaft) provides information about the system's efficiency. The mechanical power is always higher than the hydraulic power, and the difference between them represents the sum of the power lost to cover volumetric and mechanical-hydraulic losses. The analysis of the graphs shows that this difference becomes larger for higher load pressures. This means that as the load increases, the total losses increase, leading to a decrease in the overall energy efficiency of the system.

8.1.2 Simulation Research Results for Test Scenario No. 2

The presented set of simulation results illustrates the behavior of the digital hydraulic system during operation under the second test scenario. This scenario is characterized by the generation of a series of separate flow pulses with a step-increasing amplitude. The research, as previously, was conducted for five different levels of constant load pressure (10, 12.5, 15, 17.5, and 20 MPa) to investigate the influence of load on the system's performance under dynamic and intermittent conditions.

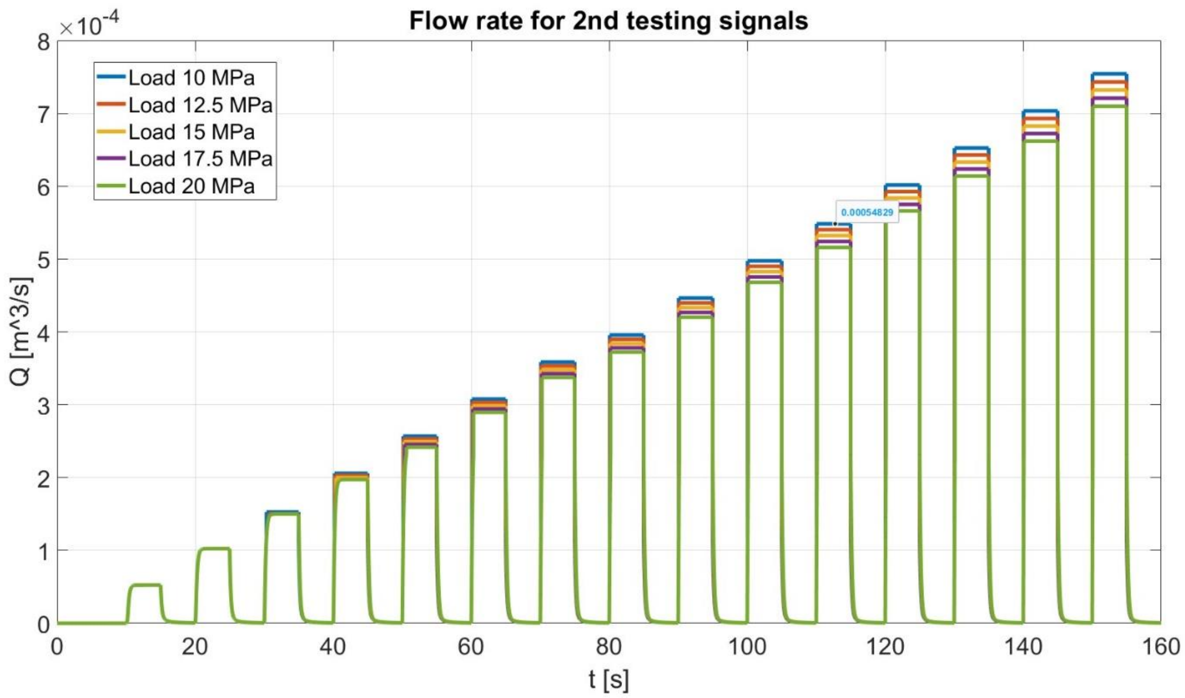

Figure 74. Flow rate Test Scenario No. 2.

Figure 74 shows the flow rate as a series of pulses with increasing amplitude, corresponding to the successive control steps. Within each pulse, a slight decrease in flow is visible with increasing load pressure (from 10 MPa to 20 MPa), which results mainly from the increase in leakages.

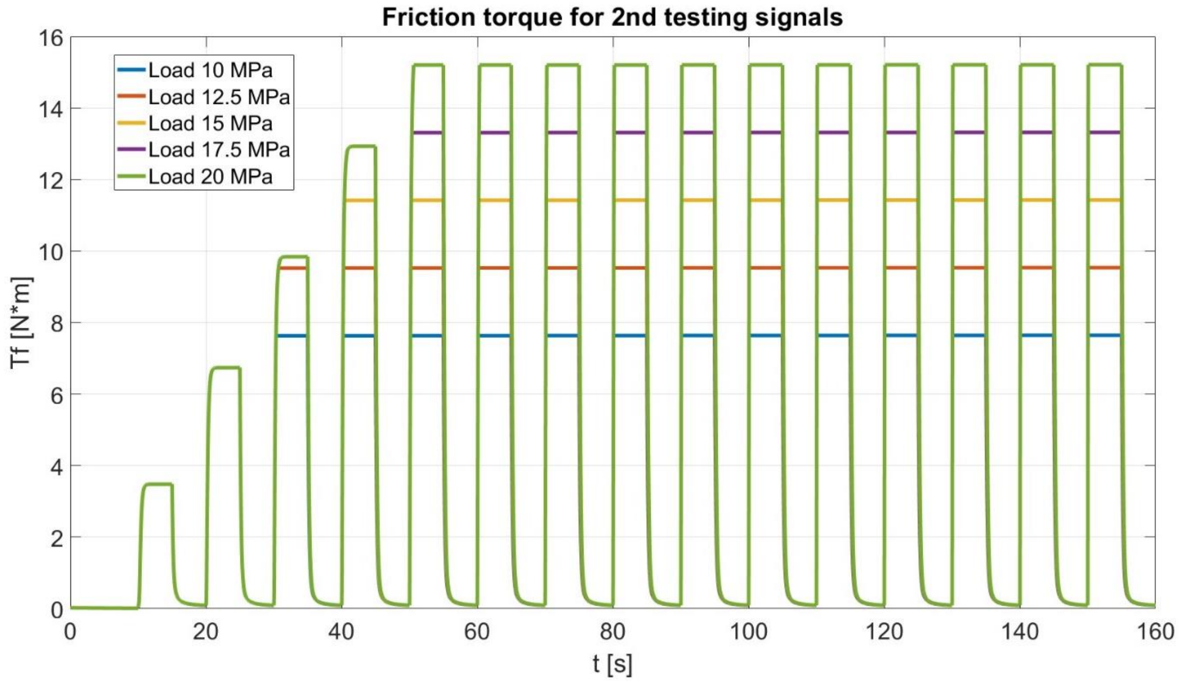

Figure 75. Friction torque Test Scenario No. 2.

Figure 75 illustrates friction torque in the pump assembly. The friction torque value is constant during each pulse and increases in steps with the load pressure, reflecting the dependence of mechanical losses on the system pressure.

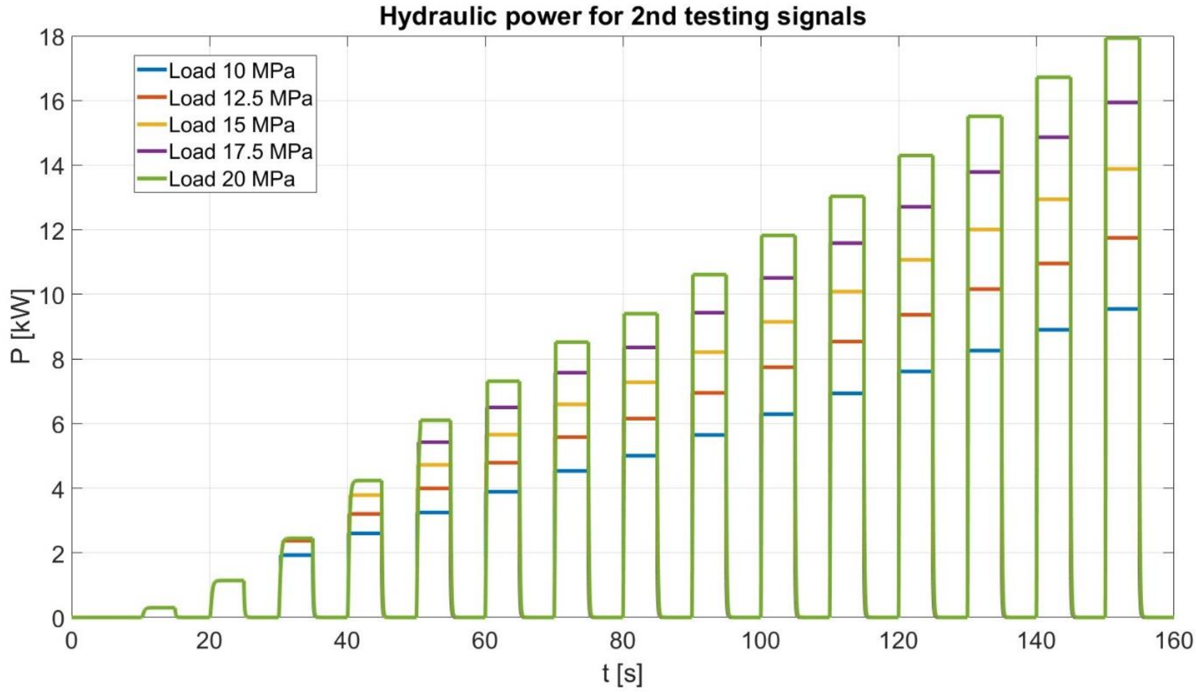

Figure 76. Hydraulic Power Test Scenario No. 2.

Figure 76 depicts the hydraulic power generated by the system during the test. Power increases in two ways: with each successive pulse (due to increased flow) and within each pulse with increasing load pressure (from 10 to 20 MPa).

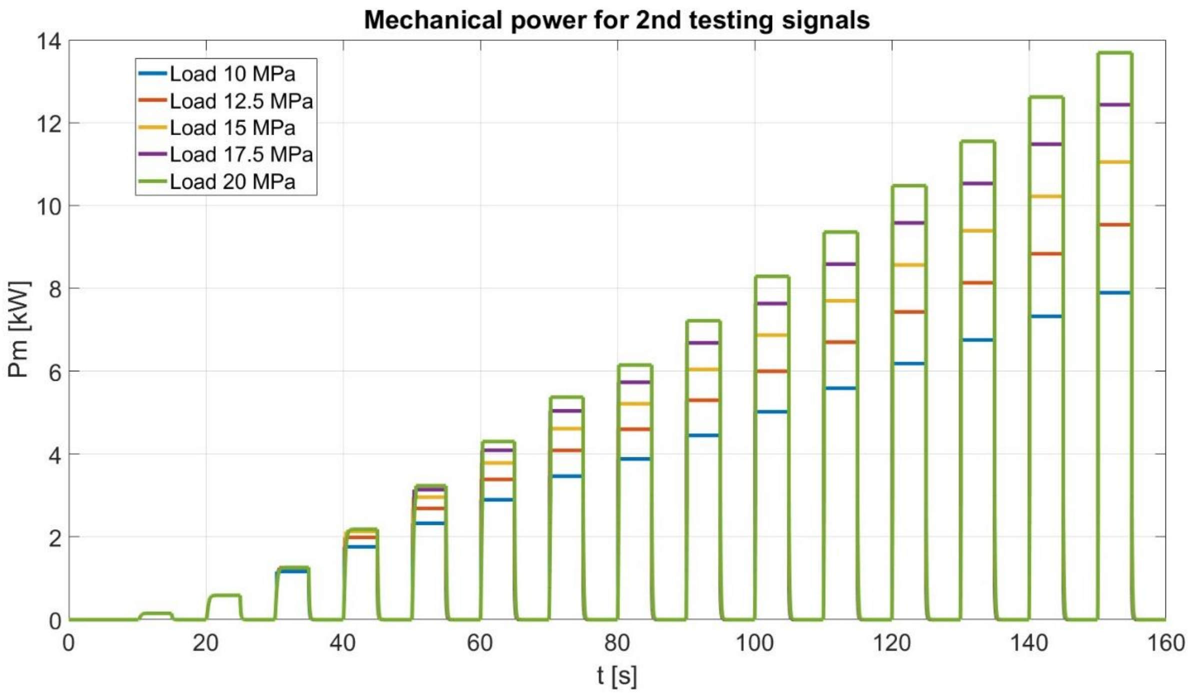

Figure 77. Mechanical Power Test Scenario No. 2.

Figure 77 shows the mechanical power supplied to the drive shaft. Its profile is analogous to the hydraulic power, but the values are higher, and the difference between them, representing the total system losses, grows with increasing load.

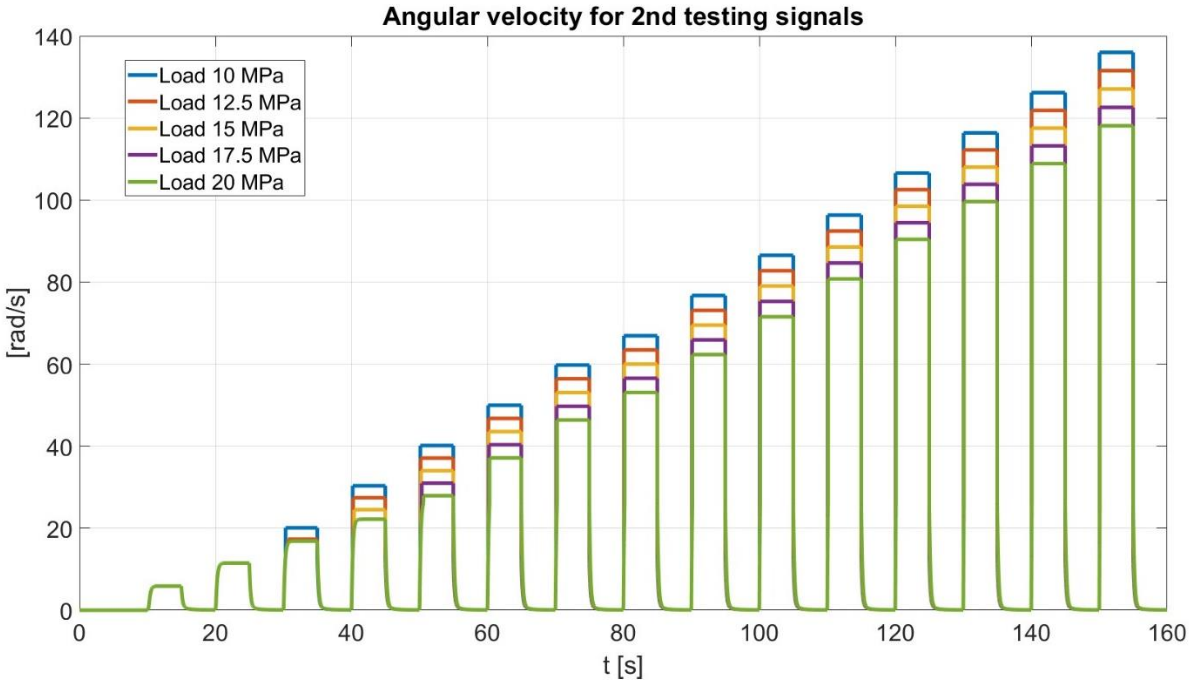

Figure 78. Angular velocity Test Scenario No. 2.

Figure 78 presents the angular velocity of the drive shaft of hydraulic motor. The overall velocity increases with each subsequent pulse; however, within each pulse, a slight drop in velocity is observed with increasing load pressure, which is mainly an effect of volumetric losses.

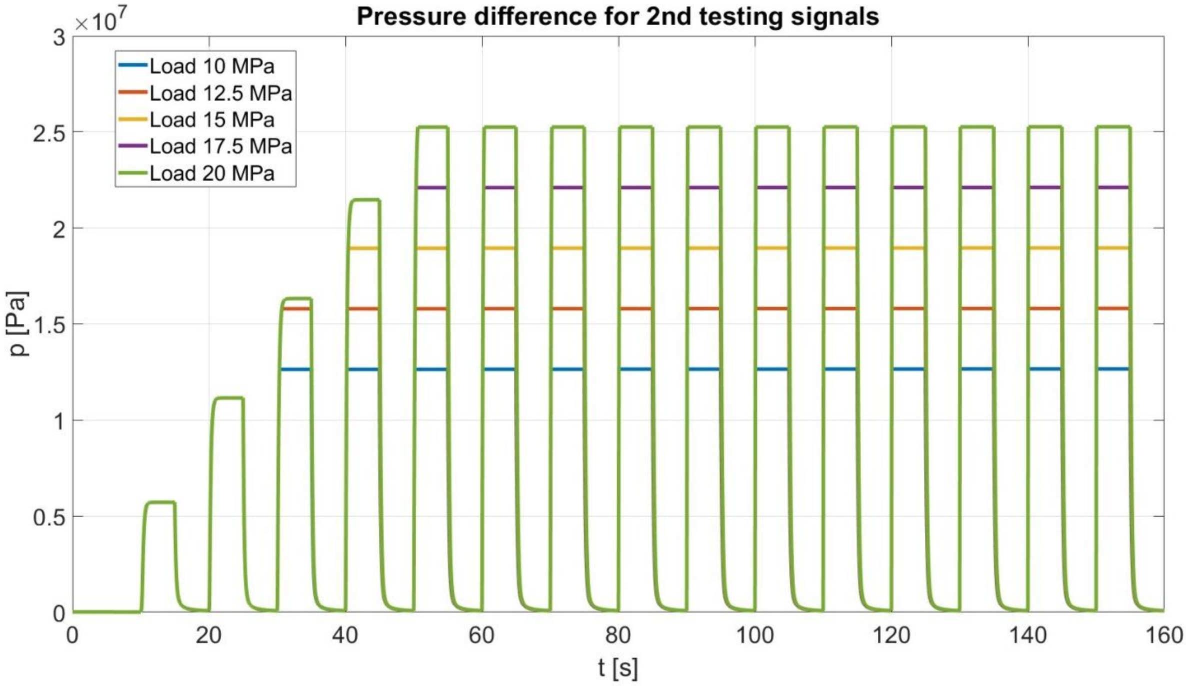

Figure 79. Pressure difference Test Scenario No. 2.

Figure 79 shows that during each pulse, the load pressure in the model was reached at the five specified, constant levels, corresponding to the five load cases of 10 MPa, 12.5 MPa, 15 MPa, 17.5 MPa, and 20 MPa.

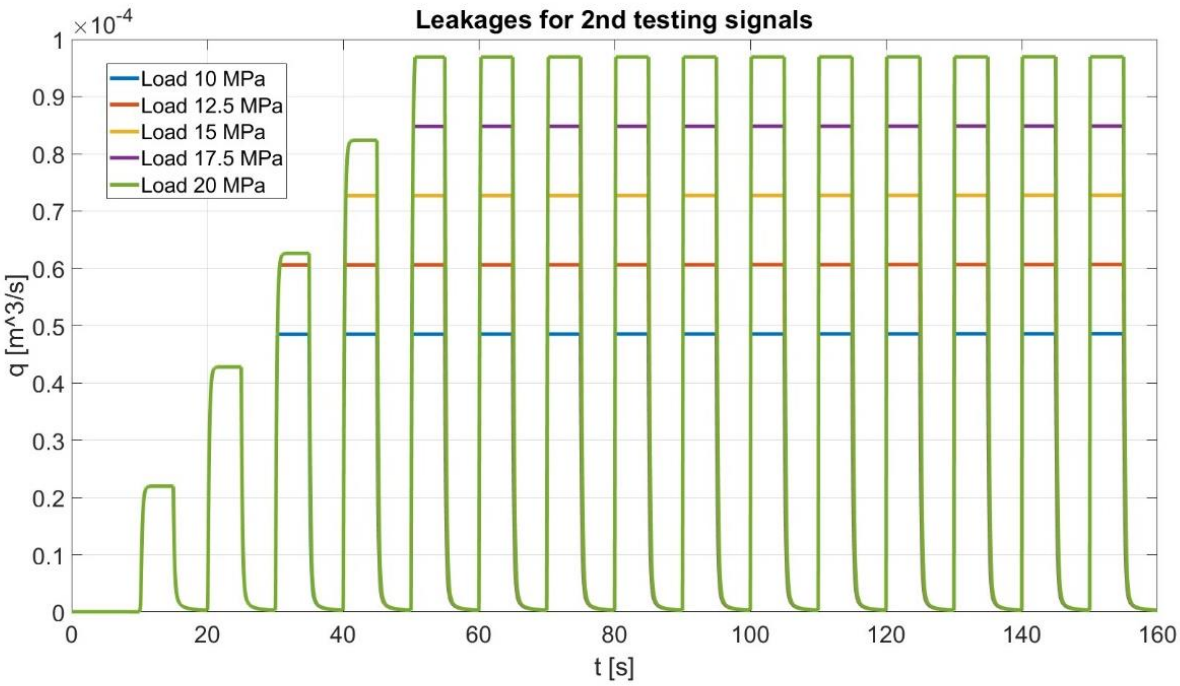

Figure 80. Leakages Test Scenario No. 2.

Figure 80 visualizes the volumetric losses (internal leakages). The magnitude of the leakage during each pulse is constant and increases in steps solely as a function of the load pressure level.

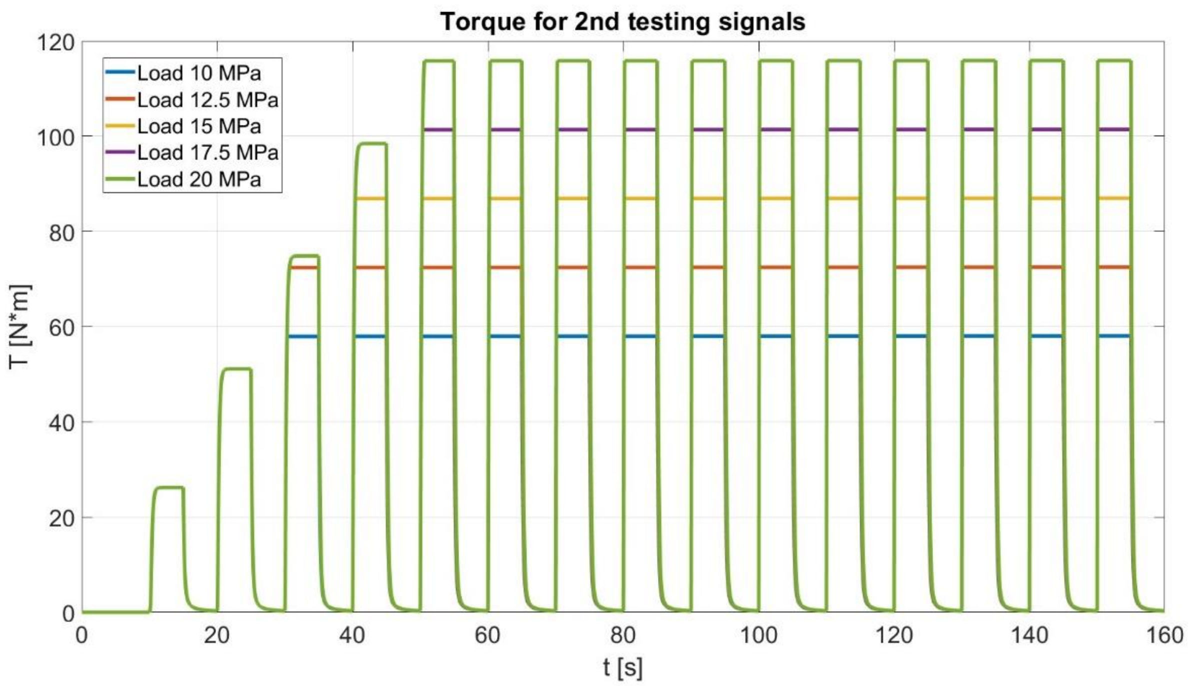

Figure 81. Torque Test Scenario No. 2.

Figure 81 illustrates the total torque required to drive the pumps assembly. According to theory, the torque is almost directly proportional to the load pressure, which is shown by the stepped increase in values for the successive pressure levels from 10 MPa to 20 MPa within each pulse.

The visualization of the results in the form of stacked bar charts perfectly illustrates the effect of load on the operating parameters within each pulse. The pressure difference graph confirms that during each pulse, the model operated under the specified, stable load, as indicated by the constant pressure levels for each of the five load cases (10 MPa, 12.5 MPa, 15 MPa, 17.5 MPa, and 20 MPa). The analysis of the angular velocity graph provides significant insights. Firstly, the height of successive pulses increases, which is consistent with the assumption of increasing displacement (activation of subsequent pump combinations) in the following steps of the test. Secondly, within each individual pulse, it is evident that the rotational speed decreases as the load pressure increases the lowest bar (representing the 10 MPa load) corresponds to the highest speed, and each subsequent bar for the higher pressure levels (12.5 MPa to 20 MPa) is slightly lower. The flow rate profile is a direct reflection of the angular velocity. The total flow increases with each successive pulse, realizing the commanded test profile. Concurrently, within each pulse, a slightly lower flow is observed for higher load pressures (higher bars on the pressure graph), which is an effect of increasing internal leakages.

The graphs of leakages and friction torque clearly visualize the losses. In both cases, the losses are almost zero during the intervals between pulses and assume a constant value during each pulse.

The total torque, much like the losses, remains constant during each pulse and depends mainly on the load pressure. The hydraulic power and mechanical power graphs show that the power demand increases in two ways: with each successive pulse (due to increasing flow) and within each pulse (due to increasing pressure). The difference between mechanical and hydraulic power, representing the total power losses, is clearly larger for higher load pressures, which confirms the decrease in the system's overall efficiency under higher loads.

8.1.3 Simulation Research Results for Test Scenario No. 3

The presented set of simulation results illustrates the behavior of the digital hydraulic system during operation under the third test scenario. This profile is characterized by a trapezoidal shape, simulating a typical machine work cycle: a ramp-up phase, a steady-state operation phase, and a ramp-down phase. The research was conducted for five different levels of constant load pressure, ranging from 10 MPa to 20 MPa, in order to investigate the influence of load on the key operating parameters of the system.

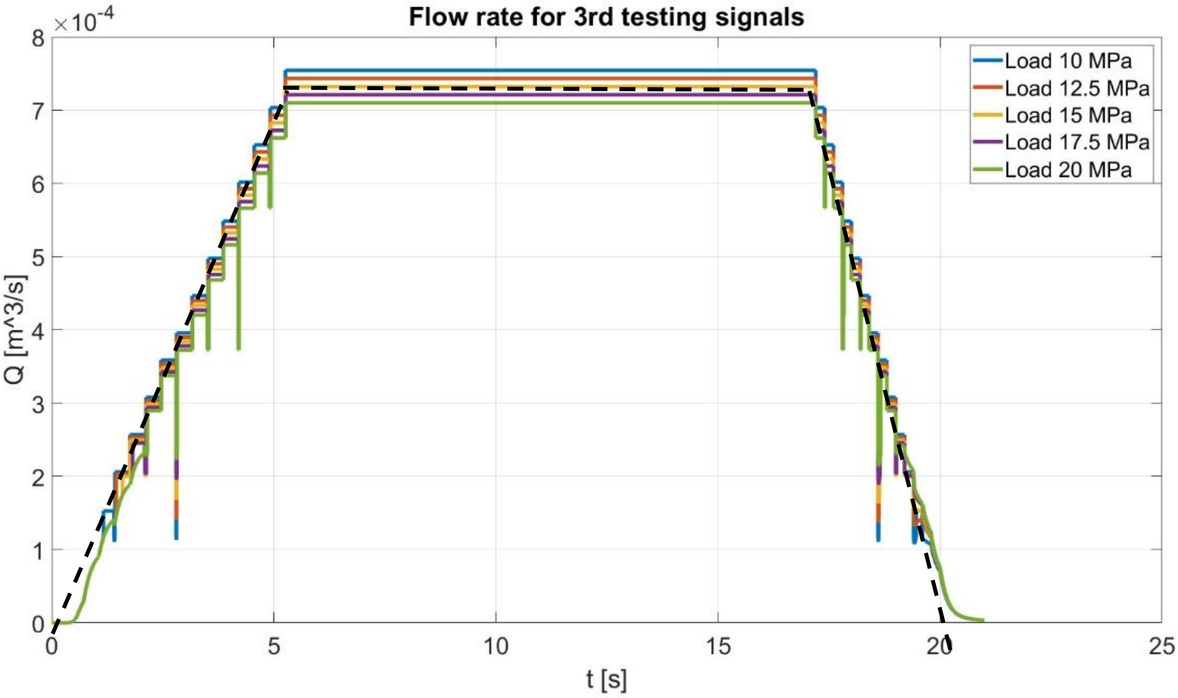

Figure 82. Flow rate Test Scenario No. 3.

Figure 82 shows the flow rate in the commanded trapezoidal cycle. The stepped character of the ramp-up and ramp-down phases is a result of the digital control strategy, and the slight decrease in flow during the steady-state phase at higher pressures is a consequence of the increase in leakages.

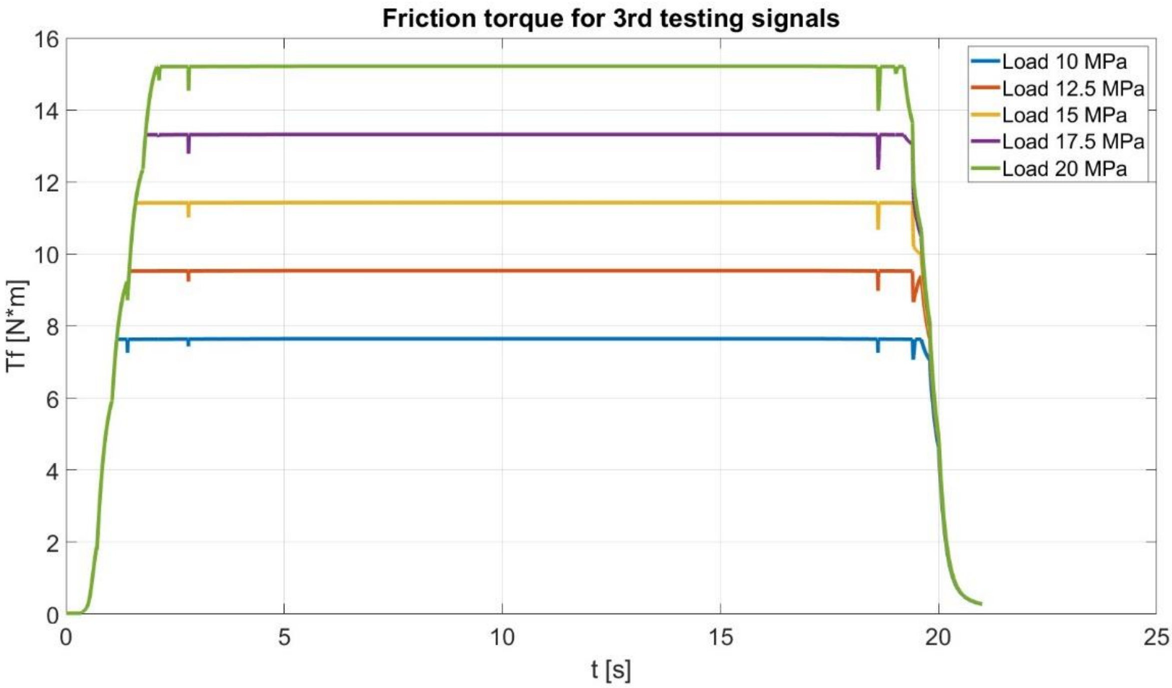

Figure 83. Friction torque Test Scenario No. 3.

Figure 83 illustrates the friction torque in the pumps assembly. The torque value is constant during the steady-state phase and increases in steps with the load pressure, reflecting the dependence of mechanical losses on the forces acting within the system.

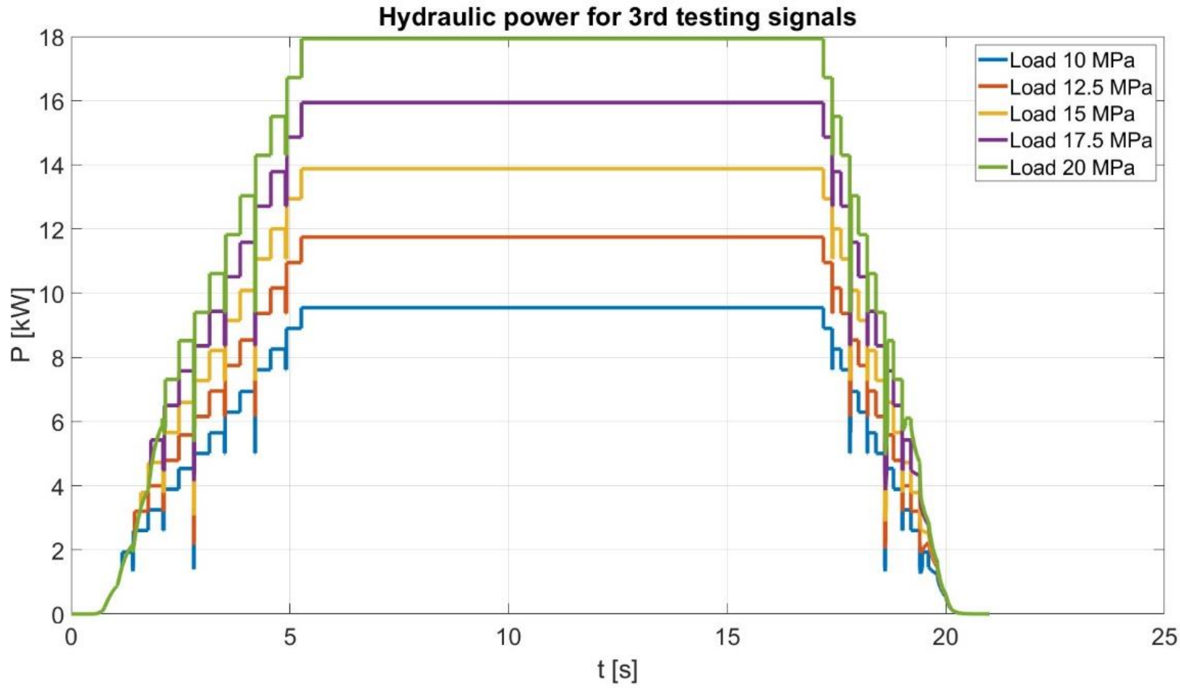

Figure 84. Hydraulic power Test Scenario No. 3.

Figure 84 depicts the hydraulic power generated by the system. The shape of the profile corresponds to the analysed cycle, and the height of the power in the steady-state phase is almost directly proportional to the load pressure.

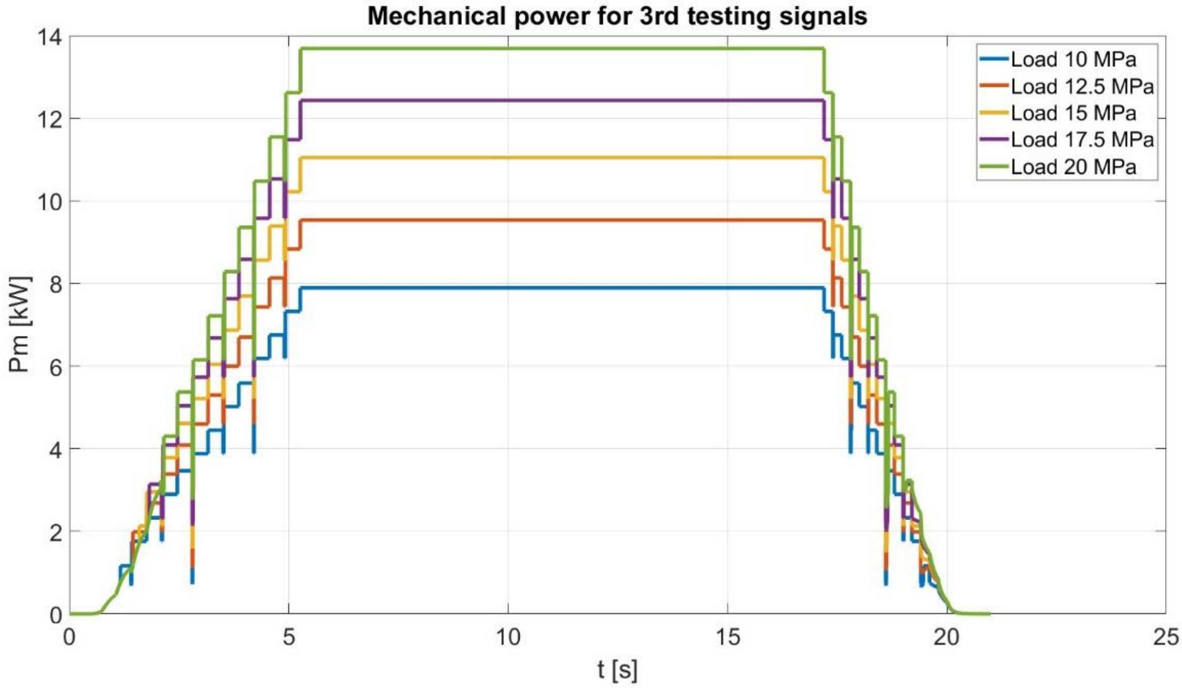

Figure 85. Mechanical power Test Scenario No. 3.

Figure 85 shows the mechanical power supplied to the drive shaft. Its profile is analogous to the hydraulic power; however, the values are higher by the sum of the system's losses, with this difference becoming clearly larger at higher operating pressures.

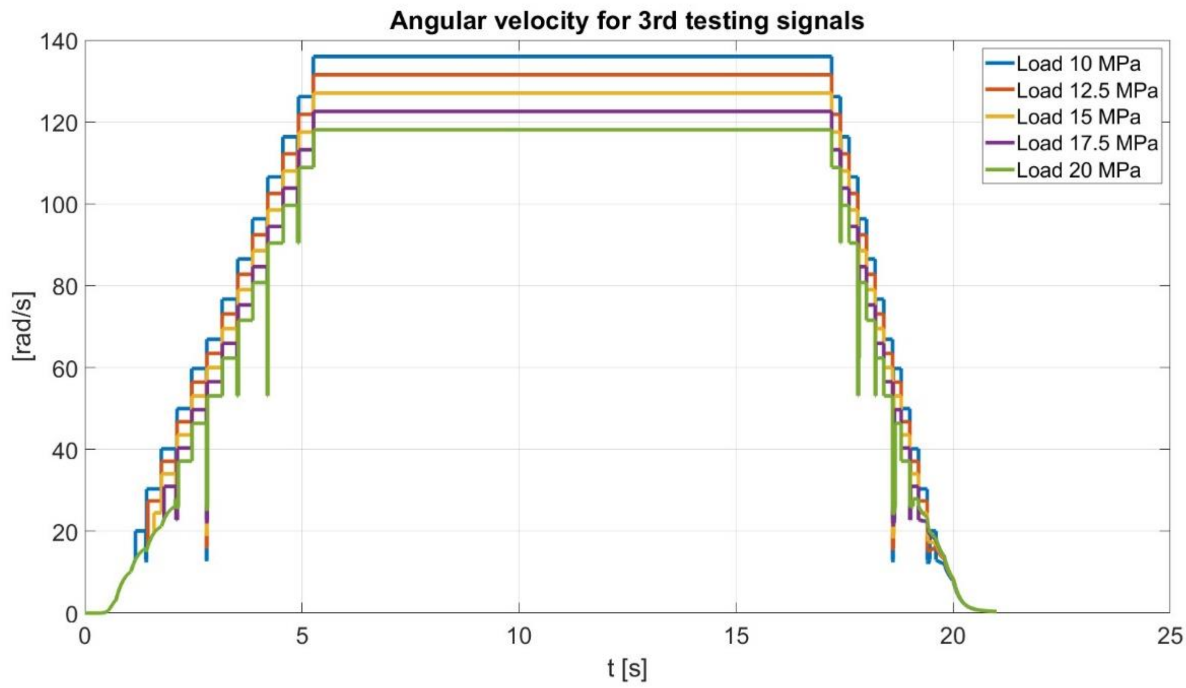

Figure 86. Angular velocity Test Scenario No. 3.

Figure 86 presents the angular velocity of the drive shaft. In the steady-state phase, a slight drop in velocity is observed with increasing load pressure (from 10 to 20 MPa).

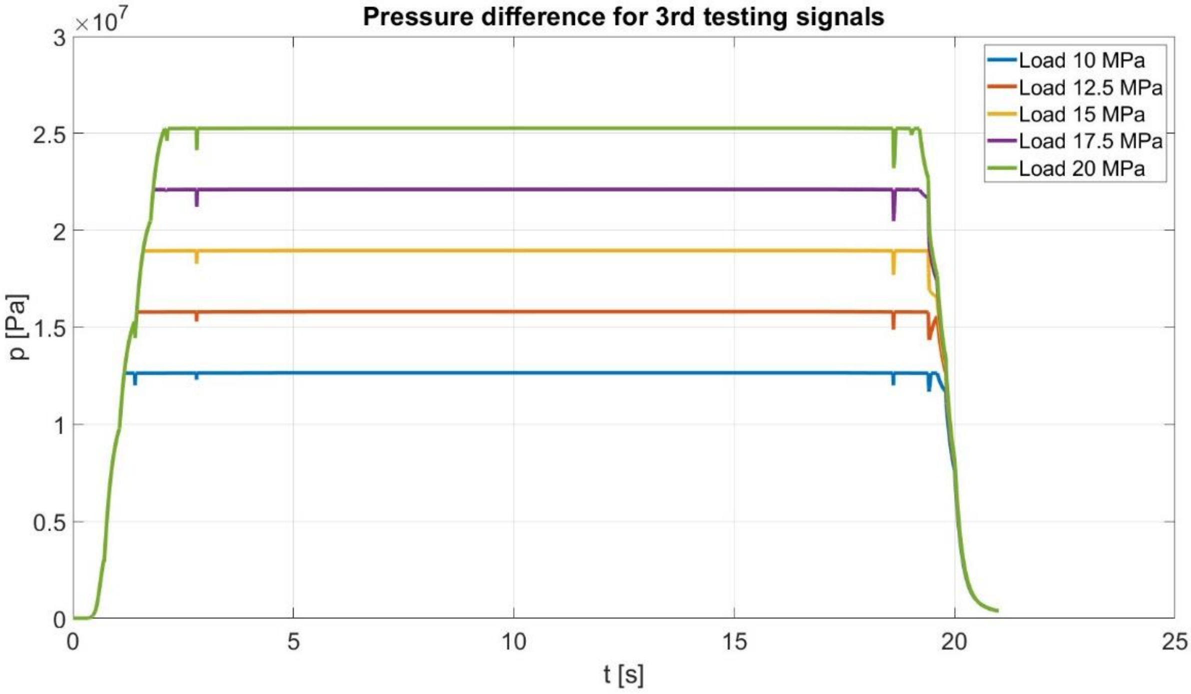

Figure 87. Pressure difference Test Scenario No. 3.

Figure 87 confirm that for each of the five test cases, the load pressure in the model stabilized at the set, constant level.

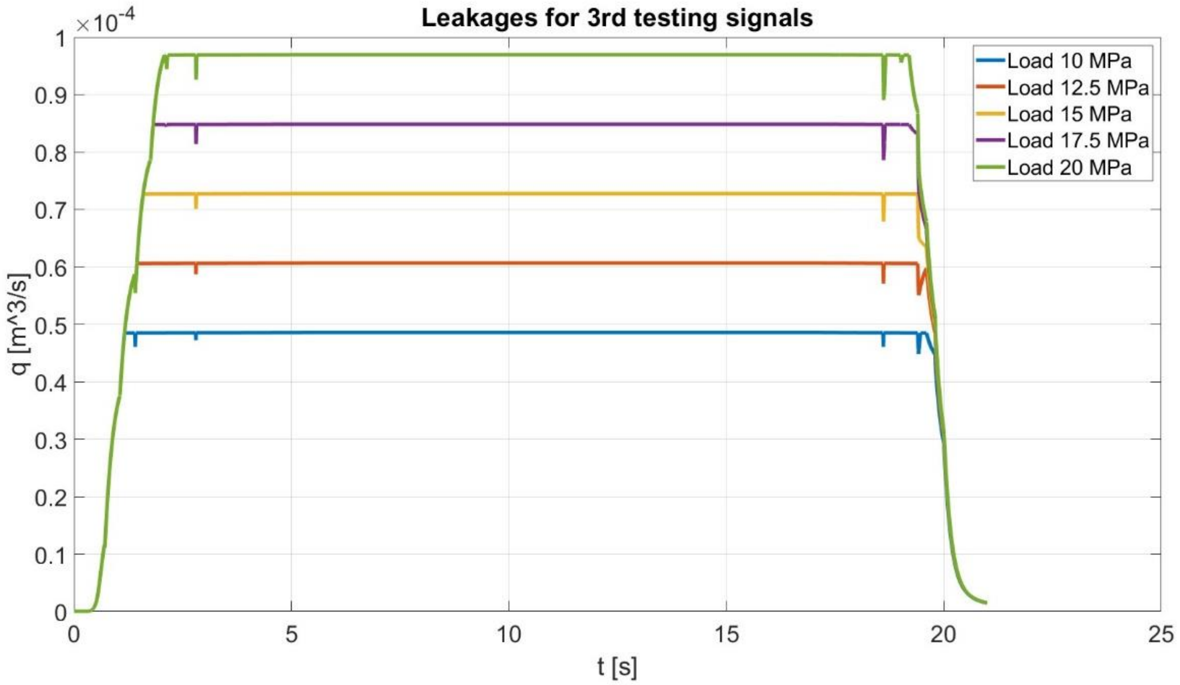

Figure 88. Leakages Test Scenario No. 3.

Figure 88 visualizes the volumetric losses (internal leakages). The magnitude of the leakage in the steady-state phase is constant and increases in steps depending on the load pressure level.

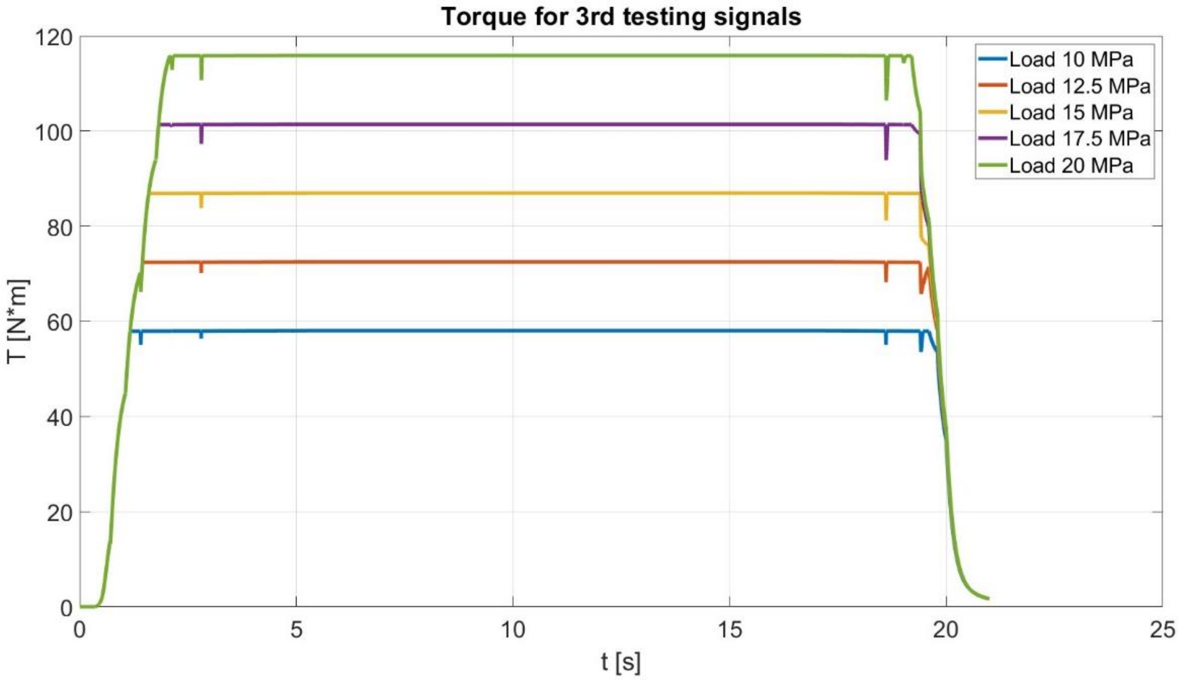

Figure 89. Torque Test Scenario No. 3.

Figure 89 illustrates the total torque required to drive the pump assembly. The torque in the steady-state phase is almost directly proportional to the operating pressure, which is visible in the clearly separated and increasing levels for the subsequent load cases.

The key kinematic parameters angular velocity and flow rate faithfully replicate the trapezoidal character of the commanded cycle. Both values increase in a stepped manner, reach a constant level during the steady-state phase (approximately from 5 to 18 seconds), and then symmetrically decrease. The stepped nature of the ramps is a clear signature of the digital control strategy, where successive combinations of pumps are sequentially engaged to approximate a smooth change in output. A significant observation, consistent with previous analyses, is the effect of load on velocity. The angular velocity graph shows that during the steady-state phase, the system reaches the highest speed at the lowest load (10 MPa) and the lowest speed at the highest load (20 MPa). This phenomenon is directly connected to the flow rate, which is also minimally lower for higher operating pressures. The graphs of leakages and friction torque show how the losses behave in this work cycle. Both loss values increase rapidly during the ramp-up phase and stabilize at a constant level during the steady-state phase. The key conclusion here is the direct, almost linear relationship between the magnitude of the losses and the load pressure. For each subsequent, higher pressure level (from 10 to 20 MPa), both the total leakages and the friction torque assume a distinctly higher, constant value. A comparison of the power and torque graphs allows for a comprehensive energy assessment of the system in the given cycle. The total torque required on the drive shaft replicates the trapezoidal work cycle with its shape. Its value in the steady-state phase is strongly dependent on the load pressure a 100% increase in pressure (from 10 to 20 MPa) results in an almost 100% increase in the required torque (from approx. 58 Nm to approx. 116 Nm). The hydraulic power and mechanical power graphs also follow the trapezoidal profile. It is clearly visible that the power (both hydraulic and mechanical) increases in steps for each subsequent pressure level. The comparison of both power graphs is crucial: the mechanical power (supplied) is always higher than the hydraulic power (useful). This difference, representing the total power losses in the system, is noticeably larger for higher load pressures. This indicates a decrease in the overall energy efficiency of the system as the load increases.

Summary of Conclusions from the Simulation for Scenario No. 1, 2 and 3

The conducted simulation studies of Scenario No. 1 and 2 effectively replicate the behavior of the digital hydrostatic transmission under varying loads. They confirm the fundamental theoretical relationships, such as the nearly linear increase in required torque, power, and internal losses with the increase in operating pressure. The simulation of the trapezoidal work cycle (Scenario No. 3) also effectively demonstrates the behavior of the digital system under continuous, multi-phase load conditions, which is typical for many work machines. Importantly, the model also reveals the interactions between components: an increase in load causes a decrease in the drive's rotational speed, which in turn slightly reduces the system's output. These results provide a solid reference baseline for further experimental verification and assessment of the digital transmission's energy efficiency.

8.1.4 Simulation Research Results for Test Scenario No. 3a

The presented set of simulation results (Fig. 90 to Fig. 97) illustrates the behavior of the digital hydraulic system during operation under the fourth test scenario. This profile, similar to Test Scenario no. 3a, has a trapezoidal character but is distinguished by a significantly shorter cycle time (approx. 10 seconds) and very rapid ramp-up and ramp-down phases of the parameters. This scenario simulates the system's operation under conditions requiring a fast dynamic response, for instance, in applications with high repeatability and short cycle times. The research was conducted for five different levels of load pressure (10-20 MPa).

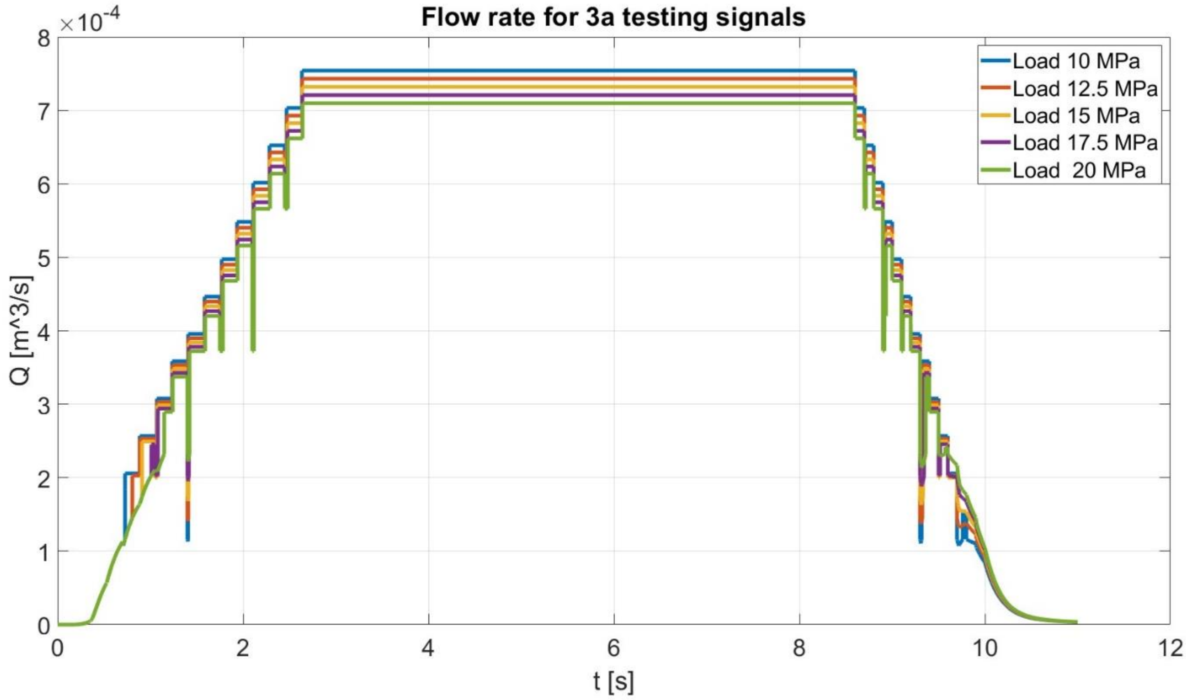

Figure 90. Flow rate Test Scenario No. 3a.

Figure 90 shows the flow rate in a rapid trapezoidal cycle. The very steep ramp-up and ramp-down phases demonstrate the system's capacity for a dynamic response, and the stepped nature of these ramps is a result of the digital pump control.

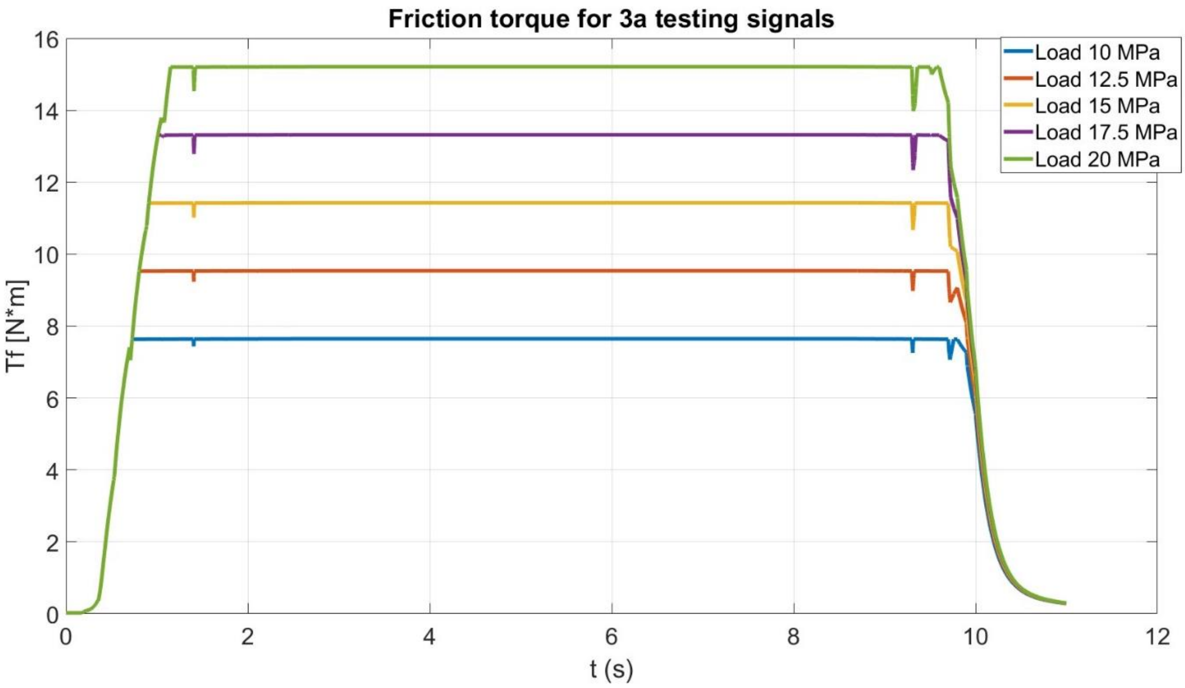

Figure 91. Friction torque Test Scenario No. 3a.

Figure 91 illustrates the friction torque in the pump assembly. The torque value increases rapidly with pressure at the beginning of the cycle and stabilizes in the steady-state phase at a level proportional to the set load pressure.

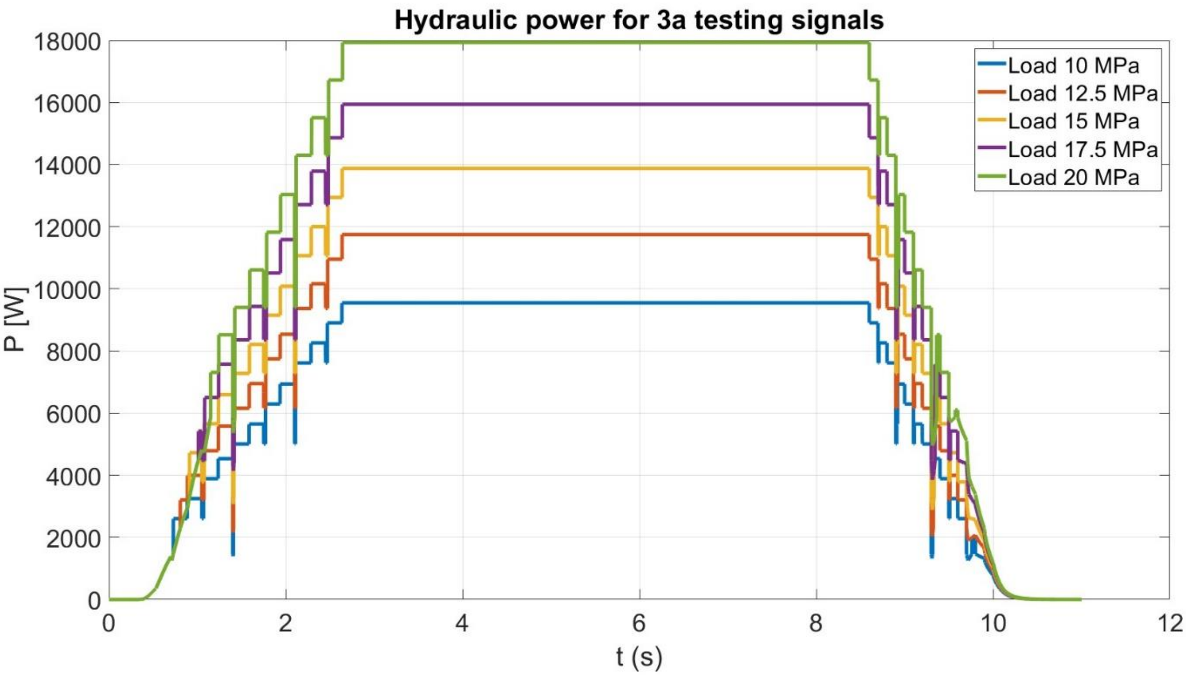

Figure 92. Hydraulic power Test Scenario No. 3a.

Figure 92 depicts the hydraulic power generated by the system in a dynamic cycle. The very steep slope of the power during the ramp-up phase indicates high instantaneous energy demand, and the power level in the steady-state grows with the increase in load pressure.

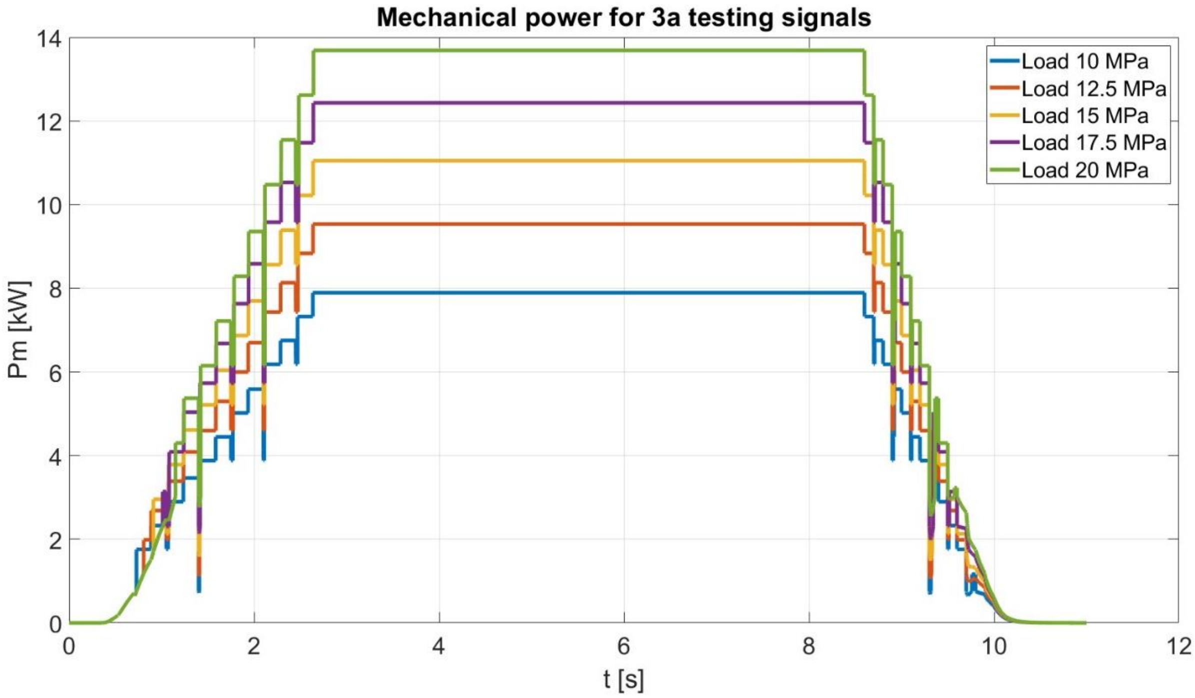

Figure 93. Mechanical power Test Scenario No. 3a.

Figure 93 displays the mechanical power supplied to the drive shaft. The curve is similar to that of hydraulic power, but with higher values by the amount of losses in the system, which increases at higher pressures.

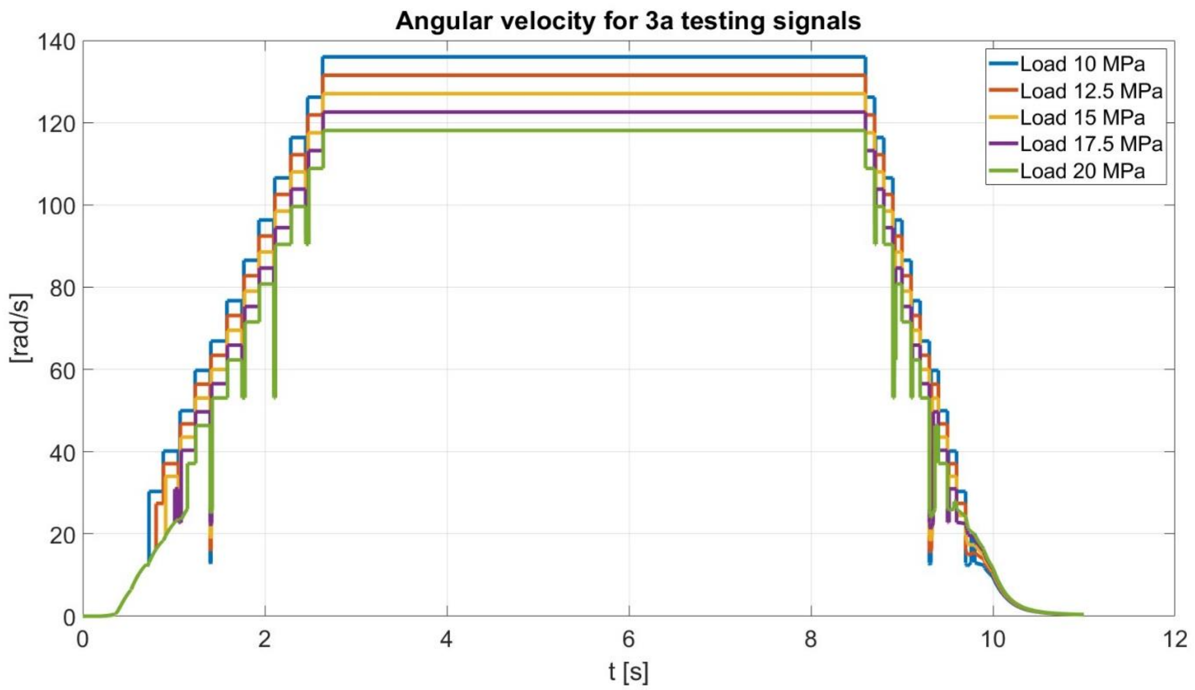

Figure 94. Angular velocity Test Scenario No. 3a.

Figure 94 illustrates the angular velocity of the drive shaft. In this short cycle, there is a small decrease in velocity during the steady state phase as the load pressure increases.

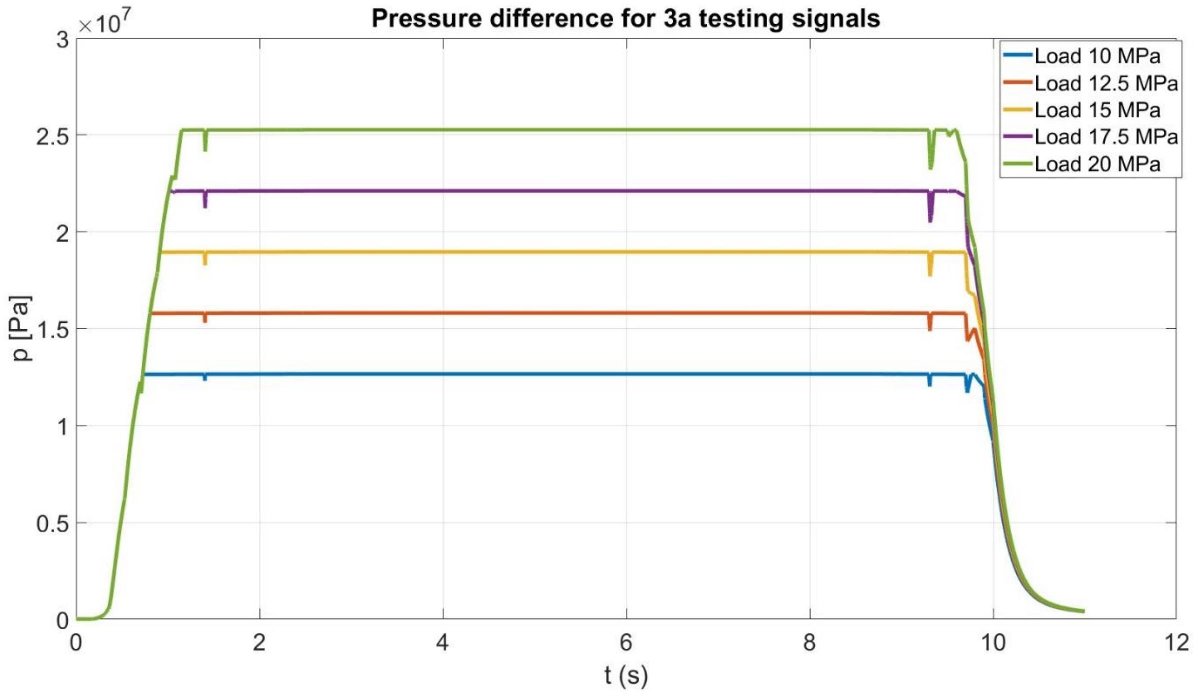

Figure 95. Pressure difference Test Scenario No. 3a.

Figure 95 confirming that the load pressure during the steady-state phase of the cycle was maintained at the five specified, constant levels. Slight pressure peaks are also visible at the beginning and end of the steady-state phase, resulting from the flow dynamics.

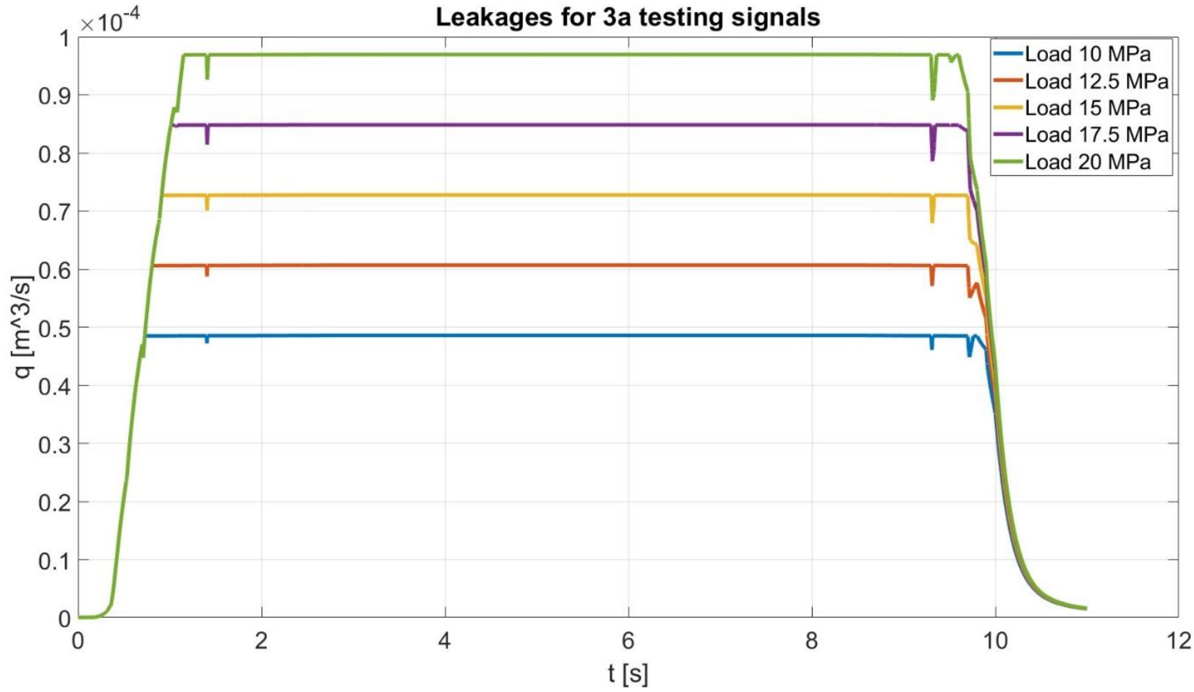

Figure 96. Leakages Test Scenario No. 3a.

Figure 96 illustrates the volumetric losses. The level of leakage in the steady-state phase is constant and grows in steps depending on the level of load pressure.

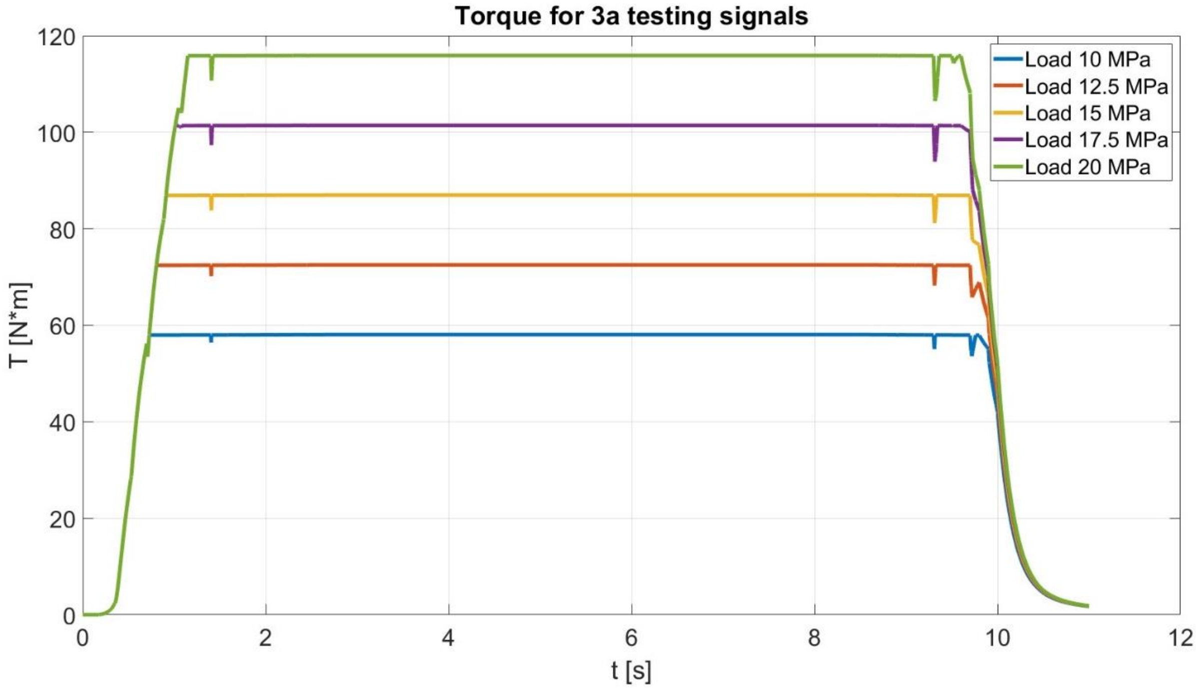

Figure 97. Torque Test Scenario No. 3a.

Figure 97 illustrates the total torque required to drive the pumps assembly. The rapid increase at the beginning of the cycle shows high dynamic demand, and the torque level in the steady-state phase is directly proportional to the load pressure.

Summary analysis of simulation results for Scenario No. 3a.

The pressure difference confirming that during the steady-state phase of the cycle (approx. 2s - 9.5s), the model operated under the specified, stable load. This graph also shows slight, momentary pressure peaks (overshoots) at the beginning and end of the steady-state phase, which is characteristic of rapid changes in flow rate and the associated dynamic fluid phenomena. The profiles of angular velocity and flow rate reflect the very fast dynamics of the commanded cycle. The ramp-up phase to full output takes about 2 seconds and, as in previous tests, has a stepped character, which is a signature of the digital pump control. Consistent with previous observations, the decrease in rotational speed is associated with a reduction in flow rate caused by an increase in internal leakage. This is more pronounced in the steady-state phase at higher load pressures. The graphs of leakages and friction torque confirm the conclusions from previous analyses. The magnitudes of both types of losses in the implemented model are primarily a function of pressure. In the steady-state phase, they assume a constant value that is higher for higher load pressures (from 10 to 20 MPa). The rapid increase in losses at the beginning of the cycle is directly correlated with the fast pressure build-up in the system.

The total torque and both mechanical and hydraulic power also follow the trapezoidal profile. The very steep slopes on these graphs during the ramp-up phase (0-2s) indicate a high demand for torque and power, necessary to rapidly accelerate the system to full output. In the steady-state phase, the torque and power values stabilize at levels directly proportional to the set load pressure. A comparison of the mechanical and hydraulic power graphs again shows that the difference between them (representing losses) increases with the load. This means that the system's energy efficiency decreases at higher pressures.

8.1.5 Simulation Research Results for Test Scenario No. 3b

The presented set of simulation results (Fig. 98 to Fig. 105) illustrates the behavior of the digital hydraulic system during operation under the fifth test scenario. This profile, similar to the previous ones, has a trapezoidal character but is distinguished by shorter cycle time (approx. 5 seconds) and rapid ramp-up and ramp-down phases of the parameters according to previous ones. The purpose of this test was to investigate the theoretical, dynamic limits of the system and its behavior under conditions requiring an immediate response. The research was conducted for five different levels of load pressure (10-20 MPa).

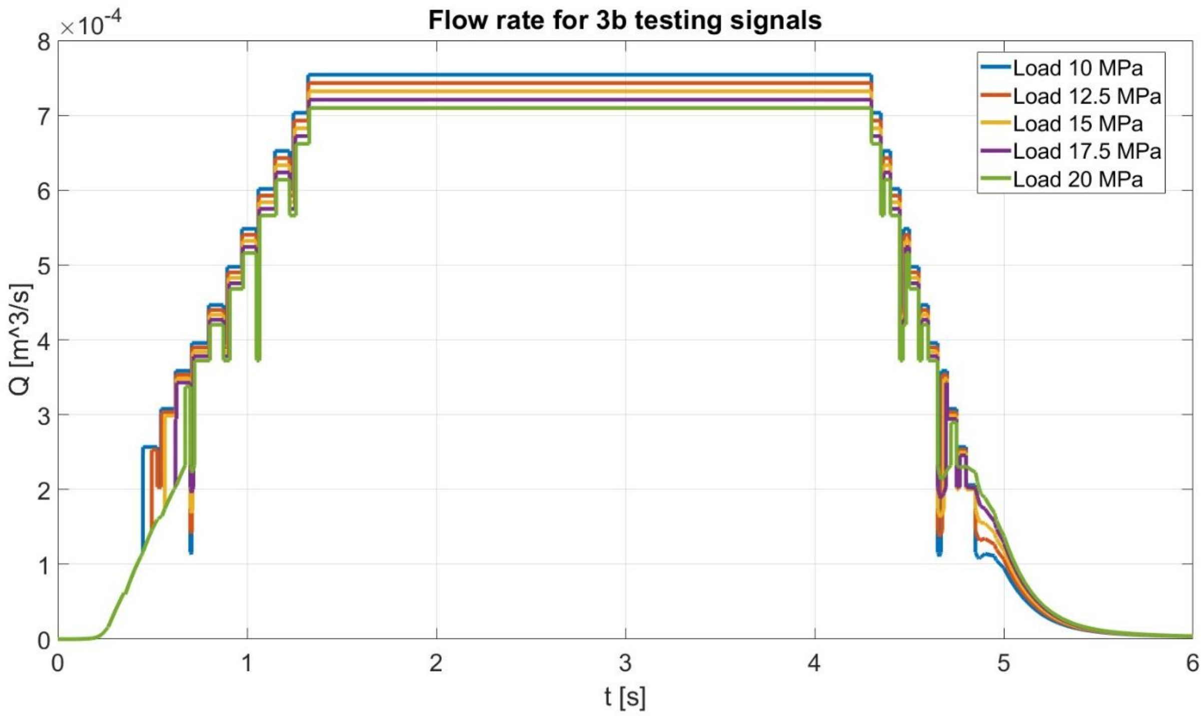

Figure 98. Flow rate Test Scenario No. 3b.

Figure 98 shows the flow rate in a fast-trapezoidal cycle. The ramp-up and ramp-down phases, lasting only about one second, demonstrate the system's dynamic capability, and the irregular, stepped nature of the ramps indicates a very aggressive pump switching strategy.

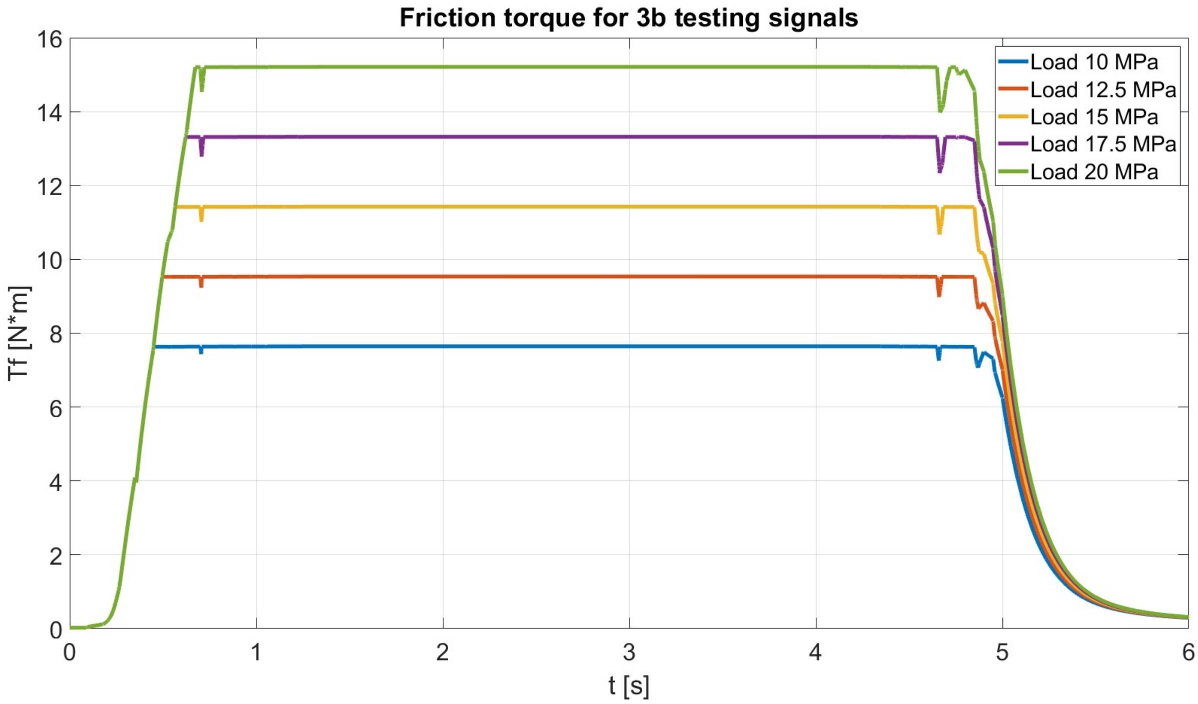

Figure 99. Friction torque Test Scenario No. 3b.

Figure 99 illustrates the friction torque. The torque value increases rapidly to a constant level in the steady-state phase, and its magnitude is directly proportional to the set load pressure.

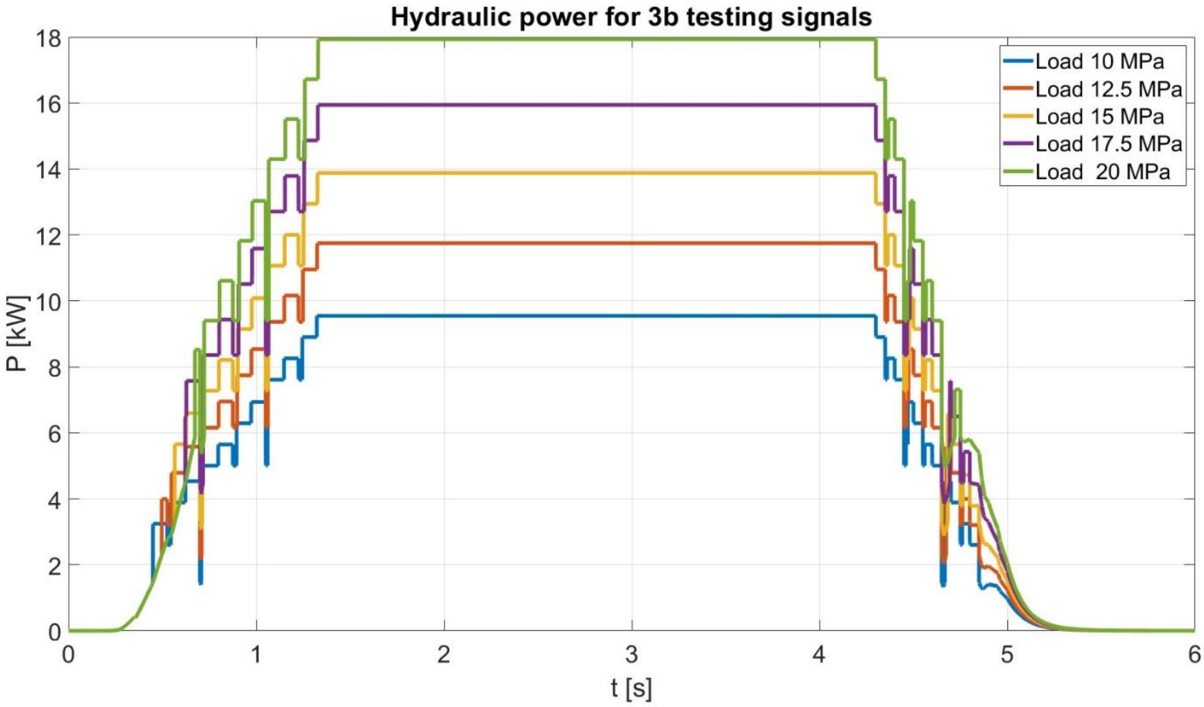

Figure 100. Hydraulic power Test Scenario No. 3b.

Figure 100 depicts the hydraulic power generated by the system. The very steep slope of the power during the ramp-up phase, reaching within a second, indicates high instantaneous energy demand, and the power level in the steady-state increases with load pressure.

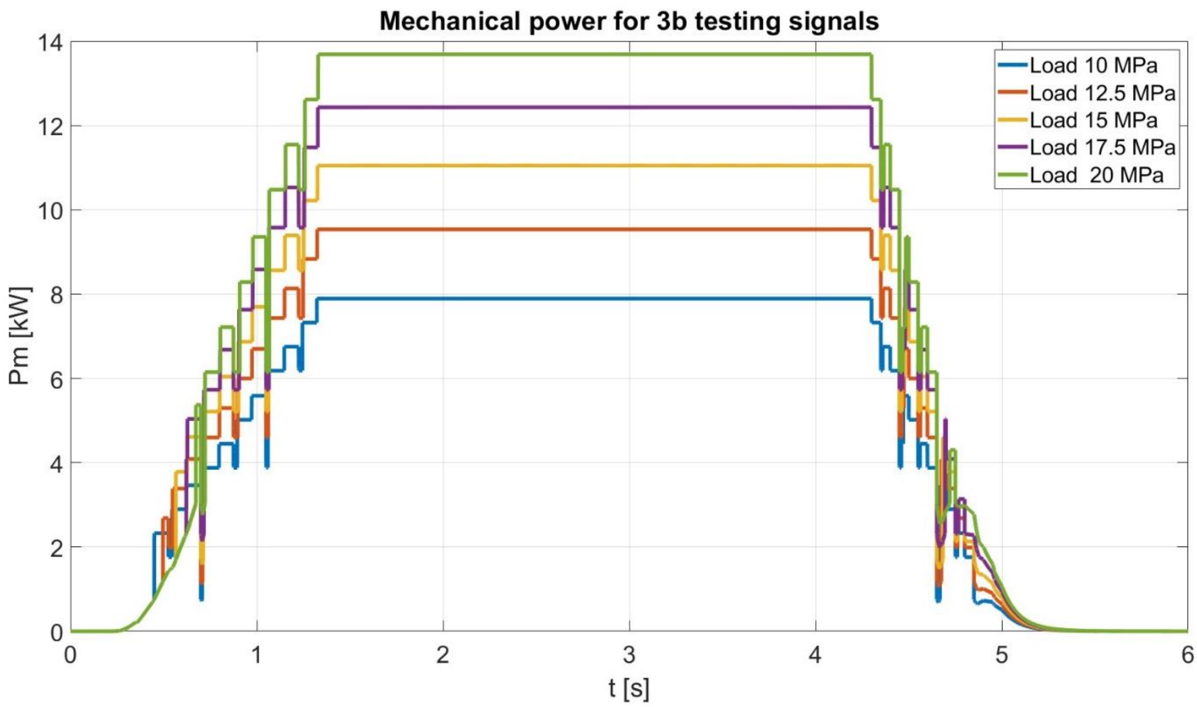

Figure 101. Mechanical power Test Scenario No. 3b.

Figure 101 reveals the mechanical power supplied to the drive shaft. It has a similar profile to the hydraulic power curve, though with higher values due to the sum of all losses occurring in the system with increasing load pressure.

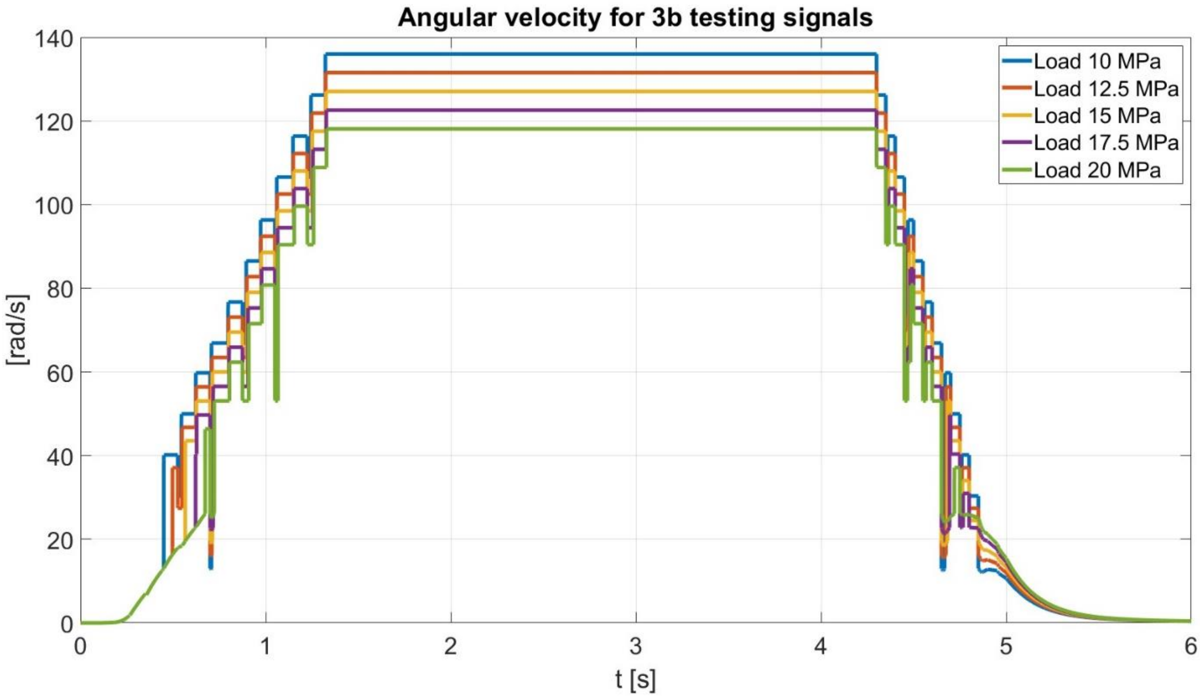

Figure 102. Angular Velocity Test Scenario No. 3b.

Figure 102 presents the angular velocity of the drive shaft of hydraulic motor. The acceleration phase to operating speed is short, and in the steady-state phase, a slight drop in speed is still visible at higher load pressures (from 10 to 20 MPa).

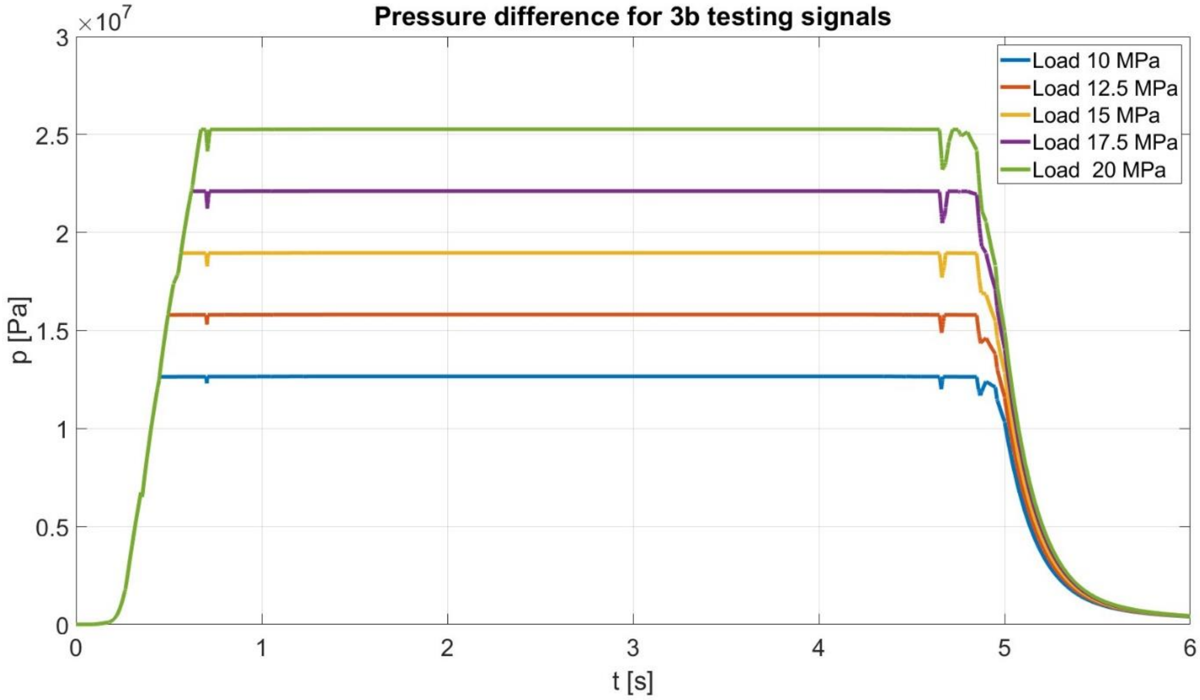

Figure 103. Pressure difference Test Scenario No. 3b.

Figure 103 present pressure in the system for the different load pressure (10-20 MPa). The pressure was maintained during the steady-state phase. The largest pressure peaks (overshoots) are clearly visible here, resulting from higher dynamics of the cycle.

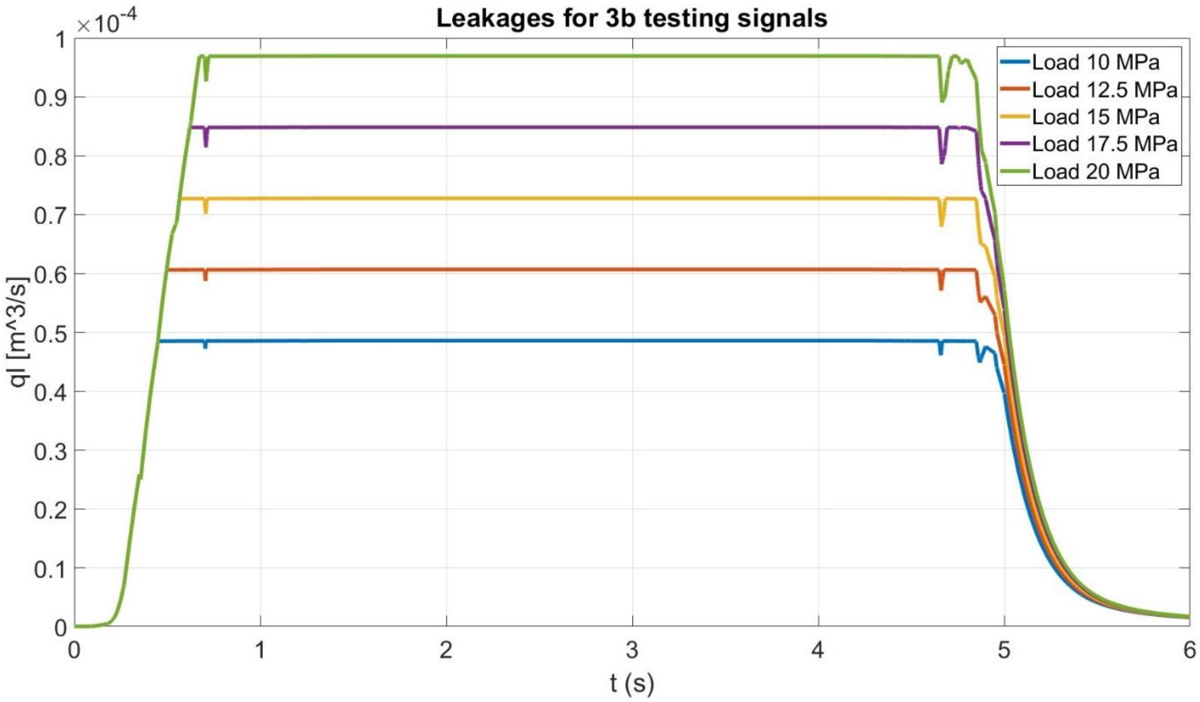

Figure 104. Leakages Test Scenario No. 3b.

Figure 104 visualizes the volumetric losses. The magnitude of the leakage in the steady-state phase is constant and depends directly on the load pressure level.

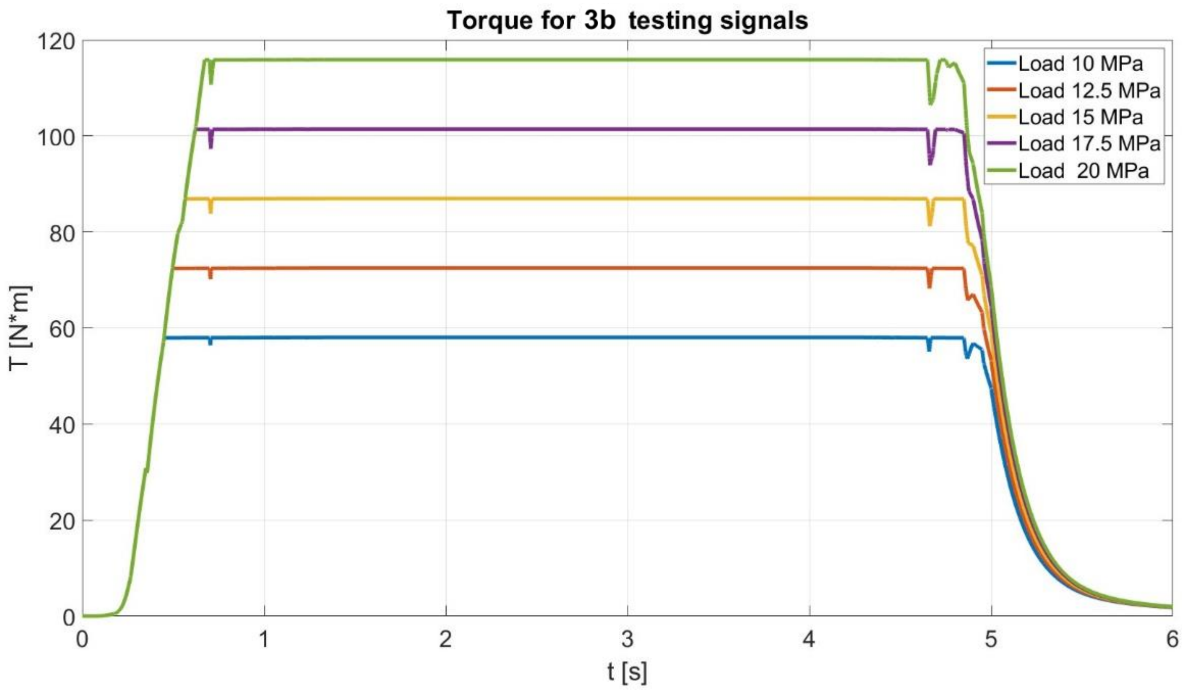

Figure 105. Torque Test Scenario No. 3b.

Figure 105 illustrates the total torque required to drive the pumps. The almost instantaneous rise to the maximum value demonstrates the high dynamic of this cycle, and the torque level in the steady-state phase is directly proportional to the operating pressure.

The pressure difference graph confirms that the specified loads (10-20 MPa) are maintained during the steady-state phase of the cycle (approx. 1s - 4.5s). In this scenario, due to higher dynamics, the most pronounced pressure peaks are visible at the beginning and end of the steady-state phase. This is a key observation, indicating that very rapid changes in flow induce significant wave phenomena (pressure shocks) in the system. The profiles of angular velocity and flow rate are characterized by a nearly vertical ramp-up phase, reaching full output in just one second. The steps on the ramps here are less regular and more dynamic than in previous tests, which may suggest that the model represents very fast, possibly overlapping, pump switching to achieve such high dynamics. The drop in speed as a function of load is visible. The graphs of leakages and friction torque consistently confirm the conclusions from previous analyses. Both forms of loss in the implemented model are almost exclusively a function of pressure. Their values increase rapidly with pressure in the first second of the cycle, after which they stabilize at a level proportional to the set load for the duration of the steady-state phase. The graphs of torque, hydraulic power, and mechanical power show an almost instantaneous increase to maximum values. The steep slopes of these profiles indicate high instantaneous demand for power and torque. The steady-state values, as in previous tests, scale linearly with the load pressure. The comparison of mechanical and hydraulic power again reveals growing energy losses at higher pressures, which translates into a decrease in the overall efficiency of the system.

8.1.6 Simulation Research Results for Test Scenario No. 3c

The presented set of simulation results (Fig. 106 to Fig. 113) illustrates the behavior of the digital hydraulic system under the sixth and most dynamically aggressive test scenario. This profile, characterized by a trapezoidal shape and a total duration of only 2,5 seconds, features an extremely fast ramp-up phase (under 0.5 seconds) and a very rapid ramp-down. The purpose of this test was to investigate the dynamic limits of the simulated system in response to a step command.

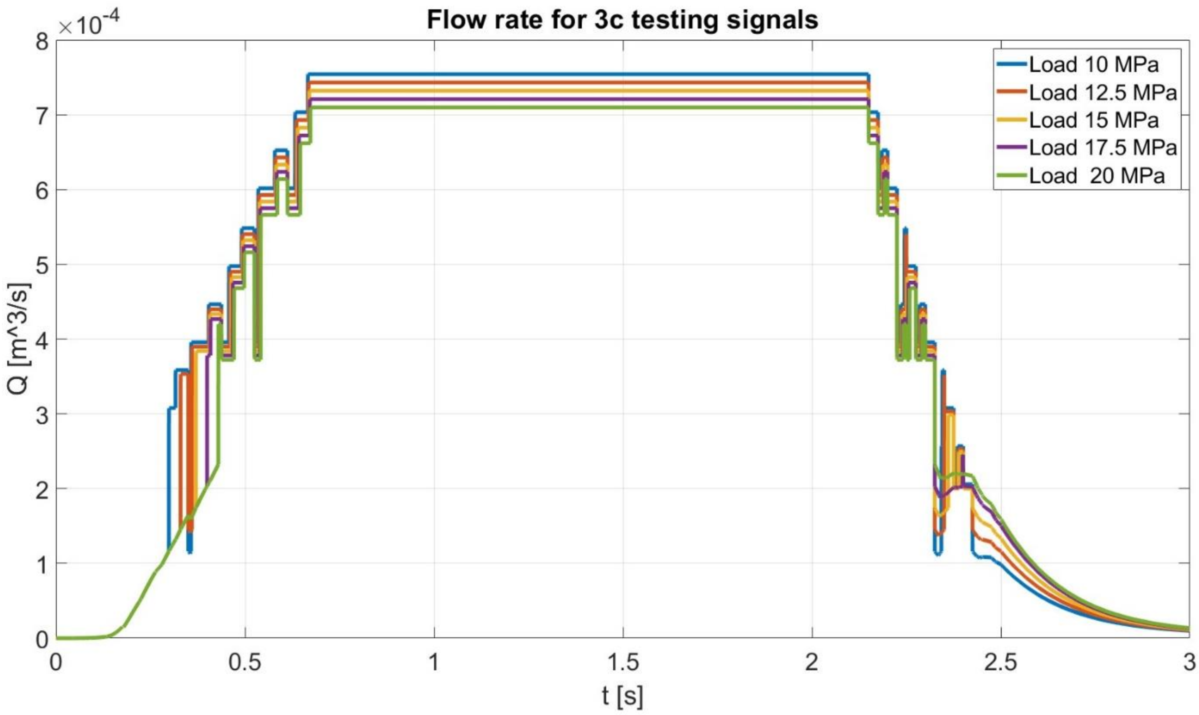

Figure 106. Flow rate Test Scenario No. 3c.

Figure 106 shows the flow rate during the most dynamic cycle tested. The ramp-up phase to full power in less than 0.5 seconds demonstrates the system's limited acceleration capabilities. A similar pattern occurs as the flow rate decreases. This suggests the beginnings of limitations for this control strategy.

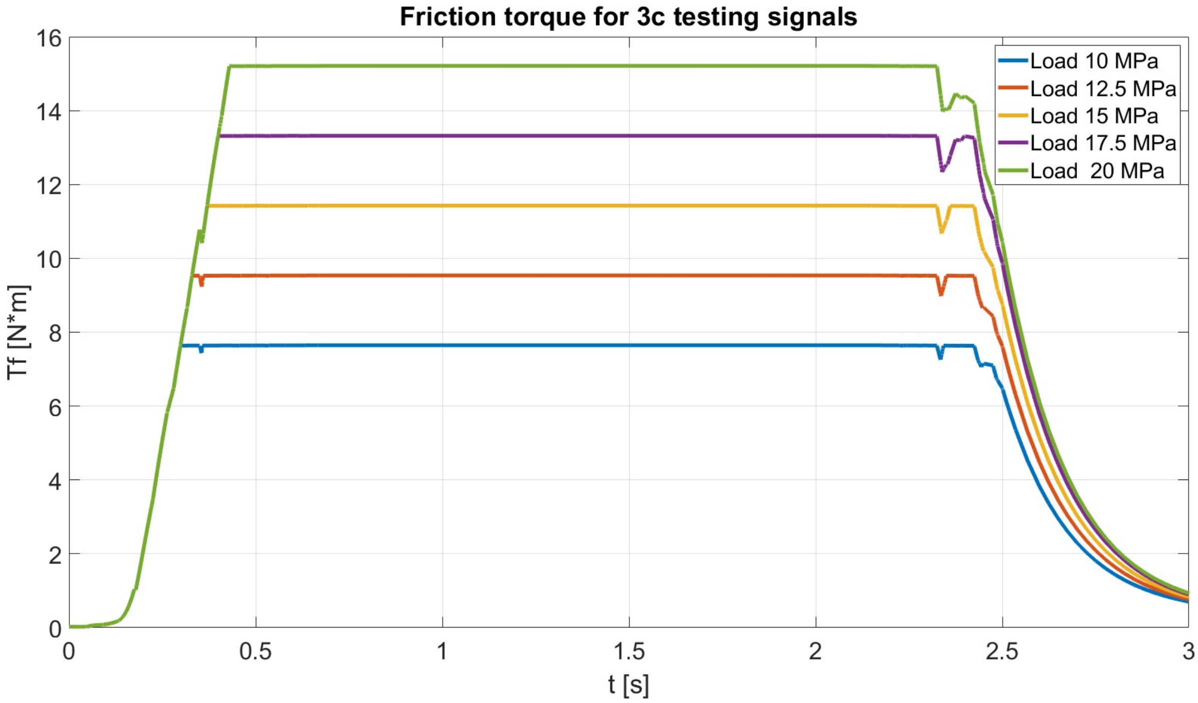

Figure 107. Friction torque Test Scenario No. 3c.

Figure 107 illustrates the friction torque in the pumps assembly. The torque value increases rapidly with pressure at the beginning of the cycle and stabilizes in the steady-state phase at a level proportional to the set load pressure.

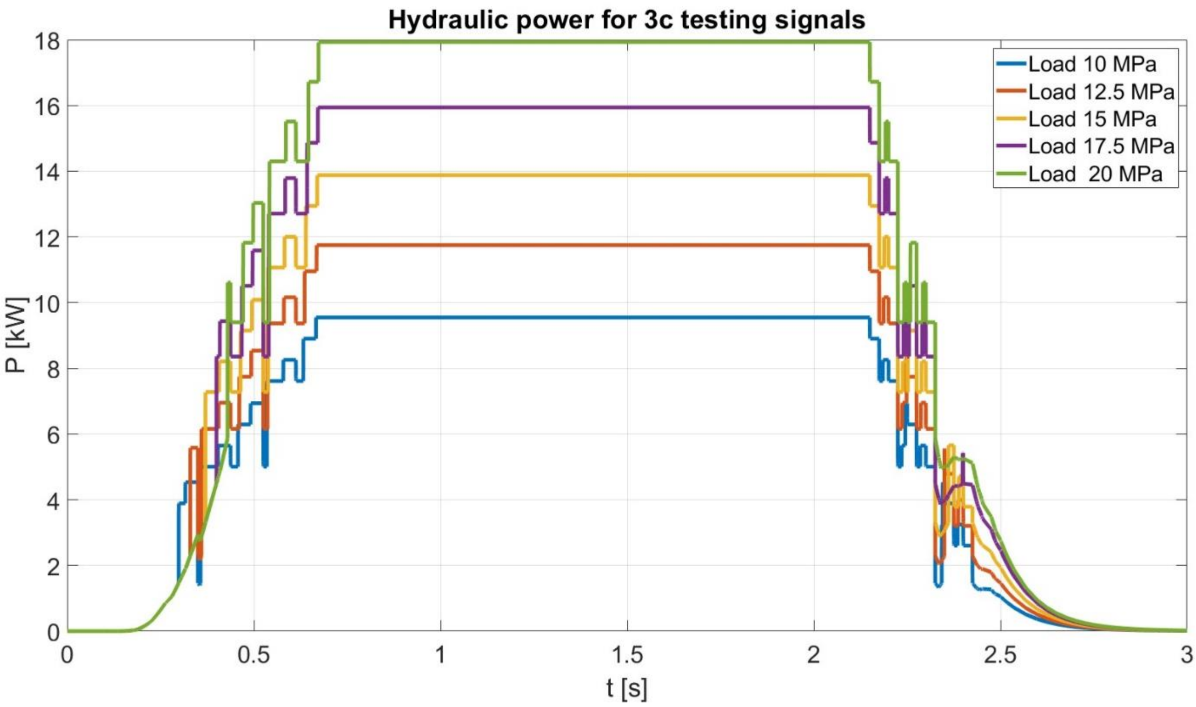

Figure 108. Hydraulic power Test Scenario No. 3c.

Figure 108 depicts the hydraulic power generated by the system. The nearly vertical slope of the power during the ramp-up phase indicates an extremely high instantaneous energy demand, and the power level in the steady-state increases with pressure.

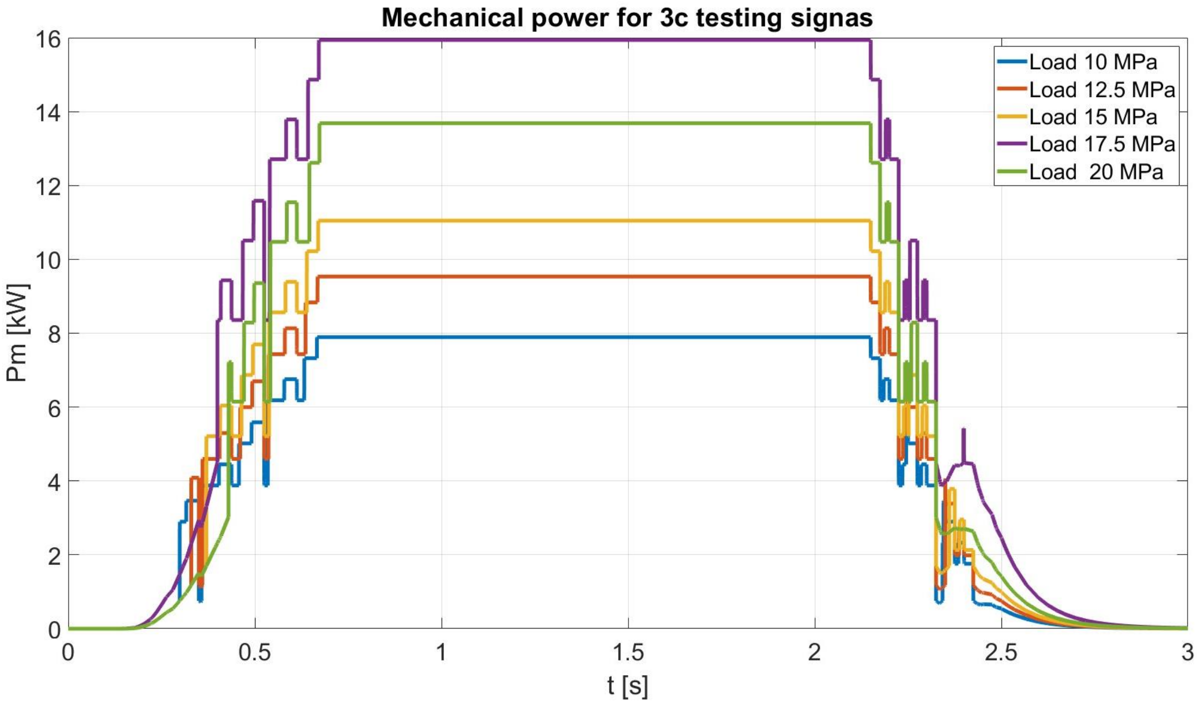

Figure 109. Mechanical power Test Scenario No. 3c.

Figure 109 represented the mechanical power supplied to the drive shaft. This profile is similar to the hydraulic power profile, but the values are greater by the sum of the losses in the system, which are proportional to the operating pressure.

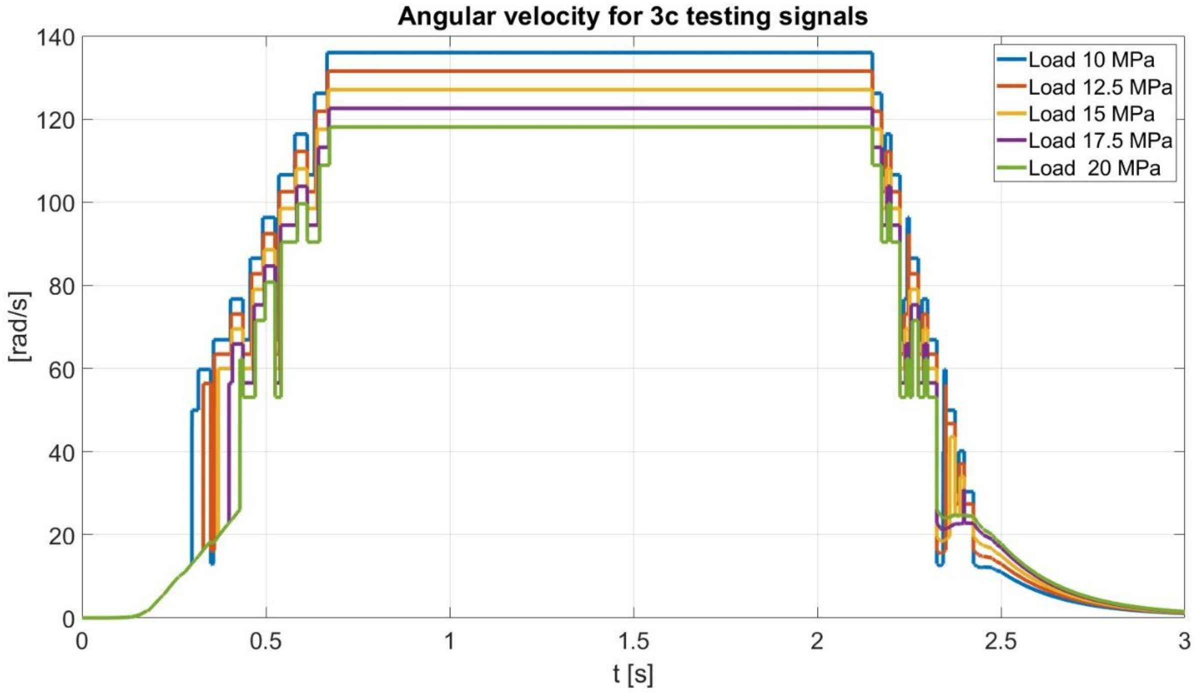

Figure 110. Angular velocity Test Scenario No. 3c.

Figure 110 presents the angular velocity of the drive shaft. The acceleration phase to operating speed is extremely short (<0.5s), and Throughout the steady-state phase, a minor speed reduction remains observable under increased load pressures. (from 10 to 20 MPa).

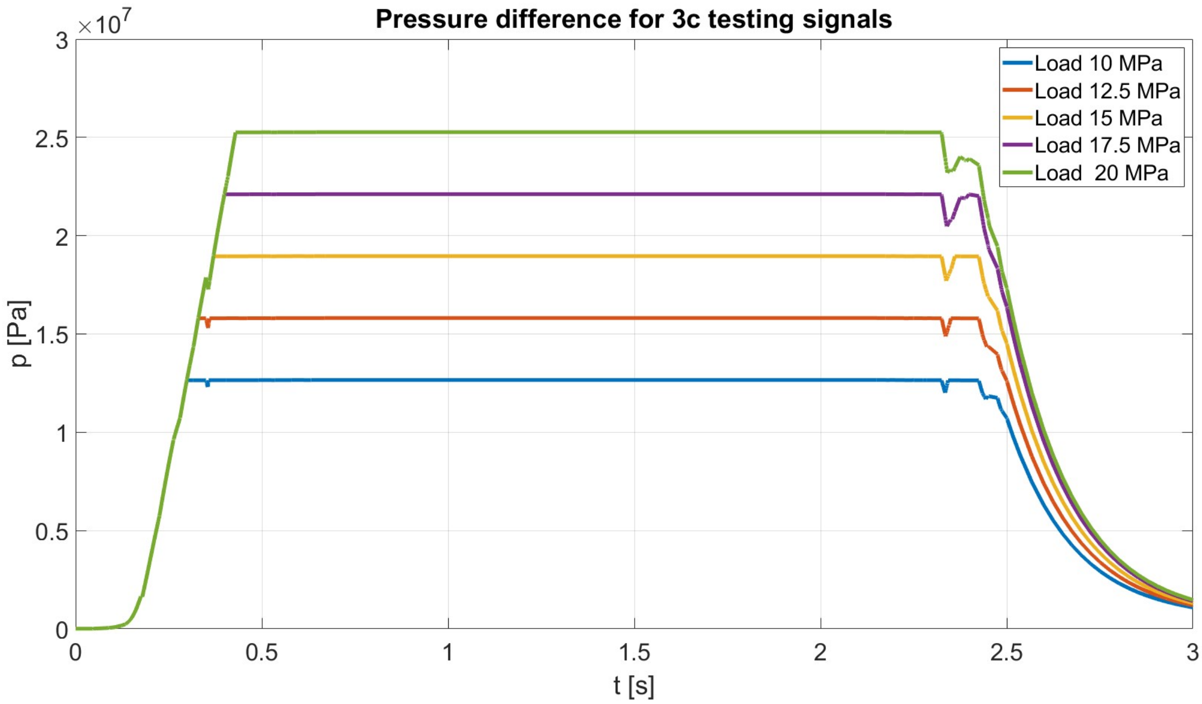

Figure 111 . Pressure difference Test Scenario No. 3c.

Figure 111 presents the pressure in the system for different load pressure (10-20 MPa). The sharpest pressure peaks (overshoots) at the beginning of the steady-state phase are clearly visible here, resulting from the dynamics of the cycle.

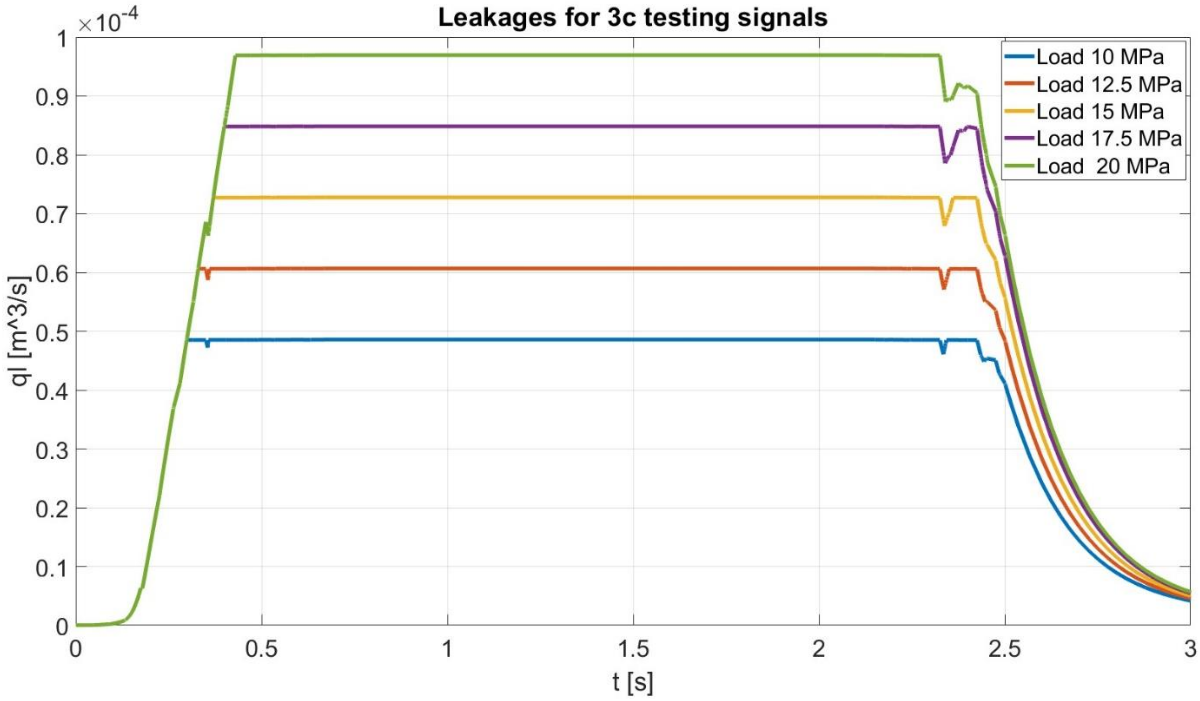

Figure 112. Leakages Test Scenario No. 3c.

Figure 112 depicts the volumetric losses. The magnitude of the leakage in the steady-state phase is constant and depends directly on the load pressure level, which is consistent with previous analyses.

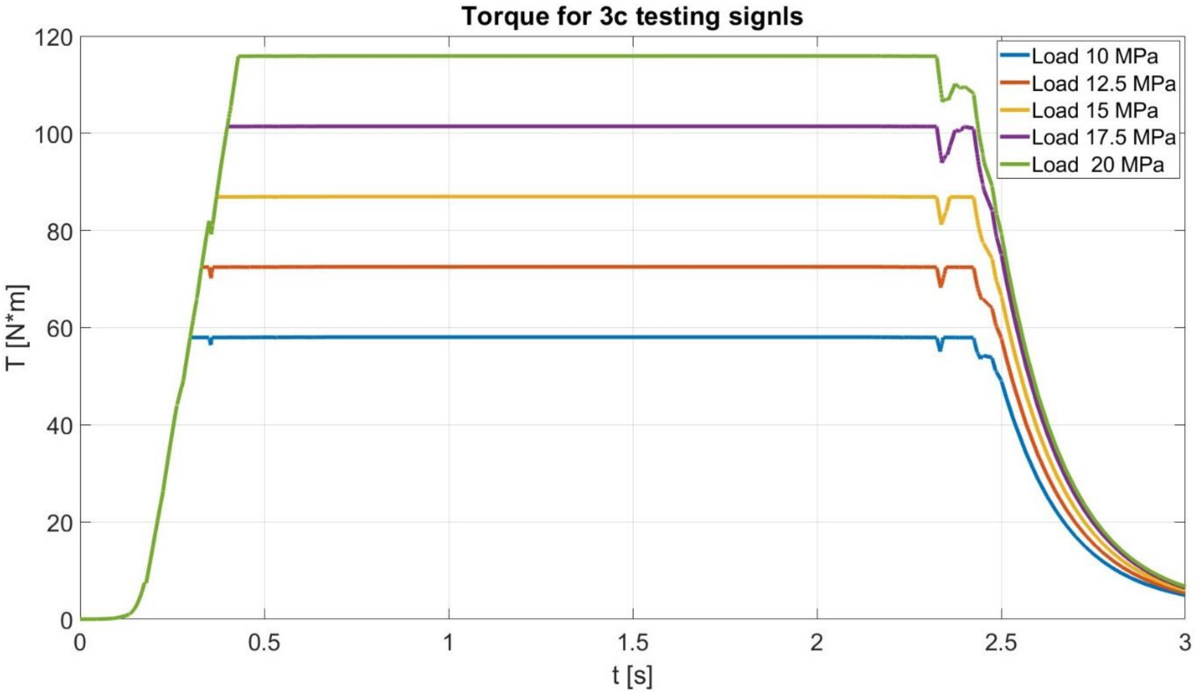

Figure 113. Torque Test Scenario No. 3c.

Figure 113 illustrates the total torque required to drive the pumps. The almost instantaneous rise to the maximum value demonstrates the extreme dynamic requirements of this cycle, and the torque level in the steady-state phase is directly proportional to the operating pressure.

The pressure difference most clearly reveals dynamic phenomena in this scenario. The rapid pressure increase at the beginning of the cycle generates a distinct overshoot (pressure peak) just after reaching the set value (approx. t=0.4s). This phenomenon confirms that the faster the required system response, the more pronounced the wave effects and pressure shocks become. The profiles of angular velocity and flow rate demonstrate the system's theoretical capability for almost instantaneous acceleration. Achieving full operating speed in under half a second is evidence of the digital system's significant dynamic potential. Interestingly, the ramp-down phase (after t≈2.3s) has a more complex, stepped character than the ramp-up phase. The graphs of leakages and friction torque once again confirm that the modelled losses are primarily a function of pressure. Their profiles almost perfectly replicate the pressure profile: they increase rapidly to a constant level that is proportional to the set load and maintain it throughout the steady-state phase. The energy and mechanical requirements in this test reach their extreme. The torque graph shows a nearly vertical line in the ramp-up phase, which indicates a huge, instantaneous demand for torque. The steady-state values, like the losses, scale linearly with the load pressure. The hydraulic power and mechanical power graphs highlight the peak power demand in the system. The system must be capable of delivering full power almost instantly. The difference between mechanical and hydraulic power (losses) is clearly larger at higher pressures, which is consistent with previous analyses and indicates a decrease in efficiency under increasing load. The simulation of the fastest duty cycle allows to investigate the theoretical limits of the system's dynamic performance. It confirms the system's ability to reach full power and flow in less than a second. However, this value appears to be close to critical – if the trapezoidal time of load is reduced, it may be impossible to achieve the desired fluid delivery profile (e.g., due to constraints related to the on/off valve switching time). The most important conclusion from this analysis is that extremely fast control, although possible in the model, generates the most severe dynamic phenomena, such as pressure peaks.

In this part of the work, a series of test scenarios were defined and analyzed, aimed at evaluating and comparing the operation of a digital hydrostatic transmission under various operational conditions. Three distinct test scenarios were defined, which simulate different machine operating conditions (for the third scenario, in-depth research was conducted, consisting of shortening the cycle duration while maintaining maximum flow rates):

- **Scenario No. 1:** A symmetrical, trapezoidal flow profile, characterized by ramp-up, steady-state, and ramp-down phases.
- **Scenario No. 2:** Pulsating (intermittent) operation with a series of pulses of step-increasing amplitude, which tests the system's behavior during frequent start-stop cycles.
- **Scenario No. 3:** A trapezoidal profile typical for vehicle motion, including acceleration, constant speed driving, and braking phases for 4 cycles differing only in their execution time, namely 20s, 10s, 5s, and 2.5s.

All scenarios were realized using the same hardware configuration and four gear pumps with displacements of : P1=3.1831×10^{-7}m³/rad (2 cm^3/rev), P2=6.3662×10^{-7}m³/rad (4 cm^3/rev), P3=1.2732×10^{-6}m³/rad (8 cm^3/rev), P4=2.5465×10^{-6} m³/rad (16 cm^3/rev), controlled by on/off valves.

For all six scenarios, simulation studies were conducted for five different levels of load pressure (from 10 to 20 MPa every 2.5 MPa). This will allow for a comprehensive analysis of the influence of load on the system's operation. The key observations from these simulations are:

- An increase in load pressure leads to:
  - An almost proportional increase in the required torque and consumed mechanical power.
  - An increase in internal losses (leakages and friction torque).
  - A slight decrease in flow rate, and consequently angular velocity, due to increasing leakages in the system.
- The simulations consistently showed the "stepped" character of the flow ramp-up and ramp-down, which is a signature of digital control (so-called resolution). They also revealed slight pressure overshoots in the transient phases.

The analysis of all presented simulation scenarios allowed for the formulation of a general conclusion that the conducted research effectively replicates the behavior of the digital hydrostatic transmission under various conditions, confirming the basic theoretical relationships. These results constitute a solid reference base that will be used to compare it with the simulation model of a classic hydrostatic transmission in order to answer the question of whether it can be used as an alternative for application in multi-source hydrostatic drive systems.

8.2 Classic Hydrostatic Transmission

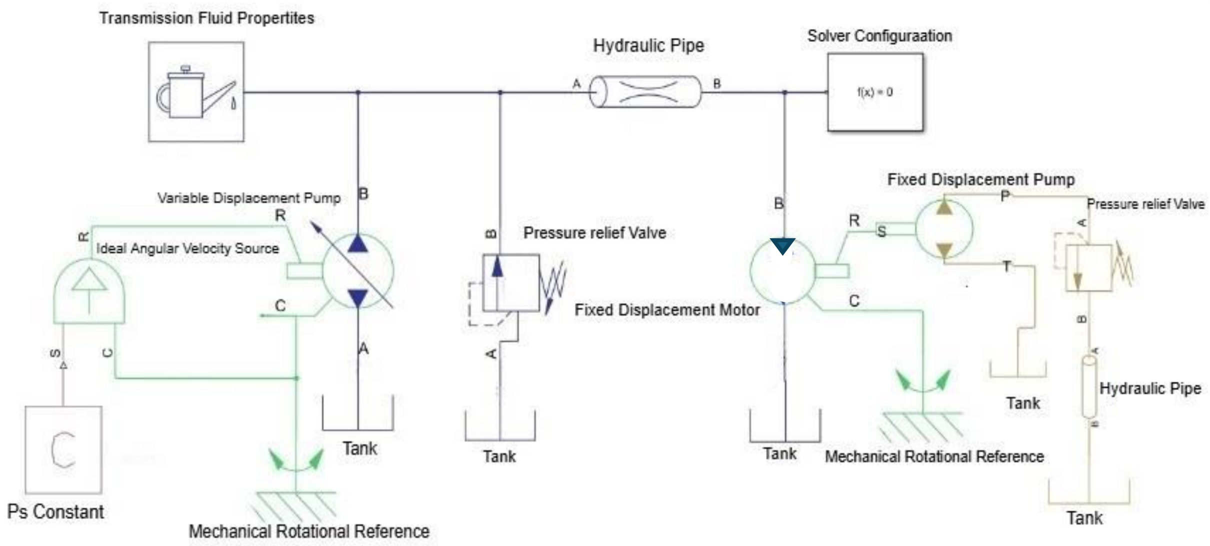

Figure 114. The simulation model of „classic" hydrostatic transmission.

The provided schematic (Fig. 114) shows a simulation model of a classic, open-loop hydrostatic transmission, built in the MATLAB/Simscape environment. This model was developed to create a comparative basis (benchmark) for the analysis and evaluation of the properties of the digital hydrostatic transmission. The system consists of a supply unit, a transmission line, a hydraulic motor and load unit, and control blocks. The main drive is represented by the Velocity Source block, which sets a constant angular velocity on the pump shaft, like an ideal electric motor. It simulates the operation of an electric or internal combustion engine at a constant rotational speed. The heart of the supply system is the Variable-Displacement Pump block (labeled as "Pump"). It represents a variable-displacement pump, (axial-piston pump) with a tilting swashplate. Its displacement is controlled by an external physical signal connected to port C. The physical properties of the working fluid (such as density, viscosity, bulk modulus) for the entire circuit are defined globally in the Transmission Fluid Properties block. The model accounts for volumetric losses for both the pump and the hydraulic motor. The system is protected from excessive pressure increase by the Pressure Relief Valve B block, which is connected to the main pressure line and opens the flow to the tank upon exceeding the set pressure. The connection between the pump and the motor is modeled using the Pipe B block. This block represents a hydraulic pipeline, accounting for pressure losses resulting from friction and the effects related to the fluid's compressibility inside the line. Hydraulic Motor is the Fixed-Displacement Motor block (labeled as "FDM"). It represents a fixed-displacement motor that converts the hydraulic energy supplied from the pump into mechanical energy in the form of torque and rotational motion on the output shaft (port R). The load for the FDM motor is simulated by another hydraulic unit a fixed-displacement pump, FDPLoad. It is mechanically connected to the FDM motor shaft and acts as a hydraulic brake. It generates a resistive torque, the value of which is controlled by throttling the flow at its outlet.

The main control signals for the model are supplied by the System Inputs block. The parameters of the individual components of the system are presented in the tables in Appendix C (Table C20 to C33).

8.2.1 Comparison of Experim. and Sim. Results for Scenario No. 2 (Load 1,2 MPa)

The presented set of graphs allows for the validation of the simulation model through its direct comparison with data obtained from the physical object. This analysis aims to assess the model's fidelity, identify any discrepancies, and understand their physical causes. It was decided that the comparison would be presented only for the second scenario.

On a macroscopic scale, the simulation model shows general agreement with the experimental results. Both, the simulation (PS) and the experiment (profiles 1 and 2) correctly replicate the pulsating nature of the second test scenario, with a series of pulses of step-increasing amplitude. This confirms that the control logic in the model is consistent with reality. In the steady-state phases of each pulse, the values of key parameters from the simulation are very close to the experimental values. The maximum flow rate, load pressure, average torque, and active power in the simulation align well with the averaged values from the measurements. This indicates the correct parameterization of the static aspects of the model, such as leakage and friction losses in steady states.

The most important conclusions come from the analysis of the differences in dynamic behavior, which are most visible on the torque graph. This is the most significant discrepancy between the model and reality. The experimental results clearly show the occurrence of sharp, very high torque peaks at the beginning of each pulse. In contrast, the torque profile from the simulation (sim torque) is "flat" and devoid of these dynamic overshoots. The absence of peaks in the simulation proves that the mathematical model in its current form is too simplified and does not sufficiently account for dynamic phenomena. The simulation shows almost perfectly rectangular pressure and flow pulses. In reality, these profiles have a slower rise time and more rounded shapes, which is also an effect of the inertia and damping present in the real system.

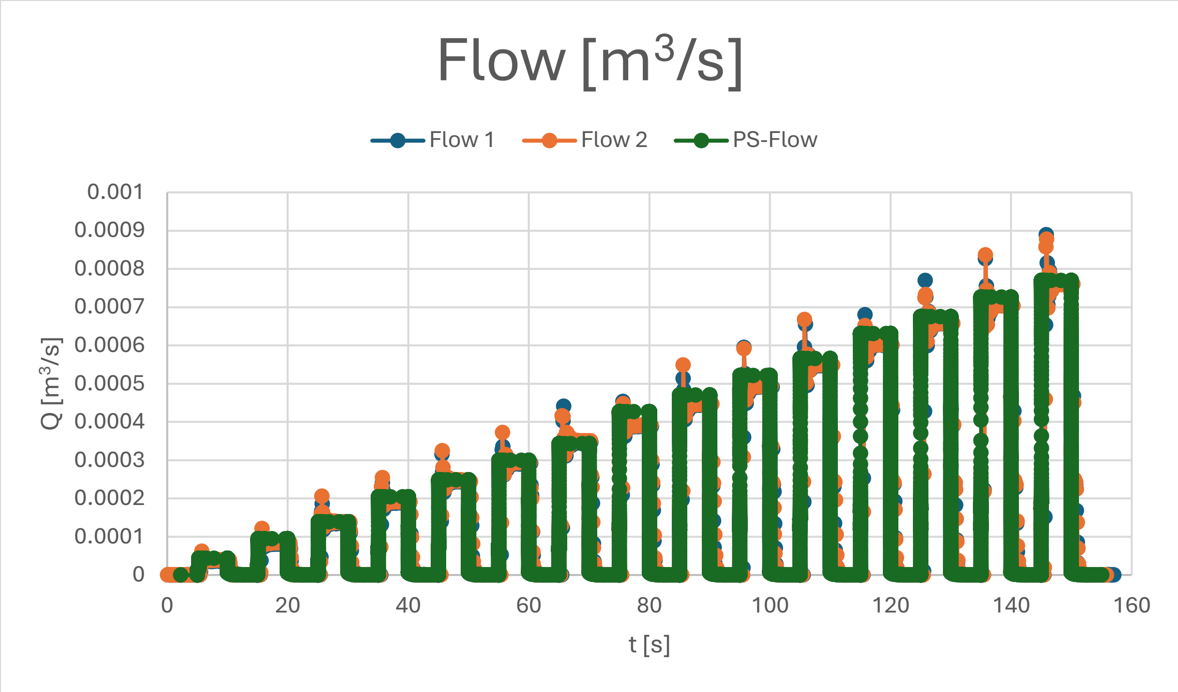

Figure 115. Flow rate Comparative Analysis of Experimental and Simulation Research Results for Scenario No. 2 (Load 1.2 MPa).

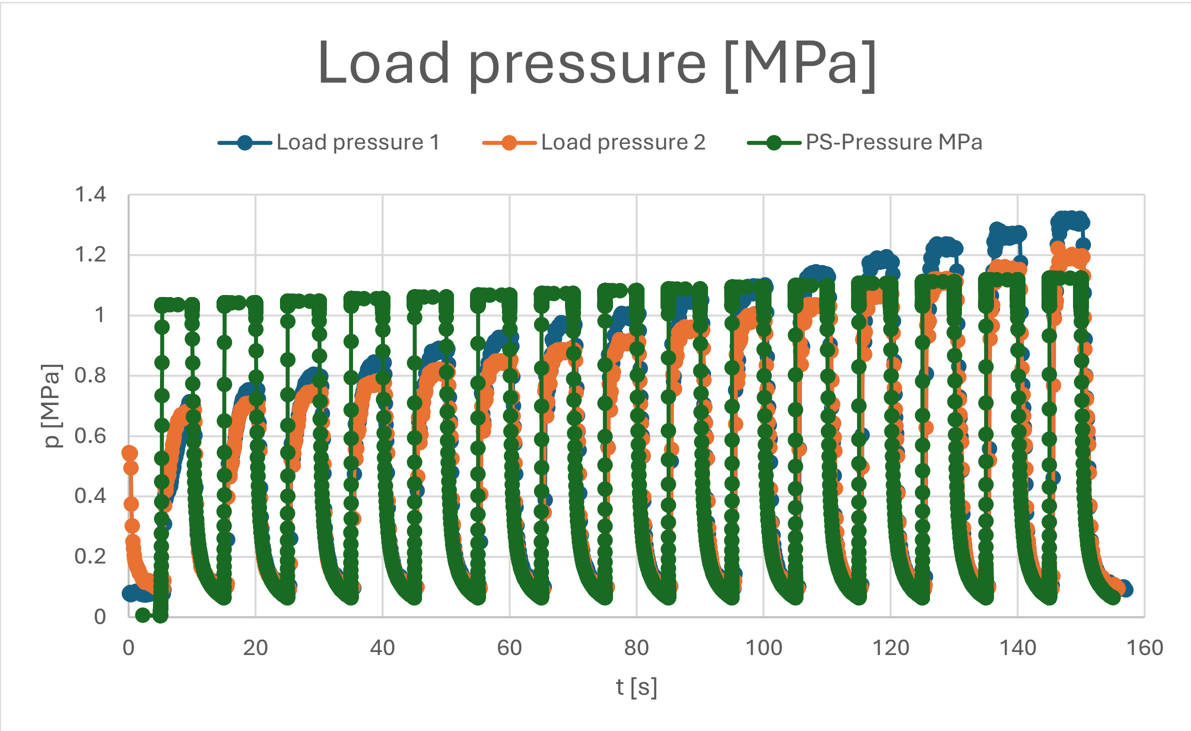

Figure 116. Load pressure Comparative Analysis of Experimental and Simulation Research Results for Scenario No. 2 (Load 1.2 MPa).

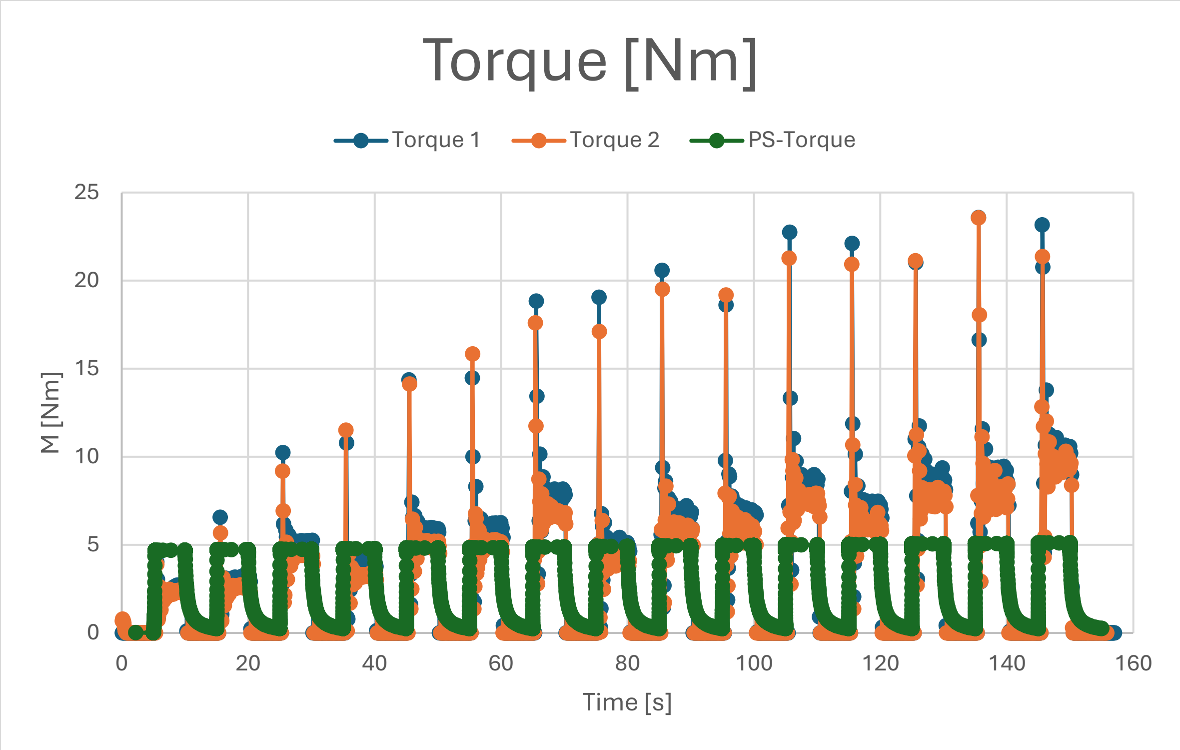

Figure 117. Torque Comparative Analysis of Experimental and Simulation Research Results for Scenario No. 2 (Load 1.2 MPa).

The simulation model has been correctly calibrated for steady states. It accurately predicts the average values of flow, pressure, power, and torque, making it a useful tool for energy and performance analysis in quasi-static conditions. The model omits dynamic phenomena such as hydraulic shocks and the associated torque peaks. For this reason, it is not suitable for analyzing fatigue loads, mechanical durability, vibrations, or noise. To increase the dynamic fidelity of the model, the simulation model should be expanded by reducing the number of simplifying assumptions.

8.2.2 Comparison of Experim. and Sim. Results for Scenario No. 2 (Load 6 MPa)

A comparative analysis at a pressure of 6 MPa allows for the assessment of the simulation model's fidelity under higher, dynamic load conditions.

On a macroscopic scale, the simulation model continues to correctly replicate the overall control strategy and operating characteristics of the system. Both the simulation and the experiment execute a pulsating profile with a step-increasing amplitude. The steady-state values for pressure and active power show good agreement, which confirms that the static aspects of the model (losses, fundamental energy relationships) are correctly parameterized even for higher pressures. However, at a pressure of 6 MPa, discrepancies are visible. The simulation model predicts a slightly higher flow rate in the final pulses than that obtained in the experiment. This difference arises from the fact that in reality, at high load, the drop in the motor's rotational speed and the increase in leakages are slightly greater than what the simplified model assumes.

Similar to the test at 1.2 MPa, the simulation model omits the sharp torque spikes at the beginning of each pulse. The experimental results show that at 6 MPa, these mechanical shock loads reach over 30 Nm, while the simulation shows a smooth, "flat" profile. The intensification of the spikes in the experiment proves that phenomena such as hydraulic shock and fluid inertia become the dominant factor during the rapid activation of flow under higher pressure.

Despite the discrepancy in the mechanical torque profile, the agreement between the simulated and experimental active power remains very high. The averaged power consumption is similar.

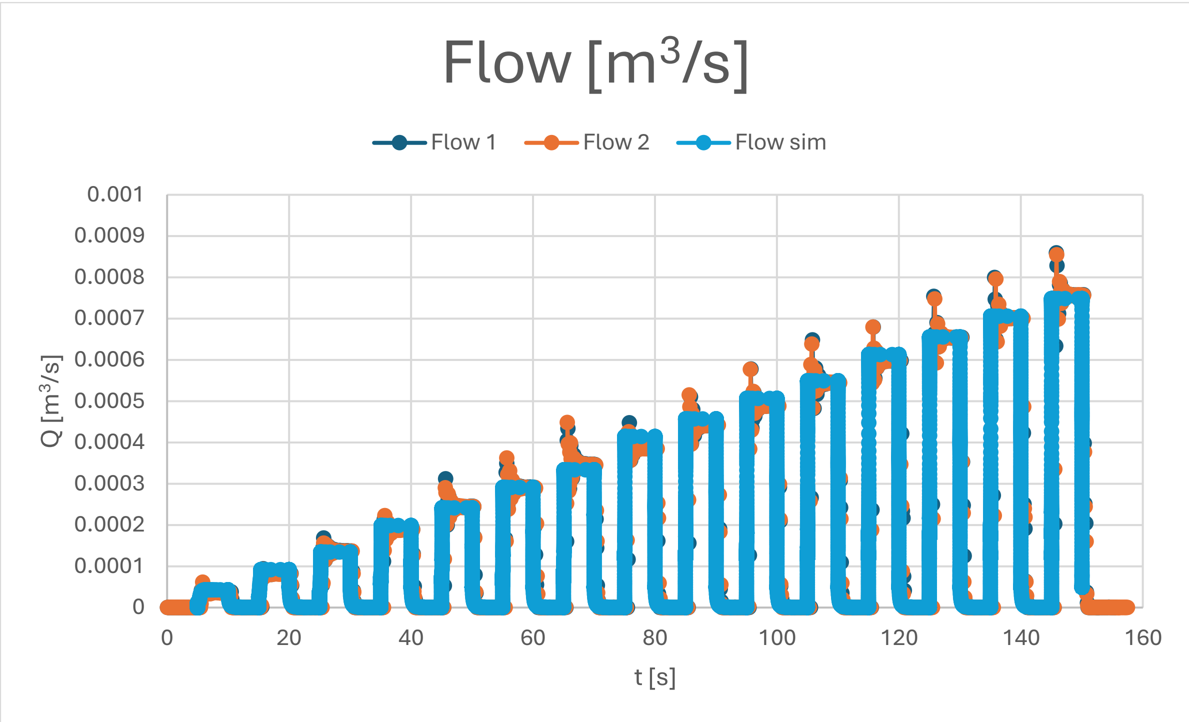

Figure 118. Flow rate Comparative Analysis of Experimental and Simulation Research Results for Scenario No. 2 (Load 6 MPa).

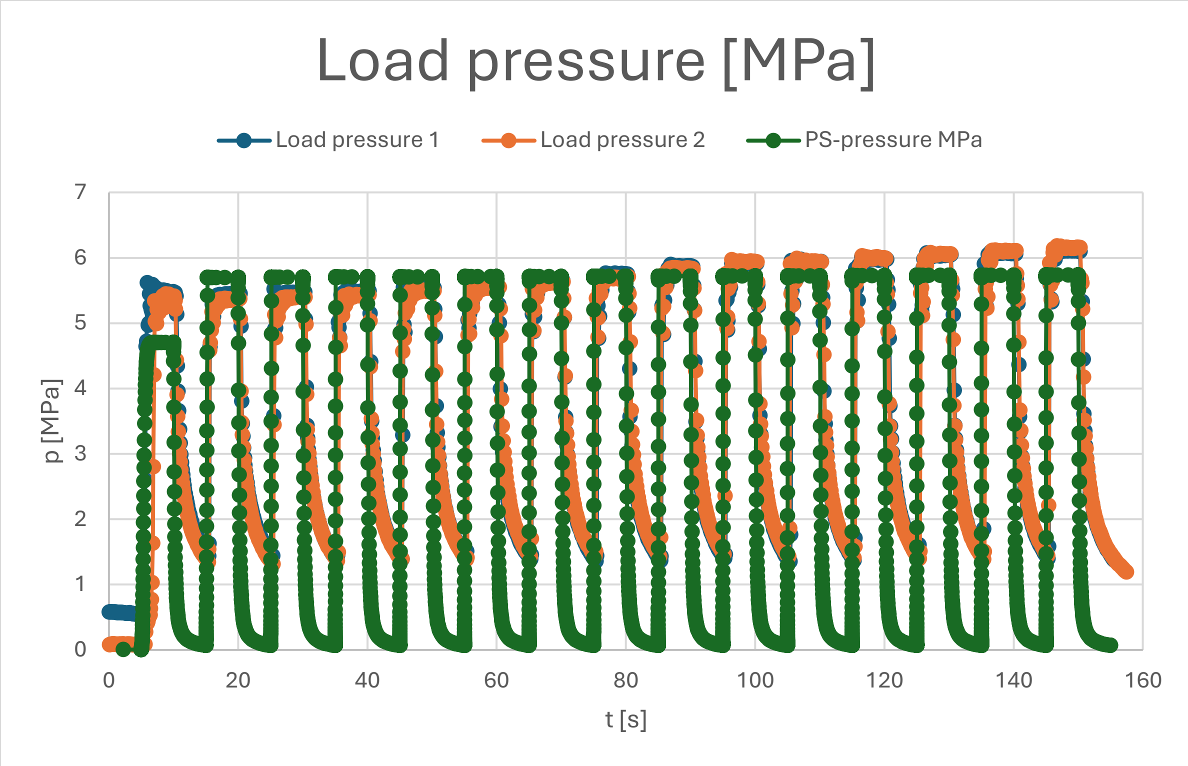

Figure 119. Load pressure Comparative Analysis of Experimental and Simulation Research Results for Scenario No.2 (Load 6 MPa).

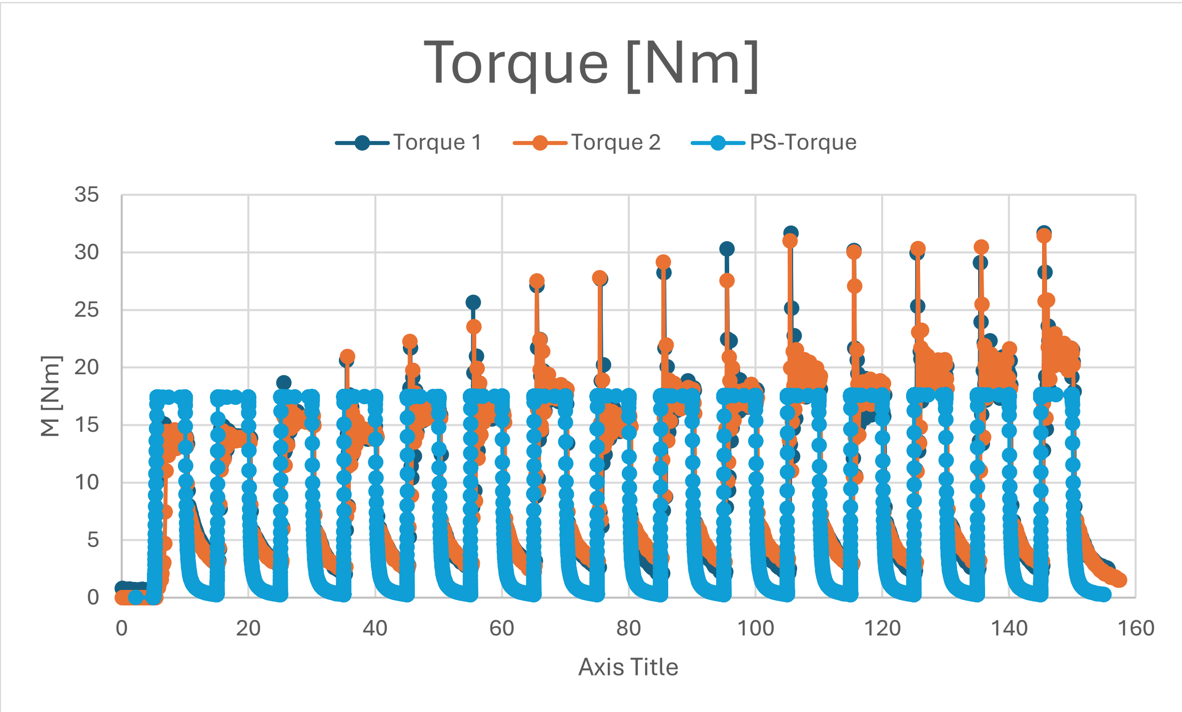

Figure 120. Torque Comparative Analysis of Experimental and Simulation Research Results for Scenario No. 2 (Load 6 MPa).

The comparison at 6 MPa confirms that the model is valid in the scope of quasi-static and energy analysis. It correctly predicts the average values of power, torque, and flow in steady states. This analysis indicates the need for further expansion of the model to include elements that account for fluid dynamics (inertia, compressibility).

8.3 Comparison of Simulation Results: Classic vs. Digital Transmission

The presented sets of graphs compare the key operating parameters for the simulation model of a classic hydrostatic transmission (designated as classic) and the model of a digital hydrostatic transmission (designated as digital). The purpose of this analysis is to assess the extent to which digital transmission can replicate the operation of the classic system and to identify the fundamental differences in their behavior, which is a key step in verifying the research hypothesis.

8.3.1 Analysis for Scenario No. 3 (20s)

The graphs (Fig. 121 - 124) allow for a direct comparison of key operating parameters for the simulation model of a classic hydrostatic transmission (classic) and the model of a digital hydrostatic transmission (digital). This analysis was conducted for a scenario with a trapezoidal profile featuring a long steady-state phase.

The analysis of the angular velocity (Fig. 121) and flow rate (Fig. 122) graphs shows that the digital transmission model is convergent with the classic system. The "stepped" profile generated by the digital system (DH) precisely approximates the smooth ramp-up and ramp-down phases of the classic system (CH). A slight difference is visible in the steady state, where the angular velocity of the digital system is minimally higher.

The pressure graph (Fig. 123) confirms that both systems operate under similar load conditions. It can be noted that the pressure in the classic system (CH) is minimally higher in the steady state. The digital profile (DH) exhibits a slightly larger overshoot at the beginning of the steady-state phase, which is characteristic of its stepwise nature.

In the steady-state phase, the required torque (Fig. 124) for the digital transmission (digital) is consistently lower than for the classic transmission (classic).

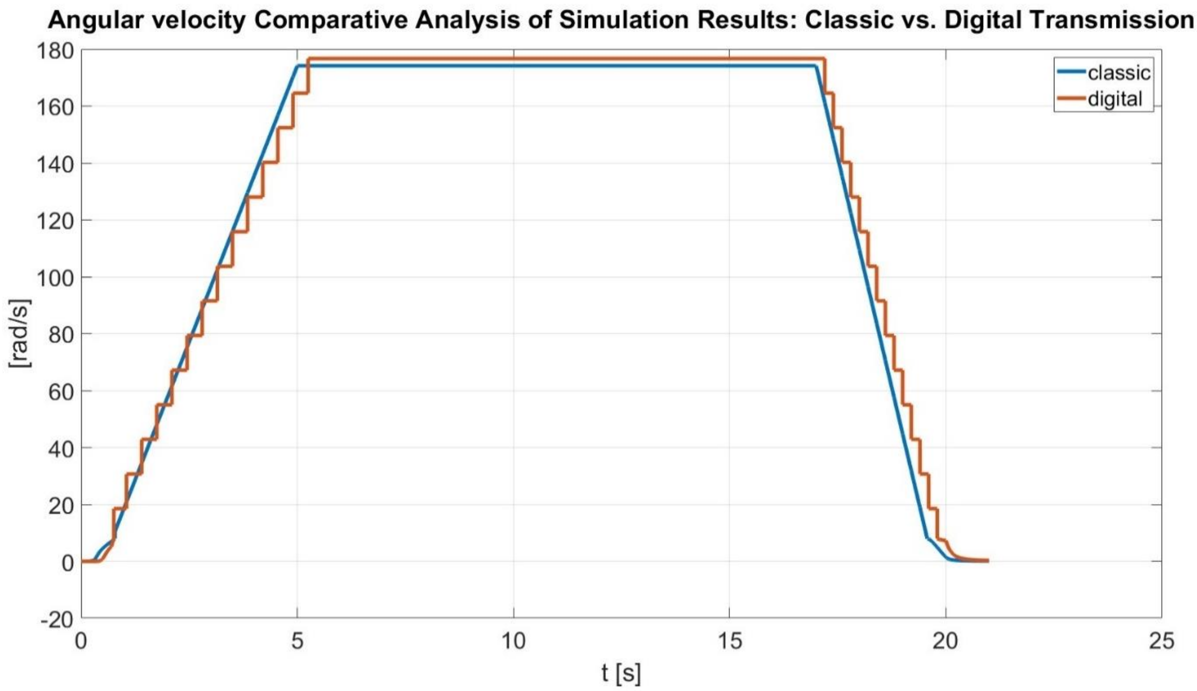

Figure 121. Angular Velocity Comparative Analysis of Simulation Results: Classic vs. Digital Transmission.

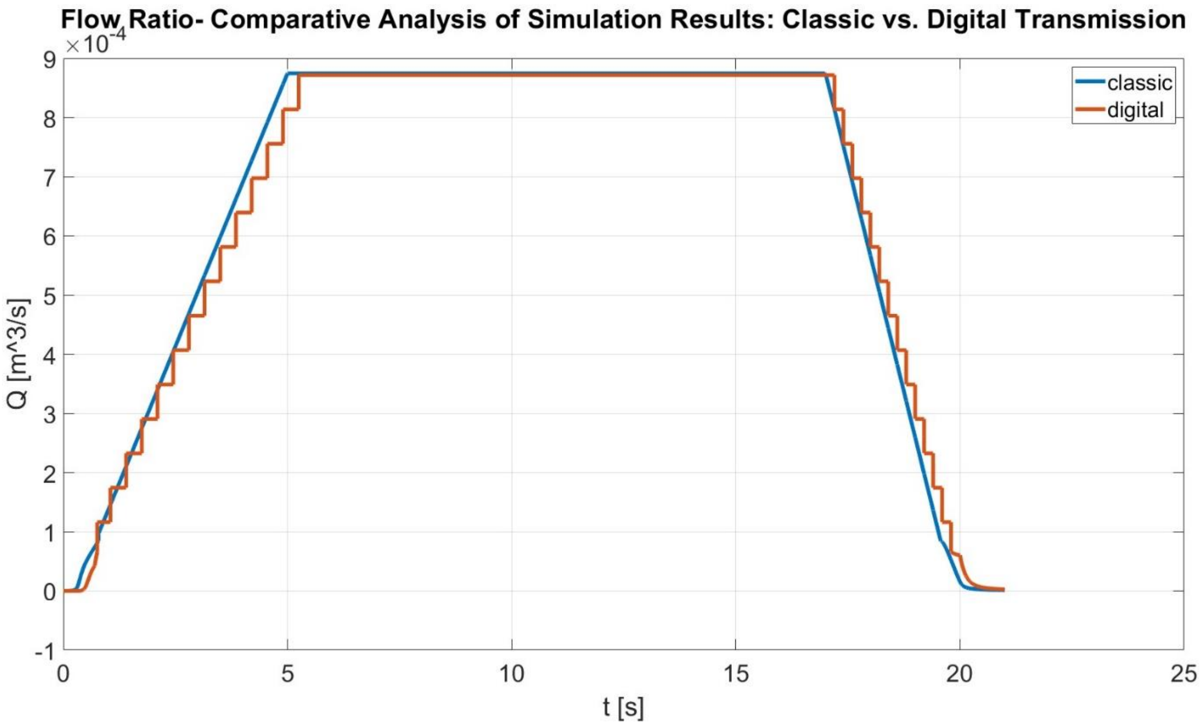

Figure 122. Flow Ratio Comparative Analysis of Simulation Results: Classic vs. Digital Transmission.

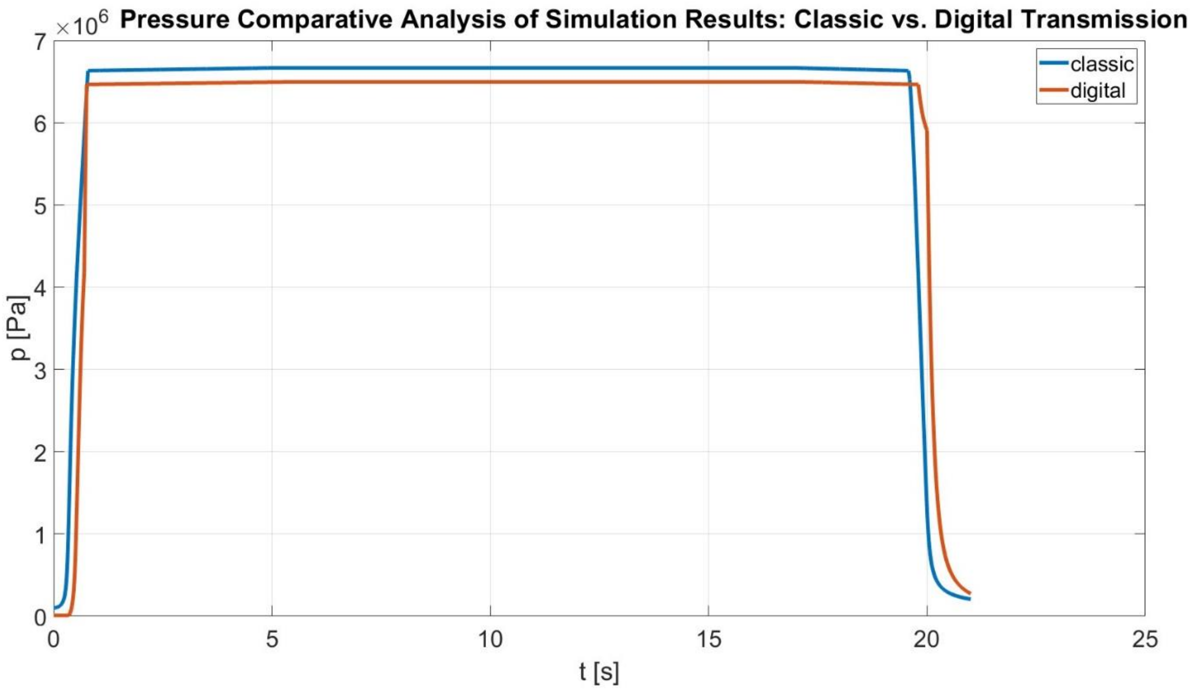

Figure 123. Pressure Comparative Analysis of Simulation Results: Classic vs. Digital Transmission.

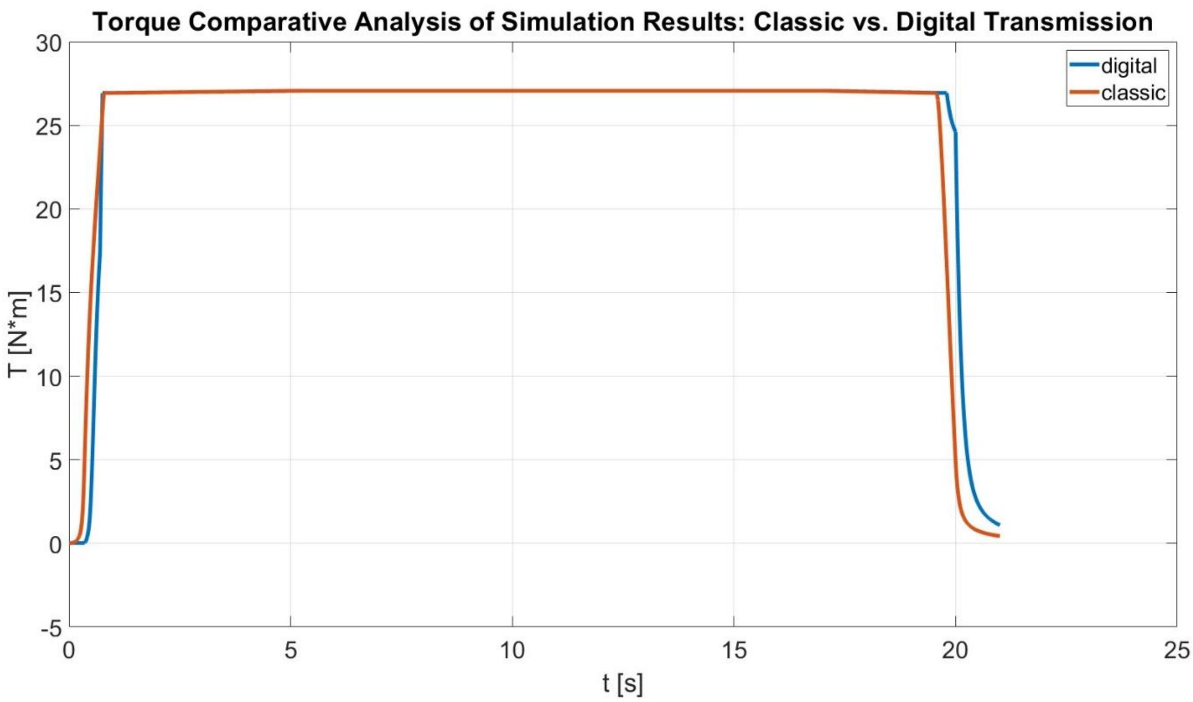

Figure 124. Torque Comparative Analysis of Simulation Results: Classic vs. Digital Transmission.

8.3.2 Analysis for Scenario No. 3a (10s)

The analysis of the angular velocity and flow rate graphs shows that the digital transmission model is able to very closely approximate (emulate) the kinematic profile of the classic system. The "stepped" flow profile generated by the digital system very faithfully follows the smooth, trapezoidal characteristic of the flow from the variable-displacement pump. This means that the digital control strategy, which involves engaging successive pumps, effectively realizes the commanded ramp-up, steady-state, and ramp-down profile. Similarly, the angular velocity in both models is nearly identical. In the digital model, the steady-state speed is minimally higher. The graph of torque clearly shows that in the steady-state phase, the required torque for the digital transmission is lower than for the classic transmission. Additionally, the torque profile for the digital system shows slight, high-frequency pulsations, which are absent in the ideal classic model and constitute the "signature" of digital switching. The pressure profile in the digital system is characterized by a faster rise time and a more pronounced overshoot (pressure peak) at the beginning of the steady-state phase. This is a consequence of the stepwise, rather than smooth, engagement of the successive pumps, which generates more intense dynamic phenomena in the model.

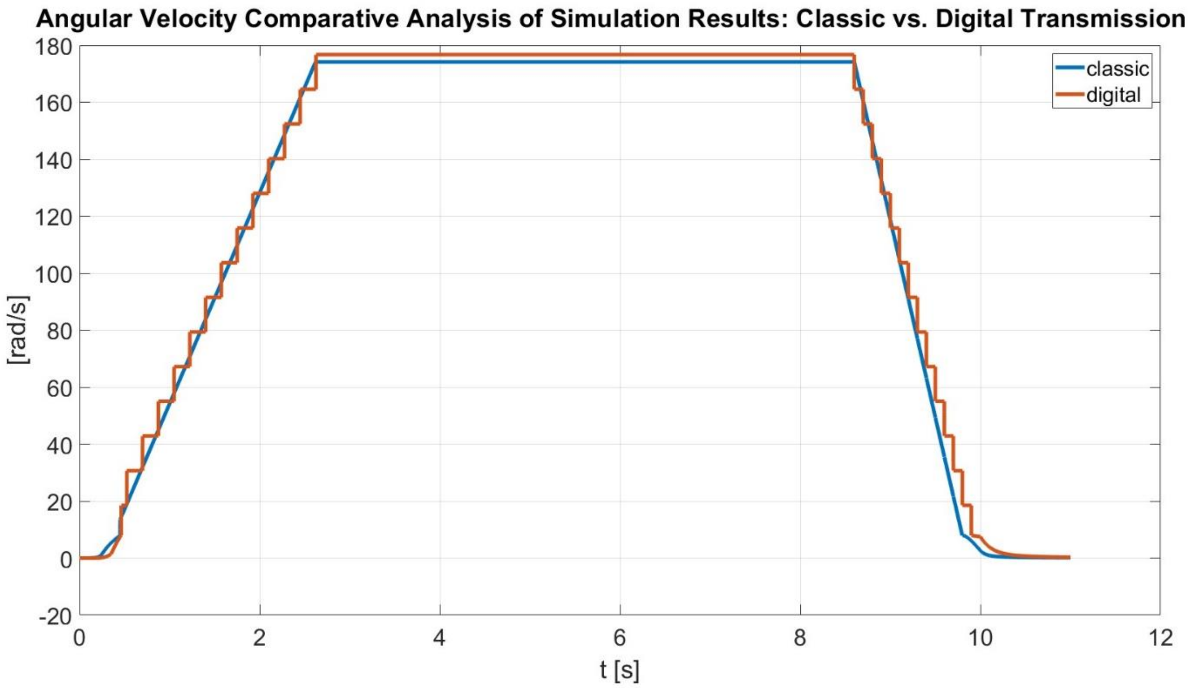

Figure 125. Angular Velocity Comparative Analysis of Simulation Results: Classic vs Digital Transmission.

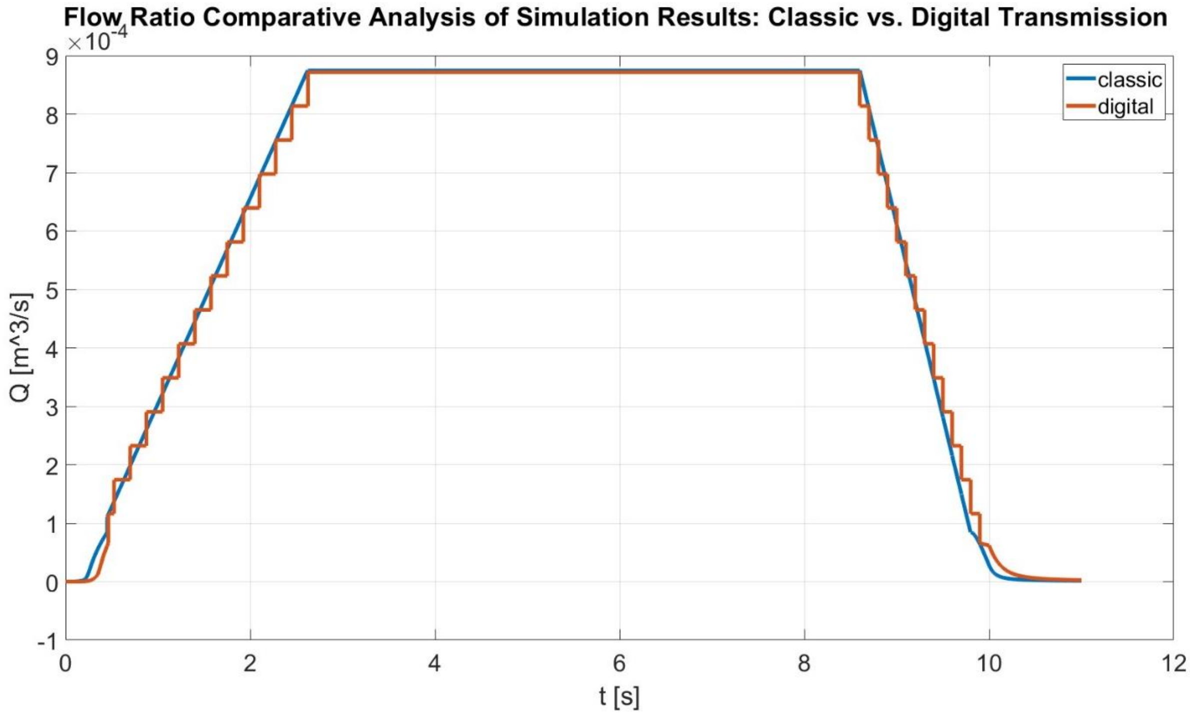

Figure 126. Flow Ratio Comparative Analysis of Simulation Results: Classic vs Digital Transmission.

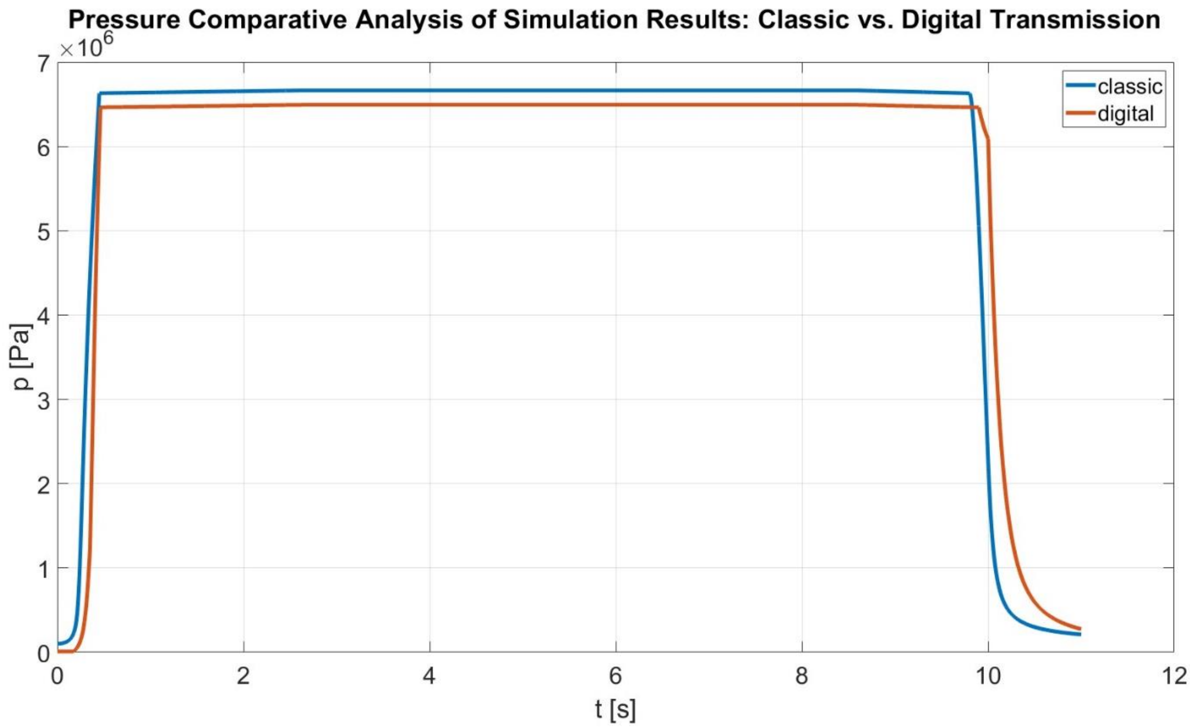

Figure 127. Pressure Comparative Analysis of Simulation Results: Classic vs Digital Transmission.

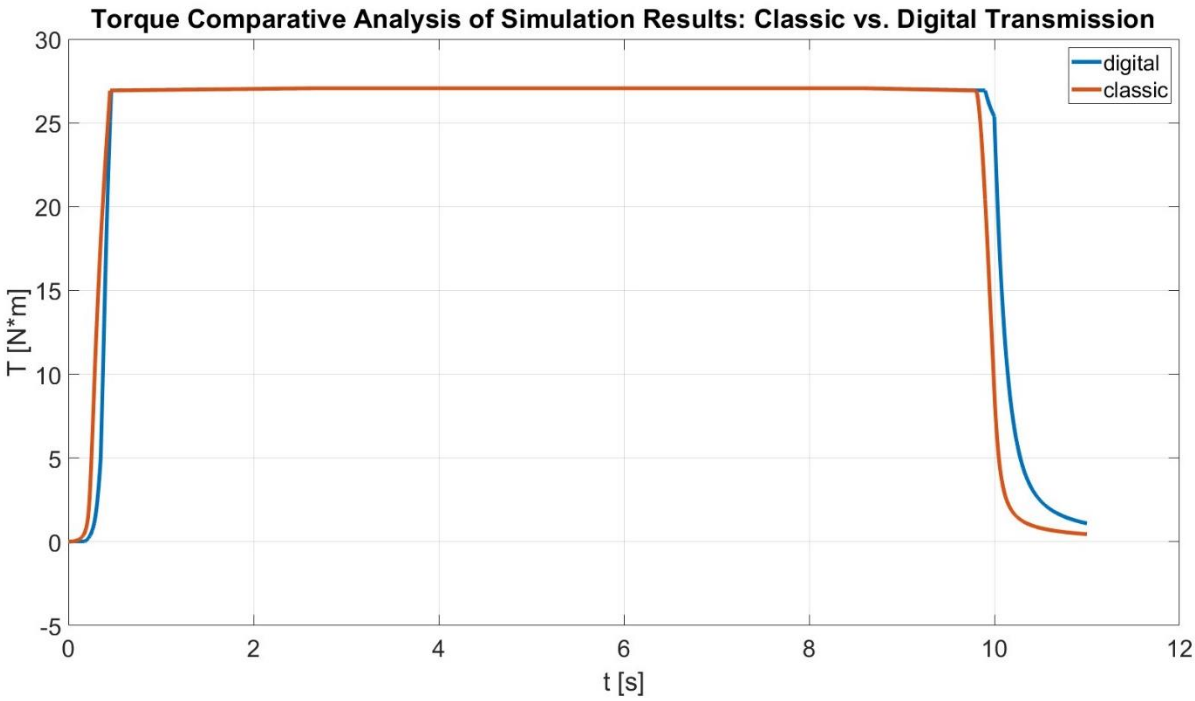

Figure 128. Torque Comparative Analysis of Simulation Results: Classic vs Digital Transmission.

8.3.3 Analysis for Scenario No. 3b (5s)

The angular velocity (Fig. 129) and flow rate (Fig. 130) graphs confirm that the digital transmission model is able to replicate the kinematic profile of the classic system with very high accuracy. The pressure graph (Fig. 131) confirms that both systems operate under similar load conditions. Similar to previous analyses, the digital profile exhibits a slightly larger pressure at the beginning of the steady-state phase, which is an inherent feature of its stepwise mode of operation, especially visible during rapid changes. The torque (Fig. 132) in the steady-state phase is consistently lower than for the classic transmission. This difference is maintained throughout the entire period of operation under constant load. The results of this simulation confirm the conclusions from previous analyses, but under more demanding, dynamic conditions.

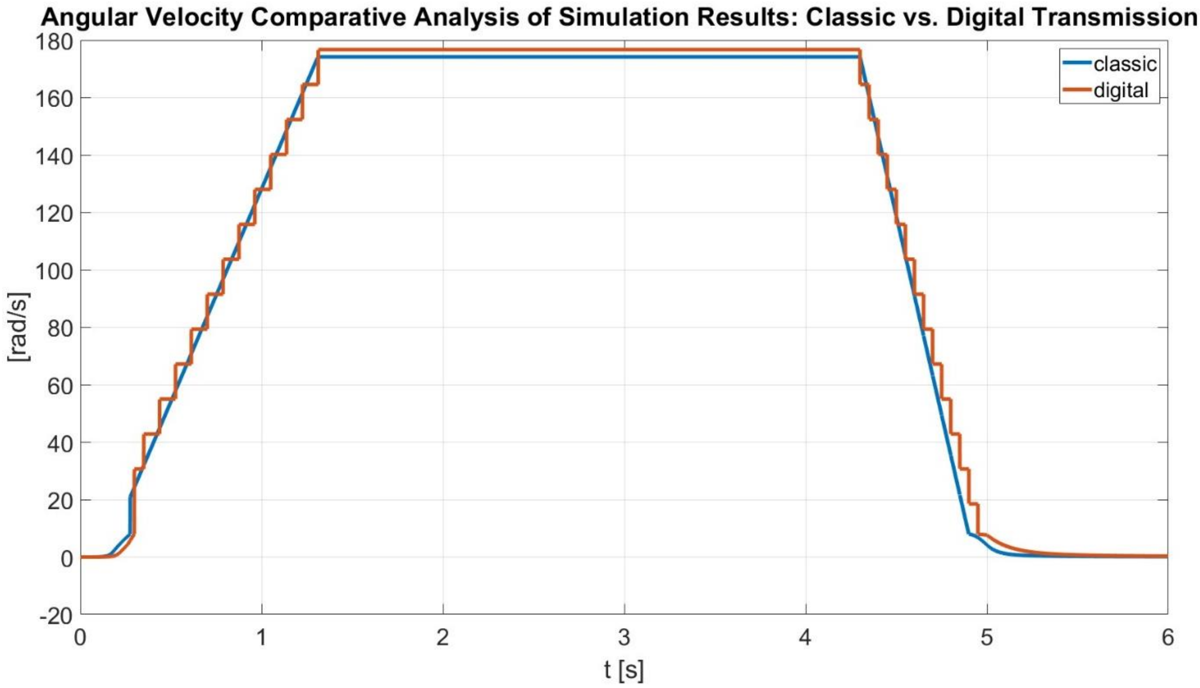

Figure 129. Angular Velocity Comparative Analysis of Simulation Results: Classic vs Digital Transmission.

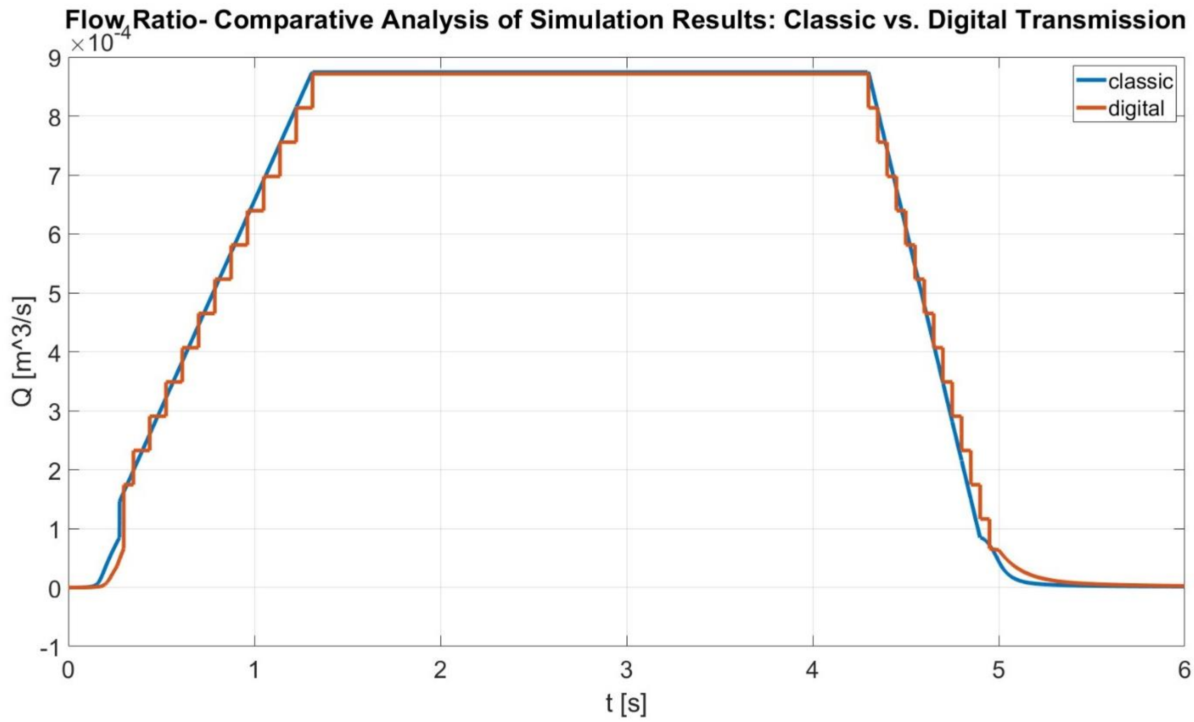

Figure 130. Flow Ratio Comparative Analysis of Simulation Results: Classic vs Digital Transmission.

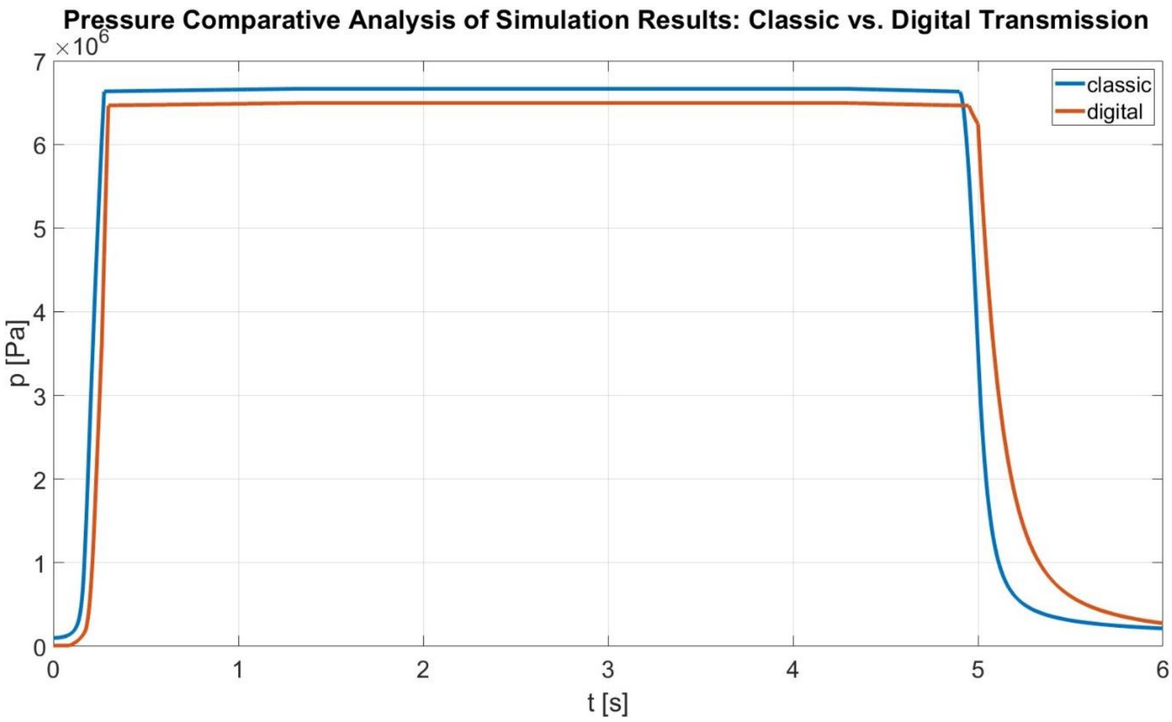

Figure 131. Pressure Comparative Analysis of Simulation Results: Classic vs Digital Transmission.

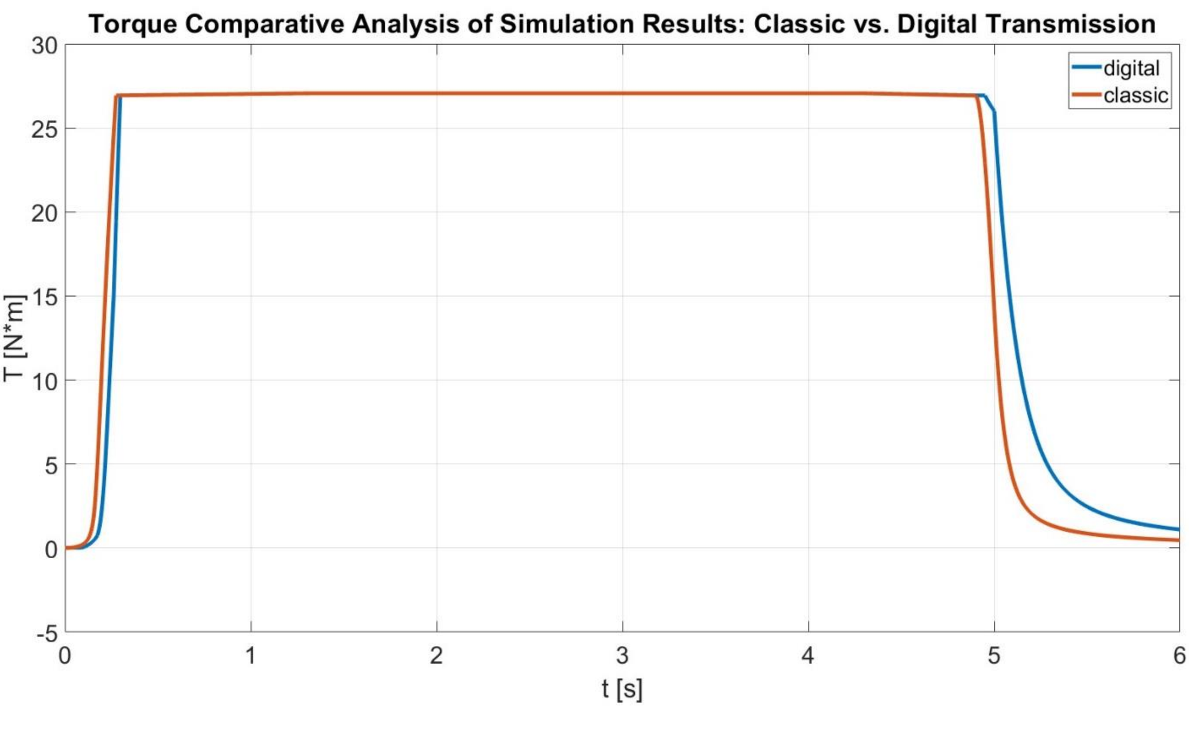

Figure 132. Torque Comparative Analysis of Simulation Results: Classic vs Digital Transmission.

To assess the quality of signal tracking achieved by the digital hydrostatic transmission system compared to its classical counterpart, a comprehensive analysis was conducted for a set of key physical variables: angular velocity, flow rate, pressure, and torque. Both short (5 s) and extended (20 s) simulation cases were considered. Results are summarized in the comparison table (Appendings A). The analysis employed several error metrics: Root Mean Square Error (RMSE), which quantifies the average squared difference between the digital and classic signals; Mean of Squared Error (MSE), representing the accumulated squared error over time; and the maximum tracking error, which indicates the largest pointwise deviation between the signals. Additionally, the time at which this maximum error occurs is noted to help diagnose specific regions of signal mismatch. The total signal area (computed as the integral over time) is compared for both transmission types, and the difference between these areas provides insights into cumulative discrepancies.

Table 6. The quality of signal tracking achieved by the digital hydrostatic transmission system compared to its classical counterpart.

Signal	Unit	RMSE	MSE	Max Error	Time of Max Error [s]
Angular Vel.(20s)	rad/s	7.61	889.04	23.92	19.40
Flow Rate (20s)	m³/s	$3.17x10^{-5}$	$1.78x10^{-8}$	$1.01x10^{-4}$	4.90
Pressure (20s)	Pa	545894	$7.08x10^{12}$	$4.61x10^{6}$	20.0
Torque (20s)	N·m	2.22	116.54	19.69	20.00
Angular Vel.(10s)	rad/s	6.57	216.58	22.72	9.8
Flow Rate (10s)	m³/s	$2.68x10^{-5}$	$3.52x10^{-9}$	$8.99x10^{-5}$	9.8
Pressure (10s)	Pa	$4.98x10^{5}$	$3.50x10^{12}$	$3.82x10^{6}$	10.0
Torque (10s)	N·m	1.998	58.40	-16.43	10.0
Angular Vel. (5s)	rad/s	6.56	111.07	22.72	4.90
Flow Rate (5s)	m³/s	$2.82x10^{-5}$	$1.94x10^{-9}$	$9.81x10^{-5}$	0.276
Pressure (5s)	Pa	5.0310^{5}	$2.53x10^{12}$	$2.76x10^{6}$	5.020
Torque (5s)	N·m	1.98	23.6	12.0	5.014

The analysis of selected cases is presented below.

Figure 121 present an angular velocity (20 s). The comparison of angular velocity signals over 20 seconds resulted in an RMSE of 7.61 rad/s, MSE-889.04 (rad/s)2 and a peak error of 23.92 rad/s.

Figure 122 present Flow Rate (20 s). For the 20-second flow rate signal, the analysis demonstrated a very low RMSE of 3. $17x10^{-5}$ m³/s, MSE-$1.78x10^{-8}$ (m3/s)2 and peak error of $1.01x10^{-4}$ m³/s, indicating high accuracy.

Figure 123 present Pressure (20 s). In the case of pressure over 20 seconds, the RMSE reached 545894 Pa, MSE-7.08x1012 (Pa)2 with a peak error of 4.61x106 Pa. Although these values may appear high, they are acceptable considering the typical operating ranges of hydraulic systems.

Figure 124 present Torque (20 s). The torque signal analysis yielded an RMSE of 2.22 Nm, MSE-116.54 (Nm)2 and a maximum error of 19.69 Nm.

Figure 125 present Angular Velocity (10 s). For the shorter 10-second case, the angular velocity signals maintained good agreement with an RMSE of 6.57 rad/s, MSE-216.58 (rad/s)2 and a maximum error 22.72 rad/s.

The most accurate tracking performance was observed for the flow rate and angular velocity signals, where both instantaneous and cumulative errors remained minimal. Larger deviations were found in pressure tracking, which may be attributed to elastic dynamics or model response discrepancies in the digital valve subsystem. Nonetheless, the overall signal areas closely matched in most cases, confirming that the digital transmission replicates the system behavior with high fidelity over time.

The digital system is able to effectively and with high accuracy execute commanded, dynamic profiles of velocity and flow. The digital system experiences slightly more intense dynamic phenomena (e.g., pressure overshoots), which are a consequence of its discrete nature.

In summary, the simulation results for the three loads described above strengthen the research hypothesis, showing that the digital hydrostatic transmission is a solution that is not only feasible but also promising in terms of energy efficiency, even in applications requiring a fast response.

8.4 Comparison of simulation of classic and digital simulation drive models

Based on the conclusions contained in the previous sections, it was concluded that simulation models can be used for simulation studies for load pressures up to 20 MPa. The results of simulation studies in this area are presented below. Models of classical and digital hydrostatic transmissions were compared for the same loads for 3rd testing scenario and load cycle time equals: 20, 10, 5 as well as 2,5 s.

8.4.1 Comparison for the 3rd testing signal at 10-20 MPa load pressure

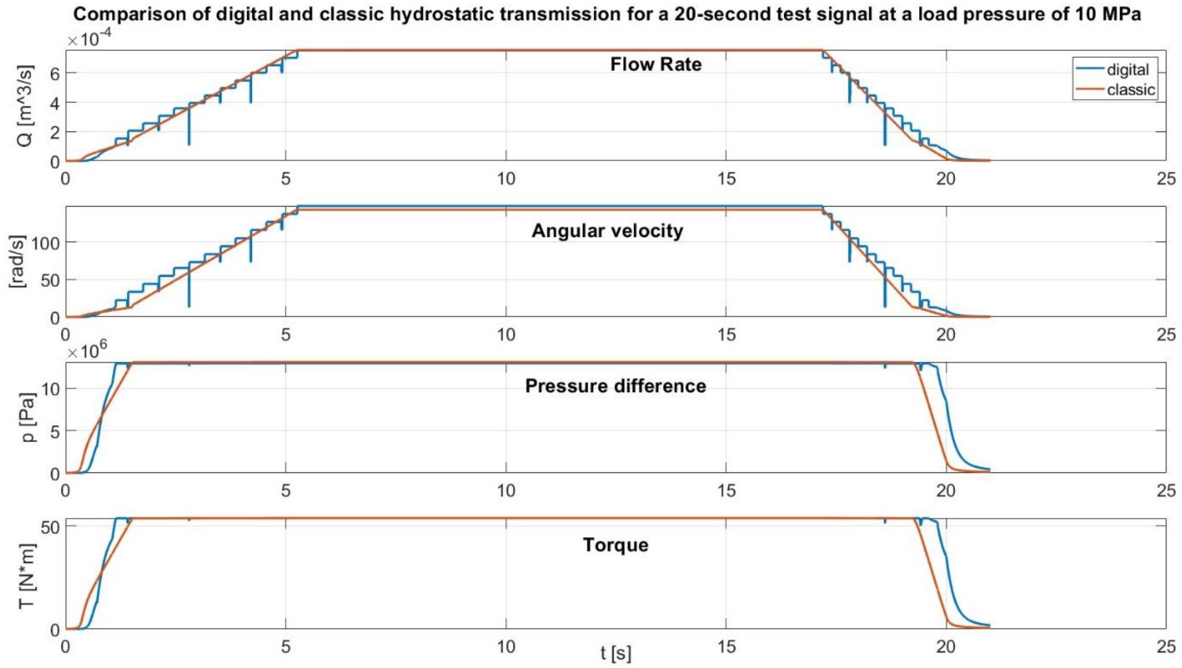

Figure 133. Comparison of digital and classic hydrostatic transmissions for a 20-second test signal at a load pressure of 10 MPa.

This figure 133 presents a simulation comparison of the classic and digital transmissions for a 20-second cycle at a 10 MPa load. The analysis of the angular velocity and flow rate graphs shows that the stepped profile of the digital system precisely approximates the smooth trajectory of the classic system.

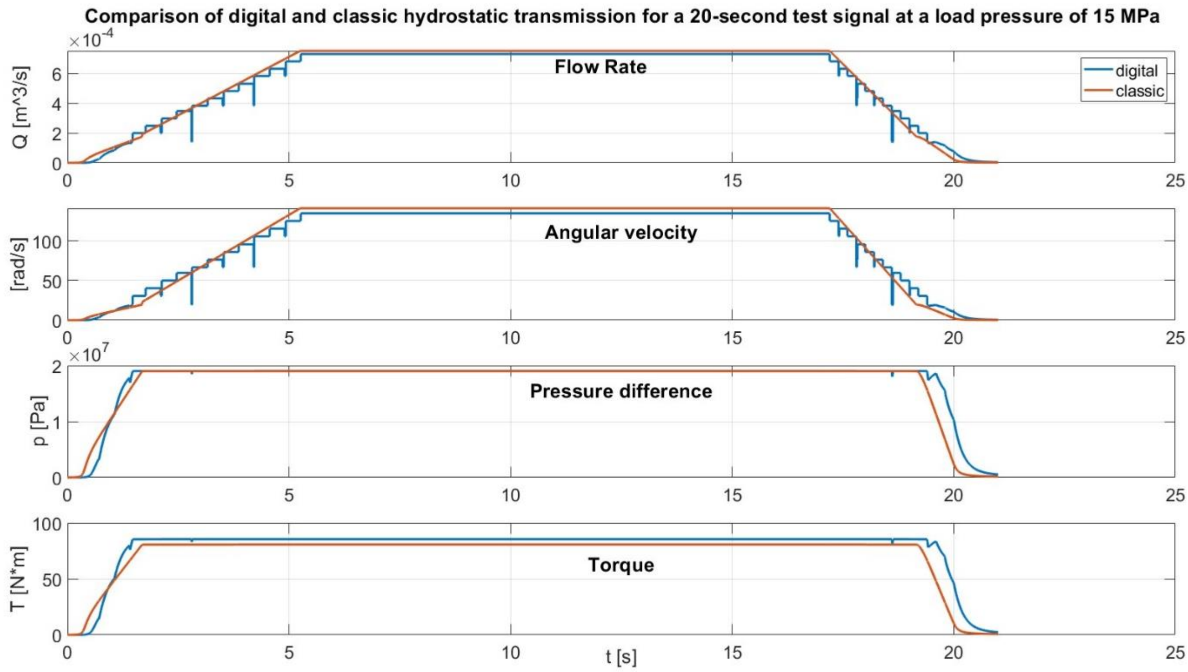

Figure 134. Comparison of digital and classic hydrostatic transmissions for a 20-second test signal at a load pressure of 15 MPa.

Again, the figure 134 shows excellent kinematic agreement of both systems is visible. The difference in the required torque in favor of the digital system is even more pronounced here.

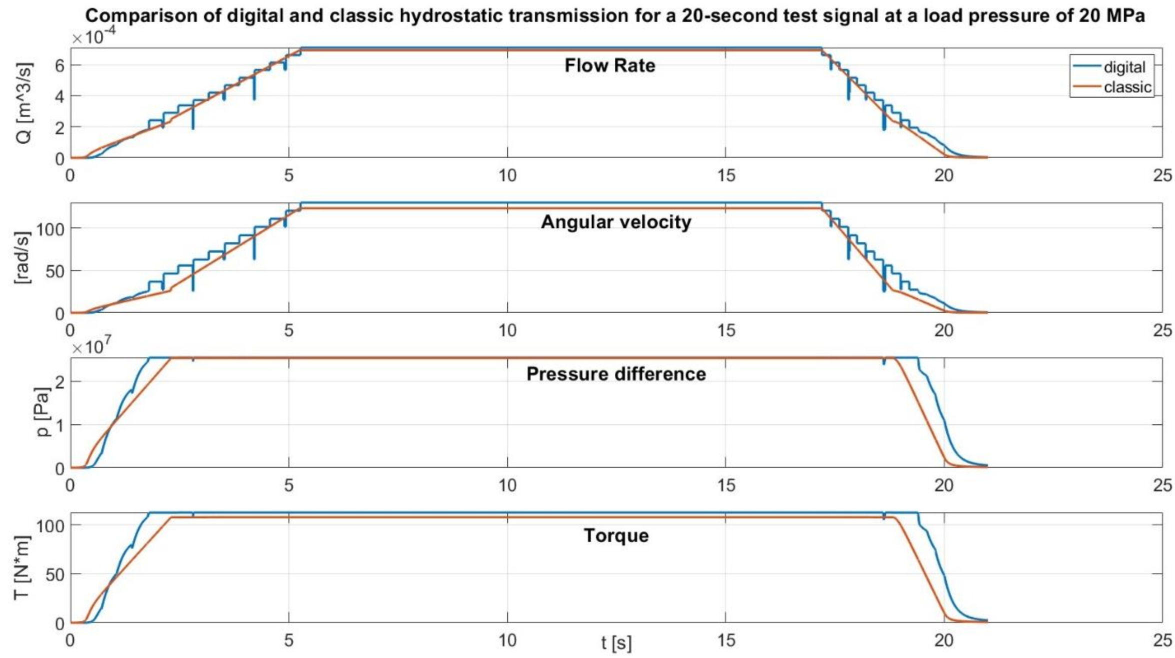

Figure 135. Comparison of digital and classic hydrostatic transmissions for a 20-second test signal at a load pressure of 20 MPa

This figure 135 presents a comparison for the highest tested load (20 MPa) in a 20-second cycle. All previously observed trends are confirmed: the ability of the digital system to mimic the classic profile and its lower torque demand. The absolute difference in torque between the systems is the largest in this case.

8.4.2 Comparison for the 3a testing signal at 10-20 MPa load pressure

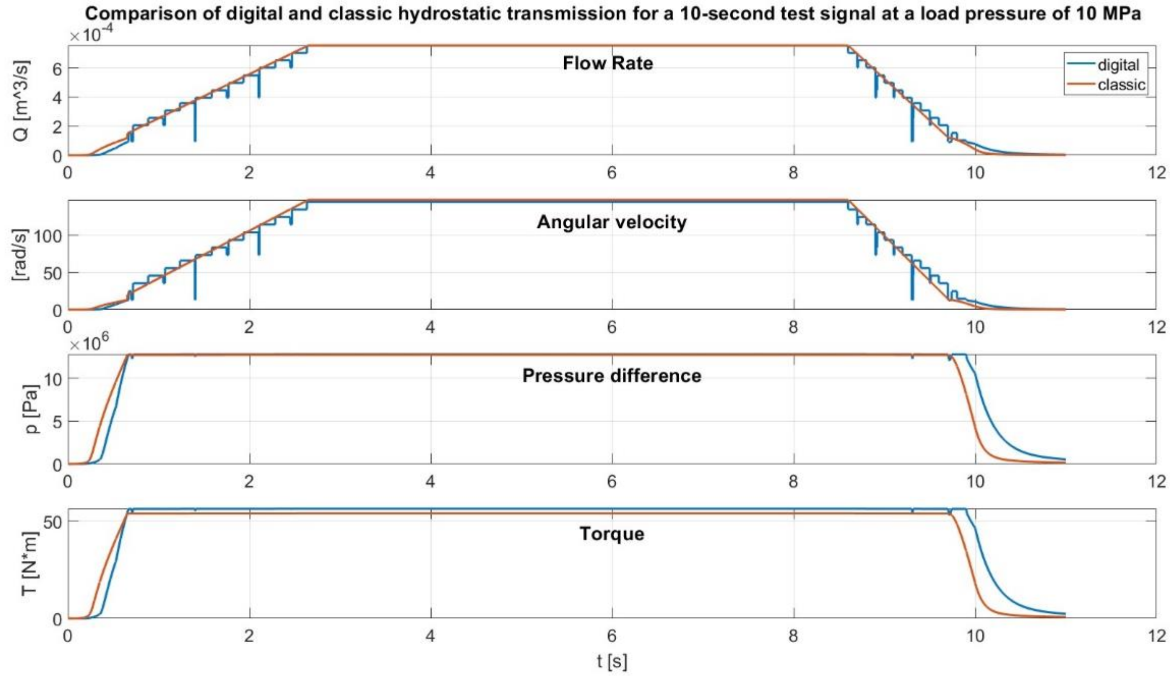

Figure 136. Comparison of digital and classic hydrostatic transmissions for a 10-second test signal at a load pressure of 10 MPa.

Figure 136 begins a series of tests for a shorter, 10-second cycle, at a load of 10 MPa. Even with greater dynamics (shorter ramps), the digital system maintains its ability to precisely track the kinematic profile.

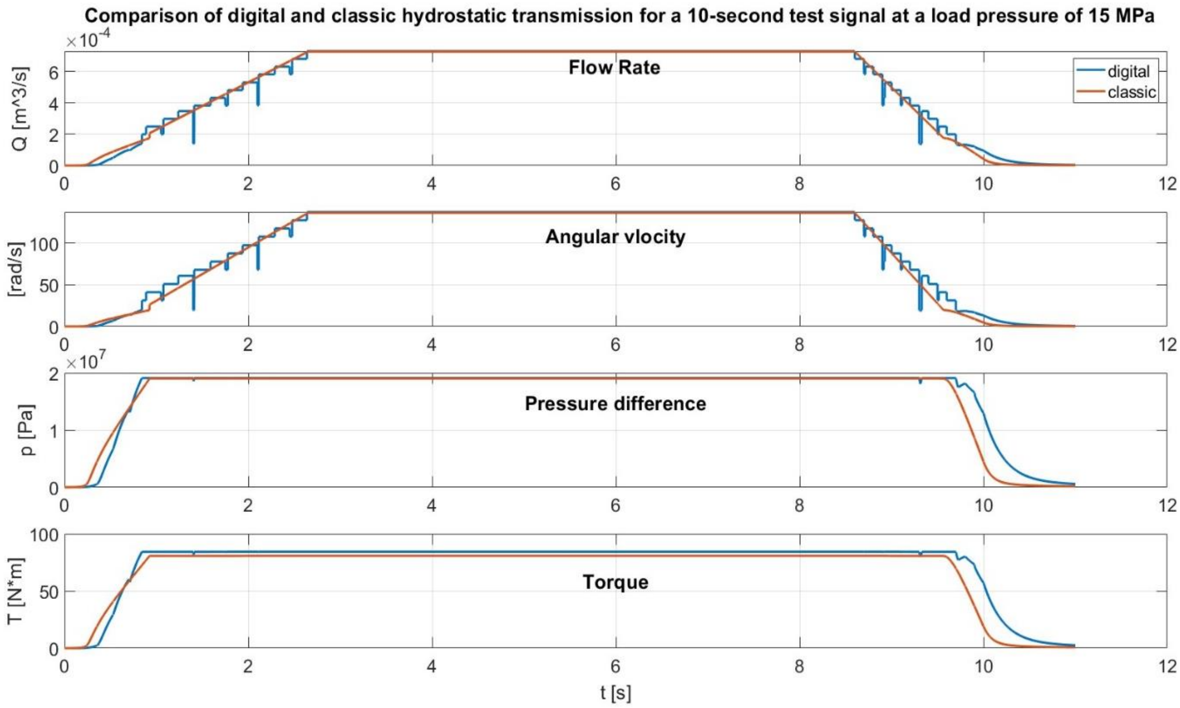

Figure 137. Comparison of digital and classic hydrostatic transmissions for a 10-second test signal at a load pressure of 15 MPa.

Figure 137 presents a comparison in a 10-second cycle for a medium load of 15 MPa. The kinematic agreement remains high. The pressure graph for the digital system shows a slightly more pronounced overshoot than in the 20-second cycle, which indicates the influence of greater dynamics.

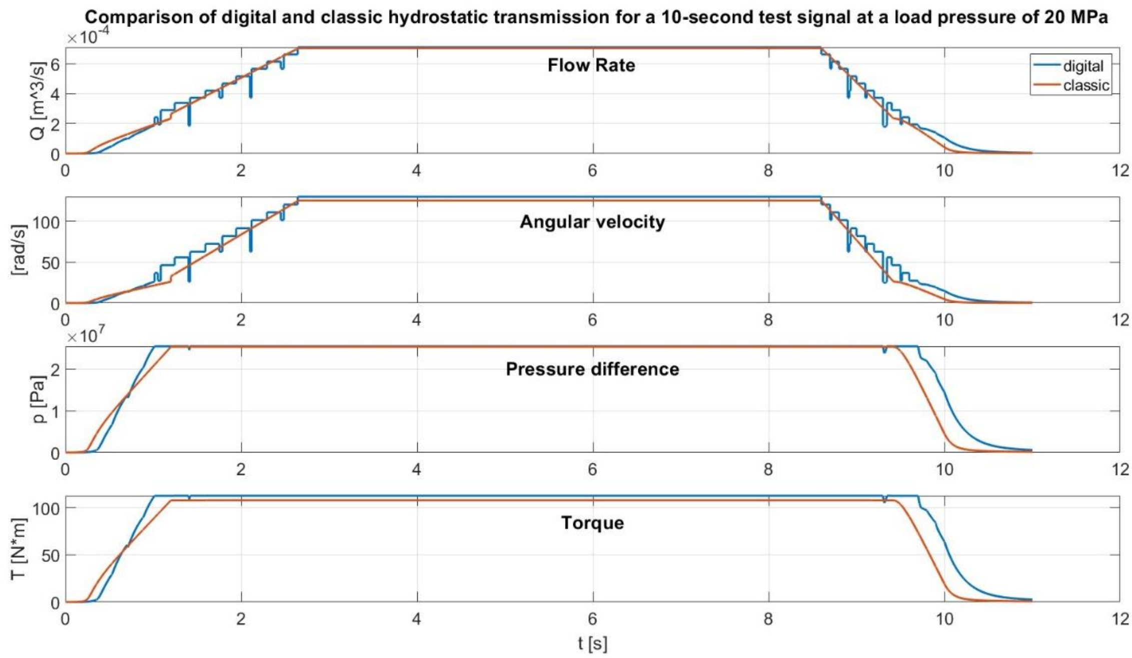

Figure 138. Comparison of digital and classic hydrostatic transmissions for a 10-second test signal at a load pressure of 20 MPa.

In figure 141 both systems were compared in a 10-second cycle under the highest load of 20 MPa.

8.4.3 Comparison for the 3b testing signal at 10-20 MPa load pressure

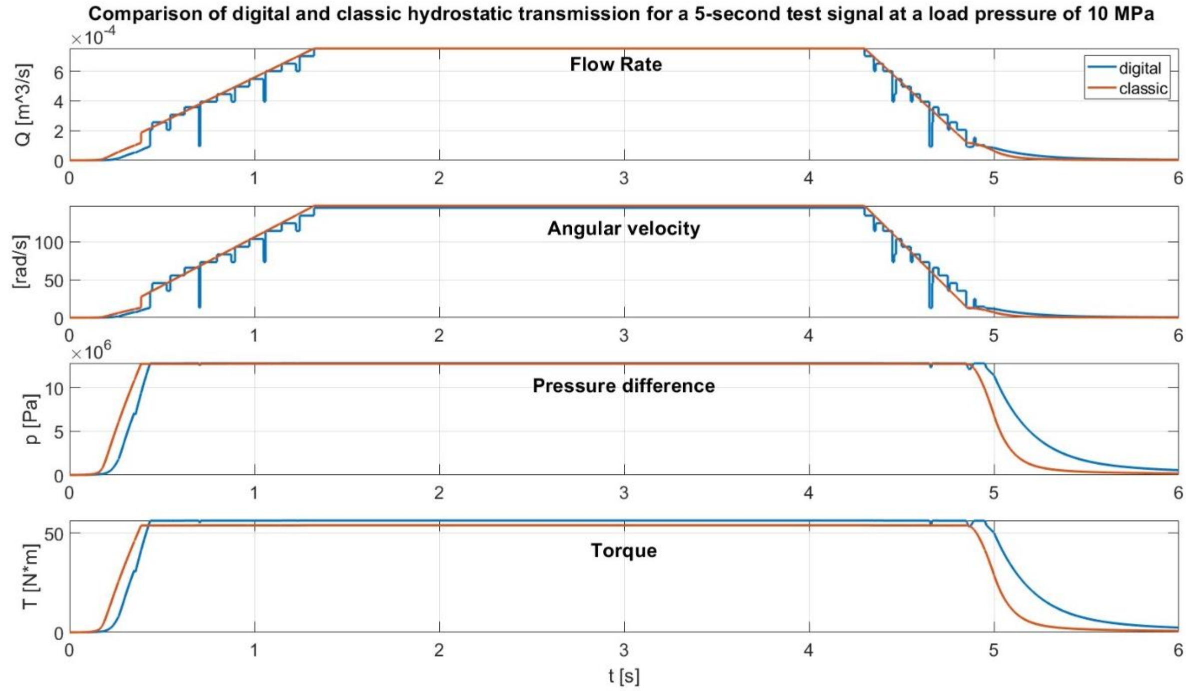

Figure 139. Comparison of digital and classic hydrostatic transmissions for a 5-second test signal at a load pressure of 10 MPa.

Figure 139 begins a series of tests for a very short, 5-second cycle, at a load of 10 MPa. The analysis shows that even with very steep ramps, the digital profile mimics the classic one well. Dynamic phenomena, such as pressure overshoot in the digital system, become more visible here.

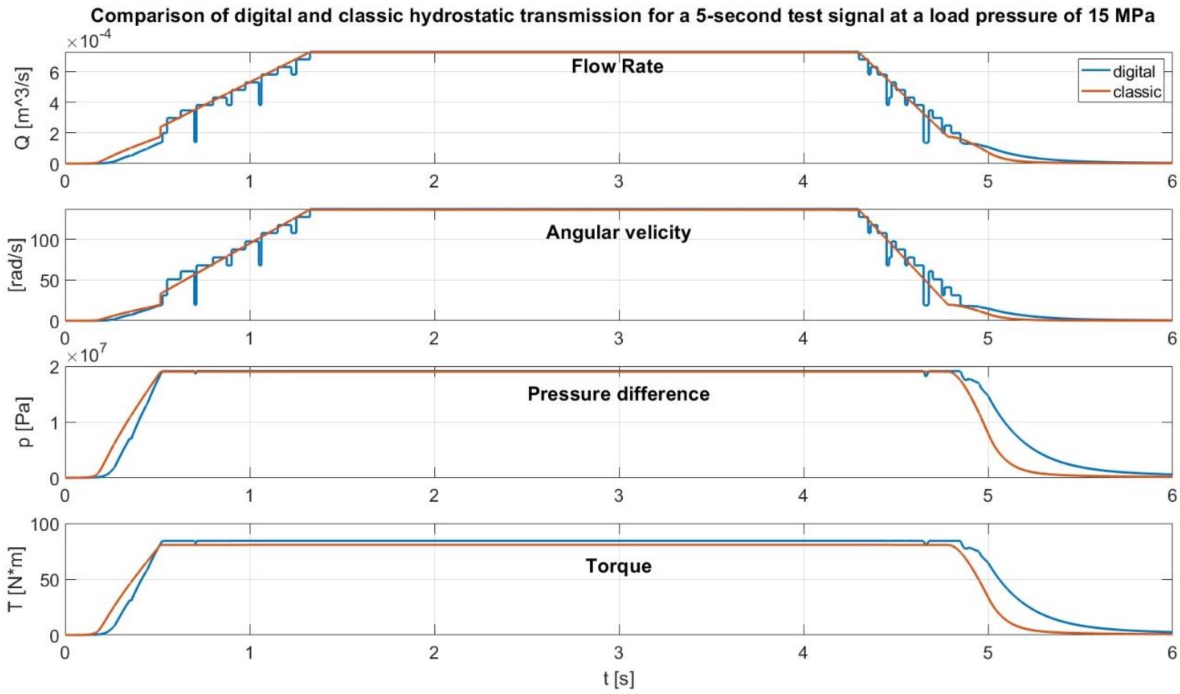

Figure 140. Comparison of digital and classic hydrostatic transmissions for a 5-second test signal at a load pressure of 15 MPa.

The figure 140 presents a comparison in a 5-second cycle for a load of 15 MPa. All key conclusions remain consistent: good kinematic agreement and lower torque for the digital system. A comparison with previous tests shows that the shorter the cycle, the more noticeable the differences in dynamic response become.

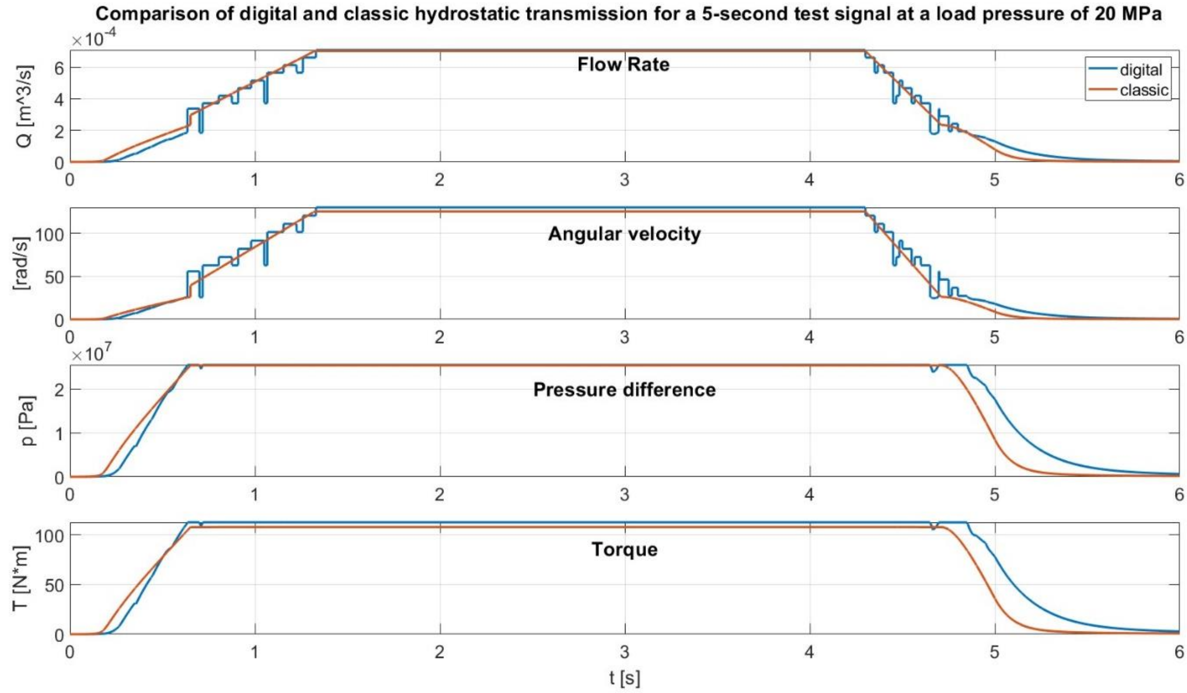

Figure 141. Comparison of digital and classic hydrostatic transmissions for a 10-second test signal at a load pressure of 20 MPa.

In this figure 141, both systems were compared in a 5-second cycle under the highest load of 20 MPa.

8.4.4 Comparison for the 3c testing signal at 10-20 MPa load pressure

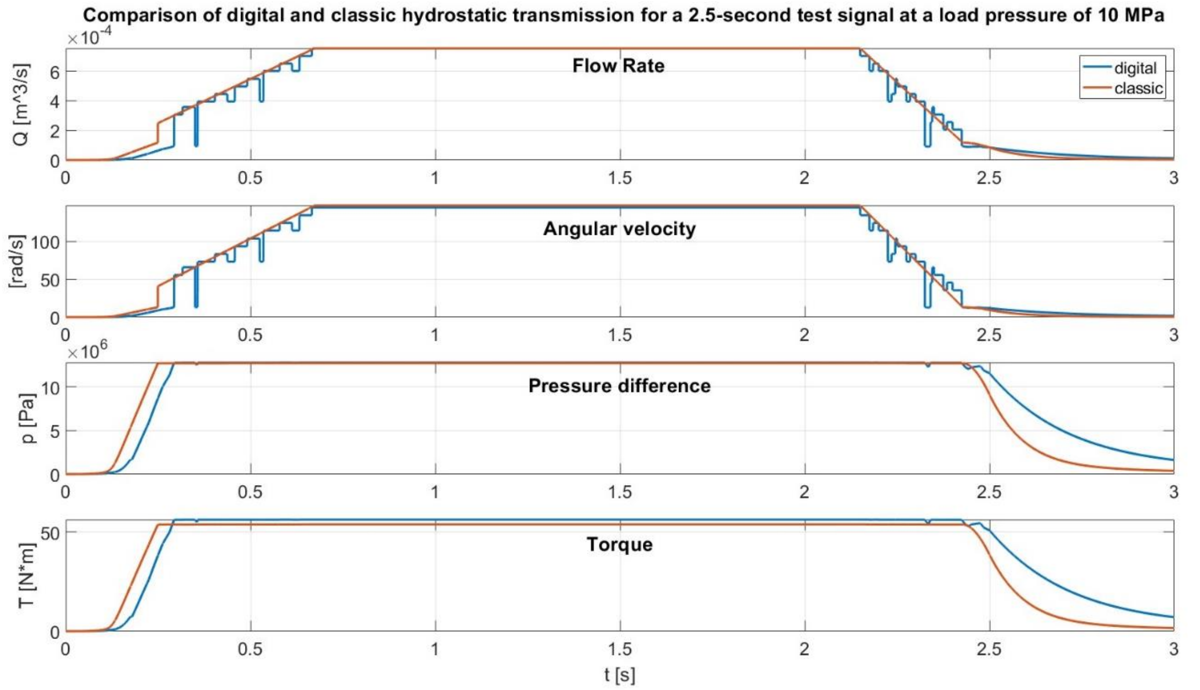

Figure 142. Comparison of digital and classic hydrostatic transmissions for a 2.5-second test signal at a load pressure of 10 MPa.

The figure 142 begins the last, most dynamic series of tests for a cycle with a duration of just 2.5 seconds, at a load of 10 MPa. Despite the extremely steep ramps, the digital system is still able to replicate the kinematic profile.

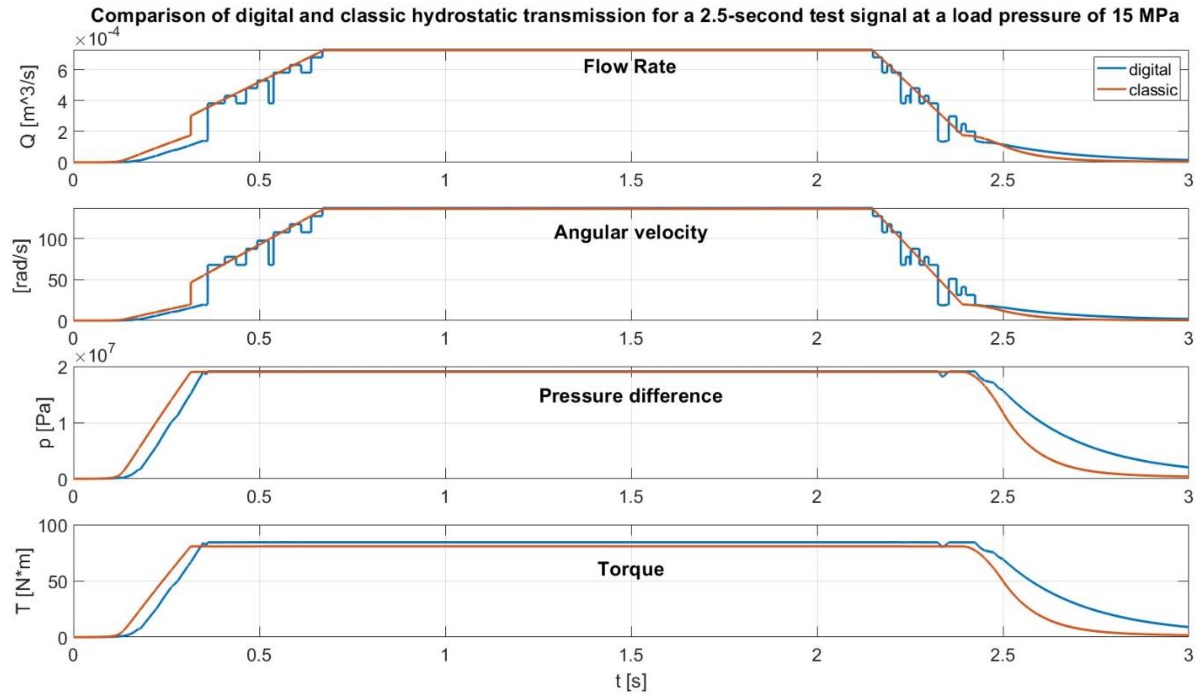

Figure 143. Comparison of digital and classic hydrostatic transmissions for a 2.5-second test signal at a load pressure of 15 MPa.

Figure 143 presents a comparison in a 2.5s cycle for a load of 15 MPa. The differences in the smoothness of the profiles become most visible under these conditions.

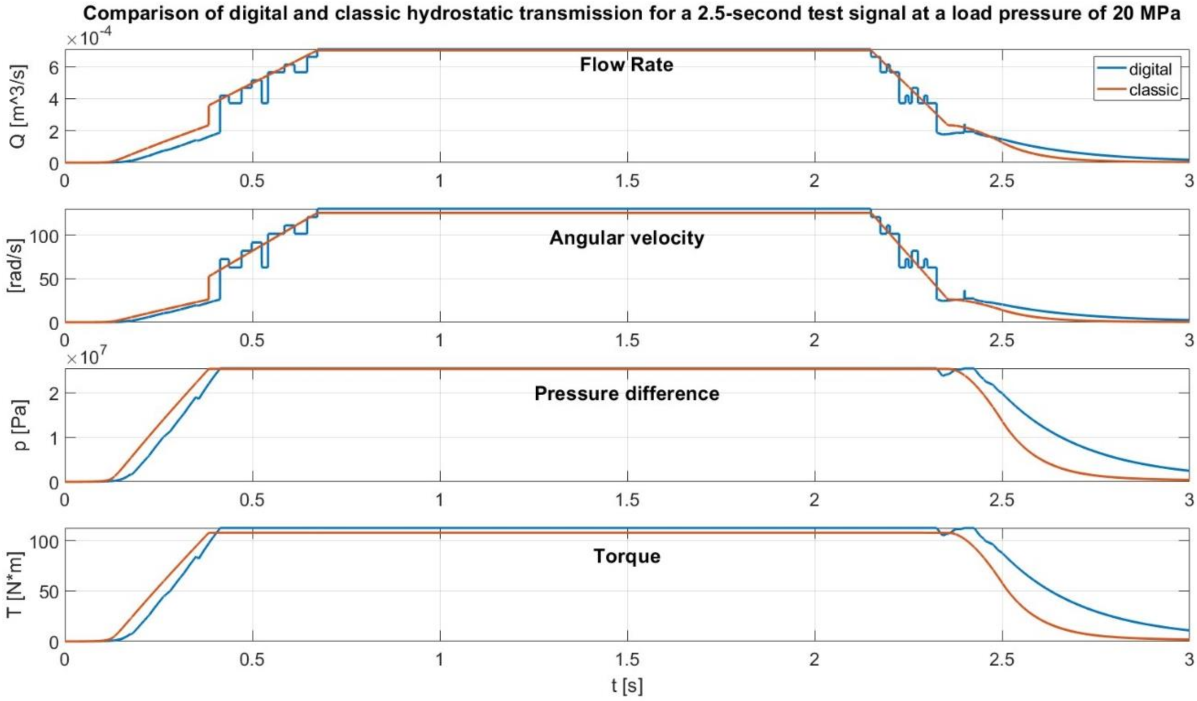

Figure 144. Comparison of digital and classic hydrostatic transmissions for a 2.5-second test signal at a load pressure of 20 MPa.

In this figure 144, both systems were compared under the most extreme conditions: the shortest cycle (2.5s) and the highest load (20 MPa).

General conclusion form of simulation research results of classic vs. digital hydrostatic transmission comparison is presented as follow.

The flow rate and angular velocity graphs consistently demonstrate that the stepped profile of the digital transmission very faithfully approximates the smooth trajectory of the classic system. This capability is maintained across the entire range of tested loads (10-20 MPa) and cycle durations (from 20s to 2.5s), which confirms the high kinematic fidelity of the digital control. The pressure graphs confirm the operation of both systems under the commanded load. A characteristic feature of the digital system is the generation of a more pronounced pressure overshoot at the beginning of the steady-state phase, with the amplitude of this phenomenon increasing as the cycle time shortens and the dynamics increase. The torque graphs provide the key conclusion from the entire simulation campaign. In all cases, the torque required by the digital transmission is lower than in the classic system, and this difference widens at higher pressures.

The conducted extensive simulation campaign provides very strong evidence in favor of the main research thesis. The digital transmission can effectively replace the classic transmission. The ability to perform the same kinematic tasks has been confirmed over a wide range of operating conditions. The main engineering challenge, which the simulations also confirm, remains the management of its unique dynamic characteristics. It is necessary to account for the loads resulting from pulsations in the mechanical design and to implement control strategies that minimize adverse phenomena, such as pressure overshoots, especially in applications with very high dynamics.

9 SUMMARY

Based on the research results described in the previous chapters, the correctness of the statement included in the thesis of this doctoral dissertation was confirmed:

“It is possible to replace the proportional technique in hydrostatic drive systems with "digital hydraulics" ensuring a similar parameters while reducing the expenditure on the construction of a system by 30%”.

Table 7. Comparison of the costs of building a classic and digital hydrostatic transmission.

Drive system component	**Classic system (Proportional) – price ranges**	**Digital system (DPH) – price ranges**	**Remarks**
Electric motor (3-phase, 11 kW, IE3)	**1,900 PLN – 3,500 PLN gross** (1,544 PLN – 2,845 PLN net) Examples: from budget imported motors to Tamel / Siemens.	**1,900 PLN – 3,500 PLN gross** (1,544 PLN – 2,845 PLN net) Examples: as above.	Cost is identical for both solutions.
Pump	**Variable displacement axial piston pump** (e.g., PWG Hydrolider, Hydro Leduc, Bosch Rexroth)	**Set of 4 gear pumps (Group 2)** (e.g., Hydrosila, Presko, Casappa)	The pumping module in the digital system is from 7 to almost 9 times cheaper, regardless of whether we compare the cheapest alternatives or high-end equipment.
	7,500 PLN – 15,000 PLN gross (6,097 PLN – 12,195 PLN net)	**850 PLN – 2,200 PLN gross** (691 PLN – 1,788 PLN net) (Total cost of 4 units with different displacements)	

Drive system component	Classic system (Proportional) – price ranges	Digital system (DPH) – price ranges	Remarks
Control elements	**Hydraulic proportional valve / directional valve** (e.g., Atos, Parker, Rexroth) **2,000 PLN – 6,000 PLN gross** (1,626 PLN – 4,878 PLN net)	**Set of 4 ON/OFF directional solenoid valves NG06** (e.g., Badestnost, Ponar Wadowice, Atos) **800 PLN – 1,800 PLN gross** (650 PLN – 1,463 PLN net) (Total cost of 4 units)	Significant cost reduction due to the elimination of sensitive proportional electronics in favor of simple and cheap on/off spool valves.
Estimated total cost of main components (Sum of ranges)	**From 11,400 PLN to 24,500 PLN gross** (From 9,267 PLN to 19,918 PLN net)	**From 3,550 PLN to 7,500 PLN gross** (From 2,885 PLN to 6,096 PLN net)	**CAPEX savings of around 68-70%** in favor of the digital drive.

The above updated summary, based on real market price ranges, unequivocally and firmly proves the proposed hypothesis regarding the possibility of reducing capital expenditures by a minimum of 30%. These savings are evident in every variant of the system's configuration.

OPEX (maintenance and service costs) in harsh conditions, such as on seagoing vessels, strongly favour digital solutions. The replacement of a simple gear pump or an on-off valve by the ship's crew generates significantly lower costs compared to the necessity of summoning an authorized service to the port for the diagnosis and calibration of sensitive multi-piston pumps, e.g., with Load Sensing systems.

Answers to the Research Problems Based on the Collected Results

Problem 1: Will the digital hydraulic system meet the requirements for power supply and control units used to build a hydrostatic drive system?

Yes, from a functional and kinematic perspective, the system built according to the "digital hydraulics" concept fully meets the requirements for power supply and control units. Both simulation and experimental studies have confirmed that the system based on a set of gear pumps and on/off valves is able to precisely and with high repeatability execute complex, commanded flow profiles. A comparative analysis of the simulation models showed that the "stepped" flow profile from the digital system very faithfully approximates the smooth characteristic of an ideal classic system over a wide range of loads and cycle dynamics. This means that from the point of view of the ability to control the hydraulic motor motion, the replacement is fully possible.

Problem 2: What will be the energy efficiency of the above-described change?

The energy efficiency of the digital system and the classic system is at a similar level. Estimated analyses based on the assessment of the static characteristics of individual components showed similar or greater efficiency of the digital system - especially in the case of throttling control of the classic system for the same load.

Problem 3: Will the dynamic parameters of the hydraulic system subjected to such modifications meet the requirements assumed for multi-source systems?

Yes, but with several caveats. The digital system introduces a specific dynamic characteristic. The digital system demonstrated in simulations and experiments the ability to execute cycles with very high dynamics, with rise times to full output of less than one second. In this respect, it meets and even exceeds the requirements of many applications in which it can be used. Unfortunately, the experimental research has clearly revealed the existence of phenomena that constitute the main challenge of this technology. Even in a steady state, the system generates significant, high-frequency torque oscillations, most likely resulting from the pump gearing process. Under intermittent (pulsating) operating conditions, very high, short-term torque spikes occur at the beginning of each flow activation cycle, which many times exceed the nominal value. These shock loads, which intensify with increasing pressure, are a significant factor for the mechanical durability of the system. The digital system meets the requirements in terms of response speed but introduces dynamic loads (pulsations, shocks) that must be considered during the design stage and in the control strategy.

Problem 4: What kinds of savings will result from such a modified system?

The modification of the system brings savings in three main areas.

First is: Investment Savings CAPEX, or capital expenditure, refers to the one-time costs incurred at the design, purchase, and implementation stage of the system. In this area, digital technology offers a fundamental and immediate advantage. The main source of savings is the replacement of the two most expensive and complex components of the classic system the variable-displacement axial piston pump and/or the precision proportional valve with their much cheaper counterparts. In the digital system, their functions are taken over by a set of standards, mass-produced gear pumps and a group of simple, reliable, and widely available on/off valves. The difference in price between a precision-made variable-displacement pump and the sum of the costs of several standard gear pumps is very large. Similarly, the cost of a proportional valve, which requires precise control electronics, significantly exceeds the cost of a set of simple solenoid valves. The realization of the research hypothesis about a 30% reduction in the system's construction costs seems fully justified in this context.

Second is Operational Savings OPEX refers to the ongoing costs associated with the use of the system throughout its life cycle. In this area, the benefits of digital technology are long-term and accumulate over time. This is the most important and measurable component of OPEX. The digital transmission is characterized by significantly higher energy efficiency when replacing a throttle-controlled system. In practice, this means a direct reduction in energy consumption (fuel in mobile machines or electricity in stationary applications) to perform the same work. These savings, although they may seem small on the scale of a single cycle, translate into huge financial benefits when summed over thousands of hours of machine operation. The simpler construction of digital components (especially ON/OFF valves) and their lower sensitivity to oil contamination compared to precision proportional valves can lead to higher reliability and fewer failures. Lower failure rates mean less unplanned machine downtime, which is crucial in industrial applications where every hour of production interruption generates measurable financial losses.

Third is Maintenance Savings and Total Cost of Ownership (TCO) This aspect is related to maintenance costs but directly concerns service and repair activities. In the event of a failure, the cost of replacing a standard gear pump or on/off valve is incomparably lower than the cost of purchasing and replacing a specialized variable-displacement pump or servo-valve. The availability of standard, "off-the-shelf" parts also shortens the repair time. Moreover, the application of this concept can be used in developing world economies in Asia, Africa and South America due to its simple construction and thus facilitating service and possible repairs (the waiting time for multi-piston pumps or hydraulic motors reaches up to 18 months). The construction of the digital system based on multiple parallel elements provides a degree of fault tolerance. The failure of one of the four pumps does not immobilize the entire system, but only limits its maximum capacity, often allowing the task to be completed or the work to be safely terminated.

In conclusion, a comprehensive economic analysis, considering the Total Cost of Ownership (TCO), clearly indicates the advantage of the digital concept. It is not only cheaper to build (lower CAPEX), but primarily generates constant, long-term savings thanks to lower operating costs (OPEX) resulting from energy savings (in the case of replacing a system with throttle control) and higher reliability.

Problem 5: What is the effect of replacing a typical hydraulic system with a system built according to the concept of "digital hydraulics" in the area of efficiency, reliability, safety and ecology (carbon footprint, emission of harmful substances, e.g. in the case of using an internal combustion engine: carbon dioxide, nitrogen oxides, solid particles)?

The main advantages of the digital system compared to the classic transmission are presented below.

- Ecology: The production of complex, precision axial piston pumps with variable displacement and proportional valves is a material- and energy-intensive process. Replacing them with a set of simpler-to-build, mass-produced gear pumps and on/off valves has the potential to reduce the carbon footprint already at the component production stage. This work largely confirms this.
- Reliability: Theoretically, reliability increases. This is due to the use of simpler, more robust components and the inherent redundancy of the system—the failure of one of the four pumps does not cause the entire system to stop, but only limits its maximum capacity.
- Safety: The basic safety systems, such as the main pressure relief valve, remain the same. Nothing changes in this area. A new challenge for safety (mainly in the context of durability) becomes the shock loads, which were not identified in the simulation models but were detected in the experiments.

9.1 Method for Replacing a Classic to Digital Hydrostatic Transmission

To replace a classic hydrostatic transmission with its digital equivalent, an algorithm in the form of a flowchart was proposed (Fig. 145).

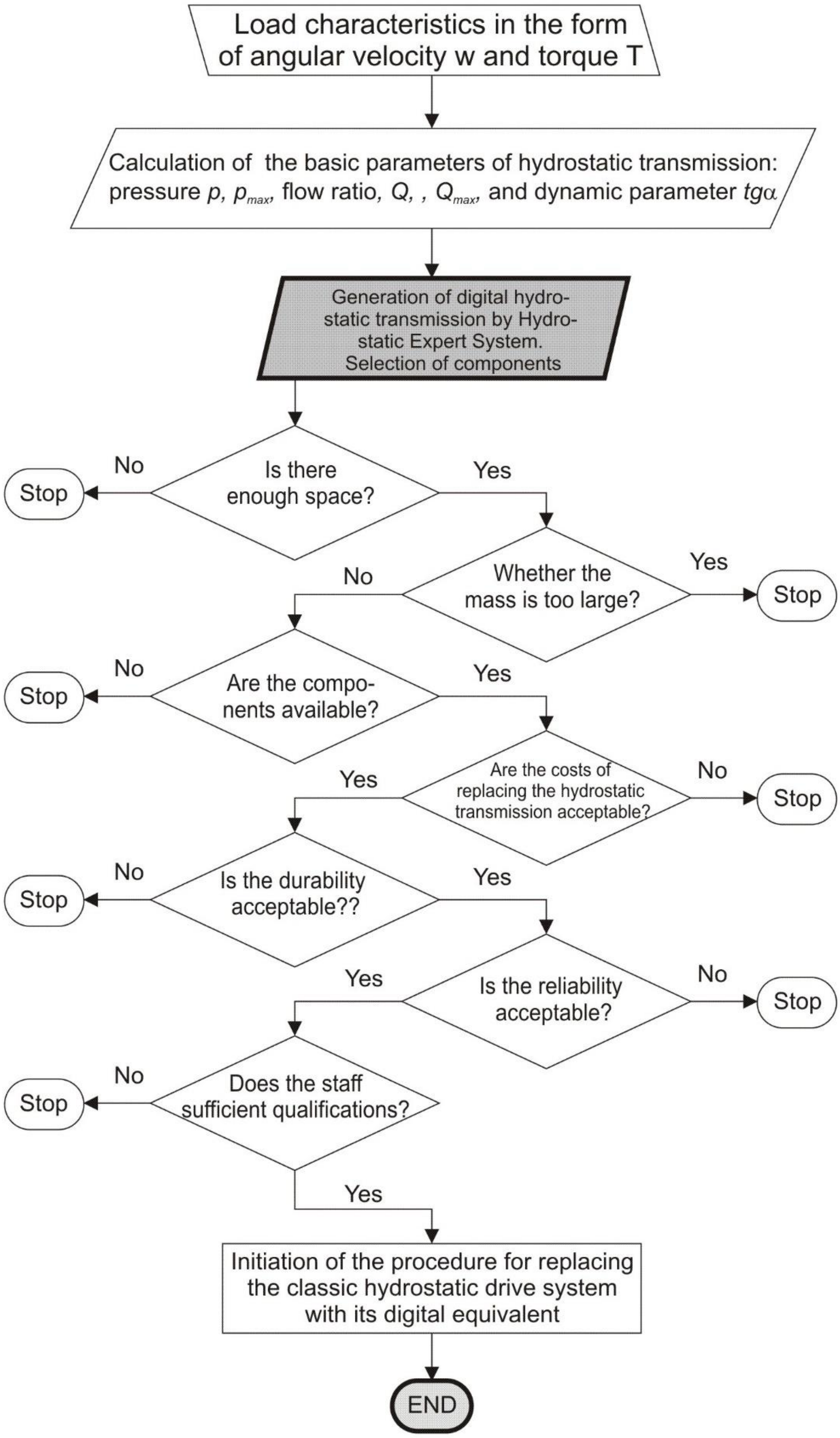

Figure 145. Schema of the method of replacement of classic hydrostatic transmission its digital equivalent.

The basis for all analyses is knowledge of the operating cycle of the system to be modified. A good example is defining the operating cycle as the load torque and angular velocity required to complete a given operating cycle over time (Fig. 146 to 148).

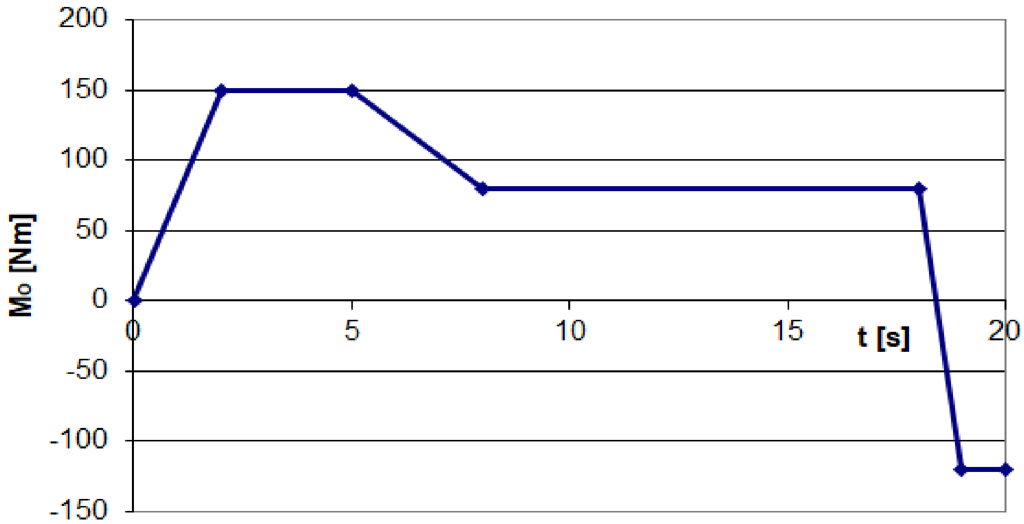

Figure 146. Example of torque of load

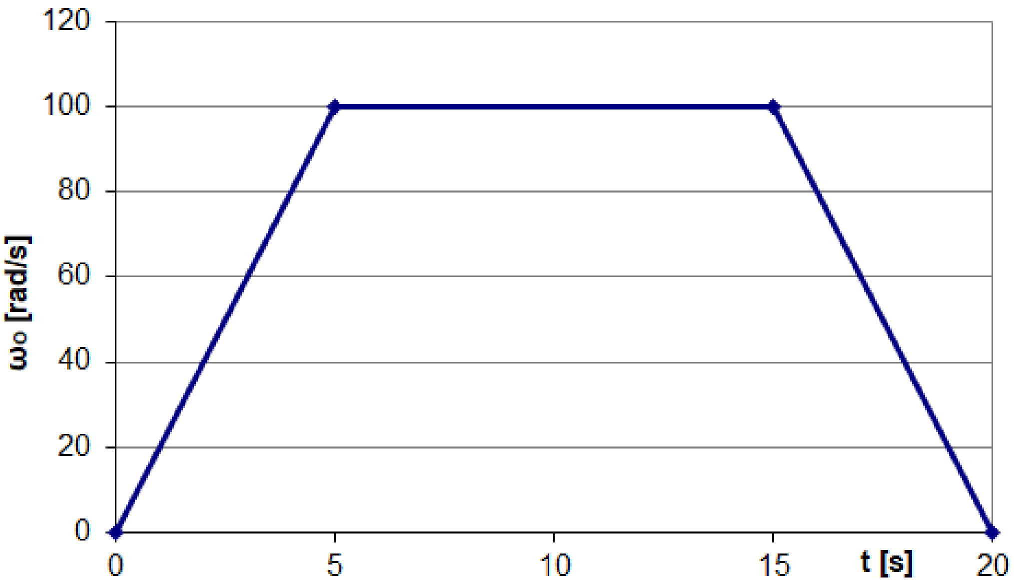

Figure 147. Example of angular velocity of load.

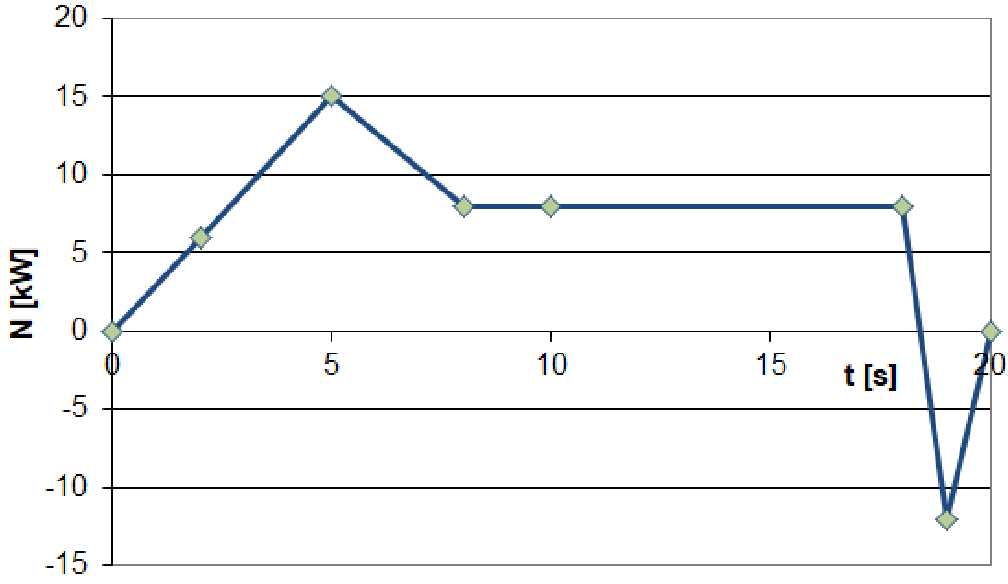

Figure 148. Example of power of the load.

The product of torque and speed is the energy over time required to complete a given work cycle. Simply analysing the power demand curve is insufficient, as a given power can be obtained for various angular velocity and load torque parameters. Therefore, it is necessary to know at least two of these curves (usually torque and angular velocity over time).

Knowing the load characteristics allows us to determine the appropriate parameters of a classic hydrostatic transmission: operating pressure (p) and flow rate (Q). These variables, analogous to a mechanical system, represent angular velocity (ω) and load torque (T). Based on this, we can determine the maximum pressures and flow rates, as well as dynamic parameters such as tangent (α) for a given work cycle.

If all conditions are met, the data is transferred to the expert system. Decisions are made there regarding the selection of digital system components, such as binary or trinary pump configuration, pump gradation, and number of pumps. The output of the expert system's operation is the appropriate technical and operational documentation for the digital system.

On this basis, verification of the feasibility of replacing the traditional hydrostatic transmission with its digital counterpart can begin. The conditions verified include energy and environmental parameters such as:

- maximum power, speed, and torque,
- adequate space,
- appropriate operator qualifications,
- transmission replacement costs,
- component availability,

- weight of the proposed solution,
- durability,
- reliability,
- noise level.

If the above conditions are met, it will be possible to replace the classic hydrostatic transmission with its "digital" equivalent.

9.2 Final Conclusions and Verification of the Research Hypothesis

The extensive analysis of simulation and experimental research conducted as part of this dissertation allows for the formulation of conclusions regarding the possibility of effectively replacing a classic hydrostatic transmission with its corresponding digital transmission concept. The analysis of the results in relation to the stated research hypothesis and problems leads to clear, albeit multifaceted, answers.

1. Verification of Functional and Kinematic Capability. The first fundamental conclusion is the confirmation that the digital hydrostatic transmission is able to fully functionally replace the classic system in terms of executing commanded motion tasks. Both simulation and experimental studies have shown that the digital control strategy, based on the sequential engagement of a set of fixed-displacement pumps, allows for the precise and repeatable replication of commanded kinematic profiles (speed and flow). The digital system approximates the "smooth" characteristics of the classic system with high fidelity, regardless of the cycle dynamics from long, 20-second processes to very fast, 2.5-second cycles.

2. Assessment of Energy Efficiency. The advantage of digital systems may become apparent when replacing systems using a throttle valve. This would be due to the elimination of throttling losses characteristic of this type of system. This makes the digital concept particularly attractive for high-load applications where energy saving is most desired.

3. Analysis of Dynamic Parameters – Identification of the Main Challenge. The experimental research, precisely identifies the key engineering challenge and the "price" to be paid for potentially replacing the classic transmission with its corresponding digital transmission. They are:

- Pulsations and Shock Loads: Research on the physical object has proven that an inherent feature of the digital transmission's operation is the generation of significant, high-frequency torque pulsations. Moreover, under intermittent operating conditions (test scenario no. 2), very high, shock torque spikes occur at the beginning of each pulse, which exceed the steady-state values. These phenomena are a real load on the mechanical components of the system.

- Filtering Effect of the Drive System: The comparison of the extremely "noisy" torque profile with the very smooth profile of the consumed active power proves that the drive system acts as an effective mechanical filter.

Answer to the Hypothesis and Research Problems In light of the above conclusions, it can be considered that the main thesis of the doctoral dissertation has been positively confirmed. Yes, it is possible to effectively replace the proportional technique with "digital hydraulics." The digital system provides comparable energy efficiency. The cost analysis, although simplified, also indicates potential savings consistent with the assumptions of the thesis. The digital system meets the kinematic and functional requirements. The biggest challenge remains its dynamic characteristic. Replacing the "smooth" operation of the classic system involves accepting and needing to manage pulsations and shock loads.

9.3 Contribution and Recommendations:

This work makes a significant contribution to the development of knowledge about digital hydrostatic systems, by identifying and quantifying the gap between idealized simulation results and complex experimental reality. It shows that while simulation models are an excellent tool for energy assessment, experimental research is absolutely key to identifying critical dynamic loads. The recommendation for further research and engineering practice is to focus on:

- **Development of advanced control strategies** that minimize torque and pressure peaks (e.g., by optimizing the sequence and timing of switching).
- **Design of mechanical components** with increased resistance to fatigue loads resulting from high-frequency pulsations.
- **Creation of more complex simulation models** to more faithfully predict dynamic phenomena.

10References:

[1] Pascal, B. (1663). Treatise on the equilibrium of liquids and the weight of the mass of air.

[2] McNeil, I. (1990). An encyclopaedia of the history of technology. Routledge.

[3] Merritt, H. E. (1967). Hydraulic control systems (Xth ed.). Wiley.

[4] Ivantysyn, J., & Ivantysynova, M. (2001). Hydrostatic pumps and motors: principles, design, performance, modelling, analysis, control and testing.

[5] Watton, J. (2009). Fundamentals of fluid power control.

[6] Jędrzykiewicz. Z, "Napędy i sterowania hydrauliczne" (Hydraulic Drives and Controls), 2009 (and other works by the author).

[7] Linjama, M. (2011, May). Digital fluid power: State of the art. In The Twelfth Scandinavian International Conference on Fluid Power (Vol. 2, No. 4, pp. 18-20).

[8] Kotlicki, T. (2023, August 28). Kiedy wynaleziono Żurawie? Historia Żurawi Budowlanych. Dźwigi Kotlicki.

[9] Heitzig, S., Sgro, S., & Theissen, H. (2012). Energy efficiency of hydraulic systems with shared digital pumps. International journal of fluid power, 13(3), 49-57.

[10] Murrenhoff, H., & Theissen, H. (2010). Hydraulic news – actual developments at IFAS. A retrospect of the 7th IFK and other developments. Contribution to conference proceedings.

[11] Kędzia, K. (2017). An algorithm for the determination of the control parameters of a multisource drive system. Technical Transactions, 3(114), 173–182.

[12] Donkov, V. H., Andersen, T., Linjama, M., & Ebbesen, M. (2020). Digital hydraulic technology for linear actuation: A state of the art review. International Journal of Fluid Power, 263-304.

[13] Winkler, B., Ploeckinger, A., & Scheidl, R. (2010). A novel piloted fast switching multi poppet valve. International journal of fluid power, 11(3), 7-14.

[14] Wang, P., Cheng, Y., Linjama, M., Yao, J., & Shan, D. (2023). A novel equivalent continuous metering control with a uniform switching strategy for digital valve system. IEEE/ASME Transactions on Mechatronics, 28(5).

[15] Huova, M., & Plöckinger, A. (2010). Improving resolution of digital hydraulic valve system by utilizing fast switching valves. In Proceedings of the Third Workshop on Digital Fluid Power, October 13-14 2010, Tampere, Finland (pp. 79-92).

[16] Scheidl, R., Kogler, H., & Winkler, B. (2013). HYDRAULIC SWITCHING CONTROL-OBJECTIVES, CONCEPTS, CHALLENGES AND POTENTIAL APPLICATIONS. Hidraulica.

[17] Eng, Bogdan Alexandru TUDOR-ROTILĂ., Eng, Radu-Iulian RĂDOI., Eng, Ștefan-Mihai ȘEFU., & Eng, Robert BLEJAN. (2024). Experimental evaluation of a digital hydraulic pumping system. Hidraulica, (4), 69-75.

[18] Vardhan, A., Dasgupta, K., Kumar, N., & Mishra, S. K. (2019). Steady-state performance investigation of open-circuit hydrostatic drives used in the rotary head of drill machine. Proceedings of the Institution of Mechanical Engineers, Part E: Journal of Process Mechanical Engineering, 233(1), 3-20.

[19] Scheidl, R., Winkler, B., & Kogler, H. (2016). Digital fluid technologies for the steel industry. Berg- und Hüttenmännische Monatshefte, 161, 504–509.

[20] McCloy, D., & Martin, H. R. (1980). Control of fluid power: analysis and design. Chichester.

[21] Kędzia, K. (2022). A method of determining optimal parameters for the secondary energy source of a multisource hydrostatic drive system in machines working in closed spaces. Energies, 15(14), 5132.

[22] Plöckinger, A., Huova, M., & Luomaranta, M. (2018). Energy efficiency of digital hydraulic light system in mobile machines. In Proceedings of the 15th International Fluid Power Conference (IFK) (pp. 372–383). RWTH Aachen.

[23] Yan, X., Chen, B., Zhang, D., Wu, C., & Luo, W. (2019). An energy-saving method to reduce the installed power of hydraulic press machines. Journal of cleaner production, 233, 538-545.

[24] Huova, M. (2017). "Energy Efficiency of Digital Hydraulic Valve Control." Journal of Fluid Power, 18(3), 188–199.

[25] Bosch Rexroth AG. (2016). Intelligent Hydraulics Fit for Industry 4.0.

[26] Ryalat, M., Franco, E., Elmoaqet, H., Almtireen, N., & Alrefai, G. (2024). The integration of advanced mechatronic systems into Industry 4.0 for smart manufacturing. Sustainability, 16(19), 8504.

[27] Tamburrano, P., Plummer, A. R., Distaso, E., & Amirante, R. (2018). A review of electro-hydraulic servovalve research and development. International Journal of Fluid Power, 19(1), 1–23.

[28] Li, C., Liu, X., Wang, X., Chen, J., & Wang, Y. (2021). Optimization of multi-way valve structure in digital hydraulic system of loader. Energies, 14(3), 700.

[29] Kärnell, S. (2020). Fluid Power Pumps and the Electrification: With a Focus on Discrete Displacement Control in Load Handling Applications (Vol. 1882). Linköping University Electronic Press.

[30] Fan, Q., Zhang, J., Li, R., & Fan, T. (2025). Review of Research on Hydrostatic Transmission Systems and Control Strategies. Processes, 13(2), 317.

[31] Kärnell, S., & Ericson, L. (2023). Classification and Review of Variable Displacement Fluid Power Pumps and Motors. International Journal of Fluid Power, 207-246.

[32]Valmet. (n.d.). FPDigHydr new technology. Valmet Insights. https://www.valmet.com/insights/articles/up-and-running/new-technology/FPDigHydr/.

[33] Zhang, Q., Kong, X., Yu, B., Ba, K., Jin, Z., & Kang, Y. (2020). Review and development trend of digital hydraulic technology. Applied Sciences, 10(2), 579.

[34] Huova, M., Linjama, M., & Huhtala, K. (2013). Energy efficiency of digital hydraulic valve control systems (No. 2013-01-2347). SAE Technical Paper.

[35] Wang, H., Chen, Z., Huang, J., Quan, L., & Zhao, B. (2022). Development of high-speed on–off valves and their applications. Chinese Journal of Mechanical Engineering, 35(1).

[36] Sciatti, F., Tamburrano, P., Distaso, E., & Amirante, R. (2024). Digital hydraulic valves: Advancements in research. Heliyon.

[37] Tamburrano.P, A. R. Plummer, E. Distaso, and R. Amirante, “A review of electro-hydraulic servovalve research and development,” International Journal of Fluid Power, 2018, doi: 10.1080/14399776.2018.1537456.

[38] Skorek, G. (2018). Study of losses and energy efficiency of hydrostatic drives with hydraulic cylinder. Polish Maritime Research, 25(4 (100)), 114-129.

[39] Shafai, E., Simons, M., Neff, U., & Geering, H. P. (1995). Model of a continuously variable transmission. In Advances in Automotive Control 1995 (pp. 105-113). Pergamon.

[40] Laamanen, M. S. A., & Vilenius, M. (2003, May). Is it time for digital hydraulics? In The eighth Scandinavian international conference on fluid power.

[41] Thakur, S., Kumar, A., & Singh, S. (2024). A critical review of the various energy-saving models used in hydrostatic power transmission drives for enhancing the efficiency of chairlift transport system. Arabian Journal for Science and Engineering, 49(8), 10327-10348.

[42] Kędzia, K. (2004). Metoda optymalizacji energetycznej i ekologicznej hydrostatycznego wieloźródłowego układu napędowego [Doctoral dissertation, Wrocław University of Science and Technology].

[43] Chrostowski, H. (Ed.). (1990). Modelowanie rozpływu mocy w hydrostatycznych wieloźródłowych układach napędowych. Centralny Program Badań Podstawowych 02.05, Politechnika Wrocławska.

[44] Chrostowski, H. (Ed.). (1998). Podstawy budowy mechano-hydraulicznych układów napędowych z akumulation energii: Sprawozdanie merytoryczne z projektu badawczego KBN nr 1309/P4/92/02. Politechnika Wrocławska.

[45] Skrocki, A., & Szlagowski, J. (2010). Badania porównawcze układu regulacji mikroprocesorowej dla układów napędzanych silnikami hydraulicznymi małych prędkości obrotowych. Przegląd Mechaniczny, 17-24.

[46] Cheong, K. L., Li, P. Y., Sedler, S., & Chase, T. R. (2011). Comparison between input coupled and output coupled power-split configurations in hybrid vehicles. International Fluid Power Exhibition (IFPE), No. 10.2.

[47] Dindorf, R. (2009). Napędy płynowe hydrostyczne i pneumatyczne: Podstawy teoretyczne i metody obliczenia. Wydawnictwo Politechniki Świętokrzyskiej.

[48] Grandall, D. R. (2010). Performance and efficiency of hydraulic pumps and motors [Master's thesis, University of Minnesota].

[49] Paszota, Z. (1999). Uściślenia teoretyczne związane z wyznaczaniem strat i sprawności dla przekładni hydrostatycznych. In A. Garbacik (Ed.), Kierunki rozwoju napędów hydraulicznych i konstrukcji maszyn roboczych (pp. 205–248). FPN Publications.

[50] Paszota, Z. (2013). Losses and energy efficiency of drive motors and systems: Replacement of the Sankey diagram of power decrease in the direction of power flow by a diagram of power increase opposite to the direction of power flow opens a new perspective of research of drive motors and systems. Polish Maritime Research, 20(1), 3–10.

[51] Paszota, Z. (2016). On power stream in motor or drive system. Polish Maritime Research, 23(4), 93–98.

[52] Schlösser, W. M. J., & Hilbrands, J. W. (1963). Der volumetrische Wirkungsgrad von Verdrängerpumpen. Ölhydraulik und Pneumatik, 7(12).

[53] Stryczek, S. (1995). Napęd hydrostatyczny (Vols. 1–2). Wydawnictwa Naukowo-Techniczne (WNT).

[54] Triet, H. H., & Ahn, K. K. (2011). Comparison and assessment of hydraulic energy-saving system for hydrostatic drives. Proceedings of the Institution of Mechanical Engineers, Part I: Journal of Systems and Control Engineering, 225(1), 21–34.

[55] Guo, T., Wu, B., Lin, T., Chen, H., & Chen, Q. (2022). Closed-Circuit Pump-Controlled Electro-Hydraulic Steering System for Pure Electric Wheel Loader. Applied Sciences, 12(11), 5740.

[56] Zhang Yanting, Wang Qingfeng, & Xiao Qing. (2007) Simulation and experimental research on energy regeneration with hydraulic motor for hybrid drive excavator. Journal of Mechanical Engineering, 43(8), 218-223.

[57] Yan, L. J., Sun, H., Liu, W., Jiang, J. H., & Han, J. W. (2014). Hydraulic hybrid technology of moving construction machinery. Journal of Jilin University (Engineering and Technology Edition), 44(2), 364-8.

[58] Nervegna, N., & Rundo, M. (2020). Steps in Hydraulics. Vol. 1-2.

[59] Vacca, A., & Franzoni, G. (2021). Hydraulic fluid power: fundamentals, applications, and circuit design. John Wiley & Sons.

[60] Costa, G., & Sepehri, N. (2015). Hydrostatic transmissions and actuators: operation, modelling and applications. John Wiley & Sons.

[61] Tamburrano, P., De Palma, P., Plummer, A. R., Distaso, E., Sciatti, F., & Amirante, R. (2021). Simulation of a high frequency on/off valve actuated by a piezo-ring stack for digital hydraulics. In E3S Web of Conferences.

[62] Mattila, M., Huova, M., & Linjama, M. (2017). Digital hydraulics - A review. Proceedings of the Institution of Mechanical Engineers, Part I: Journal of Systems and Control Engineering, 231(7), 514-531.

[63] Andersen, T. O., Hansen, M. R., & Pedersen, H. C. (2021). Energy efficient digital displacement fluid power technology. Energies, 14(3), 615.

[64] Scheidl, R., & Winkler, B. (2012). Fault tolerance of digital hydraulic valves. The 8th International Fluid Power Conference (IFK), Dresden, Germany, March 26-28, 2012.

[65] Heikkilä, M., & Linjama, M. (2013). Energy efficiency of digital hydraulic valve control. IOP Conference Series: Materials Science and Engineering, 52(1), 012004.

[66] Ding, R., & Cheng, M. (2024). Independent metering electro-hydraulic control system. Springer.

[67] Continuous And Discrete Signals. Retreved from https://zhuanlan.zhihu.com/p/675122296.

[68] Linjama, M. (2016). On the numerical solution of steady-state equations of digital hydraulic valve-actuator. The Eighth Workshop on Digital Fluid Power.

[69] Zhao, X. (2005). Research on the theory and application of HGDV pulse modulation switching digital hydraulic valve.

[70] Pan M., Plummer A., El Agha A. (2017): Theoretical and Experimental Studies of a Switched Inertance Hydraulic System in a Four-Port High-Speed Switching Valve Configuration, Energies 2017, 10(6), 780.

[71] Winkler, B. (2017). Recent advances in digital hydraulic components and applications [Paper presentation]. The Ninth Workshop on Digital Fluid Power, Aalborg, Denmark.

[72] Milecki A., Ortmann J.: Electrohydraulic linear actuator with two stepping motors controlled by overshoot-free algorithm. Mechanical Systems and Signal Processing 96 p. 45–57 (2017).

[73] Lu, W. (2020). Review of digital hydraulics technologies.

[74] Tadakuma, S., Tanaka, S., & Miura, K. (1996). Improved PWM control for GTO inverters with pulse number modulation. IEEE Transactions on Industry Applications, 32(3).

[75] Yao, C. B., Rogelio, J. P., Baldovino, R. G., & Caluyo, F. S. (2017). A fuzzy-pulse width modulation (PWM) control algorithm for a computer numerical control (CNC) laser machine. Advanced Science Letters, 23(5).

[76] Xing, Z., Ruan, X., & Xie, H. (2018). PWM control scheme for a buck/boost modular multilevel DC/DC converter with reduced submodule capacitance. IEEE Transactions on Power Electronics, 33(5).

[77] Li, P., Zhu, Z. H., & Meguid, S. A. (2016). State dependent model predictive control for orbital rendezvous using pulse-width pulse-frequency modulated thrusters. Advances in Space Research, 58(1).

[78] Song, G., & Ma, N. (2003). Control of shape memory alloy actuators using pulse-width pulse-frequency (PWPF) modulation. Journal of Intelligent Material Systems and Structures, 14(1).

[79] Heikkilä, M., & Linjama, M. (2013). Displacement control of a mobile crane using a digital hydraulic power management system. Mechatronics, 23(4).

[80] Linjama, M., Laamanen, A., & Vilenius, M. (2003). Is it time for digital hydraulics? In Proceedings of the 8th Scandinavian International Conference on Fluid Power, SICFP '03 (Vol. 1).

[81] Hansen, A. (2023). Fluid power systems. Springer.

[82] Wilson, W. E., & Lemme, C. D. (1970). Hydrostatic transmissions. Hydraulics and Pneumatics, 1970(Nos. 1, 2, 5, 6, 9).

[83] Schlösser, W. M. J., & Hilbrands, J. W. (1963). Der volumetrische Wirkungsgrad von Verdrängerpumpen. Ölhydraulik und Pneumatik, 7(12).

[84] Paszota, Z. (2015). Comparison of the powers of energy losses in a variable capacity displacement pump determined without or with taking into account the power of hydraulic oil compression. Polish Maritime Research, 22(2), 32–43.

[85] Kucybała, P., Pobędzia, J., & Sobczyk, A. (2006). Określenie sprawności hydraulicznego układu odzysku energii w mechanizmie jazdy [Paper presentation]. Problemy Rozwoju Maszyn Roboczych, Zakopane.

[86] Kumar, R., & Ivantysynova, M. (2011). An instantaneous optimization based power management strategy to reduce fuel consumption in hydraulic hybrids. International Journal of Fluid Power, 12(2), 15–25.

[87] Ocioszyński, J. (1981). Electrical power engineering of hybrid electromechanical vehicle drive systems . Warsaw University of Technology Publishing House.

[88] Paszota, Z. (1998). Podwyższanie sprawności enetgetycznej kierunkiem rozwoju napędu hydrostatycznego. Hydraulika i Pneumatyka, 9-13.

[89] Siłka, W. (1998). Analiza wpływu parametrów cyklu jezdnego na energochłonność ruchu samochodu. Polska Akademia Nauk, Oddział w Krakowie.

[90] Wrzecioniarz, P. (2001). Diagnostyka pojazdów samochodowych. Oficyna Wydawnicza PW, Wrocław.

[91] Tomasiak, E. (2001). Napędy i sterowania hydrauliczne i pneumatyczne. Wydawnictwo Politechniki Śląskiej.

[92] Osiecki, A. (1998). Hydrostatyczny napęd maszyn. Wydawnictwa Naukowo-Techniczne (WNT).

[93] Sradomski, W. (2002). Metoda Oceny Charakterystyk Energetycznych i Ekologicznych Układu Silnik Spalinowy—Przekładnia Hydrostatyczna dla Widmowej Postaci Obciążeń. Praca doktorska: Wrocław, Poland.

[94] Kutz, M. (2008). Environmentally conscious transportation. John Wiley & Sons.

[95] Lisi, I. E. (2015). Translating environmental motivations into performance: The role of environmental performance measurement systems. Management Accounting Research, 29, 27–44.

[96] Kułażyński, M., & Sroka, Z. J. (2011). Developing Engine Technology. PintPap Łódź-Wrocław.

[97] Kuranc, A., Caban, J., Šarkan, B., Dudziak, A., & Stoma, M. (2021). Emission of selected exhaust gas components and fuel consumption in different driving cycles. Communications-Scientific letters of the University of Zilina, 23(4), B265-B277.

[98] Klop, R., & Ivantysynova, M. (2011). Investigation of noise sources on a series hybrid transmission. International Journal of Fluid Power, 12(3), 17–30.

[99] Valverde-Morales, V. (2020). Overview of the light-duty vehicles tailpipe emissions regulations in the European Union: status and upcoming type-approval and market surveillance schema. Combustion Engines, 59(1), 3-7.

[100] Stone, R. (1999). Introduction to internal combustion engines (Vol. 3). London: Macmillan.

[101] Osiński, P., Rutański, J., Bury, P. J., & Cieślicki, R. A. (2020). Acoustic tests of type KPF1 high-pressure external gear pumps. Czasopismo Techniczne – Technical Transactions, 117(1), 1–10.

[102] Stosiak, M., Skačkauskas, P., Towarnicki, K., Deptuła, A., Deptuła, A., Prażnowski, K., Grzywacz, Ż., Karpenko, M., Urbanowicz, K., & Łapka, M. (2023). Analysis of the impact of vibrations on a micro-hydraulic valve using a modified induction algorithm. Machines, 11(2), Article 184.

[103] Mistewicz, E. (1999, January 31). Terror decybeli. Wprost, (5).

[104] Engel, Z. (2001). Ochrona środowiska przed drganiami i hałasem (2nd ed.). Wydawnictwo Naukowe PWN.

[105] European Union. (2019). Regulation (EU) 2019/631 of the European Parliament and of the Council of 17 April 2019 setting CO2 emission performance standards for new passenger cars and for new light commercial vehicles, and repealing Regulations (EC) No 443/2009 and (EU) No 510/2011. Official Journal of the European Union.

[106] Ellram, L. M., & Siferd, S. P. (1998). Total Cost of Ownership: A Key Concept in Strategic Cost Management Decisions. Journal of Business Logistics, 19(1), 55-84.

[107] Schmidt, L., & Andersen, T. O. (2021). Energy Efficiency and Operational Expenditures in Modern Fluid Power Systems. Energies, 14(18), 5890.

[108] Garcés, F., & de la Fuente, A. (2023). Beyond the Purchase Price: A Framework for Total Cost of Ownership Analysis in Industrial Equipment. International Journal of Production Economics, 261, 108875.

[109] Jaskóła, J. (2022). Life Cycle Costing (LCC) as a Tool for Optimizing Maintenance Strategies in Heavy Machinery. Eksploatacja i Niezawodnosc – Maintenance and Reliability, 24(3), 450-461.

[110] Kumar, S. (2020). A comparative study on total cost of ownership for conventional and alternative powertrain technologies in commercial vehicles. Transportation Research Part D: Transport and Environment, 87, Article 102530.

11 Appendix

11.1 Appendix A

An example of determining selected errors for comparisons of simulation models of classic and digital hydrostatic transmission performed in the work:

- The Root Mean Square Error (RMSE) (31), which measures the average squared difference between the digital and classical signals.
- The Mean of Squared Error (MSE) (30), which represents the total accumulated squared error over time.
- The Maximum Tracking Error, which denotes the largest pointwise deviation between the two signals.

1. Results for Scenario No. 3 (20s)

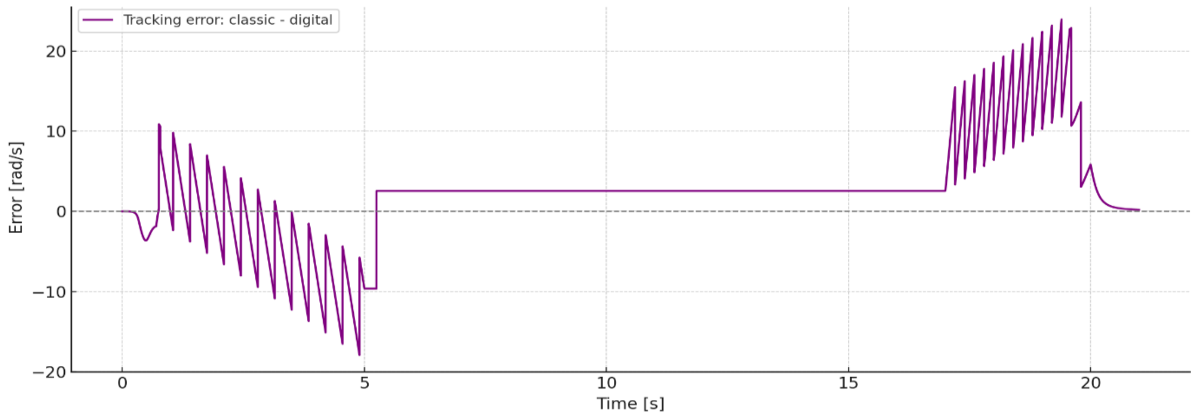

Fig. A1. Graph of angular velocity difference between classic and digital simulation model of hydrostatic transmissions (20s).

Table A1. Angular velocity comparison quality indicators between classic and digital simulation models of hydrostatic transmissions.

Metric	**Value**	**Units**
RMSE (Root Mean of Square Error)	7.61	rad/s
ISE (Integral of Squared Error)	889.04	$(rad/s)^2$
Max. Tracking Error	23.92	rad/s
Time of Occurrence	19.40	s

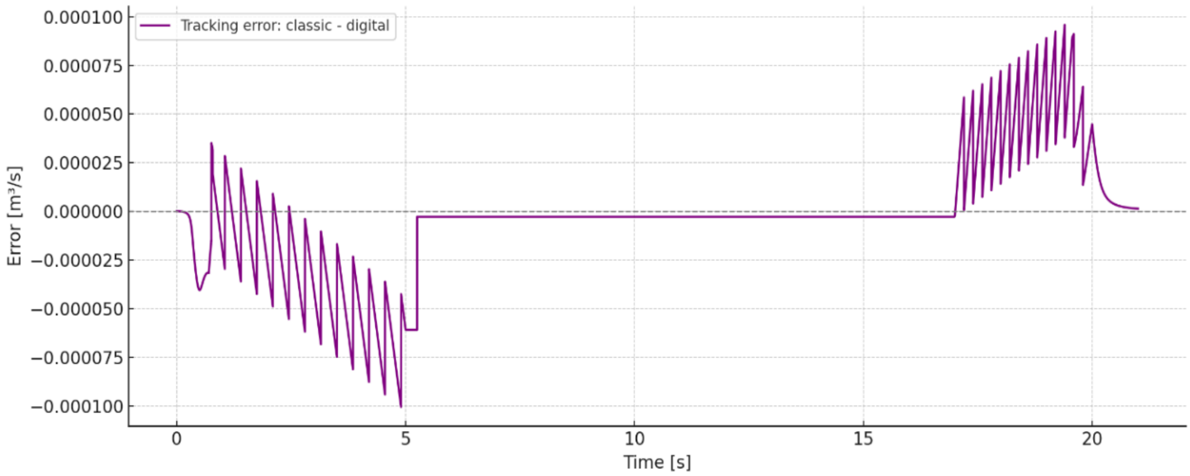

Fig. A2. Graph of flow rate difference between classic and digital simulation model of hydrostatic transmissions (20s).

Table A2. Flow rate comparison quality indicators between classic and digital simulation models of hydrostatic transmissions (20s).

Metric	**Value**	**Units**
RMSE (Root Mean of Square Error)	3.17×10^{-5}	m^3/s
MSE (Mean of Squared Error)	1.78×10^{-8}	$(m^3/s)^2$
Max. Tracking Error	1.01×10^{-4}	m^3/s
Time of Occurrence	4.90	s

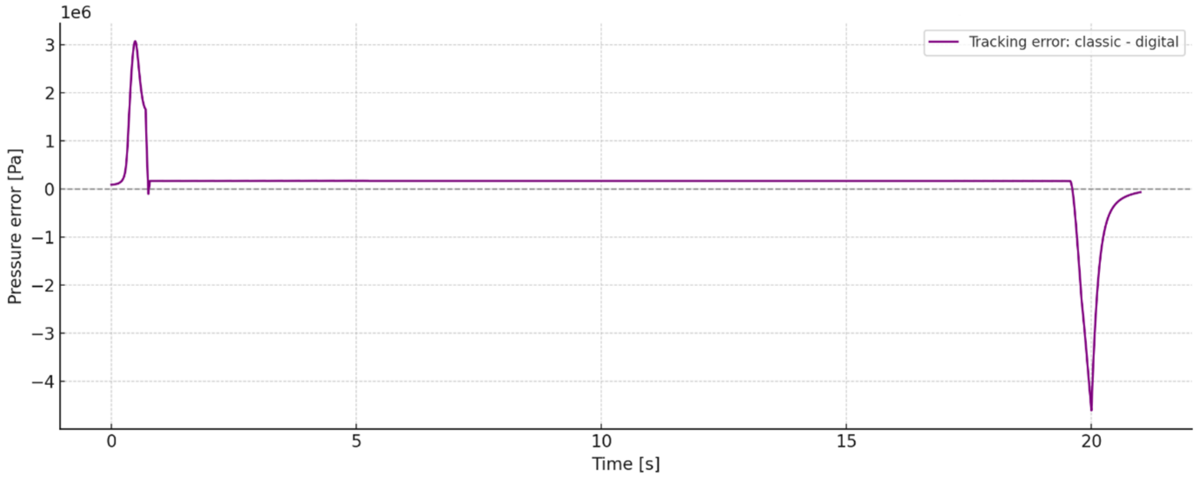

Fig. A3. Graph of pressure difference between classic and digital simulation model of hydrostatic transmissions (20s).

Table A3. Pressure comparison quality indicators between classic and digital simulation models of hydrostatic transmissions (20s).

Metric	**Value**	**Units**
RMSE (Root Mean of Square Error)	545 894	Pa
MSE (Mean of Squared Error)	7.08×10^{12}	Pa^2
Max. Tracking Error	4.61×10^{6}	Pa
Time of Occurrence	20.0	s

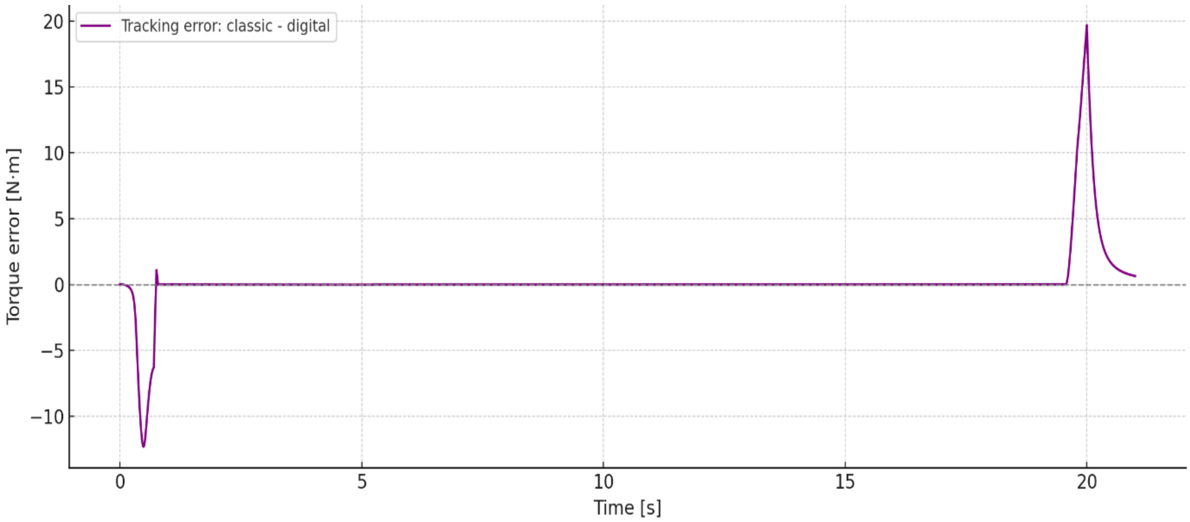

Fig. A4. Graph of torque difference between classic and digital simulation model of hydrostatic transmissions (20s).

Table A4. Torque comparison quality indicators between classic and digital simulation models of hydrostatic transmissions (20s).

Metric	**Value**	**Units**
RMSE (Root Mean of Square Error)	2.22	N/m
MSE (Mean of Squared Error)	116.54	$(N/m)^2$
Max. Tracking Error	19.69	N/m
Time of Occurrence	20.00	s

2. Results for Scenario No. 3a (10s)

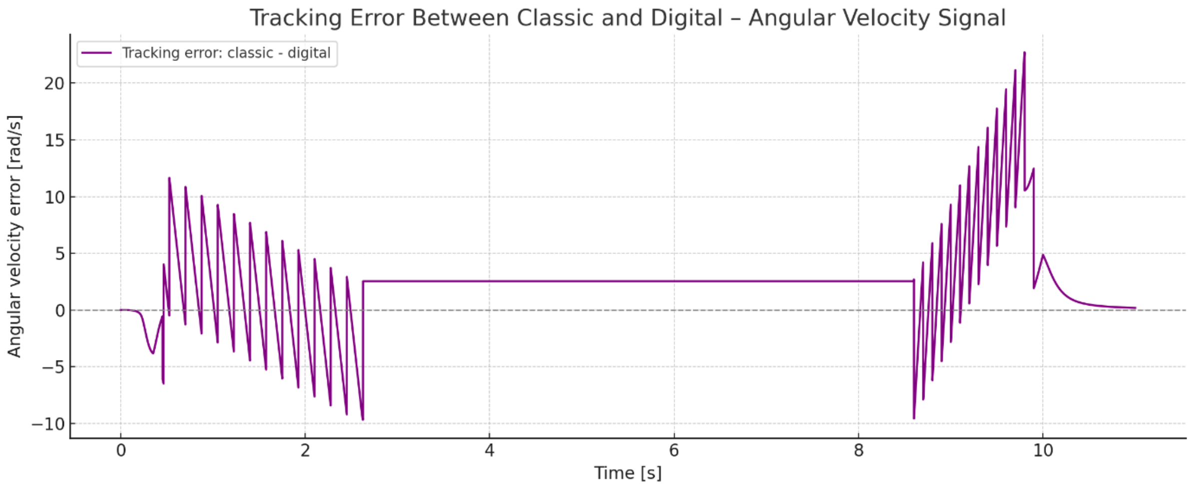

Fig. A5. Graph of angular velocity difference between classic and digital simulation model of hydrostatic transmissions (10s).

Table A5. Angular velocity comparison quality indicators between classic and digital simulation models of hydrostatic transmissions (10s).

Metric	**Value**	**Units**
RMSE (Root Mean of Square Error)	6.57	rad/s
MSE (Mean of Squared Error)	216.58	$(rad/s)^2$
Max. Tracking Error	22.72	rad/s
Time of Occurrence	9.8	s

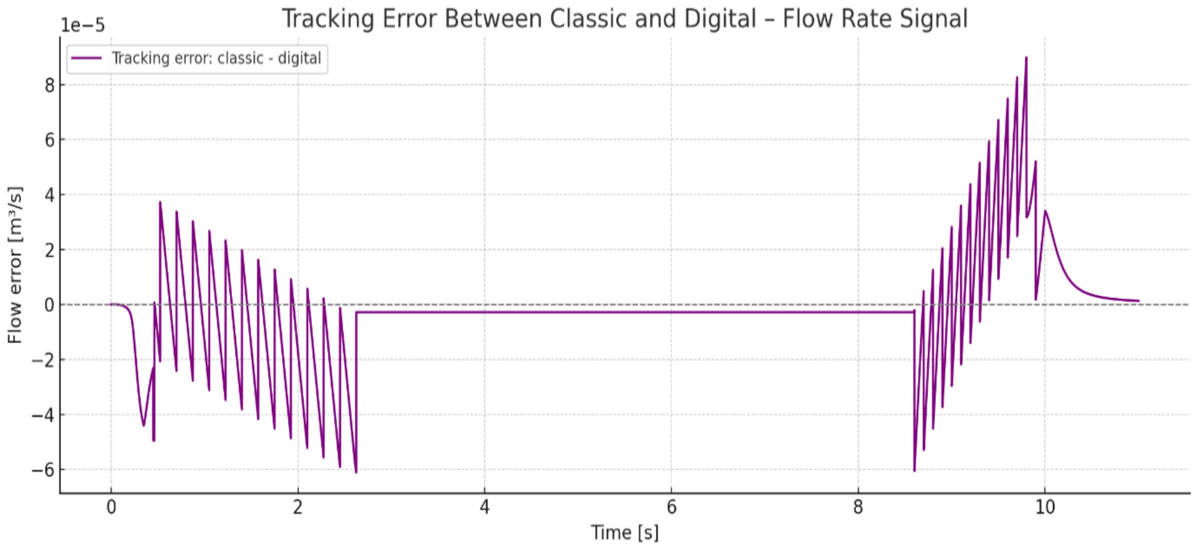

Fig. A6. Graph of flow rate difference between classic and digital simulation model of hydrostatic transmissions (10s).

Table A6. Flow rate comparison quality indicators between classic and digital simulation models of hydrostatic transmissions (10s).

Metric	**Value**	**Units**
RMSE (Root Mean of Square Error)	2.68×10^{-5}	m^3/s
MSE (Mean of Squared Error)	3.52×10^{-9}	$(m^3/s)^2$
Max. Tracking Error	8.99×10^{-5}	m^3/s
Time of Occurrence	9.8	s

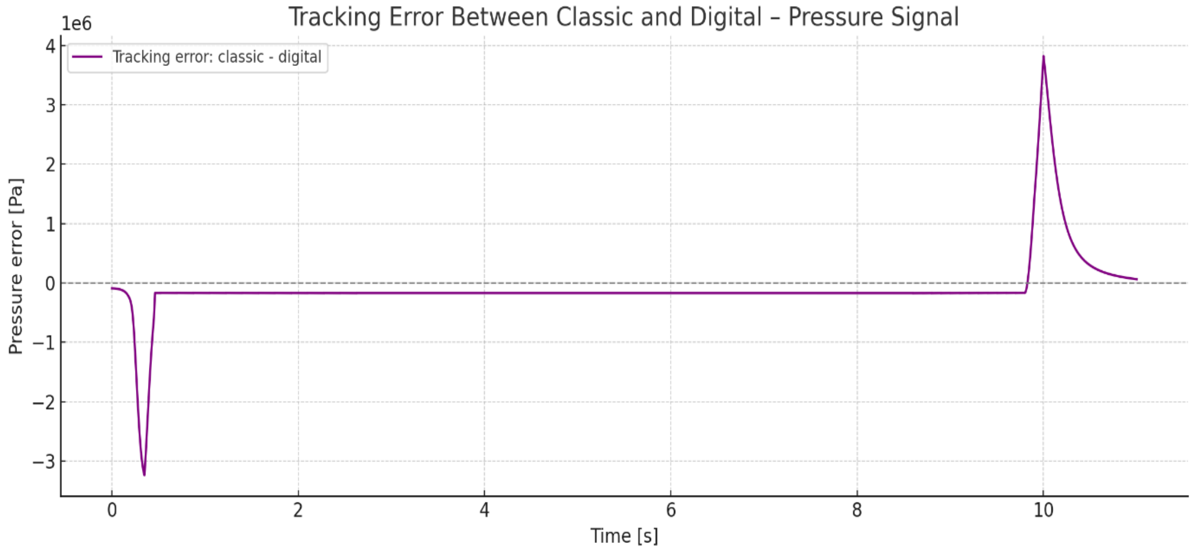

Fig. A7. Graph of pressure difference between classic and digital simulation model of hydrostatic transmissions (10s).

Table A7. Pressure comparison quality indicators between classic and digital simulation models of hydrostatic transmissions (10s).

Metric	**Value**	**Units**
RMSE (Root Mean of Square Error)	4.98×10^{5}	Pa
MSE (Mean of Squared Error)	3.50×10^{12}	Pa^2
Max. Tracking Error	3.82×10^{6}	Pa
Time of Occurrence	10.0	s

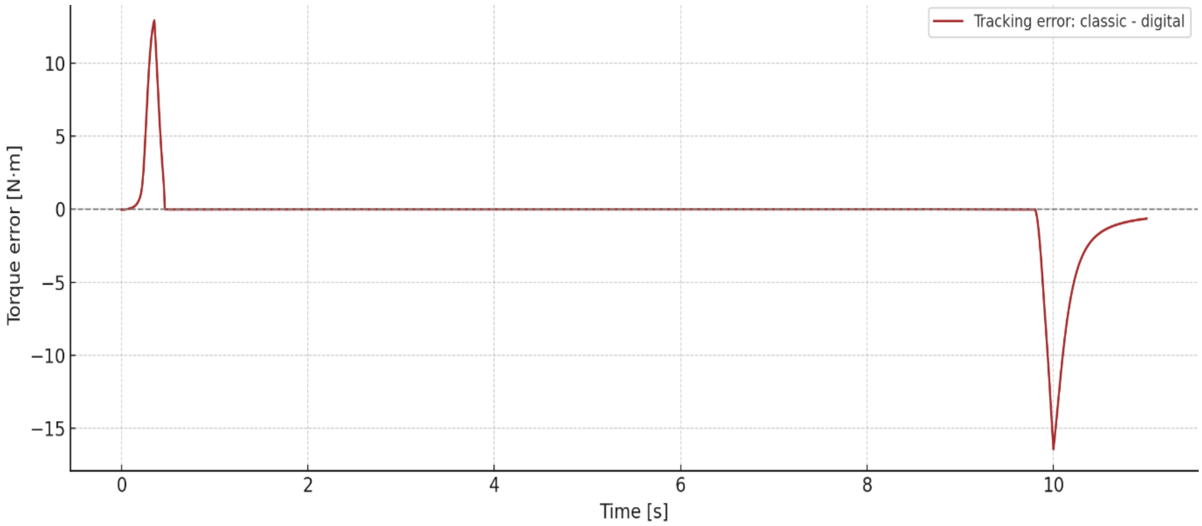

Fig. A8. Graph of torque difference between classic and digital simulation model of hydrostatic transmissions (10s).

Table A8. Torque comparison quality indicators between classic and digital simulation models of hydrostatic transmissions (10s).

Metric	**Value**	**Units**
RMSE (Root Mean of Square Error)	1.998	N/m
MSE (Mean of Squared Error)	58.40	$(N/m)^2$
Max. Tracking Error	-16.43	N/m
Time of Occurrence	10.0	s

3. Results for Scenario No. 3b (5s)

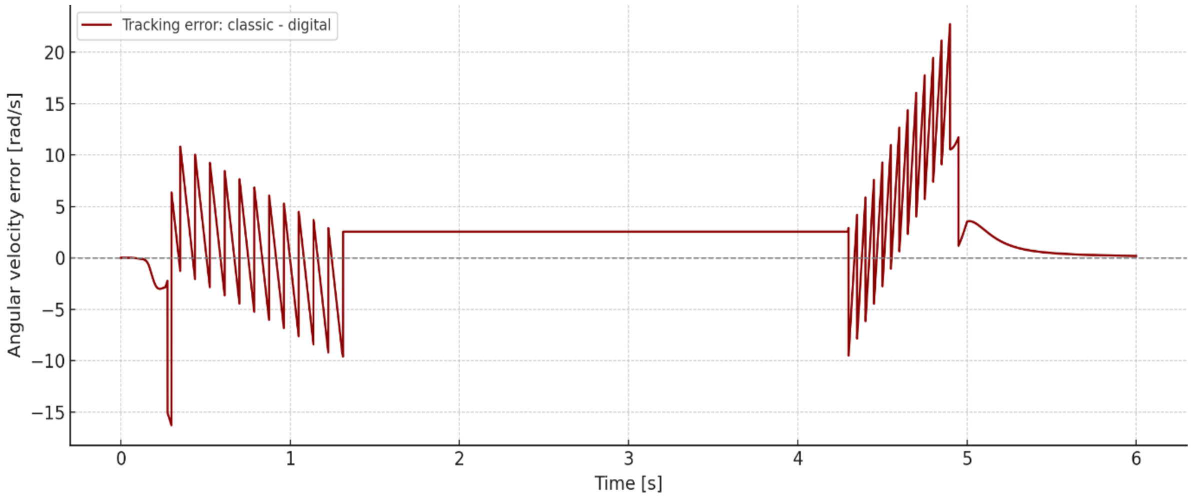

Fig. A9. Graph of angular velocity difference between classic and digital simulation model of hydrostatic transmissions (5s).

Table A9. Angular velocity comparison quality indicators between classic and digital simulation models of hydrostatic transmissions (5s).

Metric	**Value**	**Units**
RMSE (Root Mean of Square Error)	6.56	rad/s
MSE (Mean of Squared Error)	111.07	$(rad/s)^2$
Max. Tracking Error	22.72	rad/s
Time of Max. Error	4.90	s

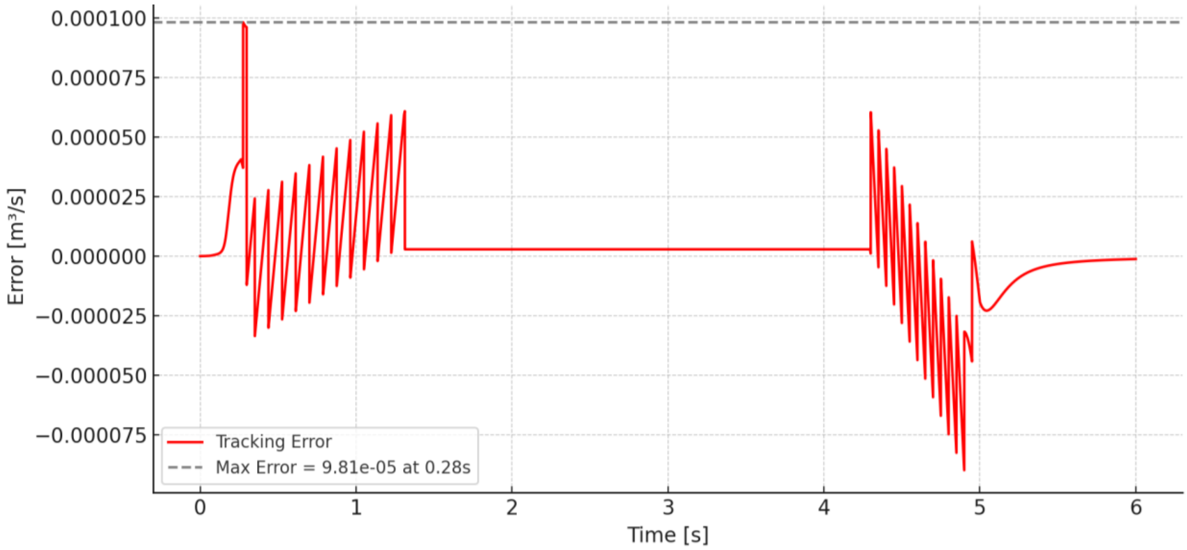

Fig. A10. Graph of flow rate difference between classic and digital simulation model of hydrostatic transmissions (5s).

Table A10. Flow rate comparison quality indicators between classic and digital simulation models of hydrostatic transmissions (5s).

Parameter	Value	**Units**
RMSE	2.82×10^{-5}	m^3/s
ISE	1.94×10^{-9}	$(m^3/s)^2$
Maximum error	9.81×10^{-5}	m^3/s
Time of maximum error	0.276 s	s

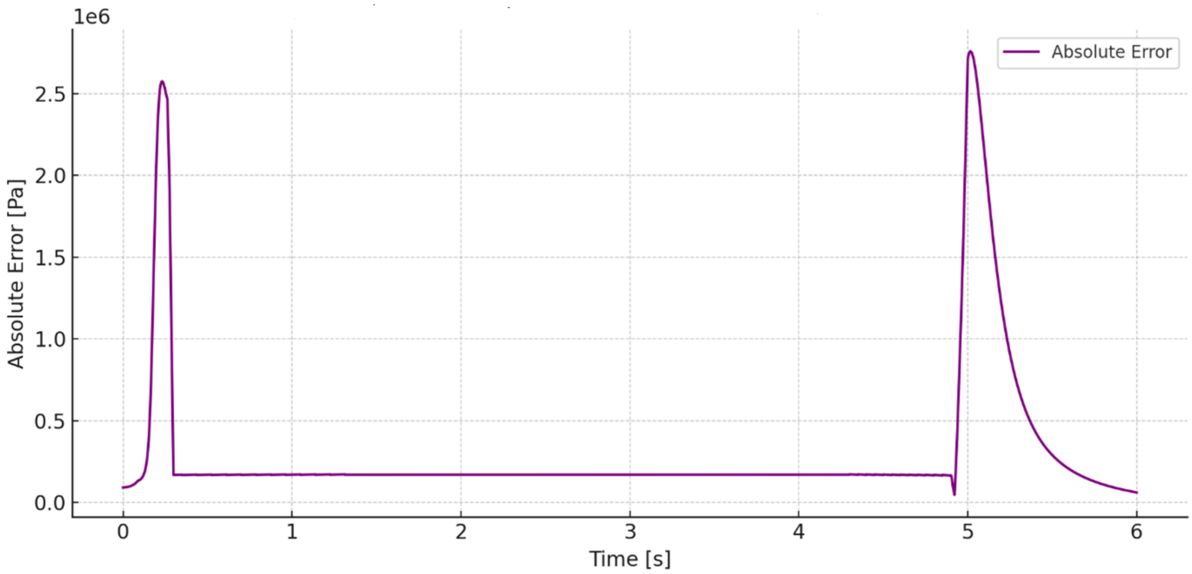

Fig. A11. Graph of pressure difference between classic and digital simulation model of hydrostatic transmissions (5s).

Table A11. Pressure comparison quality indicators between classic and digital simulation models of hydrostatic transmissions (5s).

Parameter	Value	**Units**
RMSE	5.03×10^{5}	Pa
ISE	2.53×10^{12}	Pa^2
Maximum error	2.76×10^{6}	Pa
Time of maximum error	5.020 s	s

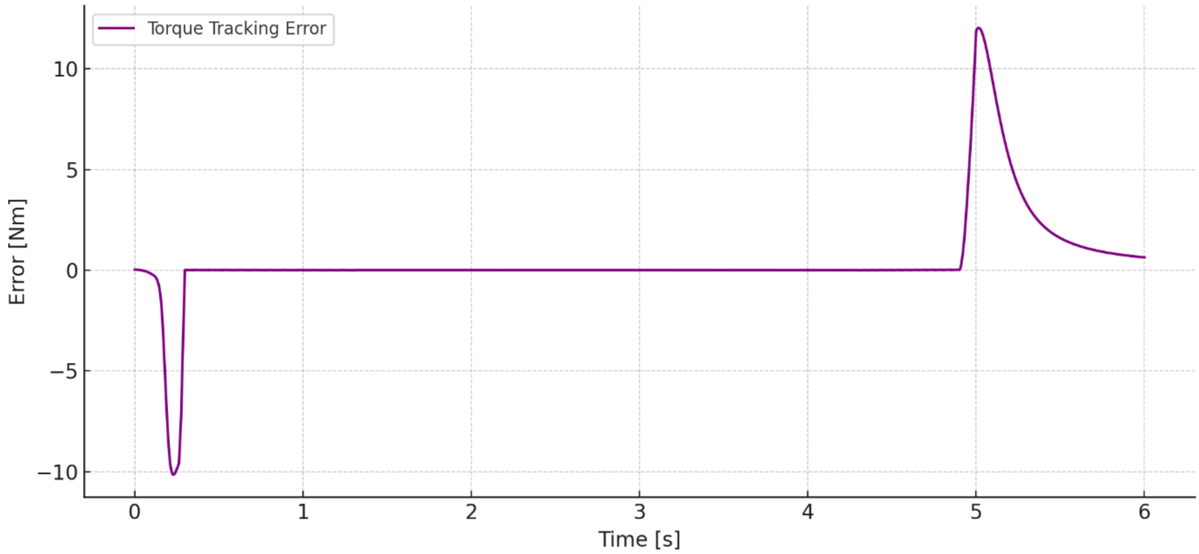

Fig. A12. Graph of torque difference between classic and digital simulation model of hydrostatic transmissions (5s).

Table A12. Torque comparison quality indicators between classic and digital simulation models of hydrostatic transmissions (5s).

Parameter	Value	**Units**
RMSE	1.98	N/m
ISE	23.6	$(N/m)^2$
Maximum error	12.0	N/m
Time of maximum error	5.014	s

11.2 Appendix B

Comparison of the costs of components of a classic and digital hydrostatic transmission.

Table B1. The prices range of 11kW three phase motor.

Type	Price Range (PLN)	Price Range (EUR)	Key Features
Standard IE2 Efficiency	2,500–4,500 PLN	~550–1,000 EUR	Basic industrial use, cast iron frame
High Efficiency IE3	3,500–6,000 PLN	~800–1,350 EUR	Energy-saving, lower long-term costs
Premium IE4 Efficiency	5,000–8,000+ PLN	~1,100–1,800+ EUR	Highest efficiency, durable construction
Explosion-Proof (ATEX)	7,000–15,000+ PLN	~1,600–3,400+ EUR	Hazardous environments (mines, chemical plants)
Brake Motor Variant	4,500–9,000 PLN	~1,000–2,000 EUR	Built-in electromagnetic brake

Table B2. The price range of proportional pressure valve.

Type	Pressure Range	Flow Rate	Price (PLN)	Price (EUR)	Brand Examples
Standard Proportional Valve	50–200 bar	10–30 L/min	1,500–5,000 PLN	~350–1,100 EUR	Bosch Rexroth, Eaton, Hydac
High-Precision (Closed Loop)	200–350 bar	30–100 L/min	5,000–15,000 PLN	~1,100–3,300 EUR	Parker, Moog, Hägglunds
Cartridge-Style (Compact)	50–300 bar	5–20 L/min	1,000–4,000 PLN	~220–900 EUR	Sun Hydraulics, Bucher
High-Flow Industrial	300–500 bar	100–500 L/min	15,000–50,000+ PLN	~3,300–11,000+ EUR	Atos, Danfoss, Linde

Table B3. The price range of gear pumps.

Displacement (cm^3/rev)	Pressure Range (bar)	Budget Brands (PLN/EUR)	Mid-Range (PLN/EUR)	Premium Brands (PLN/EUR)
2 cm^3/rev	150–200 bar	300–800 PLN (~65–175 EUR)	800–1,500 PLN (~175–330 EUR)	1,500–3,000 PLN (~330–660 EUR)
4 cm^3/rev	150–250 bar	500–1,200 PLN (~110–260 EUR)	1,200–2,500 PLN (~260–550 EUR)	2,500–5,000 PLN (~550–1,100 EUR)
8 cm^3/rev	200–250 bar	800–2,000 PLN (~175–440 EUR)	2,000–4,000 PLN (~440–880 EUR)	4,000–8,000 PLN (~880–1,750 EUR)
16 cm^3/rev	200–300 bar	1,500–3,500 PLN (~330–770 EUR)	3,500–7,000 PLN (~770–1,540 EUR)	7,000–15,000 PLN (~1,540–3,300 EUR)

Table B4. The price range of multipiston axial pump.

Type	Flow Rate	Pressure	Price Range (PLN)	Price Range (EUR)
Small fixed displacement	10–30 L/min	200–250 bar	2,000–8,000 PLN	~450–1,800 EUR
Variable displacement	50–100 L/min	300–350 bar	10,000–25,000 PLN	~2,200–5,500 EUR
High-performance industrial	150–300 L/min	350–400 bar	25,000–60,000+ PLN	~5,500–13,000+ EUR

Table B5. The price range of proportional valves.

Type	Flow Rate	Pressure	Price Range (PLN)	Price Range (EUR)	Key Brands
Small Direct-Acting (solenoid)	5–20 L/min	200–250 bar	500–3,000 PLN	~110–650 EUR	Bosch Rexroth, Parker, Eaton
Industrial Spool Valve	30–100 L/min	300–350 bar	3,000–15,000 PLN	~650–3,300 EUR	Danfoss, Moog, Hydac
High-Flow Cartridge Valve	100–300 L/min	350–400 bar	15,000–40,000+ PLN	~3,300–8,800+ EUR	Sun Hydraulics, Bucher
Digital/Closed-Loop (with feedback)	Custom	Up to 420 bar	20,000–60,000+ PLN	~4,400–13,200+ EUR	Rexroth, Sauer-Danfoss

Table B6. The price range of 2-way directional valves.

Type	Size (Ports)	Pressure Rating	Price Range (PLN)	Price Range (EUR)	Common Brands
Manual 2-way valve	1/4" – 1/2"	Up to 210 bar	50 – 300 PLN	~10 – 65 EUR	Stauff, Bosch, Hydac
Solenoid-operated	1/4" – 3/4"	250 – 350 bar	200 – 1,500 PLN	~45 – 330 EUR	Bosch Rexroth, Parker, Eaton
Proportional valve	1/2" – 1"	300 – 400 bar	1,500 – 8,000 PLN	~330 – 1,750 EUR	Moog, Danfoss, Bucher
High-flow industrial	1" – 2"	350+ bar	3,000 – 15,000 PLN	~660 – 3,300 EUR	Sauer-Danfoss, Kawasaki

11.3 Appendix C

Parameters of simulation model components of digital hydrostatic transmission (Fig. *23*).

Table C1. Parameters of gear pump (No 1) 3.1831×10^{-7} m^3/rad (2cm^3/rev).

Parameter	**Value**
Displacement	1.8 cm^3/rev
Leakage and friction parameterization	Analytical
Nominal shaft angular velocity	154 rad/s
Nominal pressure gain	200e5 Pa
Nominal kinematic viscosity	18 cSt
Nominal fluid density	900 kg/m^3
Volumetric efficiency at nominal conditions	0.92
No-load torque	0.05 N*m
Friction torque vs. pressure gain coefficient	0.6e-6 N*m/Pa

Table C2. Parameters of gear pump (No 2) 6.3662×10^{-7} m^3/rad (4cm^3/rev).

Parameter	**Value**
Displacement	3.9 cm^3/rev
Leakage and friction parameterization	Analytical
Nominal shaft angular velocity	154 rad/s
Nominal pressure gain	200e5 Pa
Nominal kinematic viscosity	18 cSt
Nominal fluid density	900 kg/m^3
Volumetric efficiency at nominal conditions	0.92
No-load torque	0.05 N*m
Friction torque vs. pressure gain coefficient	0.6e-6 N*m/Pa

Table C3. Parameters of gear pump (No 3) 1.2732×10^{-6} m^3/rad (8cm^3/rev).

Parameter	**Value**
Displacement	8.4 cm^3/rev
Leakage and friction parameterization	Analytical
Nominal shaft angular velocity	154 rad/s
Nominal pressure gain	200e5 Pa
Nominal kinematic viscosity	18 cSt

Nominal fluid density	900 kg/m³
Volumetric efficiency at nominal conditions	0.92
No-load torque	0.05 N*m
Friction torque vs. pressure gain coefficient	0.6e-6 N*m/Pa

Table C4. Parameters of gear pump (No 4) $2.5465\times10^{-6}m^3/rad$ ($16cm^3/rev$).

Parameter	**Value**
Displacement	17.5 cm³/rev
Leakage and friction parameterization	Analytical
Nominal shaft angular velocity	154 rad/s
Nominal pressure gain	200e5 Pa
Nominal kinematic viscosity	18 cSt
Nominal fluid density	900 kg/m³
Volumetric efficiency at nominal conditions	0.92
No-load torque	0.05 N*m
Friction torque vs. pressure gain coefficient	0.6e-6 N*m/Pa

Table C5. Parameters of two-way directional valve (No 1).

Parameter	**Value**
Valve passage maximum area	7e-4 m²
Valve maximum opening	0.005 m
Flow discharge coefficient	0.7
Initial opening	0 m
Leakage area	1e-12 m²
Laminar transition specification	Pressure ratio
Laminar flow pressure ratio	0.999

Table C6. Parameters of two-way directional valve (No 2).

Parameter	**Value**
Valve passage maximum area	7e-4 m²
Valve maximum opening	0.005 m
Flow discharge coefficient	0.7
Initial opening	0 m
Leakage area	1e-12 m²
Laminar transition specification	Pressure ratio
Laminar flow pressure ratio	0.999

Table C7. Parameters of two way directional valve (No 3).

Parameter	Value
Valve passage maximum area	7e-4 m^2
Valve maximum opening	0.005 m
Flow discharge coefficient	0.7
Initial opening	0 m
Leakage area	1e-12 m^2
Laminar transition specification	Pressure ratio
Laminar flow pressure ratio	0.999

Table C8. Parameters of two way directional valve (No 4).

Parameter	Value
Valve passage maximum area	10e-4 m^2
Valve maximum opening	0.005 m
Flow discharge coefficient	0.7
Initial opening	0 m
Leakage area	1e-12 m^2
Laminar transition specification	Pressure ratio
Laminar flow pressure ratio	0.999

Table C9. Parameters of hydraulic pipeline (No 1,5,6,9)

Parameter	Value
Pipe cross section type	Circular
Pipe internal diameter	0.02 m
Laminar friction constant for Darcy friction	64
Pipe length	1 m
Aggregate equivalent length of local resistance	1 m
Internal surface roughness height	15e-6 m
Laminar flow upper Reynolds number limit	2000
Turbulent flow lower Reynolds number limit	4000
Pipe wall type	Rigid wall
Specific heat ratio	1.4
Initial pressure	10000 Pa

Table C10. Parameters of hydraulic pipeline (No 2,3,7,8,4,10,11,12).

Parameter	Value
Pipe cross section type	Circular
Pipe internal diameter	0.01 m
Laminar friction constant for Darcy friction	64
Pipe length	0.5 m
Aggregate equivalent length of local resistance	1 m
Internal surface roughness height	15e-6 m
Laminar flow upper Reynolds number limit	2000
Turbulent flow lower Reynolds number limit	4000
Pipe wall type	Rigid wall
Specific heat ratio	1.4
Initial pressure	10000 Pa

Table C11. Parameters of hydraulic pipeline (No 24,27) parameters of digital simulation models of hydrostatic transmissions.

Parameter	Value
Pipe cross section type	Circular
Pipe internal diameter	0.03 m
Laminar friction constant for Darcy friction	64
Pipe length	1 m
Aggregate equivalent length of local resistance	1 m
Internal surface roughness height	15e-6 m
Laminar flow upper Reynolds number limit	2000
Turbulent flow lower Reynolds number limit	4000
Pipe wall type	Rigid wall
Specific heat ratio	1.4
Initial pressure	10000 Pa

Table C12. Fixed-displacement motor parameters of digital simulation models of hydrostatic transmissions.

Parameter	Value
Displacement	32.6 cm^3/rev
Leakage and friction parameterization	Analytical
Nominal shaft angular velocity	154 rad/s
Nominal pressure drop	100e5 Pa

Nominal kinematic viscosity	18 cSt
Nominal fluid density	900 kg/m³
Volumetric efficiency at nominal conditions	0.92
No-load torque	0.05 N*m
Friction torque vs. pressure drop coefficient	0.6e-6 N*m/Pa
Check if lower side pressure violating minimum	None

Table C13. Fixed-displacement pump $5.1885 \times 10^{-6} m^3/rad$ (32.6 cm^3/rev) parameters of digital simulation models of hydrostatic transmissions.

Parameter	**Value**
Displacement	32.6 cm³/rev
Leakage and friction parameterization	Analytical
Nominal shaft angular velocity	154 rad/s
Nominal pressure gain	100e5 Pa
Nominal kinematic viscosity	18 cSt
Nominal fluid density	900 kg/m³
Volumetric efficiency at nominal conditions	0.92
No-load torque	0.05 N*m
Friction torque vs. pressure gain coefficient	0.6e-6 N*m/Pa
Check if lower side pressure violating minimum	None

Table C14. Pressure relief load valve parameters of digital simulation models of hydrostatic transmissions.

Parameter	**Value**
Maximum passage area	2e-4 m²
Valve pressure setting	4.5e6 Pa
Valve regulation range	6e5 Pa
Flow discharge coefficient	0.7
Leakage area	1e-12 m²
Laminar transition specification	Pressure ratio
Laminar flow pressure ratio	0.999
Opening dynamics	Do not include valve opening dynamics

Table C15. Pressure relief valve 2 parameters of digital simulation models of hydrostatic transmissions.

Parameter	**Value**
Maximum passage area	2e-4 m²
Valve pressure setting	30e6 Pa

Valve regulation range	5e5 Pa
Flow discharge coefficient	0.7
Leakage area	1e-12 m²
Laminar transition specification	Pressure ratio
Laminar flow pressure ratio	0.999
Opening dynamics	Do not include valve opening dynamics

Table C16. Check valve (No 4,5,6,7) parameters of digital simulation models of hydrostatic transmissions.

Parameter	**Value**
Maximum passage area	20e-4 m²
Cracking pressure	0.3e5 Pa
Maximum opening pressure	1.2e5 Pa
Flow discharge coefficient	0.7
Leakage area	1e-12 m²
Laminar transition specification	Pressure ratio
Laminar flow pressure ratio	0.999
Opening dynamics	Do not include valve opening dynamics

Table C17. Hydraulic fluid parameters of digital simulation models of hydrostatic transmissions.

Parameter	**Value**
Hydraulic fluid index	Oil-30W
System temperature (°C)	60
Relative amount of trapped air	0.005
Viscosity derating factor	1
Pressure below absolute zero	Error
Density (kg/m³)	840
Viscosity (cSt)	34.9227
Bulk modulus (Pa)	1.47788e+09

Table C18. Solver configuration parameters of digital simulation models of hydrostatic transmissions.

Parameter	Value
Equation formulation	Time
Index reduction method	Derivative replacement
Start simulation from steady state	Yes
Consistency tolerance	1e-09
Use local solver	Yes
Use fixed-cost runtime consistency iterations	Yes
Linear Algebra	auto
Delay memory budget (kB)	1024
Apply filtering at 1-D/3-D connections when needed	Yes
Filtering time constant	0.001

Table C19. PS Constant of digital simulation models of hydrostatic transmissions.

Parameter	Value
Constant	154 rad/s

Parameters of simulation model components of classic open-loop hydrostatic transmission (Fig. 114).

Table C20. Fixed-displacement motor parameters of classic hydrostatic transmissions simulation model.

Parameter	Value
Leakage and friction parameterization	Analytical
Displacement	30 cm^3/rev
Nominal shaft angular velocity	154 rad/s
Nominal pressure gain	10 MPa
Volumetric efficiency at nominal conditions	0.92
Mechanical efficiency at nominal conditions	0.88
No-load torque	0 N*m

Table C21. Solver configuration parameters of classic hydrostatic transmissions simulation model.

Parameter	Value
Equation formulation	Time

Index reduction method	Derivative replacement
Start simulation from steady state	Yes
Consistency tolerance	Model AbsTol and RelTol
Tolerance factor	0.001
Use local solver	Yes
Use fixed-cost runtime consistency iterations	Yes
Linear Algebra	auto
Delay memory budget (kB)	1024
Apply filtering at 1-D/3-D connections when needed	Yes
Filtering time constant	0.001

Table C22. Pressure relief parameters of classic hydrostatic transmissions simulation model.

Parameter	**Value**
Set pressure control	Constant
Opening parameterization	Linear - Area vs. pressure
Opening pressure specification	Pressure differential
Set pressure differential	20 MPa
Pressure regulation range	0.35 MPa
Maximum opening area	2e-4 m^2
Leakage area	1e-10 m^2
Cross-sectional area at ports A and B	inf m^2
Discharge coefficient	0.64
Critical Reynolds number	150
Smoothing factor	0.01

Table C23. Pipe B parameters of classic hydrostatic transmissions simulation model.

Parameter	**Value**
Pipe length	6 m
Cross-sectional area	$\pi * 0.02^2 / 4 = 0.00031416\ m^2$
Hydraulic diameter	0.02 m
Aggregate equivalent length of local resistance	4 m
Internal surface absolute roughness	15e-6 m
Laminar flow upper Reynolds number limit	2000
Turbulent flow lower Reynolds number limit	4000
Laminar friction constant for Darcy friction	64

Enable dynamic compressibility	Yes
Initial liquid pressure	0.101325 MPa

Table C24. Variable-displacement pump parameters of classic hydrostatic transmissions simulation model.

Parameter	**Value**
Nominal displacement	30 cm^3/rev
Nominal shaft angular velocity	154 rad/s
Nominal pressure gain	10 MPa
Volumetric efficiency at nominal conditions	0.92
Mechanical efficiency at nominal conditions	0.88
No-load torque	0 N*m
Displacement threshold for pump-motor turnoff	0.1 cm^3/rev
Check if pressures are less than pump minimum	None

Table C25. Transmission fluid properties parameters of classic hydrostatic transmissions simulation model.

Parameter	**Value**
Density at atmospheric pressure (no entrained air)	850 kg/m^3
Isothermal bulk modulus model	Constant
Isothermal bulk modulus at atmospheric pressure	1.4 GPa
Kinematic viscosity at atmospheric pressure	18.8 cSt
Atmospheric pressure	0.101325 MPa
Minimum valid pressure	0.1 Pa
Pressure below minimum valid value	Error
Volumetric fraction of entrained air in mixture	0.005
Air polytropic index	1.0
Air density at atmospheric condition	1.225 kg/m^3

Table C26. PS constant parameters of classic hydrostatic transmissions simulation model.

Parameter	**Value**
Constant	154 rad/s

Table C27. Fixed-displacement pump lp parameters of classic hydrostatic transmissions simulation model.

Parameter	**Value**

Displacement	30 cm^3/rev
Leakage and friction parameterization	Analytical
Nominal shaft angular velocity	154 rad/s
Nominal pressure gain	100e5 Pa
Nominal kinematic viscosity	18 cSt
Nominal fluid density	900 kg/m^3
Volumetric efficiency at nominal conditions	0.92
No-load torque	0.05 N*m
Friction torque vs. pressure gain coefficient	0.6e-6 N*m/Pa

Table C28. Pressure relief valve lpv parameters of classic hydrostatic transmissions simulation model.

Parameter	**Value**
Maximum passage area	2e-4 m^2
Valve pressure setting	5e6 Pa
Valve regulation range	5e5 Pa
Flow discharge coefficient	0.7
Leakage area	1e-12 m^2
Laminar transition specification	Pressure ratio
Laminar flow pressure ratio	0.999
Opening dynamics	Do not include valve opening dynamics

Table C29. Motor leakage A parameters of classic hydrostatic transmissions simulation model.

Parameter	**Value**
Cross-sectional geometry	Custom
Linear pressure-flow resistance	1e7 s*MPa/m^3

Table C30. Motor leakage B parameters of classic hydrostatic transmissions simulation model.

Parameter	**Value**
Cross-sectional geometry	Custom
Linear pressure-flow resistance	1e7 s*MPa/m^3

Table C31. System input (displacement) parameters of classic hydrostatic transmissions simulation model.

Parameter	**Value**
Time values	[0, 5, 17, 20, 21]

Output values	[0, -31, -31, 0, 0]

Table C32. System input (load) parameters of classic hydrostatic transmissions simulation model.

Parameter	Value
Time values	[0, 20, 21]
Output values	[35, 35, 0]

Table C33. Simulink-ps converter parameters of classic hydrostatic transmissions simulation model.

Parameter	Value
Input signal unit	cm^3/rev
Apply affine conversion	No